



The
University
Of
Sheffield.

Exploring the Impact of Doxorubicin on the Perivascular Niche in Cancer

By:

Charlotte Rowan

A thesis submitted in partial fulfilment of the requirements for the degree of
Doctor of Philosophy

The University of Sheffield
Faculty of Medicine, Dentistry and Health
School of Medicine

Department of Oncology and Metabolism

August 2017

Declaration

The majority (approximately 95%) of the work presented in this thesis is my own. In experiments where assistance was provided by Dr Russell Hughes (administration of substances intravenously to mice), it is denoted in the text.

Acknowledgements

There are many people I must thank for their support during my PhD. First, I am grateful to Yorkshire Cancer Research, a fantastic charity which has funded my research during my PhD. I am also thankful for the support of my supervisors Professor Claire Lewis, Dr Carolyn Staton and Professor Gill Tozer. I would like to thank each one of you for your advice during these past few years.

I want to thank Dr Russell Hughes, who from day one of my PhD trained me in the ways of being an immunologist jedi/FACS wizard and for putting up with my terrible singing. I'd also like to thank the rest of the Tumour Targeting Group for providing me with advice on techniques, and lots of good memories.

I've been lucky to make many friends over the course of my PhD and I want to thank them all for all the fun times we've shared and for almost telepathically knowing when I needed to cut loose and sing karaoke.

I want to thank my family, for being a constant source of support. My grandmother Sadie, I thank you for always providing words of wisdom and having a brilliant sense of humour. My parents – I thank you in particular for listening to my moaning, running to the shops to buy me ice cream and cheering me on all the way to the finish line.

Last but not at all least, I need to thank Jack, my best friend of 8 years. If I were to list all the ways you've helped me during my PhD, well we'd probably have another 200 pages or so to read, so I'll keep it short but sweet. Thank you for everything, and I cannot wait to continue making memories with you.

Table of Contents

Declaration.....	i
Acknowledgements	ii
Table of Figures.....	vii
Table of Tables	ix
List of Abbreviations	x
Abstract.....	xiii
Chapter 1: General Introduction.....	1
1.1 Macrophage biology	2
1.1.1 Macrophage origins and differentiation	2
1.1.2 Macrophage functions.....	6
1.1.3 The M1/M2 paradigm	7
1.2 Tumour associated macrophages influence tumour progression.....	13
1.2.1 The ontogeny of TAMs.....	13
1.2.2 Roles in tumour progression	17
1.3 TAMs and tumour responses to chemotherapy	27
1.3.1 Use of chemotherapy in the treatment of cancer	27
1.3.2.1 Anti-tumoural functions of TAMs after chemotherapy.....	29
1.3.2.2 TAMs limit the anti-tumour effects of chemotherapy.....	31
1.4 TAM targeting strategies in the treatment of cancer	37
1.4.1 Therapies which inhibit macrophage recruitment.....	37
1.4.2 Therapies which modify TAM phenotype.	43
1.5 Summary.....	46
1.6 Hypothesis to be tested	48
1.7 Project aims	48
Chapter 2: Materials and Methods	49
2.1 Materials.....	50
2.1.1 List of reagents.....	50
2.1.2 List of materials	51
2.1.3 List of monoclonal (m) and polyclonal (p) antibodies	51
2.1.4 List of commercial kits.....	53
2.1.5 List of cell lines and animals	53
2.1.6 List of solutions	53
2.1.7 List of primers.....	54
2.1.8 List of instrumentation.....	56
2.1.9 List of software	56

2.2 Methods	57
2.2.1 Maintenance of cell lines.....	57
2.2.2 Isolation of BMDMs	58
2.2.3 Murine model of breast cancer	58
2.2.4 Dissection of FvB/n mice and preparation of samples.....	59
2.2.5 Dissociation of TS1 tumours for isolating cell populations.....	60
2.2.6 Preparation of blood from tumour bearing mice for flow cytometry	61
2.2.7 FlowJo analysis of FACS data.....	61
2.2.8 Histological analysis of tumours	62
2.2.9 Immunofluorescent staining of tumours.....	63
2.2.10 Confocal microscopy.....	64
2.2.11 Analysis of immunofluorescent images	64
2.2.12 FACS based isolation of cell populations from tumour digests.....	69
2.2.13 Laser Capture Microdissection of endothelial cells	70
2.2.14 Magnetic isolation of CD31 ⁺ cells from tumour digests.....	72
2.2.15 RNA isolation	73
2.2.16 cDNA synthesis.....	78
2.2.17 Quantitative PCR	78
2.2.18 Data representation and statistical analyses.....	80
Chapter 3: Characterisation of key features of mouse mammary (TS1) tumour implants after DOX treatment: stromal areas versus tumour cell islands	81
3.1 Introduction	82
3.2 Methods	85
3.2.1 Immunofluorescent staining of tumours.....	85
3.2.2 Analyses of immunofluorescent images	85
3.3 Results	86
3.3.1 TS1 tumours contain distinct regions of tumour cell islands and stroma.....	86
3.3.2 The stroma of PBS and DOX treated TS1 tumours is normoxic and has increased vascularity compared to tumour cell islands.	87
3.3.3 The normoxic stroma of PBS and DOX treated TS1 tumours contain increased numbers of TAMs compared to tumour cell islands.	90
3.3.4 MRC1 ⁺ TAMs are present mainly in the stroma of TS1 tumours.	92
3.3.5 DOX does not increase infiltration of immature Gr-1 ⁺ cells.....	95
3.3.6 DOX does not increase infiltration of immature Ly-6G ⁺ cells.....	98
3.4 Discussion.....	100
3.5 Concluding remarks.....	105

Chapter 4: Characterisation of the PV niche in TS1 mammary tumours: effects of DOX.....	107
4.1 Introduction	108
4.2.1 Immunofluorescent staining of tumours.....	113
4.2.2 Flow cytometric analysis of peripheral blood mononuclear cells	113
4.2.3 Preparation and staining of lymph nodes	116
4.2.4 Image analysis	118
4.2.5 Isolation of BMDMs	118
4.2.6 Flow cytometric analysis of BMDMs	119
4.3 Results	120
4.3.1 DOX significantly increases PV MRC1 ⁺ TAMs.....	120
4.3.2 DOX depletes monocytes in TS1 tumour-bearing mice.....	122
4.3.3 DOX slightly increases the abundance of MRC1 ⁺ monocytes in murine peripheral blood.....	124
4.3.4 BMDMs express MRC1 and CXCR4.....	127
4.3.5 PV MRC1 ⁺ TAMs were mainly mature, Gr1 ⁻ cells.....	127
4.3.6 The majority of PV MRC1 ⁺ TAMs were Ly-6G ⁻	131
4.3.7 CD31 ⁺ blood vessels had larger luminal areas in the stroma of TS1 tumours than those in the tumour cell islands.....	133
4.3.8 The number of PV TAMs does not correlate with the luminal area of tumour blood vessels.....	135
4.3.9 Luminal area does not impact on the number of PV MRC1 ⁺ TAMs per vessel.....	139
4.3.10 HEVs are present in mouse lymph nodes but not TS1 tumours.....	143
4.3.11 Distinct T cell populations are found within the tumour cell islands and stroma of TS1 tumours.....	145
4.3.12 FOXP3 ⁺ regulatory T cells are found at an increased density within the stroma than the tumour cell islands of TS1 tumours.....	149
4.3.13 Vessel patency was increased in the stroma of TS1 tumours compared to the tumour cell islands.....	151
4.3.14 The majority of vessels in TS1 tumours were associated with pericytes..	153
4.4 Discussion.....	155
4.5 Concluding Remarks	167
Chapter 5: Effect of DOX on the expression of selected genes by endothelial cells in TS1 tumours	169
5.1 Introduction	170
5.2 Methods	175
5.3 Results	179

5.3.1 Isolation of endothelial cells using FACS.	179
5.3.2 Isolation of endothelial cells using LCM.	181
5.3.3 Successful isolation of RNA from CD31 ⁺ cells using magnetic Dynabeads.	183
5.3.4 Assessing the enrichment of endothelial cells in the CD31-enriched fraction of cells using qPCR.	183
5.3.5 DOX significantly increases <i>Angpt2</i> expression in CD31-enriched cells....	188
5.3.6 DOX significantly increased the mRNA levels for <i>Angpt2</i> , <i>Plgf</i> and <i>Spp1</i> in CD31-depleted cell fractions.	190
5.4 Discussion.....	194
5.5 Concluding remarks.....	208
Chapter 6: General Discussion	210
6.1 Summary of major findings.....	211
6.2 DOX induces changes within the PV niche of TS1 tumours.....	212
6.3 Limitations of studies	215
6.4 Clinical implications	218
6.5 Further work and directions	224
Chapter 7: References	227

Table of Figures

Figure 1.1 Macrophage origins: yolk-sac derived and definitive haematopoiesis.....	6
Figure 1.2 Diversity in macrophage phenotypes and functions.....	12
Figure 1.3 TAMs promote tumour progression	26
Figure 1.4 Anti-tumoural TAMs synergise with chemotherapy.....	31
Figure 1.5 TAMs aid tumour survival and regrowth after chemotherapy	36
Figure 1.6 Strategies for targeting TAMs.	47
Figure 2.1 Workflow and validation of automated nuclear counting methods.	67
Figure 2.2 Laser capture microdissection.	72
Figure 2.3 Example melt curve analyses.	79
Figure 3.1: TS1 tumours contain two distinct compartments: tumour cell islands and distinct stromal areas.....	86
Figure 3.2 The stromal component of TS1 tumours is normoxic and more vascularised compared to the tumour cell islands.	89
Figure 3.3 The normoxic stroma contained a higher density of TAMs than the more hypoxic, tumour cell islands of TS1 tumours.....	91
Figure 3.4 Differences in F4/80 ⁺ and F4/80 ⁺ MRC1 ⁺ TAMs between the stromal compartment and tumour cell islands in TS1 implant tumours.....	93
Figure 3.5 Differences in F4/80 ⁺ and F4/80 ⁺ MRC1 ⁺ TAM densities between the stromal compartment and tumour cell islands in TS1 implant tumours.....	95
Figure 3.6 The number and density of Gr-1 ⁺ cells was higher in the stroma compared to the tumour cell islands of TS1 implant tumours.....	97
Figure 3.7 The density of Ly-6G ⁺ neutrophils is increased in the stroma compared to the tumour cell islands of TS1 implant tumours.....	99
Figure 3.8 Summary of differences between stromal and tumour cell island components of TS1 tumours.....	106
Figure 4.1 Isotype-matched controls do not bind to mouse PBMCs.....	115
Figure 4.2 Gating strategy for the flow cytometric analysis of murine peripheral blood monocytes.	117
Figure 4.3 DOX increases the density MRC1 ⁺ TAMs in direct contact with CD31 ⁺ blood vessels in tumours.....	121
Figure 4.4 DOX significantly lowers the proportion of myeloid cells that are monocytes in the blood of TS1 tumour bearing mice.	123
Figure 4.5 DOX increases the small proportion of MRC1 ⁺ monocytes in the peripheral blood of TS1 bearing mice.	126
Figure 4.6 Analysis of MRC1 and CXCR4 on the surface of murine BMDMs.	128
Figure 4.7 DOX did not alter the recruitment of immature PV MRC1 ⁺ Gr-1 ⁺ cells in TS1 tumours.....	130
Figure 4.8 PV MRC1 ⁺ cells expressing Ly-6G were infrequent in PBS and DOX-treated tumours.....	132
Figure 4.9 Analysis of vessel luminal area (restricted to vessels with a measurable lumen) within tumour cell islands and stroma of TS1 implant tumours, after PBS or DOX treatment.....	134
Figure 4.10 Analysis of the distribution of F4/80 ⁺ TAMs around vessels with a visible lumen in the stroma of TS1 tumours, after PBS and DOX treatment.....	137
Figure 4.11 Analysis of the distribution of F4/80 ⁺ TAMs around vessels with a visible lumen in the tumour cell islands, after PBS or DOX treatment.	138

Figure 4.12 Analysis of the distribution of F4/80 ⁺ MRC1 ⁺ TAMs around vessels with a measurable lumen in the tumour stroma, after PBS or DOX treatment.	141
Figure 4.13 Analysis of the distribution of F4/80 ⁺ MRC1 ⁺ TAMs around vessels with a measurable lumen in tumour cell islands, after PBS or DOX treatment.	142
Figure 4.14 TS1 implant tumours do not contain high endothelial venules.	144
Figure 4.15 Differences in the frequency of T cell subsets between the stroma and tumour cell islands of TS1 tumours after PBS or DOX treatment.	146
Figure 4.16 Differences in the percentages of CD4 ⁺ or CD8 ⁺ T cells between the stroma and tumour cell islands of TS1 tumours after PBS or DOX treatment.	148
Figure 4.17 Differences in the frequency of regulatory T cells between the stroma and tumour cell islands of TS1 tumours after PBS or DOX treatment.	150
Figure 4.18 DOX did not affect vessel patency in TS1 tumours.	152
Figure 4.19 The majority of vessels in the stroma and tumour cell islands have pericyte coverage after PBS and DOX treatment.	154
Figure 5.1 Various methods used to isolate tumour endothelial cells.	177
Figure 5.2 Flow cytometric analysis of CD31 and CD45 in digested tumours.	178
Figure 5.3 FACS isolation of endothelial cells from digested tumours.	180
Figure 5.4 Isolation of endothelial cells via Laser Capture Microdissection.	182
Figure 5.5 Isolation of CD31-enriched cells using magnetic bead isolation.	184
Figure 5.6 Magnetic isolation of CD31 ⁺ cells enriches <i>Pecam1</i> expression and decreases <i>Epcam</i> , <i>Itgam</i> and <i>Adgre1</i> expression in the CD31-enriched fraction of cells compared to CD31-depleted fraction of cells.	187
Figure 5.7 DOX significantly increases <i>Angpt2</i> expression in the CD31-enriched cell fractions.	191
Figure 5.8 DOX increases expression of <i>Angpt2</i> , <i>Cx3cl1</i> , <i>Plgf</i> and <i>Spp1</i> but not <i>Vegfa</i> in CD31-depleted cell fractions.	193
Figure 6.1 Summary of the effects of DOX on the PV niche.	212

Table of Tables

Table 1.1 The markers of the inflammatory and resident subsets of monocytes in humans and mice	3
Table 1.2 The ontogeny of different macrophage populations in adults	6
Table 1.3 Markers of macrophage M1 and M2a-skew in murine and human macrophages.....	9
Table 1.4 The various categories of chemotherapeutics, their mechanisms of action and the type of cancer they are used to treat.	28
Table 2.1 Concentrations of antibodies used in immunofluorescent analyses	65
Table 3.1: Antibodies used in immunofluorescent analyses in this chapter.....	85
Table 3.2 Number of Gr-1 ⁺ cells per field of view in PBS and DOX treated tumours. ...	96
Table 3.3 Gr-1 ⁺ cell density in PBS and DOX treated tumours.....	97
Table 4.1 Vessel types found within the abnormal tumour vasculature.....	110
Table 4.2 Antibodies used in the fluorescent staining of tumours.....	113
Table 4.3 Antibodies and isotype controls used in the flow cytometric analysis of peripheral blood mononuclear cells.	114
Table 4.4: Antibodies and isotype controls used in the flow cytometric analysis of BMDMs.	119
Table 5.1 Genes assayed using qPCR.....	174
Table 5.2: Antibodies used in FACS sorting of TS1 tumours.....	175
Table 5.3 Comparing gene expression in the CD31-enriched cell fractions isolated from tumours treated with PBS and DOX.....	189

List of Abbreviations

Acta2	α smooth muscle actin
Actb	β -actin
Adgre1	EGF-like module-containing mucin-like hormone receptor-like 1
Angpt2	Angiopoietin-2
BMDMs	Bone marrow derived macrophages
BrdU	5-Bromo-2'-deoxyuridine
BSA	Bovine Serum Albumin
CAMs	Cell Adhesion Molecules
CCL2	CC-Chemokine ligand 2
CFSE	Carboxyfluorescein succinimidyl ester
CFU-GM	Colony forming unit granulocyte macrophage
CSF1	Colony stimulating factor-1
CSF2	Colony stimulating factor-2
DAPI	4',6-Diamidino-2-Phenylindole, Dihydrochloride
DMEM	Dulbecco's Modified Eagle's Medium
DMSO	Dimethyl Sulfoxide
DOX	Doxorubicin
DPBS	Dulbecco's Phosphate Buffered Saline
dpc	Postcoital days
EGF	Epidermal growth factor
EMPs	Erythomyeloid precursors
Eng	Endoglin
Epcam	Epithelial cell adhesion molecule
ER	Oestrogen Receptor
FACS	Fluorescence Activated Cell Sorting
FasL	Fas ligand
FCS	Foetal calf serum
Fgf1	Fibroblast growth factor 1
FITC-lectin	Fluorescein labelled Lycopersicon Esculentum (tomato) lectin
FMO	Fluorescent Minus One
FN	Fibronectin
FOV	Field of view
FSC-A	Forward Scatter-Area
FSC-H	Forward Scatter-Height
GFR	Growth Factor Reduced
GM-CSF	Granulocyte macrophage colony stimulating factor
HBSS	Hank's Balanced Salt Solution
HEVs	High Endothelial Venules
HIF1	Hypoxia-Inducible Factor 1
HIF2	Hypoxia-Inducible Factor 2
HMGB1	High Mobility Group Box 1
HRG	Histidine-rich glycoprotein
HSCs	Haematopoietic Stem Cells
Icam1	Intercellular adhesion molecule 1

Icam2	Intercellular adhesion molecule 2
IFN- γ	Interferon- γ
IGF1	Insulin-like growth factor 1
IGF2	Insulin-like growth factor 2
IGFs	Insulin-like growth factors
IKK β	I κ B kinase
IL-10	Interleukin-10
IL-13	Interleukin-13
Il1a	Interleukin-1 α
Il1b	Interleukin-1 β
IL-1RA	IL-1 receptor antagonist
IL-4	Interleukin-4
Il6	Interleukin-6
IMDM	Iscoe's Modified Dulbecco's Medium
iNOS	Inducible nitric oxide synthase
IsoFlo	Isoflurane
ITCN	Image-based Tool for Counting Nuclei
Itgam	Integrin α M
LCM	Laser Capture Microdissection
LLC	Lewis Lung Carcinoma
LPS	Lipopolysaccharide
MAMs	Metastasis-associated macrophages
M-CFU	Macrophage colony forming unit
MDSCs	Myeloid-Derived Suppressor Cells
MHCII	Major histocompatibility complex class II
MI	Myocardial infarcts
MMP-9	Matrix metalloprotease-9
MPs	Monopotent precursors
MTMs	Mammary tumour macrophages
NF- κ B	Nuclear factor- κ B
NSCLC	Non-small cell lung cancer
OCT	Optimal Cutting Temperature Compound
PBMCs	Peripheral Blood Mononuclear Cells
PD-1	Programmed death-1
PD-L1	Programmed cell death 1 ligand
PD-L2	Programmed cell death 1 ligand 2
Pecam1	Platelet endothelial cell adhesion molecule
PFA	Paraformaldehyde
PIMO	Pimonidazole
Plgf	Placental growth factor
PNAAd	Peripheral Node Addressin
PPSCs	Pluripotent stem cells
PR	Progesterone Receptor
PTGS1	Prostaglandin-endoperoxide synthase 1
PV	Perivascular
qPCR	Quantitative real-time PCR
RIN	RNA Integrity Number

RPMI	Roswell Park Memorial Institute medium
S	Stromal compartment
Sele	E-selectin
SEM	Standard Error of the Mean
SiTRAN	Sheffield Institute of Translational Neuroscience
Spp1	Osteopontin
SSC-A	Side Scatter-Area
TAMs	Tumour associated macrophages
TCI	Tumour Cell Islands
TEMs	Tie2 expressing macrophages
TGM2	Transglutaminase 2
Thbs1	Thrombospondin-1
TMEM	Tumour microenvironment of metastasis
TNBC	Triple Negative Breast Cancer
TNF	Tumour Necrosis Factor
VCAM-1	Vascular Cellular Adhesion Molecule-1
Vegfa	Vascular endothelial growth factor A
WSX-1	IL-27 receptor chain

Abstract

Aims: Previous studies have shown that tumour associated macrophages (TAMs) limit the efficacy of chemotherapy agents like paclitaxel in mouse tumours. Furthermore, perivascular (PV) MRC1⁺ TAMs stimulate tumour regrowth after their exposure to cyclophosphamide. The aim of this thesis was to investigate the presence and origin of these PV cells in orthotopic mammary (TS1) tumours after doxorubicin (DOX) treatment. Attempts were also made to characterise their interaction with the tumour vasculature in such tumours.

Methods and Results: When TS1 tumours had become established in the mammary fat pads of FVB/N mice, their hosts were treated with a single injection of DOX or PBS. 48 hours later, mice were culled and their tumours removed for analysis. Immunofluorescent staining of tumours sections revealed the presence of increased numbers of MRC1⁺ TAMs in the well-vascularised (normoxic) stromal areas of TS1 tumours, compared to their less well-vascularised, tumour cell islands. Moreover, the number of these cells making direct contact with the tumour vasculature increased after DOX. These cells were mature Gr-1⁻ cells, rather than newly recruited monocytes or immature TAMs. They were not seen to associate with vessels of a particular size. DOX had no effect on the luminal area, patency or pericyte coverage of tumour blood vessels but increased the expression of *VegfA* mRNA by CD31⁺ endothelial cells. Moreover, both endothelial cells, and other, as yet undefined cells, upregulated mRNA for *Angiopoietin-2*, *Cx3cl1*, *Osteopontin* and *Plgf* in response to DOX.

Conclusions: DOX increases the number of MRC1⁺ TAMs associated with blood vessels in TS1 tumours, possibly in response to various genes upregulated by tumour endothelial cells (and other cells in the tumour microenvironment). The impact of these on the recruitment, retention and/or activation of TAMs in the PV niche merits further investigation.

Chapter 1

General Introduction

1.1 Macrophage biology

Metchnikoff first coined the term 'macrophage' in 1892, which he used to describe phagocytic cells in a number of different organs including the liver and lungs [1]. A great deal of work has since characterised macrophages as essential components of the innate immune system. Their major functions include phagocytosis of pathogens and dead/dying cells, antigen presentation to T cells and production of cytokines [2], [3].

1.1.1 Macrophage origins and differentiation

Macrophages originate from two distinct sources: definitive haematopoiesis and yolk-sac derived macrophages. Definitive haematopoiesis-derived macrophages begin differentiation in the colony forming unit, Granulocyte-Macrophage (CFU-GM) of the bone marrow, which contains progenitors which may form neutrophils or monocyte precursors, the monoblasts [4], [5]. Monoblasts differentiate into promonocytes, the precursors of monocytes, in the bone marrow [6]–[8]. Circulating monocytes can be divided into two subpopulations: 'classical' (formally inflammatory) and 'non-classical' (resident) subsets, both of which are capable of migrating into tissues and differentiating into macrophages [9].

In both mice and humans, fractalkine (CX₃CR1) receptor expression helps to distinguish between these two subsets; classical monocytes are CX₃CR1^{lo} and non-classical monocytes are CX₃CR1^{hi} [9]. CD62L (L-selectin) expression and CCR2 expression also differs between these monocyte subsets - with classical monocytes defined as CX₃CR1^{lo} CCR2⁺ CD62L⁺ and non-classical monocytes as CX₃CR1^{hi} CCR2⁻ CD62L⁻. Previously, human monocytes had been defined as CD14^{hi} CD16⁻ classical and CD14^{low} CD16^{hi} non-classical monocytes, which were additionally found to be defined by their CX₃CR1 expression level [9], [10]. Murine monocytes subsets, while not distinguishable by CD14 nor CD16 expression can be identified by additional

markers not expressed in humans. Ly-6C is highly expressed by classical murine monocytes, but at low levels in non-classical monocytes, whereas the opposite is true for CD43 expression [11]. CCR5 is only expressed by non-classical human monocytes [12]. Markers for these two monocytic subsets are summarised in Table 1.1 [13]. Ly-6C^{hi} classical monocytes are thought to differentiate and give rise to Ly-6C^{lo} monocytes, as Ly-6C^{hi} monocytes are the first monocytic subset to re-appear following depletion with clodronate liposomes [11]. Following depletion, an intermediate monocyte subset appears, the Ly-6C^{int}, and then the Ly-6C^{lo} monocytes reappear, suggesting that Ly-6C^{lo} monocytes are more mature monocytes [11].

Mouse Monocytes		Human Monocytes	
Classical	Non-classical	Classical	Non-classical
CX ₃ CR1 ^{lo}	CX ₃ CR1 ^{hi}	CX ₃ CR1 ^{lo}	CX ₃ CR1 ^{hi}
CCR2 ⁺	CCR2 ⁻	CCR2 ⁺	CCR2 ⁻
CD62L ⁺	CD62L ⁻	CD62L ⁺	CD62L ⁻
Gr1 ⁺	Gr1 ⁻	CD14 ^{hi}	CD14 ^{lo}
Ly6C ^{hi}	Ly6C ^{lo}	CD16 ⁻	CD16 ^{hi}
CD43 ⁻	CD43 ⁺	CCR5 ⁻	CCR5 ⁺

Table 1.1 The markers of the inflammatory and resident subsets of monocytes in humans and mice [13]

Experimentally, classical monocytes (CX₃CR1^{lo} Gr-1⁺) were shown to migrate into the inflamed peritoneum of mice. Conversely, while some CX₃CR1^{hi} Gr-1⁻ non-classical monocytes were identified in the inflamed peritoneum, most of the cells were found within the blood or non-inflamed peripheral organs [9]. As these monocytic subsets express different chemokine receptors, it is unsurprising they may respond to inflammation differently. Use of CX₃CR1^{gfp/+} mice and intravital imaging revealed that GFP^{hi} (thus CX₃CR1^{hi} non-classical) monocytes patrolled the inside of blood vessels [14]. Antibodies which inhibited CD11a/CD18 (LFA-1) showed that these integrins were integral to the 'patrolling' behaviour of these cells [14]. This patrolling behaviour is thought to be essential in the early response to inflammation as GFP^{hi} CX₃CR1^{hi} Gr-1⁻ non-classical monocytes extravasated out of blood vessels within 1 hour in order to

respond to various stimuli, including intraperitoneal infection with *Listeria monocytogenes*, where they then differentiated into macrophages [14].

Another study examining monocyte recruitment to myocardial infarcts (MI), showed classical Ly-6C^{hi} monocytes were initially recruited to the injury site (peaking at day 3 post-MI), followed by non-classical Ly-6C^{lo} recruitment (peaking at day 7 post-MI), which appeared to be dependent on the increased expression of CC-Chemokine ligand 2 (CCL2) during the wave of classical (CCR2⁺) monocyte recruitment [15]. This experimental model also revealed functional differences between the two monocytic subsets: Ly-6C^{hi} classical monocytes had produced more TNF when stimulated and had increased matrix metalloprotease (MMPs -2, -3, -9 and -13) and cathepsin (cathepsins -B, -L and -S) activity, suggesting they are important in proteolysis and inflammation [15]. By contrast, non-classical Ly-6C^{lo} monocytes had increased VEGF expression, suggesting a role for these cells in angiogenesis [15]. It is unknown, however, if the response of monocytic subsets to stimuli is due to their intrinsic programming, or due to the context and nature of the stimuli they are exposed to - i.e. Ly-6C^{lo} monocytes arrive later at the MI and, therefore, will be exposed to a different microenvironment (i.e. different chemokine expression etc) compared to the Ly-6C^{hi} monocytes which arrive at the MI site earlier.

Peripheral blood monocytes are known to extravasate into tissues, where they can differentiate into macrophages or specialised antigen presenting dendritic cells in a context-dependent manner [13]. Studies have revealed different roles for the two major monocytic subsets [16], however this could be due to differential expression of chemokine receptors and thus migratory behaviour, which results in these subsets reacting to different stimuli. Peripheral blood monocytes are not the only source of macrophages, and yolk-sac derived macrophages are discussed below (see Figure 1.1).

Prior to the onset of definitive haematopoiesis within the bone marrow, macrophages exist during embryonic development [17]. These embryonic “yolk-sac

derived" macrophages are now considered to be very important in the development of some adult tissue macrophages. Three different waves of embryonic macrophages can be identified in the embryos of mice. First, at 7.5-8 postcoital days (dpc), a maternally derived CD45⁺ F4/80⁺ c-Kit⁻ subset of macrophages can be identified just below the blood islands of the yolk sac [18]. These maternally derived macrophages constitute 0.4% of yolk sac cells at 7.5-8 dpc, yet by 8.5-9 dpc only 0.03% of yolk sac cells are maternally derived macrophages, demonstrating they colonize the embryonic yolk sac for only a short period of time.

Within the early (2-8 somite stage) yolk-sac two additional sources of embryonic macrophages exist, which are precursor subpopulations that are CD45⁻ c-Kit⁺: erythromyeloid precursors (produce erythrocytes and myeloid cells) and monopotent precursors (myeloid cells only) [18].

Foetal liver haematopoiesis is the final wave in macrophage development prior to definitive haematopoiesis [17]. By embryonic day 11.5, erythromyeloid progenitors have migrated from the yolk sac to the foetal liver, where they proliferate and differentiate [19]. Many tissue resident macrophage populations (for example Kupffer cells of the liver, microglia in the brain) are now believed to be derived from these embryonic macrophages (summarised in Table 1.2), although definitive haematopoiesis may also help maintain these populations [17]. A summary of the different macrophage differentiation pathways is shown in Figure 1.1.

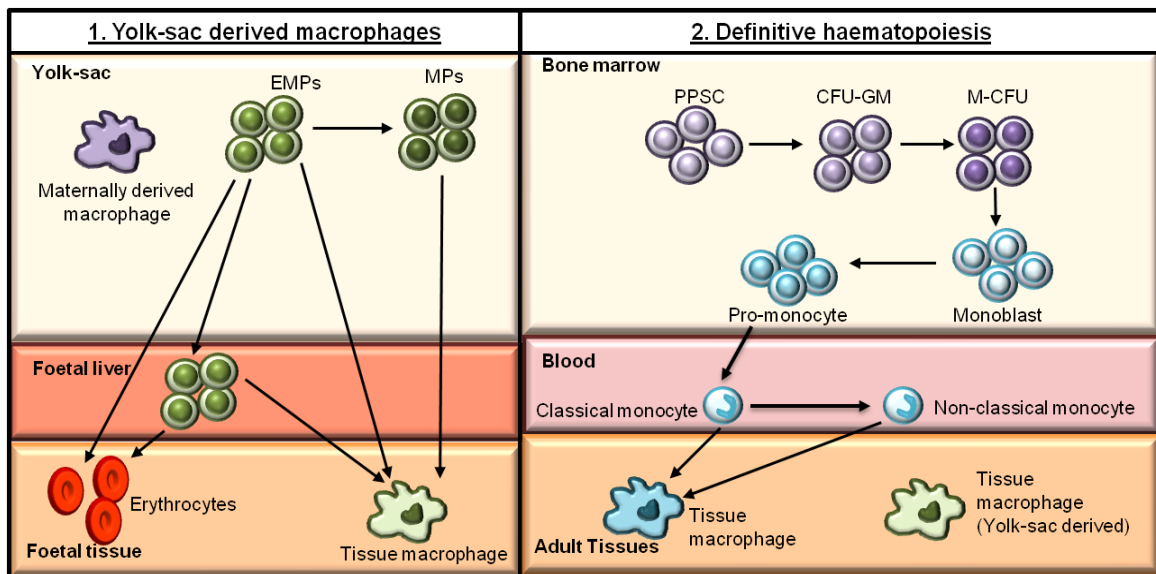


Figure 1.1 Macrophage origins: yolk-sac derived and definitive haematopoiesis. Macrophages originate in the yolk-sac of the embryo (1) or from definitive haematopoiesis in the bone marrow of adults (2). In the yolk-sac, maternally derived macrophages (purple, above) provide a short-lived source of macrophages. Following this erythromyeloid (EMPs) and monopotent progenitors (MPs) are a source of yolk-sac derived macrophages. EMPs can also form other myeloid cells and erythrocytes. During embryonic development EMPs migrate to the foetal liver and continue to produce erythrocytes and myeloid cells. In definitive haematopoiesis (2), pluripotent stem cells (PPSCs) exist within the bone marrow niche. The colony forming unit granulocyte macrophage (CFU-GM) contains progenitors of macrophages and neutrophils, some of which form macrophage progenitors (M-CFU). These develop into monoblasts which then form pro-monocytes within the bone marrow. Monocytes are released from the bone marrow into the blood as classical monocytes, which may either be recruited into tissues to form macrophages (blue), or mature into non-classical monocytes, which can also extravasate and form tissue macrophages (blue). Yolk-sac derived macrophages (green) continue to exist within healthy adult tissues as described in Table 1.2.

Tissue	Macrophage type	Origin
Liver	Kupffer cells	Yolk-sac derived
Brain	Microglia	Yolk-sac derived
Lung	Alveolar macrophage	Yolk-sac derived
Spleen	Red pulp macrophage	Yolk-sac derived
Bone	Osteoclasts	Definitive haematopoiesis
Skin	Langerhans cells	Yolk-sac derived
Blood	Circulating monocytes	Definitive haematopoiesis

Table 1.2 The ontogeny of different macrophage populations in adults [20]

1.1.2 Macrophage functions

Macrophages are a diverse and plastic cell type, with various functions that contribute to the elimination of pathogens and also play key roles in tissue homeostasis and wound healing [21]. There are also tissue-specific subsets of macrophages which have roles in supporting the tissues in which they reside, as follows.

Key players in the body's "first line of defence" are alveolar macrophages which reside in the lungs. As well as defending against pathogens and suppressing allergic responses, these cells also maintain the optimal height of the air-liquid interface and breakdown the surfactant layer, which is crucial to maximise gaseous exchange [22]. Langerhans cells are a population of antigen presenting cells in the skin which are crucial in triggering immune responses [23]. Microglia reside in the brain and provide immunological surveillance and appropriate responses to both pathogens and other damaging stimuli such as the build-up of amyloid- β plaques. Furthermore, microglia play roles in synaptic pruning during embryonic development [24]. Osteoclasts are found within bone and are multinucleate cells derived from macrophages which have merged together. These cells are vital in bone resorption, an important homeostatic process in bone growth and repair [25]. In the liver, Kupffer cells line the sinusoids and perform a variety of roles such as clearance of erythrocytes and bacteria [26], [27]. Kupffer cells are also thought to be important in liver regeneration [27].

1.1.3 The M1/M2 paradigm

Attempts to describe macrophage phenotypes have resulted in the 'M1/M2 activation' paradigm. Macrophage phenotypes have, therefore, been described as 'classically activated (also known as 'M1-skewed') or an 'alternatively activated' (also known as 'M2-skewed') [2], [28]. However, it is important to recognise the plasticity of macrophages means that they can express a phenotype anywhere on the sliding scale between these two polarized states, rather than being just one or the other, depending upon the balance of local signals acting on them at any one time [29]–[31].

Macrophages can be 'classically' activated by Interferon- γ (IFN- γ) in combination with the pathogen associated molecule lipopolysaccharide (LPS) or tumour necrosis factor (TNF) [2], [32]. Such M1-skewed macrophages have an increased expression of pro-inflammatory molecules such as IL-1 β , inducible nitric oxide synthase (iNOS), CXCL9, CXCL10, and CXCL11 [33]–[35]. These pro-

inflammatory molecules are essential for drawing in other immune cells to the site of the insult e.g. a bacterial infection, and killing the pathogen responsible [2], [34], [36]. The stimulation and recruitment of immune cells such as cytotoxic T cells and natural killer cells can also be important for killing tumour cells [37], [38].

Equally important are anti-inflammatory 'M2-skewed' macrophages which are essential for the resolution of inflammation and tissue repair [2], [39]. These M2-skewed macrophages are believed to provide protection from excessive and unwanted inflammatory responses [40], [41]. Interleukin-4 (IL-4) and Interleukin-13 (IL-13) are able to polarise macrophages to an M2 phenotype [2]. Further studies revealed two other methods which contributed to 'M2-skewing'. Macrophages activated with IL-4 and IL-13 are described as M2a; those activated with TLR ligands and immune complexes are described as M2b and activation with IL-10 or glucocorticoids gives an M2c phenotype [42]. Additionally, the macrophage growth factor colony stimulating factor-1 (CSF1) is thought to be an M2-skewing signal, whereas CSF2 is an M1-skewing signal [43].

IL-4 can inhibit the expression of pro-inflammatory genes such as IL-1 β , TNF, IL-6 and iNOS in murine monocytes or macrophages [44], [45] and upregulates anti-inflammatory gene expression such as arginase-1, IL-27 receptor chain (WSX-1) and IL-1 receptor antagonist (IL-1RA) [46]–[48].

Genes upregulated in murine macrophages when treated with IL-4 include MRC1 (a mannose receptor) [49], Arginase-1 [50], Ym1 and Fizz1 [51], with MRC1 commonly used as a marker of anti-inflammatory macrophages. In humans, arginase-1 expression is not regulated by IL-4, and so is not considered is not a marker of M2 phenotype in humans [52], [53]. Ym1 and Fizz1, are only markers of M2 phenotype in mice, as humans do not express homologues of these genes [33], [53]. However, some markers, first identified in mice, remain useful for distinguishing polarisation in human macrophages. For example, human M2 polarised macrophages express the markers

MRC1, the mannose scavenger receptor MSR1 and CD163 amongst others described in Table 1.3 [33].

Microarray and proteomic studies examining genes induced by IL-4 in both murine and human macrophages have been conducted to reveal 'M2a' markers which appear to be conserved between species. Genes upregulated in murine and human macrophages treated with IL-4 included the previously described mannose receptor MRC1 [49], Kruppel-like factor 4 (gut) [54], Prostaglandin-endoperoxide synthase 1 (PTGS1) [55] and interferon regulatory factor 4 [53], [56]. Moreover, this microarray and proteomics analysis revealed transglutaminase 2 (TGM2) as a novel marker of the M2a phenotype [53]. A summary of M2a markers induced by IL-4 are summarised in Table 1.3.

M2-activation can relate to functional differences, for example murine bone marrow derived macrophages (BMDMs) cultured with IFN- γ and immune complexes (M2b activation) had increased IL-10 production, whereas those cultured with IL-4 alone (M2a activation) did not produce IL-10 [57]. Moreover, the M2b-skewed macrophages were able to stimulate T cell proliferation and caused T cells to upregulate activation markers CD25 and CD69, possibly as they expressed the antigen presenting proteins CD86 and major histocompatibility complex class II (MHCII).

Murine macrophages		Human macrophages	
M1 phenotype	M2a Phenotype	M1 phenotype	M2a Phenotype
CXCL9	MRC1	CXCL9	MRC1
CXCL10	MSR1	CXCL10	MSR1
CXCL11	CD163	CXCL11	CD163
IL-12	IL-1RA	IL-12B	IL-1RA
TNF	TGM2	TNF	TGM2
iNOS	Arginase-1	COX2	CCL17
COX2	Stabilin-1	IL-6	CCL22
IL-6		IL-15	

Table 1.3 Markers of macrophage M1 and M2a-skew in murine and human macrophages [2], [33], [53].

IL-4 is known to affect arginine metabolism by upregulating arginase-1 and downregulating iNOS in murine M2a-skewed macrophages [45], [46]. However, skewing murine macrophages with immune complexes and LPS had the converse effect on arginine metabolism, as these macrophages produced large amounts of nitric oxide and low amounts of urea, demonstrating they had increased iNOS activity and decreased arginase-1 activity [57].

M2c-skewed macrophages are described as being activated by IL-10 or glucocorticoids, and their effects on the phenotype of human macrophages have been studied [58]–[60]. Of note, pre-incubating human monocyte-derived macrophages (MDMs) with the glucocorticoid fluticasone propionate significantly altered their responses to activation with IFN- γ and IL-4 [60]. Activation of macrophages with IFN- γ typically caused an upregulation of the Fc receptor CD64, but pre-incubating with fluticasone propionate (a glucocorticoid) prevented this response. Only IL-10 and fluticasone propionate treated MDMs showed CD163 expression, however when these macrophages were pre-incubated with fluticasone propionate, macrophages activated with IFN- γ , IL-4 and IL-10 all showed an upregulation of CD163, compared to activation with the respective stimulus alone [60]. These data suggest that while the M1/M2 paradigm is a traditional way to describe macrophage activation, the activation status of macrophages is complex, and can be modulated by additional stimuli. This is particularly important when considering relevance of *in vitro* models of macrophage activation, as a multitude of likely stimuli affect macrophage phenotype *in vivo*.

Martinez and Gordon suggest a new outline for the M1/M2 paradigm in which many more factors are considered when describing macrophage phenotype, including growth and survival factors, interactions with other immune cells, pathogen interactions and resolution of the inflammatory response [28]. It is clear from this new perspective, that while ‘M1-skew’ and ‘M2-skew’ are traditional and useful general terms, terms need to be used to describe the activation status of macrophages that take on board the immunological context of these cells, so it is not over-simplified. For example,

Mosser and Edwards also define 'M2-skewed' macrophages into two different categories, specifically relating to their functions, with those that produce anti-inflammatory cytokines such as IL-10 and can present antigens to T cells (e.g. express CD86 and MHCII) being referred to as 'regulatory' macrophages [2], [57]. In contrast, macrophages that express low amounts of pro-inflammatory cytokines and produce molecules involved in wound healing such as arginase-1, were categorised as 'wound healing' macrophages [2], [57]. This paradigm of macrophage phenotype is illustrated in Figure 1.2.

Given their anti-microbial pro-inflammatory phenotype, M1-skewed macrophages are believed to be anti-tumoural as they could activate the immune system to promote an anti-tumour response. Macrophages with an M2-skew however, produce immunosuppressive molecules and molecules associated with tissue remodelling and are believed to be mainly tumour-promoting [2], [61].

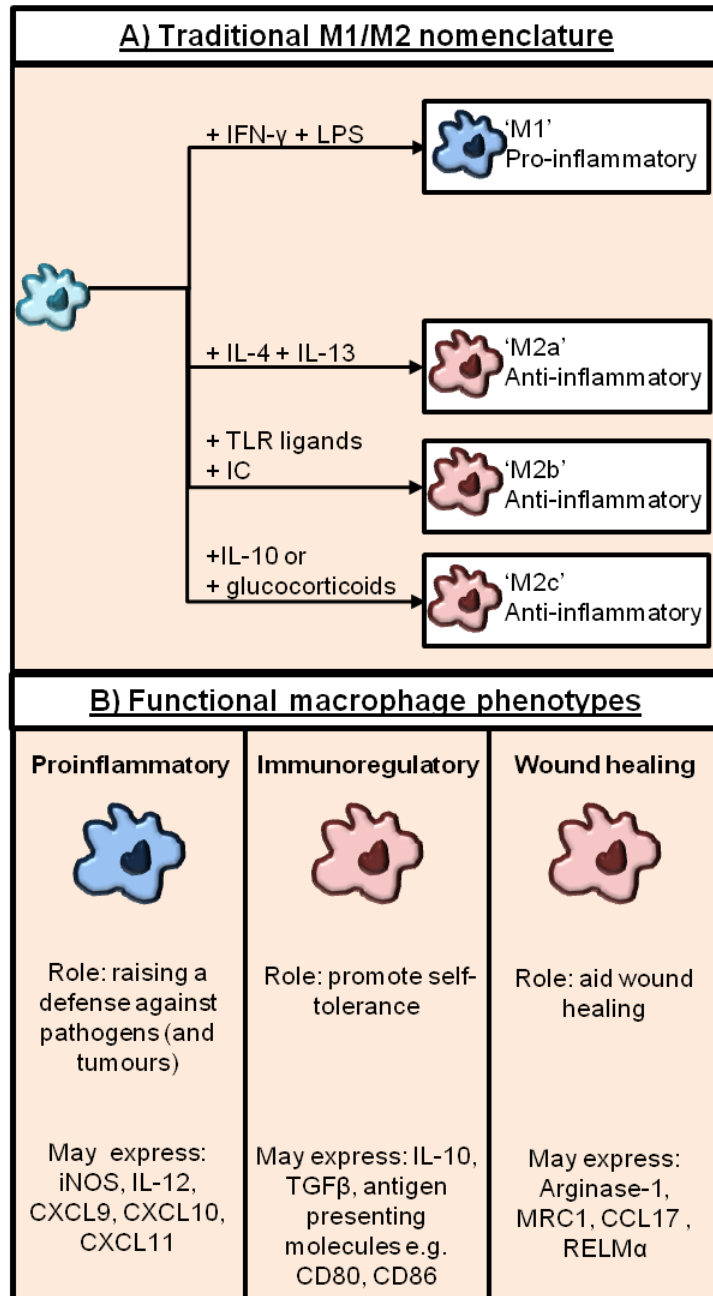


Figure 1.2 Diversity in macrophage phenotypes and functions.

(A) Traditionally, macrophages were described as having an 'M1-skewed' pro-inflammatory phenotype (i.e. expression of inflammatory cytokines) or an 'M2-skewed' anti-inflammatory phenotype (i.e. expression of immunosuppressive molecules, proangiogenic functions). Activation with IFN- γ and LPS leads to an M1-skewed macrophage. M2-skewed macrophages can be split into 3 subcategories – M2a (as activated by IL-4 and IL-13), M2b (activated by TLR activation and immune complexes) and M2c (IL-10 or glucocorticoid) activation. Csf-1 (not shown) also promotes M2-skewedness in macrophages.

(B) Functional macrophage phenotypes accurately describe macrophage behaviour. Proinflammatory macrophages, probably would be considered as M1-skewed, and express many immunostimulatory molecules. Immunoregulatory macrophages are able to promote self-tolerance with immunosuppressive molecules such as IL-10 and can present antigens to T cells. Wound-healing macrophages promote angiogenesis and fibroblast functions. Both regulatory and wound-healing macrophages share phenotypic features associated with M2-skewed macrophages.

1.2 Tumour associated macrophages are a key component of the tumour microenvironment

The tumour microenvironment consists of many components which can influence tumour growth and progression, including tumour associated macrophages (TAMs) and the tumour vasculature [62]. In addition to TAMs, other immune cells such as T cells, myeloid-derived suppressor cells (MDSCs), and neutrophils can infiltrate and interact with the tumour microenvironment to impact on tumour progression [63]. It is thought that TAMs support tumour progression by influencing immunosuppression, metastasis, angiogenesis and response to therapy [64]–[66].

1.2.1 The ontogeny of TAMs

An important, much debated question about TAMs is the origin of these cells. As previously denoted, peripheral blood monocytes, derived from definitive haematopoiesis can give rise to mature macrophages within tissues. Yolk-sac derived macrophages also remain within certain adult tissues, and continually populate them by proliferating [17].

Recently, monocyte tracing studies have been employed to understand the origin(s) of TAMs. Fluorescent latex beads (0.5µm in size) were used to label the two monocytic subpopulations on the basis of their Gr-1 expression status in the peripheral blood of mice. Intravenous injection of 0.5µm microspheres was able to label cells within the peripheral blood and 10-12% of peripheral blood monocytes (identifiable as side scatter low, CD115⁺ F4/80⁺ cells within the circulation) were labelled with latex beads [67]. Initially all 3 monocytic subpopulations (Gr-1^{hi}, Gr-1^{int} Gr-1^{lo} monocytes) could be detected within the latex bead labelled population of monocytes, but over time the percentage of latex bead⁺ Gr-1^{hi} monocytes decreased until at 24 hours only Gr-1^{lo} monocytes were detected within the latex bead⁺ population of peripheral blood

monocytes [67]. These latex bead⁺ Gr-1^{lo} monocytes could be detected in the circulation for up to one week.

In order to label Gr-1^{hi} monocytes, circulating monocytes were first depleted with clodronate liposomes. 18 hours later, latex beads were injected into the mice intravenously. Importantly, latex bead⁺ Gr-1^{hi} monocytes were also detectable for 1 week after labelling using this method [67]. These Gr-1^{hi} monocytes acquired their latex beads from neutrophils and B cells, which in the absence of circulating monocytes (i.e. after clodronate liposome administration) became latex bead⁺ and migrated to the bone marrow where the monocytes acquired latex beads [67].

This technique was also used in a study by Movahedi and colleagues [68]. TS/A tumours were established following monocytic labelling with latex beads to identify the contributions of monocytic subpopulations to TAM subsets within the tumour microenvironment [68]. When circulating Ly-6C^{lo} monocytes were labelled with latex beads, no latex bead⁺ CD11b⁺ cells could be identified within tumours, which were taken 6 days after monocyte labelling [68]. However, labelling the Ly-6C^{hi} monocytes demonstrated that this subset of cells are recruited into tumours, as 4% of tumoural CD11b⁺ cells were also latex bead⁺. These cells could be identified within tumours up to 19 days after the initial labelling. This demonstrates that Ly-6C^{hi} monocytes are recruited into and contribute to TAM populations within these tumours. In this model, 6 days after tumour initiation, some Ly-6C^{hi} monocytes had started to differentiate into MHCII^{hi} TAMs and MHCII^{lo} TAMs; whereas by day 12 most monocytes had converted into the two aforementioned TAM subsets [68]. These data suggest that TAMs derive from circulating Ly-6C^{hi} classical monocytes.

The limitations of these studies, however, are that only 10-15% of circulating monocytes are labelled using this latex bead technique and it appears that, as Ly-6C^{hi} classical monocytes mature, they lose their Ly-6C expression, which in turn could lead to questions over the relevance of monocytic subsets when investigating macrophage origins [67], [68]. If Ly-6C^{hi} monocytes mature into Ly-6C^{lo} monocytes, then the

question still remains – are the monocytes Ly-6C^{hi} cells upon entry into tumours, or must they have already become Ly-6C^{lo} monocytes prior to tumour entry? A small population of Ly-6C^{hi} monocytes was detectable within TS/A tumours, which decreased over time [68]. Conversely, only 0.06% of total CD11b⁺ tumoural cells were considered to be Ly-6C^{lo} monocytes [68]. These data therefore suggest that Ly-6C^{hi} monocytes were able to infiltrate tumours to a greater extent compared to Ly-6C^{lo} monocytes.

Tie2-expressing macrophages (TEMs) are thought to form from a subset of circulating non-classical monocytes and are found within tumours [69], [70]. It is therefore possible that non-classical monocytes also infiltrate tumours [69]–[71]. As previously discussed, different monocytic subsets do express different levels of chemokine receptors, e.g. non-classical monocytes are Cx₃CR1^{hi} CCR2⁻ whereas classical monocytes are Cx₃CR1^{lo} CCR2⁺, which could explain differences in monocytic subset recruitment to different tumour types, as it is likely that a range of tumours may express different chemokines [9].

Another pool of monocytes which may contribute to the TAM pool are the reservoir of monocytes which reside in the spleen [72]. Studies in mice bearing genetically induced lung adenocarcinomas (induced by oncogenic Kras and loss of p53) demonstrate that monocytes from the spleen infiltrate these tumours [73]. Splenectomised mice had significantly fewer TAMs [73]. There was also a decrease in the circulating CD11b⁺ Ly-6C^{hi} monocytes in splenectomised mice, yet bone marrow numbers were unaffected by the splenectomy suggesting that the spleen releases monocytes into the circulation and acts as a separate store of monocytes to the bone marrow [73]. The recruitment of cells into these tumours was shown to be in a CCL2-CCR2 dependent manner, as targeting monocytes with lipid nanoparticles which contained CCR2-targeted siRNA, reduced TAMs [73]. This splenic pool of monocytes was also increased in patients with invasive cancers compared to spleens from patients without signs of malignancy, demonstrating a possible clinical significance of these data [73].

More recently, studies utilising a photoconvertible protein in monocytes were used to trace the contributions of bone marrow and splenic monocytes to TAMs within Lewis Lung Carcinomas (LLCs), which demonstrated bone marrow monocytes migrated to these tumours to a much greater extent than splenic monocytes [74]. Taken together, these studies suggest splenic monocytes contribute to TAM populations, however perhaps not to the same extent as bone marrow monocytes; it is also likely that differences in animal model may account for differences in splenic vs. bone marrow contributions to TAM populations in these two studies [73], [74].

Yolk-sac derived macrophages also contribute to resident macrophage populations within a variety of tissues [17]. A recent study described the role of the resident 'mammary tissue macrophages' (MTMs) in the progression of the MMTV-PyMT murine mammary tumours [75]. MTMs were identified in healthy mammary glands as CD11b^{hi} MHCII^{hi} cells, which were also found within mammary tumours. As these tumours increased in growth there was a decrease in the proportion of MTMs, as the proportion of TAMs (CD11b^{lo} MHCII^{hi} cells) increased [75]. Parabiosis was used to identify whether the increase in TAMs was due to recruitment from cells derived from definitive haematopoiesis or expansion of tissue resident (yolk-sac derived) macrophages. Both parabionts contributed to the MTMs, TAMs and monocytes as shown by chimerism of these cell populations, demonstrating that recruitment from definitive haematopoiesis-derived precursors plays a role in the expansion of TAMs during tumour progression [75].

Depletion of CCR2⁺ cells using mice with diphtheria toxin receptor (DTR) expression driven by the CCR2 promoter decreased both TAM and MTM populations within the tumours [75]. These data suggest that classical CCR2⁺ monocytes contribute at least in part, to both TAMs and MTMs within these tumours [75]. Previously, classical monocytes were shown to contribute to TAM populations, using labelling experiments, whereas these data show that by depleting the classical monocytes, you can reduce TAM populations within tumours [68], [75]. Interestingly, MTMs are also

described within this study, which does indicate a potential role for 'resident' tissue macrophages in tumour progression. The MTMs in these tumours are clearly derived at least in part, from classical monocytes. Further studies using models which differentiate between definitive haematopoiesis and yolk-sac derived macrophages, such as the *Myb* knockout mouse which lacks cells derived from definitive haematopoiesis, but not embryonic macrophages, could give novel insights into the contributions of embryonic macrophages to tumour progression [76].

In summary, Ly-6C^{hi} classical monocytes have been traced and shown to enter tumours, where they can give rise to numerous TAM subpopulations within the tumour [68]. TEMs, which arise from circulating non-classical monocytes also infiltrate tumours, although evidence suggests that Ly-6C^{hi} monocytes mature into Ly-6C^{lo} monocytes and tracing studies demonstrated non-classical monocytes form a very low percentage of cells recruited into tumours [68], [70], [71]. Questions still remain over the source of resident tissue macrophages which could affect tumour progression, as studies demonstrated they were at least in part maintained by definitive haematopoiesis, and further studies are required to fully understand embryonic contributions to these macrophage subsets [75]. It is likely that the contributions of embryonic macrophages and macrophages which differentiate from monocytes will depend on the location and type of the tumour.

1.2.2 Roles in tumour progression

It is now widely accepted that TAMs can influence cancer growth, metastasis and response to therapy [65], [66], [77]. The presence of high numbers of TAMs is associated with poor prognosis in many types of human cancer including breast, thyroid, bladder, oesophageal and astrocytic tumours [78]–[82].

Cancer has several defining features, best described by Hanahan and Weinberg as "Hallmarks of Cancer" [83]. In order to survive and grow, tumours must proliferate, develop a blood supply (angiogenesis), invade and metastasise to other

tissues and escape the immune system [83]. The evidence that TAMs can aid tumour progression by increasing tumour invasiveness, increasing tumour angiogenesis or immunosuppression of anti-tumoural cells e.g. cytotoxic T cells will now be discussed and summarised in Figure 1.3 [64], [66].

1.2.2.1 Angiogenesis

Angiogenesis, the process by which new vessels arise from pre-existing vessels, is required for tumour growth [84], [85]. Implanting tumour spheroids that were infiltrated with macrophages demonstrated increased angiogenic potential *in vivo*, providing evidence that macrophages may support angiogenesis [86]. In the MMTV-PyMT model of mammary cancer, Lin and colleagues describe the 4 stages of tumour progression, starting with hyperplasia, then adenoma/MIN stage [87]. Following this tumours enter the early carcinoma stage which can progress to a late carcinoma stage [87]. Vessel density increases as these tumours transition from the premalignant adenomas to the malignant early carcinoma stage, which suggests increases in angiogenesis is related to tumour progression. This lead to this increase in vessel density being described as an 'angiogenic switch' – an increase in angiogenesis required for tumour progression [88]. Interestingly, macrophages infiltrate MMTV-PyMT tumours prior to the increase in angiogenesis, and Csf1 deficient mice (Csf1^{op/op}) with depleted macrophages [89], showed a delayed angiogenic switch and tumour progression, which implicates macrophages in promoting the angiogenic switch which is key for tumour survival and progression [88]. TAMs are known to express many pro-angiogenic molecules including VEGFA, angiopoietin-1 and angiopoietin-2, cathepsin B and thymidine phosphorylase [71]. Moreover, depletion of macrophages using clodronate liposomes resulted in a decrease in tumour vessel density and halted tumour growth [90].

De Palma *et al.* identified a new subpopulation of macrophages: TEMs [69]. It was later revealed that these TEMs had a strongly pro-angiogenic and M2-skewed phenotype. Originally, De Palma and colleagues set out to target endothelial cells as a

possible way to inhibit tumour angiogenesis. The TIE2 receptor was originally thought to be exclusively expressed in endothelial cells [91]. Transfecting cell lines with a construct expressing GFP under the control of the *Tie2* promoter, demonstrated GFP expression (and therefore *Tie2* expression) was restricted to endothelial cell lines *in vitro* [69]. However, when examining Tie2-driven GFP expression *in vivo*, it was clear that there were CD45⁺ (pan-leucocyte marker) CD11b⁺ (myeloid lineage marker) cells which also expressed *Tie2* [69]. Interestingly these myeloid cells were found at the periphery of tumours and at sites of angiogenesis [69]. Furthermore, when TEMs were ablated in mice carrying LLCs or TS/A mammary tumours, there was a decrease in tumour volume and weight as well as in tumour vascular density, demonstrating that TEMs support tumour growth and angiogenesis [69].

The subsequent characterization of TEMs revealed they have a marked pro-angiogenic macrophage-like phenotype, rather than that of endothelial or haematopoietic stem cells (HSCs) [70]. Human monocytes and MDMs were also found to express functional TIE2, as they responded to angiopoietin-2 treatment by chemotaxis and exerted increased pro-angiogenic activity [92], [93]. Venneri *et al.* described the presence of TEMs within human tumours, supporting the notion that TEMs are clinically relevant and may be a potential target for new anti-cancer therapies [93]. Moreover, a recent study correlated the presence of TEMs with increased angiogenesis in hepatocellular carcinomas, supporting their possible role in promoting tumour angiogenesis [94].

Pucci *et al.* extracted TEMs, TIE2⁻ TAMs and endothelial cells from N202 mammary tumours grown subcutaneously in Tie2-GFP transgenic mice in order to compare their gene expression profiles [71]. Quantitative PCR (qPCR) analysis of 280 genes demonstrated that TEMs and TAMs express typical hematopoietic genes such as CD45, CD11b and F4/80 and low amounts of typical endothelial cell genes e.g. VEGFR2. qPCR analysis also showed differential gene expression between the TAMs and TEMs. Arginase-1 and other M2 genes such as MRC1 and CD163 were

upregulated in TEMs in comparison to TAMs, whereas pro-inflammatory genes such as iNOS, IL-1 β and COX2 were downregulated in TEMs. Interestingly, TEMs were found to be a population of non-classical Gr1⁻ and CD43⁺ cells in peripheral blood [71]. In order to confirm the TEMs were definitely hematopoietic cells, Pucci *et al.* used a microRNA targeting system [95] to ensure that Tie2-GFP expression would be suppressed in hematopoietic cells. Haematopoietic cells express microRNA miR142 [96] which causes degradation of GFP tagged with miR142 targeting sequences exclusively in haematopoietic cells. They showed that TEMs and endothelial cells express GFP in a Tie2-GFP transgenic mouse; however this GFP expression is lost in TEMs in the Tie2-GFPmiR142T mouse as the miR142 expression in hematopoietic cells causes degradation of the GFP [71]. Taken together, these three papers suggest that a population of bone marrow derived TEMs have a proangiogenic role, support tumour growth and are of an anti-inflammatory phenotype [69]–[71]. Interestingly, while TEMs are heavily M2-skewed, it should be noted that Tie2 expression is also strongly upregulated in human macrophages treated with IFN- γ and so is not a prototypical marker of the “M2” phenotype [97]. It is therefore important to assess the functions of TEMs within tissues, rather than assuming their behaviour based on the expression of one marker.

Gene expression profiling of TEMs also demonstrated they express a variety of pro-angiogenic molecules including thymidine phosphorylase, vegfa and placental growth factor (plgf) [71]. The TIE2 ligand, angiopoietin-2 [98], has been shown to influence TEMs, acting as a chemoattractant and promoting their proangiogenic behaviour [92], [93], [99]. Angiopoietin-2 increased the pro-angiogenic activity of human TEMs as measured by sprouting and endothelial cell tubule formation assays [99]. Using qPCR and protein assays, angiopoietin-2 was found to increase the expression of pro-angiogenic genes such as VEGFA, matrix metalloprotease-9 (MMP-9), cathepsin B and thymidine phosphorylase [99].

Moreover, double transgenic mice, with endothelial cells over expressing angiopoietin-2 (ANG2-DT) [100] were used to demonstrate the effect of angiopoietin-2 *in vivo* [99]. Tumours grown in the ANG2-DT mice did not grow faster, but showed increased infiltration by TEMs and had increased numbers of immature vessels, which were CD31⁺ but lacked pericyte coverage [99]. The increased angiopoietin-2 expression also increased the expression of thymidine phosphorylase, cathepsin B and MRC1 in TEMs [99]. The overall effect of angiopoietin-2 overexpression was an increase in immature vessels, which could be partially due to the increased population of pro-angiogenic TEMs within the tumour [99], as well as the direct effects angiopoietin-2 may exert on the tumour endothelial cells [101].

Knockdown of Tie2 in TEMs resulted in fewer TEMs around the vasculature, and a decrease in CD31⁺ area (endothelial cell coverage) in MMTV-PyMT tumours, demonstrating angiopoietin-2 may play a role in attracting TEMs to the vasculature [102]. However, knockdown of the Tie2 receptor in TEMs did not significantly inhibit tumour growth [102]. An antibody targeting angiopoietin-2 however significantly reduced tumour growth and metastasis suggesting that this antibody inhibits tumour growth by a mechanism other than its effects on TEMs alone i.e. effects on the vasculature [102]

TEMs were also revealed to have increased immunosuppressive functions when treated with angiopoietin-2 [103]. Both *in vitro*, *in vivo* and *ex vivo*, angiopoietin-2 increased the immunosuppressive effects of TEMs. TEMs pre-treated with angiopoietin-2 were shown to inhibit T cell proliferation, measured using a carboxyfluorescein succinimidyl ester (CFSE) assay [103]. There was also an increase in the percentage of T cells *in vitro* which were CD4⁺ CD25⁺ FOXP3⁺ Tregs, and a decreased percentage of CD8⁺ cytotoxic T cells, demonstrating another role for TEMs in aiding tumour progression [103]. These *in vitro* studies utilised an anti-IL-10 antibody to demonstrate the immunosuppressive activity of TEMs was dependant on IL-10. In tumours with endothelial cells overexpressing angiopoietin-2 (ANG2-DT) there was

also an increase in Tregs [103]. *Ex vivo*, TEMs isolated from tumours were capable of inhibiting T cell proliferation to a greater extent than that of Tie-2⁻ TAMs. Interestingly CD11b⁺ Gr1⁺ cells isolated from the spleens of these mice were also more immunosuppressive than the Tie2⁻ TAMs [103].

1.2.2.2 Immunosuppression

Immunosuppression promotes tumour progression, as tumour cells evade the immune system and continue to proliferate [83]. Natural killer cells are part of the innate immune system and can kill tumour cells [37]. Natural killer cells isolated from mice bearing LLCs had decreased cytotoxic activity as the tumours increased in size [104]. Both tumour cells and macrophages were found to produce prostaglandin E₂ which suppressed the natural killer cells [104]. Moreover the depletion of macrophages was found to prevent tumour suppression of natural killer cells, demonstrating one way in which TAMs promote tumour tolerance [104].

Within the adaptive immune system, CD4⁺ FOXP3⁺ regulatory T cells (Tregs) suppress T cell responses and promote tumour self-tolerance, whereas CD8⁺ T cells (cytotoxic T cells) can mediate tumouricidal activity [105]. TAMs suppress T lymphocyte proliferation, preventing the adaptive immune system from promoting an anti-tumour response [106], [107]. Depletion of macrophages by inhibiting the CSF1 receptor in murine models of cancer, following treatment with chemotherapy, significantly increased the amount of cytotoxic CD8⁺ T cells and reduced the amount of Tregs in tumours, indicating a role for TAMs in skewing the tumour microenvironment towards immune escape [108], [109].

It is likely that TAMs mediate T cell suppression via IL-10 [57], [103], as IL-10 was highly expressed by TAMs isolated from MMTV-PyMT tumours [110], and anti-IL-10 therapy in combination with chemotherapy increased the amount of granzyme B expressing cells (cytotoxic T cells) within tumours and reduced tumour volume [110].

Mechanistically, TAM-derived IL-10 was shown to suppress dendritic cell production of IL-12 which is important in the activation and proliferation of cytotoxic T cells [110].

In order to promote self-tolerance, T cells express 'checkpoint molecules' such as programmed death-1 (PD-1), which allows them to be inactivated when necessary [111]. However, tumour cells and TAMs express ligands for these checkpoint molecules such as programmed cell death 1 ligand (PD-L1) and PD-L2, which also deactivate T cells [112]. Evidence suggests that tumours can encourage TAMs to become more immunosuppressive by inducing their expression of PD-L1 [113].

In sum, TAMs aid tumours to escape the immune system by many mechanisms, including preventing T cell proliferation and de-activating T cells through expression of immunosuppressive molecules such as IL-10 and checkpoint molecules.

1.2.2.3 Metastasis

Invasion and metastasis spread tumour cells throughout the body. TAMs release a number of factors implicated in these two processes [71]. TAMs have been implicated in both the initiation of metastasis (i.e. within the primary tumour) and the survival and growth of metastases (i.e. within the metastatic niche).

Macrophage-derived epidermal growth factor (EGF) increased the invasive behaviour of carcinoma cells both *in vitro* and in mouse tumours [114], [115]. Moreover intravital imaging was used to visualise TAM-tumour cell interactions *in vivo* and demonstrated that tumour cells were more motile when in the proximity of TAMs near blood vessels in tumours [116]. In $Csf1^{op/op}$ macrophage deficient mice, there are significant delays in the onset of metastasis compared to $Csf1^{+/op}$ littermates [117]. The $Csf1$ deficient mice had fewer circulating tumour cells, indicating the loss of TAMs in these mice reduced tumour cell intravasation [116]. Inhibition of the EGF receptor or the CSF1 receptor had similar effects on the numbers of circulating tumour cells, implicating these molecules further in the promotion of metastasis [116].

TAMs and TEMs express many molecules which may impact on metastasis, and one of these molecules is MMP-9 [99], [118]. *In vitro*, macrophages co-cultured with tumour cells upregulated MMP-9 expression, which increased the invasion of cancer cell lines (measured using matrigel invasion assays) [118]. Moreover, LLC-bearing mice that were deficient in MMP9 exhibit reduced lung metastasis [119].

TAMs are a well-documented source of factors which can increase vascular permeability such as VEGF-A [120] and thus may influence intravasation by increasing vascular permeability, enabling tumour cells to enter the blood from the tumour [121]. Indeed tumours with a more normalised, less “leaky” vasculature, form fewer metastases [30], [121]. Mena, a protein involved in actin regulation, was found to be a gene upregulated in invasive tumour cells [122], [123]. Research has recently focussed on trios of cells consisting of tumour cells which overexpress Mena, coupled with an endothelial cell and a perivascular (PV) TAM, to form a complex called the ‘tumour microenvironment of metastasis’ (‘TMEM’) [124]. Ablation of VEGF-A in PV TAMs within these TMEMs reduced vascular permeability and circulating tumour cells, demonstrating TAMs produce factors which promote intravasation [124]. High numbers of TMEMs in ER⁺ HER2⁻ breast tumours are associated with increased risk of distant metastasis [125].

Tumour cells also require macrophages to be present if they are to extravasate and survive at the metastatic site [126]. Depletion of macrophages (using the Csf1^{op/op} mouse) results in fewer experimental lung metastases following an intravenous injection of mouse mammary tumour cells [126]. Using clodronate liposomes, it became clear that depletion of macrophages during the time of tumour cell injection reduced the number of lung metastases, indicating their role in metastatic seeding at this site [126]. Depletion of macrophages at later time points (2 days and 4 days after tumour cells were injected) did not reduce the number of metastases established in the lungs, but decreased the size of metastases and the amount of alive, proliferating tumour cells within the metastases, suggesting that metastasis-associated

macrophages (MAMs) are also important for the growth of metastases [126]. Depletion of resident lung macrophages by intra-tracheal administration of clodronate liposomes however did not impact on metastasis, suggesting MAMs are a distinct sub-population of macrophages [126].

In fact, the lung MAMs are thought to be derived from classical Ly-6C^{hi} monocytes, as monocyte tracing studies demonstrated there was an increase in the numbers of classical monocytes infiltrating lung metastases compared to the non-classical monocytes [127]. Moreover, an anti-CCL2 antibody inhibited the recruitment of the classical monocytes (which are CCR2⁺) to the lung metastases and reduced the number macrophages within metastases [127]. Anti-CCL2 therapy also significantly reduces metastatic burden, demonstrating macrophages have a role in promoting metastasis, which could be targeted with anti-CCL2 therapies [127]. Unfortunately, the clinical benefits of anti-CCL2 may be limited as a recent study revealed that metastatic growth accelerated after the cessation of anti-CCL2 therapy in mice, as monocytes previously sequestered in the bone marrow during anti-CCL2 therapy are released into circulation and promote metastasis [128]. Ongoing research into novel targets has revealed CCL3 and VEGFR1 are also expressed by and essential for the metastasis-promoting activity of MAMs and therefore could be potential anti-metastatic targets in future [129], [130].

In short, PV TAMs support metastasis by aiding the intravasation of tumour cells and MAMs then promote the seeding, survival and growth of the tumour cells within the metastatic niche, as demonstrated in Figure 1.3.

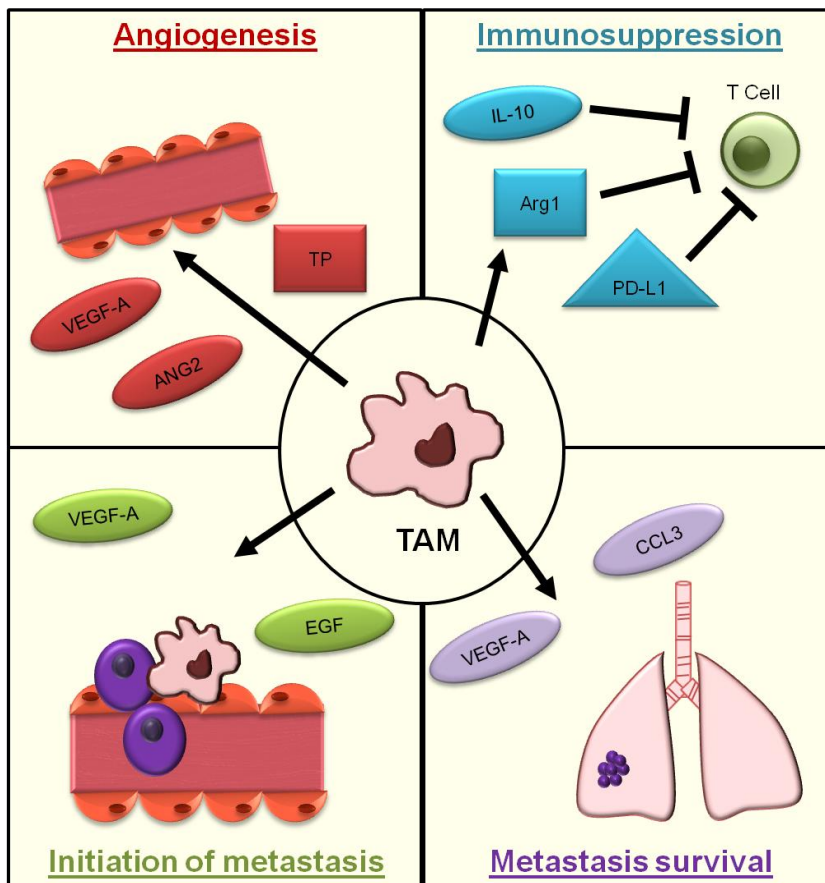


Figure 1.3 TAMs promote tumour progression

TAMs can promote angiogenesis through a number of proangiogenic molecules including VEGF-A, Angiopoietin-2 (ANG2) and thymidine phosphorylase (TP). TAMs also promote tumour tolerance by suppression of immune cells via molecules such as IL-10, Arginase-1 (Arg1) and PD-L1. TAMs increase the initiation of metastasis by increasing tumour cell invasiveness (via EGF signalling) and vascular permeability (via VEGF-A). Metastases require macrophages to survive, and macrophages produce molecules such as VEGF-A and CCL3 to increase tumour cell extravasation, metastatic seeding, survival and growth.

1.3 TAMs and tumour responses to chemotherapy

1.3.1 Use of chemotherapy in the treatment of cancer

The type of cancer and extent of tumour progression contribute to the choice of treatment offered. Chemotherapy is a standard-of-care treatment for many types of cancer. There are a range of chemotherapeutic drugs available and their mechanism of action varies. Paclitaxel and docetaxel belong to the taxane family of drugs and stop cells from proliferating as they enter mitosis by increasing their microtubule stability [131]. Anthracyclines such as doxorubicin disrupt DNA synthesis by intercalating base-pairs (guanine-cytosine and adenine-thymine) and inhibiting DNA topoisomerase activity [131]. DNA synthesis is also disrupted by the platin family of drugs, e.g. cisplatin, by inducing DNA cross-links [131]. Table 1.4 describes the other main types of chemotherapeutics currently in use.

Class of chemotherapy drug	Example	Mechanism of action	Useful in the treatment of
Anthracyclines	Doxorubicin	Intercalates base pairs and prevents DNA unwinding by inhibiting DNA topoisomerases	Many types including breast, bladder and myeloma
Anti-metabolites	Gemcitabine	Interferes with DNA and RNA synthesis	Bladder, breast, lung, ovarian and pancreatic cancers
Camptothecin analogs	Irinotecan	Inhibits topoisomerase I, disrupting DNA synthesis	Colon and rectal cancer
Epipodophyllotoxins	Etoposide	Inhibits topoisomerase II activity, preventing DNA unwinding and thus DNA synthesis	Lung, lymphomas, ovarian and testicular cancers
Nitrogen mustards	Cyclophosphamide	Alkylates DNA, causing DNA damage which leads to tumour cell death	Many types including breast, lung, leukaemias, lymphomas and myeloma
Nitrosoureas	Carmustine	Another alkylating agent, and causes DNA damage	Lymphoma, myeloma and brain tumours
Platinum agents	Cisplatin	Form DNA cross-links and causes DNA damage	Bladder, head and neck, lung, ovarian and testicular cancers
Taxanes	Paclitaxel	Increases microtubule stability and causes cells to halt in mitosis	Breast, lung and ovarian cancer
Vinca Alkaloids	Vinblastine	Bind to tubulin and inhibits mitotic spindle formation, preventing mitosis	Bladder, breast, lymphomas, Kaposi's sarcoma and testicular cancer

Table 1.4 The various categories of chemotherapeutics, their mechanisms of action and the type of cancer they are used to treat [131], [132].

1.3.2 TAMs modulate the response to chemotherapy

Increasing evidence has shown that TAMs modulate the response of the tumour to chemotherapy [65]. TAMs can promote the regrowth of mouse tumours after chemotherapy, probably by expressing a wound-healing, immunosuppressive phenotype. However there is also evidence for TAMs helping to destroy tumours following chemotherapy. These differences within the literature are likely due to differences in tumour type and the form of chemotherapeutic agent used (i.e. its effect on tumour cells). If TAMs take a pro-inflammatory phenotype following chemotherapy, it is likely they will increase the effects of tumouricidal chemotherapy.

1.3.2.1 Anti-tumoural functions of TAMs after chemotherapy

Despite evidence demonstrating that high TAM numbers often correlate poorly with prognosis in cancer patients [77], some studies demonstrate TAMs are important in raising an anti-tumoural response after chemotherapy. Cyclophosphamide was shown to increase macrophage infiltration in xenografted tumours (consisting of murine embryonic fibroblasts transformed with oncogenic K-RAS and E1A) [133]. However, depletion of macrophage precursors (peripheral blood monocytes) with gadolinium chloride caused tumours to show diminished responses to sustained therapy with cyclophosphamide [133]. Interestingly, cyclophosphamide increased the number of IL-1 β -expressing cells, suggesting that cyclophosphamide induced a pro-inflammatory phenotype within the tumour microenvironment.

High mobility group box 1 (HMGB1) is usually a nuclear protein but is released into the extracellular environment when cells undergo necrosis [134]. HMGB1-deficient tumours had a decreased response to cyclophosphamide, accompanied by a decrease in macrophage, neutrophil and natural killer cell recruitment to these tumours, compared to tumours expressing HMGB1 [135]. Furthermore, HMGB1-deficient tumours exhibited increased expression of M2-polarising genes like IL-4 whereas tumours expressing HMGB1 had an increase in proinflammatory gene expression such

as IL-1 β following cyclophosphamide treatment. These data demonstrate HMGB1 as a possible chemoattractant for immune cells which are anti-tumoural.

Interestingly, docetaxel was shown to skew myeloid-derived suppressor cells (MDSCs, immature CD11b⁺ Gr-1⁺ cells) to an immunostimulatory phenotype and increased T cell proliferation and cytolytic killing in 4T1-Neu tumours [136]. Further investigations are now required to show which chemotherapeutic drugs can trigger TAMs to take on such an immunostimulatory phenotype, as this could improve chemotherapeutic regimens by providing an immunostimulatory microenvironment within the tumour. Figure 1.4 summaries how TAMs can potentially improve the response to chemotherapy.

Importantly, strategies that have focussed on re-educating TAMs towards a proinflammatory phenotype rather than an immunosuppressive phenotype, have had success in improving the response to chemotherapy [30]. Histidine-rich glycoprotein (HRG) overexpressing tumours were shown to polarise TAMs to be more immunostimulatory by increasing expression of genes such as CXCL9 and decreasing expression of immunosuppressive genes such as arginase-1 and IL-10 [30]. Accompanying this switch in macrophage phenotype was a decrease in tumour growth and metastases, a more normalised vascular network and an improved response to doxorubicin treatment [30]. Depletion of macrophages with clodronate liposomes decreased tumour growth in wild type tumours, whereas in tumours overexpressing HRG, macrophage depletion increased tumour growth, supporting the idea that the HRG overexpression skews TAMs towards an anti-tumoural phenotype [30]. These data demonstrate the importance of macrophage phenotype in the context of improving current front-line therapies.

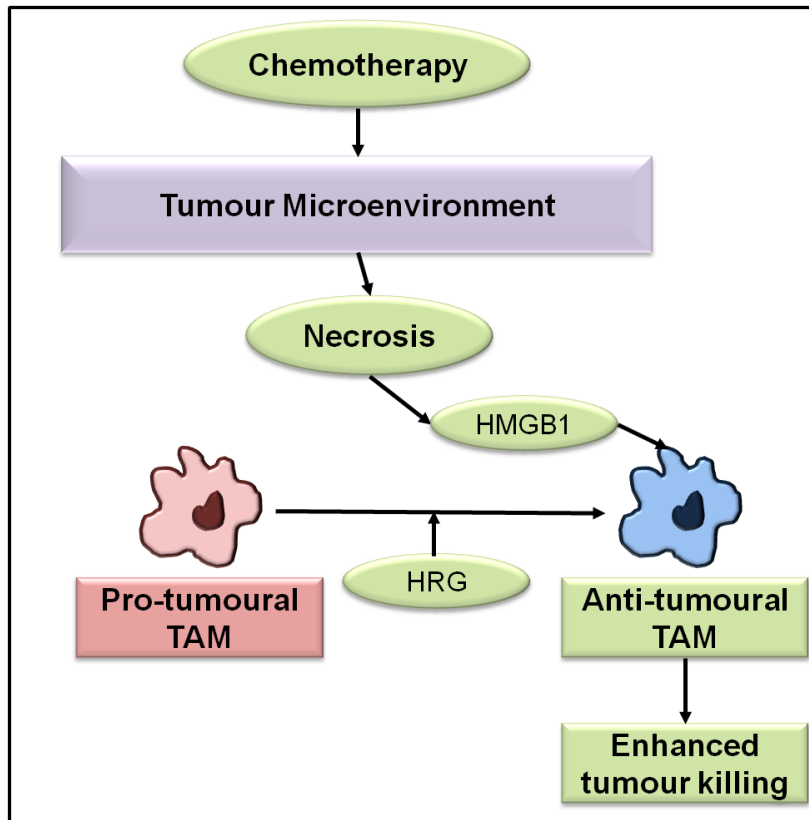


Figure 1.4 Anti-tumoural TAMs synergise with chemotherapy

Chemotherapy may induce necrotic cell death. Necrotic cells can release high mobility group box 1 (HMGB1) which attracts anti-tumoural pro-inflammatory cells into tumours, enhancing the effects of chemotherapy. Re-education of pro-tumoural immunosuppressive TAMs to an anti-tumoural phenotype e.g. in tumours overexpressing histidine-rich glycoprotein (HRG) also improves response to chemotherapy.

1.3.2.2 TAMs limit the anti-tumour effects of chemotherapy

Many studies have described TAMs as having an immunosuppressive and proangiogenic phenotype [66]. It is, therefore, not surprising to find that TAMs contribute to tumour survival and regrowth during/following chemotherapy in some mouse tumour models [65].

In vitro primary mammary tumour cells were equally sensitive to doxorubicin, regardless of the stage of the MMTV-PyMT tumour they were isolated from. However, *in vivo*, early carcinomas showed increased doxorubicin sensitivity compared to late carcinomas and hyperplasias, despite all stages of the mammary tumour displaying similar amounts of cell proliferation, indicating doxorubicin sensitivity is not mediated by a property intrinsic to the tumour cells [137]. TAMs and monocytes/neutrophils were

shown to express MMP-9, and MMP9^{-/-} mice had an increased response to doxorubicin and increased vascular leakage, suggesting that MMP-9 limited the ability of doxorubicin to diffuse within the tumours [137]. Doxorubicin increased tumour infiltration of CCR2⁺ monocytes, and this increase was not seen in CCR2^{-/-} mice, suggesting that CCL2-CCR2 signalling is important in the recruitment of these monocytes after doxorubicin [137]. Moreover, CCR2^{-/-} mice had an increased sensitivity to doxorubicin, showing these monocytes in particular are responsible for decreased sensitivity to doxorubicin *in vivo* [137].

The cathepsins B and S promote tumour growth and angiogenesis [138]. After observing an increased expression of these enzymes in lysates from paclitaxel-treated tumours, Shree and colleagues further investigated the source of these cathepsins [139]. Paclitaxel increased macrophage infiltration into tumours and using a fluorescent probe to detect cathepsin activity, they observed these macrophages were a source of cathepsins [139]. *In vitro*, they used co-cultures to demonstrate that macrophages also protect tumour cells from cell death (as detected by Annexin-V surface expression) [139]. Moreover inhibition of cathepsins with JPM abrogated the tumour-protective effects of macrophages and use of this inhibitor *in vivo* increased the efficacy of paclitaxel, doxorubicin and etoposide [139].

Insulin-like growth factors (IGFs) have been implicated in chemoresistance in pancreatic cancer [140]. *In vitro*, macrophage conditioned medium containing IGF1 and IGF2 increased the survival of pancreatic cell lines and, in addition, TAMs were shown to express IGF1 and IGF2 in patients with pancreatic ductal adenocarcinoma [140]. Murine pancreatic tumours also showed expression of IGF1 and IGF2 in TAMs and fibroblasts [140]. Inhibition of IGF signalling using IGF-blocking antibodies, in combination with the chemotherapy drug gemcitabine significantly increased tumour cell death (measured by tumour size and cleaved caspase-3 expression) in a murine model of pancreatic cancer, demonstrating IGFs, which are expressed by TAMs, can contribute to chemoresistance [140].

TAMs are known to express a number of pro-angiogenic molecules [71], [99], [141]. The role of myeloid cell VEGF-A was investigated using mice which had a loxed *Vegfa* allele and expressed Cre recombinase enzyme under the control of the LysM promoter [142], which specifically removed myeloid cell-derived VEGF-A [143]. Tumours grown in LysMCre/VEGF^{f/f} mice grew more quickly than in wild type mice and had a more normalised vasculature, with increased pericyte coverage and a less tortuous, less permeable vascular network, suggesting vascular normalisation had aided tumour growth [143]. Furthermore, the LysMCre/VEGF^{f/f} mice actually responded much better to cyclophosphamide therapy, perhaps because the more normalised vasculature allowed the chemotherapy to permeate further into the tumour mass [143]. These data implicate TAMs as hindering both tumour growth and responses to chemotherapy, and demonstrate the importance of normalising the vasculature to improve response to chemotherapy.

More recently, TAM-derived VEGF-A was ablated using the Csf1r-Mer-iCre-Mer inducible, macrophage-specific knockout of VEGF-A [127], and this resulted in significantly delayed tumour regrowth in implanted MMTV-PyMT tumours treated with doxorubicin, demonstrating these TAMs promote relapse in a VEGF-A dependent manner [144]. These TAMs infiltrated tumours treated with chemotherapy – as demonstrated by increases in both TAMs and MRC1⁺ (a marker of M2-skewed phenotype) TAMs in 3 different tumour models given 3 different types of chemotherapy (LLC + cyclophosphamide; 4T1 + paclitaxel and MMTV-PyMT implants + doxorubicin) [144]. Adoptive transfer of MRC1^{hi} TAMs isolated from LLCs into other LLCs following chemotherapy increased the rate of tumour regrowth compared to transfer of MRC1^{lo} TAMs, suggesting that MRC1⁺ TAMs are responsible for aiding the regrowth of tumours [144]. MRC1⁺ VEGF-A⁺ TAMs were found within the PV niche (the area of tumours directly in contact with the vasculature) of these LLCs [144]. Interestingly, AMD3100, an inhibitor of the CXCR4 receptor [145], delayed LLC regrowth after cyclophosphamide treatment [144]. AMD3100 inhibited the accumulation of PV MRC1⁺

TAMs, demonstrating that they promote relapse [144]. This means that targeting the CXCL12-CXCR4 axis could improve the efficacy of some forms of chemotherapy by reducing PV TAMs that promote tumour relapse [144].

Further studies utilised the LysM-Cre system to ablate *Tie2* in myeloid cells which resulted in delayed regrowth of MCA205 fibrosarcomas after chemotherapy (both cyclophosphamide and doxorubicin used as single agents) [146]. Tumours grown with TAMs lacking TIE2 were less vascular after doxorubicin treatment, compared to those grown in wildtype mice [146]. It is worth noting however, that the LysM-Cre system was not inducible and so these studies are conducted with TAMs that are unable to express *Tie2* from the beginning of the study, not exclusively during the regrowth phase, and previous studies have highlighted that angiopoietin2-TIE2 signalling can increase the proangiogenic activity of TEMs [99]. Questions therefore remain about whether the *Tie2* ablation reduces relapse because of initial changes in the tumour microenvironment prior to therapy, or due to changes which occur after therapy. Interestingly, *Tie2* expression *in vitro* did not increase survival of RAW264.7 macrophages treated with doxorubicin, but did offer survival benefits when they were grown under serum starvation conditions, suggesting TAMs which express *Tie2* are more likely to survive stressful conditions [146].

Immunosuppression is another method by which TAMs may promote tumour growth by evading anti-tumour responses. Patient biopsies (treated with chemotherapy prior to surgery) and MMTV-PyMT tumours treated with paclitaxel showed increased TAM infiltration compared to tumours not exposed to chemotherapy [109]. In the murine MMTV-PyMT tumour model, macrophage infiltration was found to be dependent on the macrophage growth factor and chemokine, CSF1, which was upregulated in these tumours following paclitaxel treatment [109]. PLX3397, an inhibitor of the CSF1 receptor and the stem cell receptor c-kit, inhibited recruitment of macrophages to tumours and increased the efficacy of paclitaxel and carboplatin chemotherapy, causing an increase in tumour shrinkage [109]. In addition to this, T cell recruitment

(CD3⁺ CD8⁺ cells and CD3⁺ CD4⁺ cells) was increased in paclitaxel-treated tumours when TAM recruitment was inhibited by PLX3397. TAMs isolated from MMTV-PyMT tumours suppressed cytotoxic T cell proliferation (CD3⁺ CD8⁺ cells) *in vitro* and anti-CD8 antibodies abolished the effects of PLX3397 on mammary tumours *in vivo*, demonstrating that the macrophages recruited by CSF1 after chemotherapy are pro-tumoural and exert some of their effects via suppression of CD8⁺ cytotoxic T cells [109]. The importance of CSF1 was also demonstrated when a CSF1 blocking antibody reduced macrophage recruitment into MCF-7 chemoresistant tumour xenografts and rendered them sensitive to chemotherapy [147].

An increase in TAMs was also observed following treatment of pancreatic tumours in mice with gemcitabine [108]. TAMs were shown to increase the number of tumour initiating cancer stem cells, tumour growth and metastasis and to mediate cytotoxic T cell suppression. Again, inhibition of CSF1R caused a decrease in macrophage accumulation and improved response of pancreatic tumours to gemcitabine. It therefore appears that the CSF1 signalling pathway is a useful target for improving response to chemotherapy, as these data suggest CSF1 is a key factor for recruiting TAMs which limit the efficacy of chemotherapy.

Paclitaxel was shown to increase IL-10 expression in TAMs, and anti-CSF1 reduced the expression of IL-10 in these tumours [110]. Combining paclitaxel with either an anti-CSF1 or an anti-IL10 significantly decreased tumour growth compared to tumours treated with paclitaxel alone [110]. Inhibition of IL-10 in combination with paclitaxel increased the numbers of tumour dendritic cells and granzyme B⁺ (marker of cytotoxic T cells) cells, suggesting IL-10 triggers immunosuppression in paclitaxel treated tumours. Additional studies also showed inhibition of CSF1R prevented TAMs from adopting an immunosuppressive, proangiogenic phenotype and increased survival in a murine glioma model [31].

In this context, TAMs represent a population of immune cells which respond to chemotherapy-induced tumour damage by upregulating their wound-healing properties, to promote tumour repair and regrowth (as summarised by Figure 1.5).

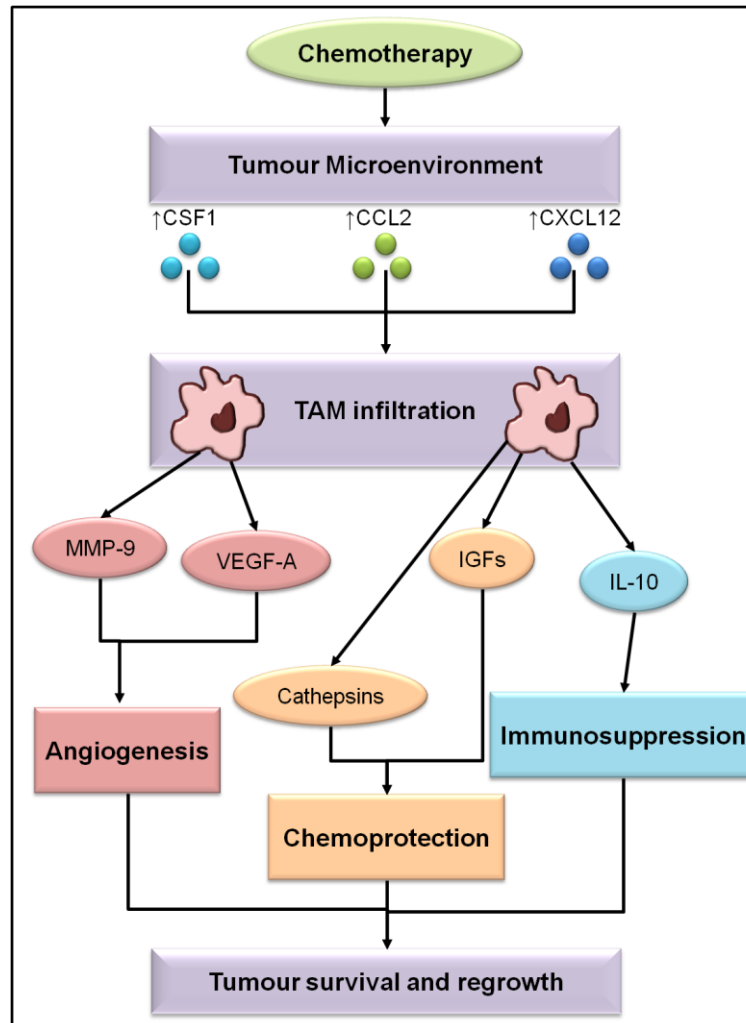


Figure 1.5 TAMs aid tumour survival and regrowth after chemotherapy

Tumours can upregulate macrophage chemoattractants CSF1, CCL2 and CXCL12 following chemotherapy which increases TAM infiltration. These TAMs can promote angiogenesis (for example via MMP-9 and VEGF-A), enhance chemoprotection (e.g. via IGF-1 and IGF-2 or cathepsins) and aid immunosuppression (e.g. via IL-10). These three mechanisms all promote tumour survival and ultimately surviving tumour cells will be able to continue to grow following therapy.

1.4 TAM targeting strategies in the treatment of cancer

Not only do TAMs modulate the response of tumours to chemotherapy [65] but they can also limit the efficacy of other cancer treatments like anti-angiogenic agents, radiotherapy and immunotherapy, demonstrating these cells are a potential target for increasing the efficacy of a number of anti-cancer therapies [65]. Research investigating new ways of inhibiting the recruitment, and/or modulating the phenotype of TAMs is now warranted (see Figure 1.6). Previous strategies that were developed to target TAMs are described below.

1.4.1 Therapies which inhibit macrophage recruitment

1.4.1.1 Targeting the CCL2-CCR2 axis

Inhibiting CCL2-CCR2 signals reduces monocyte recruitment, metastasis and increases sensitivity to doxorubicin [127], [137]. Moreover, several types of cancer have shown increased CCL2 expression in patients and in some cases, CCL2 expression correlates with poor prognosis [148]. CCL2-CCR2 signalling could be exploited to improve current therapies by increasing chemosensitivity and reducing metastasis. However, it was recently shown that halting treatment of mice with anti-CCL2 antibodies rapidly increases metastasis, as monocytes migrate into both primary tumours and the metastases and promote growth by IL-6 and VEGF-A signalling [128]. A first-in-human phase I trial tested the safety and efficacy of the human anti-CCL2 mAb, also known as carlumab (or CNTO 888) [149]. While carlumab reduced serum CCL2 initially (24 hours after treatment), 8 days later serum CCL2 levels had rebounded to pre-treatment CCL2 levels and in some cases the serum CCL2 concentration was even higher than pre-treatment concentrations [149]. Given the rapid rebound of serum CCL2, this trial suggests that serum CCL2 is not successfully suppressed with carlumab treatment. Potentially, antibodies with different

pharmacokinetic properties, that are able to sequester CCL2 in patients for longer, may be more successful at suppressing CCL2 signalling [149].

Another study showed that combining four different chemotherapy regimens (docetaxel, gemcitabine, paclitaxel and carboplatin) with carlumab was reasonably well-tolerated in patients, however total and free (not bound to carlumab) CCL2 was increased in patient sera during the course of therapy, suggesting carlumab was unable to successfully sequester CCL2 [150]. Additionally patients with metastatic castration resistant prostate cancer did not respond to carlumab, and carlumab again failed to sequester CCL2 in the serum for long periods of time [151]. These unsuccessful clinical trials, which revealed no benefit of CCL2-targeting and the pre-clinical mouse model suggesting that halting anti-CCL2 therapy can lead to accelerated metastasis and death, brings into question whether targeting CCL2 should be pursued further.

Anti-VEGFA and anti-IL6 antibodies were able to prevent rebound of metastases after anti-CCL2 therapy was halted in mice, suggesting these molecules could potentially be targeted in combination with CCL2 to improve the anti-tumoural and anti-metastatic effects [128]. Indeed, further studies investigating CCL2 signalling in metastases, have revealed roles for CCL3 and VEGFR1 and inhibiting these pathways reduced metastasis [129], [130]. These studies highlight that while CCL2 targeting may not be a good therapy, investigating pathways downstream of CCL2 signalling may reveal alternative therapeutic targets.

1.4.1.2 Inhibiting the CXCL12-CXCR4 axis

Several studies demonstrate TAMs infiltrate tumours using the CXCL12-CXCR4 axis following treatment with the vascular disrupting agent, combretastatin A4 phosphate [152], radiotherapy [153], [154] and chemotherapy [144]. AMD3100, a CXCR4 inhibitor [145], has been shown to significantly improve responses to therapy and inhibits TAM infiltration of tumours following these treatments [144], [152]–[154]. AMD3100 also acts

as an agonist of CXCR7 [155] and CXCR4 is present on cells other than macrophages, including HSCs [156], which brings into question the specificity of AMD3100 as a potential therapeutic. Indeed, one use for AMD3100 is to mobilise HSCs from the bone marrow, which can then be collected and used for stem cell transplants following intensive chemotherapy [157]–[159]. It would therefore be important to investigate any undesirable effects AMD3100 may have, due to its non-specificity, and especially due to this mobilisation of HSCs in clinical trials.

Due to the lack of specificity of AMD3100, additional CXCL12-CXCR4 disrupting drugs have been developed [160]. One such drug is LY2510924, a peptide antagonist of CXCR4 [161]. Clinical trials have shown LY2510924 induces stem cell mobilisation and is reasonably tolerated in cancer patients [162]. A phase II trial combining LY2510924 with chemotherapy (carboplatin and etoposide) was carried out in patients with extensive-disease small cell lung cancer, and while the drug combination was tolerable, LY2510924 did not improve progression free- or overall survival of patients [163]. Somewhat disappointingly, these early clinical trials indicate CXCR4 inhibition is not impacting patient survival as well as pre-clinical studies have suggested. Reasons for this could be differences between the pre-clinical models and the patients themselves and combining the CXCR4 inhibitors with different types of chemotherapy and different tumour types may still yield interesting results. Further investigations into targeting mechanisms which upregulate CXCL12 within the tumour stroma, such as hypoxic signalling pathways like HIF-1 transcription factors [164], or by targeting downstream effectors of CXCR4 signalling may also reveal novel ways to inhibit TAMs and improve chemotherapy.

1.4.1.3 Targeting CSF1 signalling

As mentioned previously, CSF1 acts as a growth factor for macrophages, and promotes their M2-polarisation within tumours [31]. Inhibiting the CSF1 signalling pathway improves the outcome of chemotherapy [108]–[110], [147], radiotherapy [165]

and anti-angiogenic therapies in murine models of cancer [166], most likely due to its effects on TAMs within the tumour microenvironment. Current clinical trials should reveal if the CSF1R inhibitor PLX3397 can improve the outcome of chemotherapy in patients. It should be noted, that PLX3397 also inhibits the stem cell receptor cKIT, so it may be important to investigate whether PLX3397 has any additional effects on stem cell survival or proliferation [109]

Inhibition of the CSF1 pathway may also affect macrophage phenotype as CSF1 increases the proangiogenic activity of monocytes *in vitro* [28], [167]. Inhibition of CSF1R (using the compound BLZ945) resulted in decreased expression of immunosuppressive genes by TAMs such as arginase-1, and the M2a-phenotype marker MRC1, as well as the pro-angiogenic molecule adrenomedullin in a murine model of glioma [31]. In this model, there was no decrease in the number of TAMs [31], which may have seemed unprecedented, as CSF1R inhibition has reduced TAM numbers in other models [108]–[110], [165], [166]. Potentially this could be because the CSF1R inhibitor was administered into mice 2.5 weeks after the original tumour was initiated [31], and macrophage recruitment can be time dependant. Moreover, BLZ945 is a more selective CSF1R inhibitor, whereas PLX3397 also inhibits c-kit, which could account for these differences in macrophage recruitment. CSF1 is also a survival factor for macrophages [168], however using glioma-conditioned media, it appeared that macrophages were protected against cell-death, despite a lack of CSF1 signalling, due to glioma cell-derived CSF2, IFN- γ and CXCL10 [31].

Interestingly CSF2, can alter macrophage phenotype, as immunofluorescent staining demonstrated mammary tumours injected with CSF2 have an increase in iNOS expressing (pro-inflammatory) TAMs and a decrease in arginase-1 expressing (immunosuppressive) TAMs [169]. Indeed, in gliomas treated with BLZ945, TAMs were less proangiogenic and immunosuppressive, which may be attributed to blockade of CSF1 M2-polarising signals, as well as an increased reliance on M1-polarising signals: IFN- γ and CSF2 [31].

Several clinical trials using PLX3397 are currently underway [170]. Tenosynovial giant cell tumours (which overexpress CSF1) were treated with PLX3397 as a single agent in patients [171]. As a single agent, PLX3397 was able to reduce tumour volume in patients on average by 61%, demonstrating PLX3397 was successful in treating these patients [171]. Some of these patients experienced adverse effects, such as periorbital oedema; despite this, most patients continued their treatment, suggesting that the drug was mostly well-tolerated [171]. PLX3397 was also used in a phase II trial as a single agent in the treatment of glioma [172]. While PLX3397 was well-tolerated, and reduced IBA1 (a macrophage marker) staining could be detected in glioma samples, demonstrating its ability to cross the blood-brain barrier, it had no effect on progression free or overall survival [172]. These data suggest that tumour type may well influence the response of tumours to CSF1R inhibitors. While CSF1R inhibition as a single agent failed to treat recurrent glioma, it was well-tolerated and potentially PLX3397 may reveal tumouricidal properties in different tumours (particularly if they overexpress CSF1), and in combination with other anti-cancer therapies.

1.4.1.4 Targeting Angiopoietin-2/Tie2 signalling

As angiopoietin-2 both recruits and activates the tumour-promoting functions of TEMs [71], [92], [99], [103], blocking this cytokine in the tumour microenvironment could possibly be seen as a way to inhibit TEMs in tumours. MEDI3617 is an anti-angiopoietin-2 antibody, which is well tolerated in patients with solid tumours, either when used as a single agent or in combination with chemotherapy (carboplatin/paclitaxel or paclitaxel alone) and the anti-angiogenic anti-VEGF drug bevacizumab [173]. These trials need to examine the effects of MEDI3617 on both the vasculature (i.e. direct effect) versus TEM number and phenotype.

On the other hand, a humanised monoclonal antibody developed to sequester angiopoietin-2 (PF-04856884) was tested in metastatic renal cell cancer patients in

combination with axitinib (inhibitor of VEGFRs, c-Kit and PDGFR), but as some patients had thromboembolic events, the trial was terminated [174]. The differences in tolerability could be due to the differences in antibody, or the combination of axitinib with anti-angiopoietin-2 therapy could have led to increased risk of thromboembolism. Clearly these toxicities must be considered when combining novel therapeutics with pre-existing drugs.

An antibody which targets both VEGF and angiopoietin-2 has been developed and elicited greater anti-tumoural effects than anti-VEGF or anti-angiopoietin-2 antibodies alone [175]. In a murine glioma model, MEDI3617 (targeting angiopoietin-2) and cediranib (targeting VEGFR) were combined and demonstrated increased tumouricidal activity [176]. Tumours treated with cediranib and MEDI3617 had a more normalised vasculature (increased pericyte coverage and reduced oedema, suggesting more functional vessels) [176]. TAMs in combination treated tumours were less pro-tumoural, and depletion of TAMs with anti-CSF1, abrogated the effects of the combination therapy, suggesting that this combination was successful due to its effects on TAMs and the vasculature [176]. In keeping with this, the bispecific antibody A2V (targeting angiopoietin-2 and VEGFA) increased survival in murine glioma models compared to antibodies targeting VEGFA alone, and was shown to skew TAMs towards an proinflammatory phenotype and reduced the percentage of MRC1⁺ M2-skewed TAMs [177]. Patients with solid tumours were shown to tolerate treatment with the antibody CVX-241 (targeting both angiopoietin-2 and VEGFA) [178]. However a more recent trial (ClinicalTrials.gov Identifier: NCT01004822) investigating the efficacy of CVX-241 in patients with advanced solid tumours was suspended due to no significant effects when testing the efficacy of the antibody alone; these issues were thought to be due to the antibody being unable to bind VEGFA for as long as predicted [179].

In summary, while therapies which target TAM recruitment have shown promise in pre-clinical mouse models, their efficacy in patients has, to date, been disappointing.

Differences between the mouse tumour models and tumours growing in patients may account for these discrepancies.

1.4.2 Therapies which modify TAM phenotype.

A common theme between the different anti-tumoural therapies, (e.g. chemo-, radio- or anti-angiogenic therapies) is that inhibiting the *recruitment* of monocytes into tumours can improve the efficacy of the treatment. However, some studies have demonstrated that altering the phenotype of TAMs can also enhance tumour response to some forms of therapy [30], [180]. As macrophages are recruited to tumours following anti-tumoural therapy these cells could potentially be a resource for killing the tumour. Therefore re-educating TAMs from an anti-inflammatory, pro-tumoural phenotype to a pro-inflammatory, tumouricidal phenotype may be more beneficial to the treatment of tumours, rather than simply blocking their recruitment.

1.4.2.1 Promoting a tumouricidal TAM phenotype

One strategy proposed for increasing the proinflammatory, tumouricidal behaviour of TAMs was the targeting of the nuclear factor- κ B (NF- κ B) signalling pathway [29]. NF- κ B activation in TAMs was inhibited as these macrophages had no functional I κ B kinase (IKK β , removed by genetic deletion or expression of a non-functional IKK β) [29]. This genetic manipulation skewed TAMs towards a proinflammatory phenotype – with an increased expression of M1-like genes such as iNOS and increased tumouricidal activity [29]. In terms of translating this strategy to patients, IKK β inhibitors have been suggested. However, ways of targeting IKK β inhibition specifically in TAMs would need to be developed. Another, more specific method would be to isolate monocytes from patients, modify them *ex vivo* to disrupt their NF- κ B signalling, and then return them intravenously to the patient – or perhaps by intratumoural injection, if that was feasible.

More recently, phosphoinositide-3 kinase γ (PI3K γ) was shown to stimulate the tumour-promoting phenotype of TAMs in some mouse models. Inhibition of PI3K γ

using the inhibitors TG-100-115 or IPI-549 resulted in decreased tumour growth [181]. Myeloid (CD11b⁺) cells isolated from PI3K γ deficient (p110 γ ^{-/-}) tumours had decreased arginase-1, IL-10 and TGF β expression, and had increases in proinflammatory gene expression such as iNOS and IL-12 [181]. TAMs isolated from p110 γ ^{-/-} tumours were also less immunosuppressive and had decreased arginase activity [181]. This study identified PI3K γ as a target within myeloid cells in tumours – as this would diminish the immunosuppressive tumour microenvironment. Clinical trials using the PI3K γ inhibitor IPI-549 are now recruiting patients to test the safety profile of this drug. Further trials will show if this promising new target has a future in the clinic [182].

DC101, an anti-VEGFR2 antibody has been used to target the tumour vasculature, and lower, ‘vascular normalising’ doses of DC101 increased pericyte coverage and vessel functionality (measured by FITC-lectin perfusion of vessels) [180]. These lower doses of DC101 also modulated the phenotype of TAMs which were located near to vessels (labelled by intravenous Hoescht dye). It reduced their expression of immunosuppressive genes e.g. CCL17, CCL22, and increased expression of proinflammatory genes such as iNOS and IL-12 α [180]. An additional study used overexpression of HRG in tumours to normalise the vasculature, which reduced tumour burden and metastasis, increased the efficacy of doxorubicin and induced a proinflammatory phenotype in TAMs, demonstrating perhaps vascular normalisation may be one strategy for re-educating TAMs [30].

These findings are supported by a more recent study in which a bispecific antibody targeting both Angiopoietin-2 and VEGF helped normalise the tumour vasculature (increased pericyte coverage and vessel diameter) and also reduced M2-skewed TAMs in tumours [177]. Anti-angiogenic drugs such as bevacizumab are clinically available, however tumours become resistant to these therapies, so they are not as effective in patients as expected [183]. Treatment with lower doses of anti-angiogenic drugs to generate vascular normalisation may be a new way to utilise these

drugs in targeting both TAMs and increasing drug delivery [184], although this may be difficult to achieve.

Elucidating the mechanism by which vascular normalisation affects macrophage phenotype could be very interesting – indeed tumour hypoxia decreases when vessels are normalised, and this may influence TAM function [184]. However, TAMs from PHD2^{+/-} haplodeficient mice (i.e. isolated from more oxygenated tumours) expressed the same levels of M2-skewed markers MRC1 and arginase-1, as those isolated from wildtype mice with more hypoxic tumours [185]. Only genes regulated by hypoxia i.e. proangiogenic factors such *vegfa* were downregulated in PHD2^{+/-} TAMs [185]. Therefore, it may be that endothelial cells influence TAM phenotype rather than hypoxia. Indeed, *in vitro*, macrophages co-cultured with endothelial cells showed an upregulation of the M2a marker MRC1 [186]. Therefore the impact of vascular normalisation on TAM phenotype may be due to the effects on the vasculature and not tumour hypoxia. These novel strategies to modulate TAM phenotype are promising, and require further investigation. Given the emerging evidence that PV TAMs are tumour-promoting and that vascular normalisation appears to re-educate TAMs to an anti-tumoural phenotype, research characterising the role of the vasculature after therapy should also be considered [141].

1.5 Summary

TAMs are associated with poor prognosis in many different tumour types [77]. They can promote tumour progression by influencing angiogenesis, immunosuppression and metastasis [66], [141]. Moreover, TAMs can limit the effects of chemotherapy, making them an ideal target for new therapies which could improve the efficacy of current frontline treatments [65]. Current TAM-targeting drugs work by either inhibiting their recruitment or by re-educating them to be a more tumouricidal. However, when tested in clinical trials, so far, TAM-targeting drugs are yet to show the promising results as seen in pre-clinical models, demonstrating the need to further understand mechanisms of TAM recruitment and phenotype [170]. It is known that chemotherapy alters the tumour microenvironment, and these changes could potentially lead to recruitment or skewing of TAMs towards to a tumour-promoting phenotype. Further characterisation of the tumour microenvironment and tumour vasculature and how it changes following chemotherapy is needed to identify novel mechanisms of TAM recruitment and/or education.

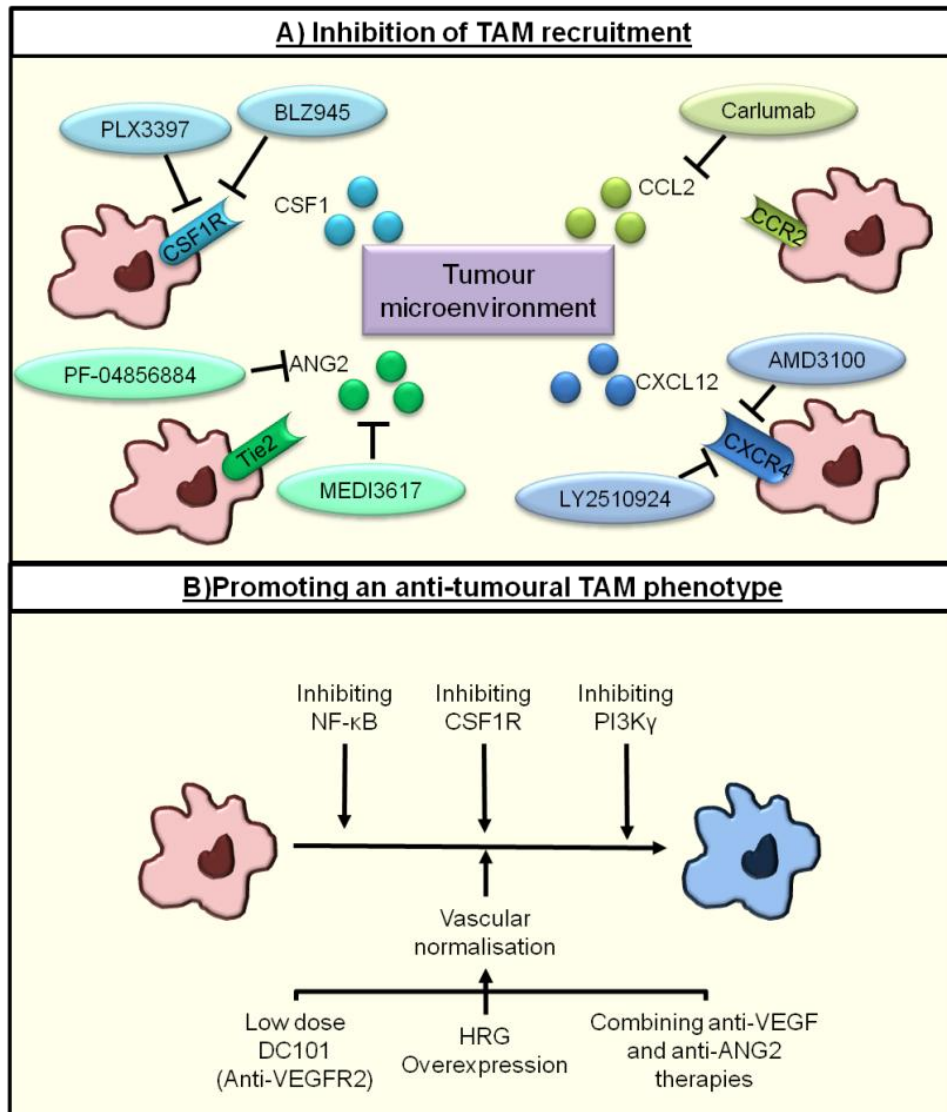


Figure 1.6 Strategies for targeting TAMs.

A) A summary of drugs which may be used to target TAM recruitment – in particular CSF1-CSF1R, CCL2-CCR2, CXCL12-CXCR4 and ANG2-TIE2 signalling have been shown to affect TAM recruitment into tumours.

B) Re-educating protumoural TAMs (red) to be antitumoural (blue) could improve response of tumours to current frontline therapies. Strategies include inhibition of macrophage signalling pathways such as CSF1, NF-κB and PI3Kγ. Moreover vascular normalisation by methods including low dose anti-VEGFR2, overexpression of HRG and combining anti-VEGF and anti-angiopoietin-2 (ANG2) therapies has also skewed TAMs to a tumouricidal phenotype.

1.6 Hypothesis to be tested

I, therefore, hypothesised that chemotherapy induces changes within the tumour microenvironment, which ultimately stimulate TAMs to adopt a tumour-promoting phenotype. In particular, endothelial cells may influence PV TAMs to take on an M2-skewed, wound-healing activation state.

1.7 Project aims

Therefore the aims of this thesis were as follows:

- 1) Characterise the location of TAMs within orthotopic MMTV-PyMT (TS1) implant tumours following their exposure *in vivo* to the chemotherapeutic agent, doxorubicin.
- 2) Characterise the relationship between TAMs and the tumour vasculature in doxorubicin-treated tumours.
- 3) Isolate endothelial cells from doxorubicin-treated tumours and profile gene expression to understand how endothelial cells might stimulate TAMs to drive tumour relapse and repair.

Chapter 2

Materials and Methods

2.1 Materials

2.1.1 List of reagents

Reagent	Supplier
5-Bromo-2'-deoxyuridine (BrdU)	Sigma Aldrich
Absolute Ethanol	Thermo Fisher Scientific
Acetone	Thermo Fisher Scientific
BD FACS Lysing Solution	BD Biosciences
Bovine serum albumin solution, 35% in DPBS	Sigma Aldrich
Butanol	Sigma Aldrich
CapSure Macro LCM caps	Thermo Fischer Scientific
Collagenase type IV from <i>Clostridium histolyticum</i>	Sigma Aldrich
4',6-Diamidino-2-Phenylindole, Dihydrochloride (DAPI)	Invitrogen
Dimethyl Sulfoxide (DMSO)	Sigma Aldrich
Dispase II	Gibco
Doxorubicin Hydrochloride	Sigma Aldrich
DPX Mounting medium	Sigma Aldrich
Dulbecco's Modified Eagle's Medium (DMEM) Ultraglutamine, 4.5g/L glucose	Lonza
Dulbecco's Phosphate Buffered Saline (DPBS)	Lonza
Dynabeads Sheep anti-Rat IgG	Invitrogen
Eosin Y	Thermo Fisher Scientific
FcR blocking reagent, mouse	Miltenyi Biotec
Fluorescein labelled Lycopersicon Esculentum (tomato) lectin (FITC-lectin)	Vector Laboratories
Foetal calf serum (FCS)	Gibco
Growth Factor Reduced (GFR) Matrigel	Corning
Haematoxylin Solution Gill No. 2	Sigma Aldrich
Hank's Balanced Salt Solution (HBSS)	Gibco
Iscove's Modified Dulbecco's Medium (IMDM)	Lonza
L-glutamine	Lonza
Normal Goat Serum	Vector Laboratories
Nuclease free water	Qiagen
Cryo-M Bed Optimal Cutting Temperature Compound (OCT)	VWR International
Paraformaldehyde	Sigma Aldrich
Penicillin-Streptomycin	Lonza

Pimonidazole	Hypoxyprobe
PrecisionPlus qPCR mastermix with SYBR green and ROX	Primer Design
ProLong Gold Antifade mountant	Invitrogen
Recombinant mouse CSF1	Biolegend
Roswell Park Memorial Institute (RPMI) medium	Lonza
Sucrose	Sigma Aldrich
Super PAP pen	Thermo Fisher Scientific
Tri-sodium citrate	BDH Laboratories Suppliers
Trypsin-EDTA	Lonza
TWEEN 20	Thermo Fisher Scientific
Xylene	Thermo Fisher Scientific
Zombie NIR Fixable Viability kit	Biolegend
Zombie UV Fixable Viability kit	Biolegend

2.1.2 List of materials

Material	Supplier
Tissue culture flasks (Nunc EasYFlask) 25cm ² ; 75cm ² ; 125cm ²	Thermo Fisher Scientific
Superfrost Plus Microscope Slides	Thermo Fisher Scientific
Coverslips	Scientific Laboratory Supplies
Fisherbrand 384-well skirted PCR plate	Thermo Fisher Scientific

2.1.3 List of monoclonal (m) and polyclonal (p) antibodies

Antibody (clone or cat no. if polyclonal)	Supplier
Goat (p) Anti-Rabbit IgG AlexaFluor555	Invitrogen
Goat (p) Anti-Rat IgG AlexaFluor488	Invitrogen
Goat (p) Anti-Rat IgG AlexaFluor555	Invitrogen
Goat (p) Anti-Rat IgG AlexaFluor647	Invitrogen
Mouse (m) Anti-pimonidazole Dylight549 (4.3.11.3)	Hypoxyprobe
Purified Rat (m) Anti-Mouse (MEC13.3)	BD Bioscience
Purified Rat (m) Anti-Mouse Gr-1 (RB6-8C5)	Biolegend
Purified Rat (m) Anti-PNAd (MECA-79)	Cardiff University, Prof Gallimore

Rabbit (p) Anti- α -smooth muscle actin (ab5694)	Abcam
Rabbit (p) Anti-angiopoietin-2 (ab8452)	Abcam
Rabbit (p) Anti-Collagen IV (ab6586)	Abcam
Rabbit (p) Anti-Mannose Receptor (ab64693)	Abcam
Rat (m) Anti-CD11b AlexaFluor488 (M1/70)	Biolegend
Rat (m) Anti-CD11b Brilliant Violet 421 (M1/70)	Biolegend
Rat (m) Anti-FOXP3 FITC (FJK-16s)	eBioscience
Rat (m) Anti-Mouse CD3 AlexaFluor647 (17A2)	Biolegend
Rat (m) Anti-Mouse CD31 AlexaFluor488 (MEC13.3)	Biolegend
Rat (m) Anti-Mouse CD31 AlexaFluor647 (MEC13.3)	Biolegend
Rat (m) Anti-Mouse CD31 PE (MEC13.3)	Biolegend
Rat (m) Anti-Mouse CD4 AlexaFluor488 (GK1.5)	Biolegend
Rat (m) Anti-Mouse CD4 PE (GK1.5)	Biolegend
Rat (m) Anti-Mouse CD8 α PE (53-6.7)	Biolegend
Rat (m) Anti-Mouse CXCR4 PE (2B11)	eBioscience
Rat (m) Anti-Mouse F4/80 AlexaFluor488 (Cl:A3-1)	Biorad
Rat (m) Anti-Mouse Ly-6C APC (HK1.4)	Biolegend
Rat (m) Anti-Mouse Ly-6G PE (1A8)	Biolegend
Rat (m) Anti-Mouse Ly-6G PerCP/Cy5.5 (1A8)	Biolegend
Rat (m) Anti-Mouse MRC1 APC (C068C2)	Biolegend
Rat (m) Anti-Mouse MRC1 Brilliant Violet 421 (C068C2)	Biolegend
Rat (m) Anti-Mouse MRC1 PE (C068C2)	Biolegend

2.1.4 List of commercial kits

Kit	Supplier
Agilent RNA 6000 Nano kit	Agilent Technologies
Agilent RNA 6000 Pico kit	Agilent Technologies
DAB Peroxidase (HRP) substrate kit	Vector Laboratories
PicoPure RNA isolation kit	Thermo Fisher Scientific
QuantiTect Reverse Transcription Kit	Qiagen
RNeasy Mini kit	Qiagen
RNeasy Mini Plus kit	Qiagen
Vectastain ABC HRP kit (Peroxidase, Rabbit IgG)	Vector Laboratories

2.1.5 List of cell lines and animals

Cell line or Animal	Supplier
TS1 cell line (in vivo passaged MMTV-PyMT derived tumour cells)	Memorial Sloan Kettering Cancer Research Centre, Prof Johanna Joyce
FvB/N female mice	Envigo

2.1.6 List of solutions

Solution	Instructions
FACS buffer	DPBS with 0.5% FCS
Sodium citrate solution	DPBS with 0.76% sodium citrate + 1% FCS
14% Sucrose solution	14g sucrose in 100mL DPBS
30% Sucrose solution	30g sucrose in 100mL DPBS
4% Paraformaldehyde	4g paraformaldehyde in 100mL DPBS
PBST	250µL TWEEN 20 in 50mL DPBS
DAPI staining solution	50µg/mL DAPI in PBST
TS1 cell line growth medium	DMEM Ultraglutamine with 10% FCS, 0.5 units/mL penicillin and 0.5 units/mL streptomycin
Tumour dissociation medium	IMDM with 0.2mg/mL collagenase type IV and 2mg/mL dispase II
Bone marrow derived macrophage medium	RPMI with 10% FCS, 0.5 units/mL penicillin, 0.5 units/mL streptomycin, 2mM L-glutamine and 50ng/mL recombinant murine CSF1
Water saturated butanol	10mL nuclease free water vigorously mixed with 10mL butanol until separation into two layers: the top layer is the water saturated butanol

2.1.7 List of primers

All primers were either previously published or designed using PrimerBlast and MFEprimer2.0. Primers were validated using melt-curve analysis and efficiency was assessed using a standard curve. Primers were obtained from Invitrogen, dissolved in nuclease free water at a stock concentration of 100µM.

Gene	Sequence 5'-3'
Acta2	FWD: AGCCATCTTTCATTGGGATGGAG REV: CATGGTGGTAACCCCTGACA
Actb	FWD: AGAGGGAAATCGTGCGTGAC REV: CAATAGTGATGACCTGGCCGT
Adgre1	FWD: CCACTTCCAAGATGGGTTAACAT REV: AAACAAAACCTGCCATCAACTCA
Angpt2	FWD: GCATGTGGTCCTTCCAACCTT REV: GATCCTCAGCCACAACCTTC
Ccl12	FWD: GCCTCCTGCTCATAGCTACC REV: GGGTCAGCACAGATCTCCTT
Ccl2	FWD: CACTCACCTGCTGCTACTCATTAC REV: GGATTCACAGAGAGGGAAAAATGG
Ccl3	FWD: CGGAAGATTCCACGCCAATTC REV: GGTGAGGAACGTGTCCTGAAG
Ccl4	FWD: CCCACTTCTGCTGTTTCTC REV: GAGCAAGGACGCTTCTCAGT
Ccl5	FWD: GTGCCACGTCAAGGAGTAT REV: AGCAAGCAATGACAGGGAAG
Ccl7	FWD: GACAAAGAAGGGCATGGAAG REV: CATTCTTAGGCGTGACCAT
Ccl8	FWD: TCTACGCAGTGCTTCTTTGC REV: CCACTTCTGTGTGGGGTCTA
Ccl8	FWD: TCTACGCAGTGCTTCTTTGC REV: CCACTTCTGTGTGGGGCTTA
Ccl9	FWD: CCAGATCACACATGCAACAG REV: CTATAAAAATAAACACTTAGAGCCA
Csf1	FWD: CCCAACGAGTCAGCAACTCA REV: AATGCCCCAAGAGTGGCTTT
Csf2	FWD: GAGGATGTGGCTGCAGAATTT REV: CTACCTCTTCATTCAACGTGACAG
Cx3cl1	FWD: ACTCCTTGATTGGTGGGAAGC REV: CAAAATGGCACAGACATTGG
Cxcl12	FWD: CCGCGCTCTGCATCAGT REV: GCGATGTGGCTCTCGAAGA
Eng	FWD: TGTCTGCCCCTCTGTAAGTGG REV: GGGGCCACGTGTGTGAGAA

<i>Epcam</i>	FWD: TTGCTCCAAACTGGCGTCTAA REV: GTTGTCTGGATCGCCCCTT
<i>FasL</i>	FWD: CTGGTGGCTCTGGTTGGAAT REV: GGTTGGCTCACGGAGTTCTG
<i>Fgf1</i>	FWD: AAAGTGCGGGCGAAGTGTAT REV: CTCATTTGGTGTCTGCGAGC
<i>Fn1</i>	FWD: ACGGTTTCCCATTACGCCAT REV: GGCACCATTTAGATGAATCGCA
<i>Icam1</i>	FWD: AGCCTCCGGACTTTTCGATCT REV: TGTTTGTGCTCTCCTGGGTC
<i>Icam2</i>	FWD: TTCACTCCCCGACCTGTAGC REV: CCAGACCCTGGGCTGTAGAAC
<i>Ifng</i>	FWD: TCAAGTGGCATAGATGTGGAAGAA REV: TGGCTCTGCAGGATTTTCATG
<i>Il10</i>	FWD: GGCCTGTGCATCGATTTCTC REV: ATGGCCTTGTAGACACCTTGG
<i>Il1a</i>	FWD: CGCTTGAGTCGGCAAAGAAAT REV: TGGCAGAACTGTAGTCTTCGT
<i>Il1b</i>	FWD: GCCACCTTTTGACAGTGATGAG REV: AGCTTCTCCACAGCCACAAT
<i>Il6</i>	FWD: TCCAGTTGCCTTCTTGGGAC REV: TGCCATTGCACAACTCTTTTCTC
<i>Itgam</i>	FWD: TCGCTACGTAATTGGGGTGG REV: AGCTGGCTTAGATGCGATGG
<i>Pecam1</i>	FWD: GCCAACAGCCATTACGGTTA REV: GTCGACCTTCCGGATCTCAC
<i>Plgf</i>	FWD: CCCTGTCTGCTGGGAACAA REV: CTGCGACCCCACTTC
<i>Sele</i>	FWD: ACGTCCCAGGAAAGATGAAC REV: GACTGGGGCTTACAGGTAG
<i>Spp1</i>	FWD: CTTTCACTCCAATCGTCCCTA REV: GCTCTCTTTGGAATGCTCAAG
<i>Thbs1</i>	FWD: GCAAAGACGTCGATGAGTGC REV: CGGTTTGCACACCTGTTTGT
<i>Tnf</i>	FWD: CCTTCACAGAGCAATGACTC REV: GTCTACTCCCAGGTTCTCTTC
<i>Vcam1</i>	FWD: TTTATGTCAACGTTGCCCCC REV: GAGGCTGCAGTTCCCCATTA
<i>Vegfa</i>	FWD: CAGGCTGCTGTAACGATGAA REV: AATGCTTTCTCCGCTCTGAA

2.1.8 List of instrumentation

Instrument	Supplier
Agilent 2100 Bioanalyzer	Agilent Technologies
Aperio ScanScope CS	Leica Biosystems
Applied Biosystems 7900 Real-time PCR machine	Applied Biosystems
DynaMag-15 Magnet	Thermo Fisher Scientific
Dyna-Mag-2 Magnet	Thermo Fisher Scientific
FACS Aria	BD Bioscience
LSR II Flow cytometer	BD Bioscience
NanoDrop 2000	Thermo Fisher Scientific
Nikon A1 Confocal	Nikon
Zeiss LSM510 NLO Inverted confocal microscope	Zeiss

2.1.9 List of software

Software	Supplier
Primer Blast	National Institute of Health, USA
MFEPrimer-2.0	http://biocompute.bmi.ac.cn/CZlab/MFEprimer-2.0/ [187]
Fiji	https://imagej.net/Fiji [188]
Flow Jo	TreeStar Inc
Graph Pad Prism 7	Graph Pad Inc
BD FACSDiva	BD Bioscience

2.2 Methods

2.2.1 Maintenance of cell lines

TS1-IVP1 PyMT (referred to as TS1) cells were obtained from Professor Joyce, Memorial Sloan Kettering Cancer Research Centre [139]. TS1 cells were derived from primary tumours of the MMTV-PyMT mice, then re-implanted and grown *in vivo* in order to increase the reliability of the cell line when transplanting them [139]. These cells were cultured in DMEM Ultraglutamine with 10% FCS, penicillin (0.5 units/mL) and streptomycin (0.5 units/mL). Cells were incubated at 37°C with 5% CO₂ and passaged when approximately 80% confluent. To passage, cells were washed twice with Dulbecco's Phosphate Buffered Saline (DPBS) and then incubated with trypsin-EDTA (200mg/ml EDTA; 170,000 units trypsin) until they no longer adhered to the T75 flask. The trypsin-EDTA was then neutralised with media, the cells washed off the flask and into a centrifuge tube before centrifuging at 1400rcf for 5 minutes. The cell pellet was then re-suspended in 5mL DPBS and an aliquot of the cell suspension was counted using a haemocytometer. Using the grid of the haemocytometer, cells within a grid (4 squares made of 16 squares each) were counted. This was divided by 4 and multiplied by 10,000 to calculate number of cells/mL. If the cell suspension aliquot had been diluted e.g. 1 in 100, this number was multiplied by the dilution factor (e.g. x100) to calculate the number of cells/mL in the undiluted cell suspension. Cells were then seeded at the appropriate density (usually 3x10⁵ cells per mL) in a T75 flask with fresh media before incubating at 37°C with 5% CO₂, with regular media changes.

Cells were cryopreserved using cryobuffer consisting of 90% FCS and 10% DMSO. In order to cryopreserve the cells, they were trypsinised as described above, and following centrifugation were resuspended in cryobuffer at a density of 3x10⁶ cells/mL. They were then slowly frozen at -80°C using a 'Mr Frosty' before transferring to the liquid nitrogen store within a week.

2.2.2 Isolation of BMDMs

FvB/N female mice were obtained from Envigo and housed and cared for according to the University of Sheffield code of ethics and Home Office regulations. In order to isolate the BMDMs, 8 week old mice were first culled using cervical dislocation, and then the bones were dissected from these mice and placed in 70% ethanol to disinfect. Inside a laminar flow hood, the bones were cut to reveal the marrow. HSCs were then collected by flushing the bone marrow into a 50mL Falcon tube with 10mL 2% FCS in DPBS using a syringe with a 25 gauge needle. The cells were then centrifuged at 500 x g for 10 minutes before resuspending in 1mL DPBS and counting cells with a haemocytometer. Cells were then resuspended in the appropriate amount of RPMI media (to yield a density of 8×10^5 cells/10mL) containing 10% FCS, penicillin (0.5 units/mL) and streptomycin (0.5 units/mL), 2mM L-glutamine and recombinant murine CSF1 (50ng/mL). Cells were then incubated at 37°C with 5% CO₂. Every 3 days, media was replaced with fresh media and macrophages were used between 7-14 days after isolation. This incubation of HSCs with CSF1 allowed macrophages to differentiate from precursors [189]. Cells which differentiated into macrophages adhered to the plastic they were cultured on. To remove the macrophages from the plastic for use in further experiments, they were first washed in DPBS, and then incubated with trypsin-EDTA (200mg/ml EDTA; 170,000 units trypsin) for 30 minutes, as macrophages adhere strongly to plastic, and scraping macrophages from plastic drastically reduces their viability. The trypsin was neutralised with FCS once cells had detached.

2.2.3 Murine model of breast cancer

FvB/N female mice were obtained from Envigo and were housed in the University of Sheffield Biological Services Unit and cared for according to the University of Sheffield code of ethics and Home Office regulations. At 8 weeks old, these mice received a mammary fat pad injection of 1×10^6 TS1 cells using the following protocol. Mice were

anaesthetised using the inhalant isoflurane (IsoFlo). They were then shaved and the skin was disinfected with Hibiscrub. Following this a 1cm midline incision was made with sterile surgical scissors, and the skin peeled back to reveal the 4th mammary fat pad located in the inguinal region of the mouse. 1×10^6 TS1 cells (which were collected from flasks during their exponential growth phase) in a 20 μ L 1:1 mixture of DPBS and growth factor reduced (GFR) Matrigel were injected into the 4th mammary fat pad. Following this, the incision was closed using surgical staples. The staples were removed 1 week after surgery to allow the wound sufficient time to heal and the body weight of the mice was carefully monitored throughout the time course of the experiment, weighing mice a minimum of 3 times a week.

Murine tumour volume was measured every other day using callipers and calculated using the formula: length x width²/2 [99]. Mice received 1 intraperitoneal injection of doxorubicin at 8mg/kg (DOX) or vehicle (DPBS) when tumours reached approximately 500mm³ in volume. 48 hours after this injection, mice received 1 intraperitoneal injection of BrdU (100mg/kg – to assess cell proliferation) and pimonidazole (PIMO, 60mg/kg – to assess hypoxia) and were culled 2 hours later by cervical dislocation.

2.2.4 Dissection of FvB/n mice and preparation of samples

Mice, as described in 2.2.3, were culled by cervical dislocation. Confirmation of death was carried out by exsanguination. Blood was collected by injecting 10mL of 0.76% sodium citrate solution with 1% FCS into the left ventricle of the heart to prevent blood clots. Blood flowed out of an incision made in the right atrium, and was collected using a syringe. Approximately 5mL of blood diluted with sodium citrate solution was collected per mouse in this manner.

Subsequently, the tumours were dissected from the mice, and then divided into three parts. One part of the tumour was first dissected into small chunks and then placed in cryobuffer (90% FCS with 10% DMSO) and frozen at -80°C, before

transferring these into liquid nitrogen stores 24 hours later, to be stored before use in fluorescence activated cell sorting (FACS) experiments (2.2.12) or magnetic isolation of tumour associated endothelial cells (2.2.14).

Some tumours parts were snap frozen immediately in OCT. The other tumour parts were placed in 4% paraformaldehyde (PFA) along with the lungs, liver and spleen of the mice for 2 hours at room temperature. 2 hours later, the organs and tumours were washed in DPBS and then placed in a 14% sucrose solution overnight. They were then left in 30% sucrose solution for at least a week before mounting organs into disposable mounts with OCT and freezing them. Tumours were prepared in this way to maximise the possible antibodies which could be used on these samples – some antibodies (the majority) work best with snap frozen tissue. Others work better on PFA-fixed frozen samples and PFA-fixing tumours also helps preserve tissue architecture. Samples were not embedded in paraffin as this drastically alters the antigens and antigen retrieval would have been required for antibodies to work. The majority of previously optimised antibody stains within the research group worked best with snap-frozen tissue.

14µM thick frozen sections were cut using the cryostat and collected onto Superfrost Plus slides and stored at -80°C prior to use in immunofluorescent staining.

2.2.5 Dissociation of TS1 tumours for isolating cell populations

Tumour chunks (see 2.2.4) were thawed and washed 3 times with DPBS prior to incubation with 5mL tumour dissociation media consisting of 0.2mg/mL collagenase and 2mg/mL dispase II in Iscove's Modified Dulbecco's Medium (IMDM). Tumour chunks were incubated at 37°C, while rotating in tumour dissociation media for 30 minutes. The enzymes within the media were then neutralised with 10% FCS, prior to filtering the dissociated tumour using a 40µM filter. Any larger tumour chunks were crushed against the filter to collect the remaining cells. The cell suspension was then centrifuged at 4500 rpm for 5 minutes, and the cell pellet was washed 3 times in 500µL

DPBS before use in isolating cell populations by FACS (see 2.2.12) or magnetic isolation (see 2.2.14)

2.2.6 Preparation of blood from tumour bearing mice for flow cytometry

Blood was collected from mice, as described in 2.2.4, and then pelleted by centrifugation at 500 x g for 5 minutes. The supernatant was discarded and the cell pellet was then resuspended in 200µL 0.76% sodium citrate solution with 1% FCS, to prevent clotting of blood while staining samples. The samples were then blocked by adding 1% Bovine Serum Albumin (BSA, 5.7µL to 200µL) and 5% Normal Goat Serum (10µL to 200µL) to samples for 30 minutes while rocking on ice. Samples were then incubated with the primary antibodies (as specified, in a total volume of 200µL, as described in Chapter 4) and Zombie UV viability dye (1µL in 200µL) while rocking on ice and kept in the dark for 40 minutes. Cells were then pelleted in a microcentrifuge at 4500rpm for 5 minutes and washed by resuspending in 500µL FACS buffer (50mL DPBS with 25µL FCS). Cells were centrifuged again at 4500rpm for 5 minutes, before resuspending in 500µL 1X BD FACS Lysing solution (diluted in dH₂O from a 10X stock) to lyse erythrocytes. Samples were incubated for 5 minutes on ice with 1 X BD FACS Lysing solution, before centrifuging at 4500rpm for 5 minutes. Cells were then washed with 500µL FACS buffer and centrifuged at 4500rpm for 5 minutes. Finally, samples were resuspended in 500µL FACS buffer before FACS analysis using the BD LSR II flow cytometer. The gating strategy for the FACS analysis of murine peripheral blood is detailed in Chapter 4.

2.2.7 FlowJo analysis of FACS data

FACS files were analysed using FlowJo Software. As multiple different markers were used (a total of 7 different fluorophores for peripheral blood analysis), fluorescent minus one (FMO) controls were imperative in the analysis of these samples, in order to

determine if fluorescence was due to fluorescent spectral overlap (i.e. false positive signals) or due to actual antibody binding.

Some fluorophores emit fluorescence which will bleed into the detection of others e.g. AlexaFluor488 emission bleeds into the PE detector, which means any cells which are positive for AlexaFluor488 can appear to have PE fluorescence. FMO controls contain every antibody, except one, and allow the user to determine background fluorescence from all the other fluorophores, before considering the impact of their antibody of interest. FMO controls were used to compensate samples i.e. determine spectral overlap, and minimise this by allowing the software to assign parts of a fluorescent signal to the appropriate fluorophore e.g. in the case in of AlexaFluor488 and PE, approximately 20% of the PE signal may be attributed to spectral overlap from AlexaFluor488 (although this can vary and should be determined for each experiment using the appropriate FMO controls).

FMO controls, given their ability to detect background which occurs due to the specific binding of multiple fluorophores, are favoured by flow cytometry users [190]. They were therefore used to set the gating strategy in these flow cytometry experiments as multiple fluorophores were used in these experiments, some of which had spectral overlap. The details of the different gating strategies and FMO controls are in the relevant chapters.

2.2.8 Histological analysis of tumours

Haematoxylin and Eosin staining

Tumours which were immersion fixed in PFA prior to freezing, were sectioned using the cryostat (14µm thick sections) and then air dried at 37°C for 30 minutes, to allow the section to attach firmly to the slide. PFA fixed tumours were used as these tumours had better preservation of their architecture compared to those which were snap frozen. Sections were then placed in tap water for 5 minutes to rehydrate the sample. They were then placed in Gill's Haematoxylin solution No.2 for 2 minutes and then rinsed in

tap water until the water was clear. Slides were then left in tap water for an extra minute, to allow the haematoxylin stain to become blue before placing slides in 70% ethanol for 3 minutes then 90% ethanol for a further 2 minutes. Following this slides were placed in eosin (2g eosin dissolved in 400mL 95% ethanol) before bathing slides in 3 baths of 100% ethanol for 5 minutes per bath. Slides were then cleared twice in xylene for 5 minutes and mounted using DPX mounting medium. Slides were scanned using the Aperio ScanScope CS with a 40x objective lens.

2.2.9 Immunofluorescent staining of tumours

Snap frozen tumour sections were fixed for 10 minutes in acetone. They were then rehydrated with PBST for 1 minute. Following this, all incubations were carried out at room temperature, in a dark humidified chamber, to prevent evaporation of liquid from the samples and to prevent fluorescent antibodies from reacting with light. Super PAP barrier pen was used to surround the tissue and the tissue was then blocked with a blocking solution, containing 1% BSA, 5% Goat serum and 10% Murine FcR blocking solution made in PBST, for 30 minutes at room temperature.

Slides were incubated with primary or conjugated antibodies, at concentrations as specified in Table 2.1 for 1 hour, and then washed three times in PBST for 5 minutes, to remove excess antibody. They were then incubated with the appropriate secondary antibodies, diluted in PBST with 1% normal goat serum, for 40 minutes. Slides were then washed three times in PBST for 5 minutes and then incubated with a 50ng/mL DAPI solution for 2 minutes before washing another three times in PBST. Finally, 1 drop of ProLong Gold Antifade mountant was added to each slide before adding coverslips. Slides were then kept in the dark for a maximum of 2 days until imaging using the Nikon A1 confocal microscope or in some cases the Zeiss LSM510 NLO Inverted confocal microscope.

It is important to note that where unconjugated rat antibodies were used alongside conjugated rat antibodies, the blocking solution did not contain murine FcR

block (a rat anti-mouse antibody), as the secondary antibody would also detect the murine FcR block. In this case following incubation with the unconjugated rat primary, slides were washed and incubated with the appropriate secondary antibody. Slides were then washed three times with PBST for 5 minutes before incubating with a Rat IgG blocking solution of 0.5mg/mL, which was used to bind to any unsaturated sites of the primary antibody. Slides were then washed and incubated with conjugated primary antibodies. Finally, slides were washed again, then stained with DAPI and mounted as described above.

2.2.10 Confocal microscopy

Tumour sections were stained as described in 2.2.9. Using the 20x objective lens, random fields of view (FOV) were selected from the tumour. At least 5 FOV were analysed per tumour. Depending on microscope availability, either the Nikon A1 confocal microscope, or the Zeiss LSM510-Inverted confocal microscope was used for imaging – importantly, images taken for one set of analyses were always taken on the same microscope to avoid variability which may have arose from using the different microscopes.

2.2.11 Analysis of immunofluorescent images

Image analysis was carried out using Fiji (Fiji Is Just ImageJ), accessed via <http://fiji.sc/Downloads>, as previously published [188]. The number of nuclei per FOV needed to be assessed, so cell counts could be normalised to the total number of cells in the FOV. Two different regions of the TS1 tumour sections could be identified on the basis of their nuclear density and morphology: the stroma and the tumour cell islands. Tumour cell islands had an increased nuclear density and a more uniform appearance compared to the stroma. For this reason, two different methods were used for counting the nuclei of the different regions.

Antibody	Fluorophore	Clone	Conc (µg/mL)
Goat (p) Anti-Rabbit IgG	AlexaFluor555		10
Goat (p) Anti-Rat IgG	AlexaFluor647		10
Goat (p) Anti-Rat IgG	AlexaFluor488		10
Goat (p) Anti-Rat IgG	AlexaFluor555		4
Mouse (m) Anti-pimonidazole	Dylight549	4.3.11.3	5
Purified Rat (m) Anti-Mouse Gr-1	unconjugated	RB6-8C5	1
Rabbit (p) Anti- α-smooth muscle actin	unconjugated	ab5694	1
Rabbit (p) Anti-Mannose Receptor	unconjugated	ab64693	2.5
Rat (m) Anti-FOXP3	FITC	FJK-16s	5
Rat (m) Anti-Mouse CD3	AlexaFluor647	17A2	5
Rat (m) Anti-Mouse CD31	AlexaFluor647	MEC13.3	5
Rat (m) Anti-Mouse CD31	AlexaFluor488	MEC13.3	5
Rat (m) Anti-Mouse CD31	PE	MEC13.3	2
Rat (m) Anti-Mouse CD4	AlexaFluor488	GK1.5	5
Rat (m) Anti-Mouse CD4	PE	GK1.5	2
Rat (m) Anti-Mouse CD8α	PE	53-6.7	2
Rat (m) Anti-Mouse F4/80	AlexaFluor488	Cl:A3-1	2
Rat (m) Anti-Mouse Ly-6G	PE	1A8	4
Rat (m) Anti-Mouse MRC1	APC	C068C2	2
Rat (m) Anti-Mouse MRC1	PE	C068C2	2
Rat (m) Anti-PNAd	unconjugated	MECA-79	~10

Table 2.1 Concentrations of antibodies used in immunofluorescent analyses

(m) indicates monoclonal antibody; **(p)** indicates polyclonal antibody. ~ indicates approximate concentration of antibody used, as the antibody was isolated from ascites.

Semi-automatic nuclear counting for tumour cell islands

The Image-based Tool for Counting Nuclei (ITCN) cell counter plug-in [191] was installed to Fiji, and was used to automate nuclear counts as follows. Images were first split into the respective colour channels to produce an image of the DAPI (nuclei staining) channel only. This image was used to outline the tumour cell island region of interest. The ITCN automated counter works by setting a minimum distance between

cell nuclei for cell counts. False positive events could be seen in blank areas, as the minimum distance set would randomly cause events to be 'detected'. These events could be identified on the image as red dots which were not associated with a nucleus (see Figure 2.1A). Manually, false positive events were counted (orange triangles indicating red dots not on a nucleus, Figure 2.1A) and then subtracted from the total nuclei number. This gave the final cell count per area.

To ensure that this method was accurate a correlation analysis was performed, analysing 10 images to see how the semi-automatic method worked in comparison with manually counting each nucleus (clicking on one nucleus at a time with a mouse). Manually counting each nucleus took several hours per image whereas the semi-automatic counting method only took 10 minutes per image. There was a significant ($p < 0.0001$) positive correlation, (Pearson's correlation co-efficient $r = 0.9621$) between manual and the semi-automatic counts, meaning this method was then used for all future tumour cell island cell counts.

Automatic nuclear counting for stroma

As the ITCN counter worked on the principle of a uniform distance between cells, like that in the tumour cell island, the counter did not work in the stroma, where the distance between cells was not as consistent. Therefore the "Analyse particles" tool, which does not rely on setting a minimum distance between cells, but does rely on accurately setting a threshold for the image, was used to count cell nuclei (see Figure 2.1B). The processing tool "Make Binary" applied a simple threshold to the image and then "Watershed" was used to ensure any large cell clumps were broken into individual cell outlines. The binary and watershed processing tools were used for each image, as that made the analysis consistent. Following this, the "Analyse Particles" tool was used to count the nuclei in the stroma. This method was validated by comparing the automated cell counts with manual cell counts for 10 different images and there was a

significant ($p < 0.0001$) positive correlation (Pearson's correlation co-efficient $r = 0.9623$) between the two. This method was then used for all future nuclei counts in the stroma.

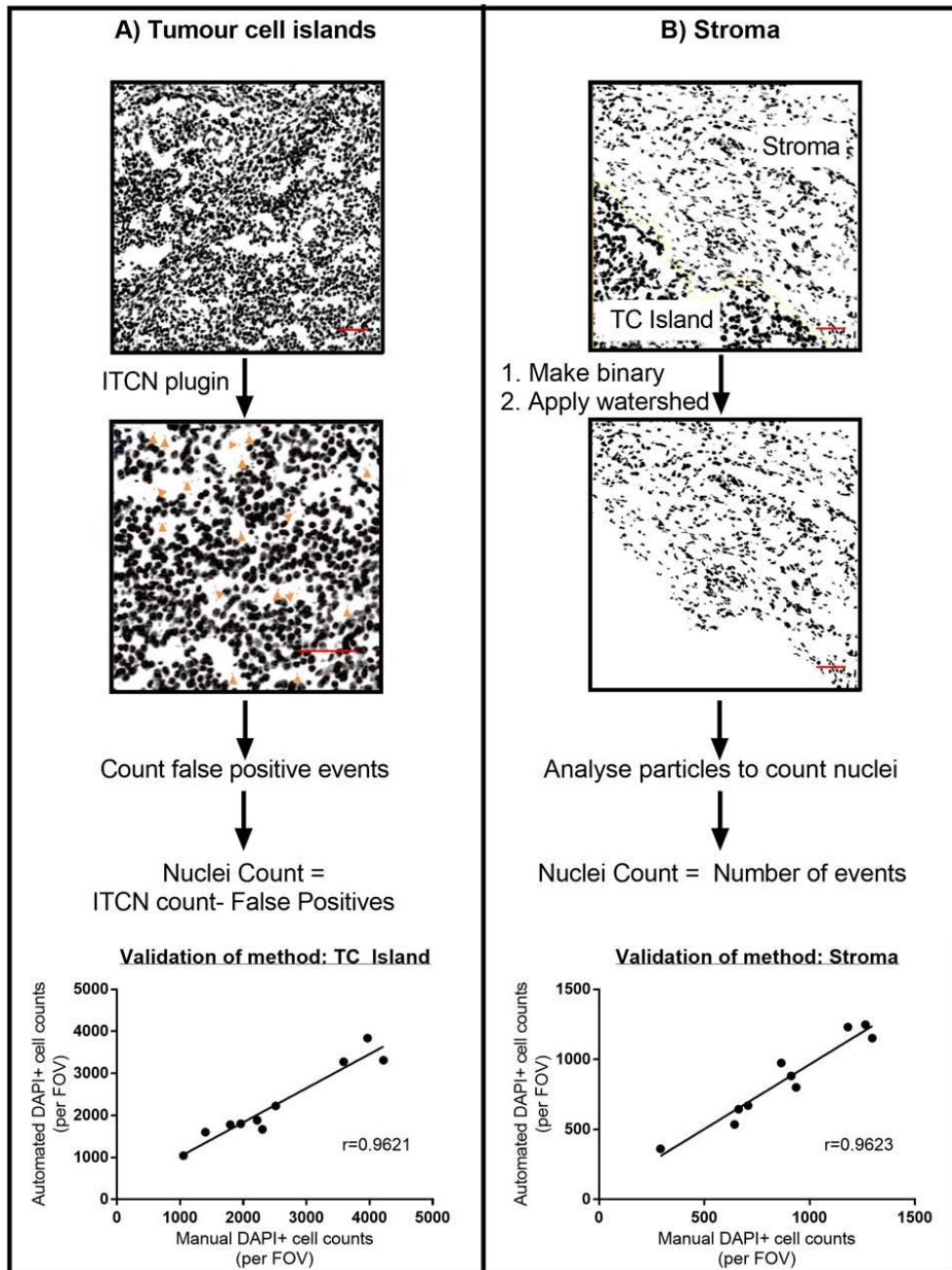


Figure 2.1 Workflow and validation of automated nuclear counting methods.

(A) Tumour cell island nuclei were counted using the ITCN plugin. False positive events (identified by orange triangles) were counted and subtracted from the ITCN count. (B) To count stromal nuclei, images were first converted to binary and the watershed function was applied. The 'Analyse Particles' function was then used to count events. Both methods were validated by comparing the automated counts to counting the nuclei by eye. $n = 10$ images for both methods. Two tailed Pearson's correlation test used. Scale bar = $50\mu\text{m}$.

Identification of tumour leucocyte populations

The cell counter plug-in on Fiji [192] was used to count individual cells and allowed the counting of cells which were dual, or even triple positive for various markers.

When counting TAMs, the marker F4/80 was used. In the case of identifying MRC1⁺ TAMs, the cell counter was first used to identify F4/80⁺ TAMs, and a secondary marker was used to identify the F4/80⁺ cells which co-expressed MRC1⁺. In the case of identification of immature myeloid cells – Gr-1 was used as a marker of neutrophils/monocytes and Ly-6G was used as a marker of neutrophils. PV cells were counted if they were in direct contact with a CD31⁺ blood vessel. When analysing the maturity of MRC1⁺ PV cells, the MRC1⁺ cells which were in contact with CD31⁺ blood vessels were first identified using one marker before assessing if they expressed either Gr-1 or Ly-6G with a second marker.

T cells were identified as CD3⁺ cells, with one marker. If these T cells expressed CD8, a second marker was placed over them, and if they were CD4⁺ a third marker was placed over them – which allowed quantification of total T cells, and the CD4⁺ and CD8⁺ T cells. FOXP3 was used to identify CD3⁺ CD4⁺ regulatory T cells. First, CD3⁺ cells were identified with one marker, and then CD3⁺ cells which expressed CD4 were marked. Finally CD3⁺ CD4⁺ T cells expressing FOXP3 were counted with a third marker.

Hypoxia analyses

PIMO was used to mark regions of hypoxia. To quantify, the number of cells within the region of hypoxia were counted and then normalised to the total number of cells in a FOV. TAMs were quantified as F4/80⁺ cells and normalised to the number of cells in the region of interest e.g. TAMs in hypoxia were normalised to the total number of hypoxic cells.

Blood vessel analyses

CD31 was used as a marker of blood vessels. PV cells were counted as cells which were in direct contact with a CD31⁺ cell. CD31 area was calculated as a percentage of total area analysed which was covered in CD31⁺ staining. To do this images of CD31 staining were converted to binary to set a threshold and the analyse particles tool was used to calculate the area.

Blood vessel sizes were analysed by selecting vessels which had a visible lumen. The lumens were measured by drawing a region of interest around the lumen outlined by the CD31 staining. The area of the region of interest was then measured using the Measure function in ImageJ.

When analysing whether blood vessels were covered in α -smooth muscle actin (α -SMA positive cells) or were perfused by FITC-lectin, the CD31 stain and respective stain were converted to binary. The CD31⁺ area was converted to a mask and applied to the stain – the percentage of CD31 area which was also positive for α -SMA or FITC-lectin was then calculated using the analyse particles tool. In addition to this, the number of CD31⁺ blood vessels were counted using the cell counter and whether these vessels were positive for FITC-lectin or had PV α -SMA⁺ cells was then quantified and a percentage of vessels which were positive for the respective marker was calculated.

2.2.12 FACS based isolation of cell populations from tumour digests

Tumour digests were prepared as described in 2.2.5, and the cell pellets were resuspended in 500 μ L DPBS with 1% FCS. The tumour samples were then incubated with the appropriate antibodies and the viability dye Zombie NIR (see Chapter 5 for details) for 40 minutes while rocking and covered on ice. Following this the samples were washed twice with 500 μ L DPBS with 1% FCS to remove excess unbound antibody and then centrifuged at 4500rpm for 3 minutes to pellet the cells. These cells were then resuspended in 2mL DPBS with 1% FCS and sorted using the BD

Biosciences FACS Aria. FMO controls were used to set a gating strategy, which is shown in Chapter 5. Briefly, viable cells were selected using the viability dye Zombie NIR and 3 cell populations were selected on the basis of their CD45 and CD31 expression (CD45⁻ CD31⁻ cells; CD45⁺ CD31⁻ cells and CD45⁻ CD31⁺ cells). Cell populations were collected into 3mL RLT buffer (Qiagen RNeasy kit) for further analysis.

2.2.13 Laser Capture Microdissection of endothelial cells

10µM thick frozen sections were cut from snap frozen OCT embedded tumours using the cryostat and collected onto uncharged glass slides. Sections were stained using a Rapid-Immuno technique, developed by the neuropathology team at Sheffield Institute of Translational Neuroscience (SiTRAN). Rapid-Immuno works similar to regular immunohistochemistry, only the reagents used are much more concentrated, reducing the staining time and thus potential damage to the RNA within samples.

Collagen IV was previously shown to stain the basement membrane of the endothelium in murine tumours (LLCs, RIP-Tag2 pancreatic tumours and MCa-IV mammary tumours), and co-localises with CD31 staining [193]. Moreover, this marker was previously optimised for Rapid-Immuno staining and therefore Collagen IV was used to identify endothelial cells during LCM. All solutions (except DAB) were prepared prior to staining. Slides were first brought to room temperature and then fixed in acetone at 4°C for 3 minutes. The acetone was then removed from the slides and the slides were blocked at room temperature for 3 minutes in a blocking solution made of 2.5mL sterile PBS and 3 drops blocking solution from the Vectastain Rabbit ABC kit. Excess block was then tipped off and slides were incubated with the primary antibody, rabbit anti-collagen IV at a concentration of 10µg/mL made up in blocking solution, for 3 minutes at room temperature. Slides were then washed by flooding them with PBS. The PBS was then tapped off, and the slides were incubated with the secondary antibody solution (1mL sterile PBS with 1 drop of biotinylated goat anti-rabbit IgG) for 3

minutes at room temperature. The slides were washed again by flooding them with PBS after tapping off the secondary antibody solution. The slides were then incubated with the ABC reagent solution (2.5mL sterile PBS with 1 drop of reagent A and 1 drop reagent B) for 3 minutes at room temperature. At this point the DAB solution was prepared with 2.5mL dH₂O, 1 drop buffer solution, 2 drops DAB reagent and 1 drop hydrogen peroxide. After washing off the ABC reagent with PBS, the slides were incubated with DAB and the stain was allowed to develop for approximately 2 minutes, while watching under a light microscope. When the stain had developed, the reaction was stopped by washing slides with dH₂O. Slides were then washed in dH₂O and dehydrated by quickly dunking the slides in 70% ethanol, 90% ethanol and 100% ethanol baths and then leaving the slides in 100% ethanol for 5 minutes. Slides were then cleared in xylene for 5 minutes. Xylene was then tapped off and slides were dried in the fume hood for 1 hour.

Collagen IV⁺ cells in vessel-like structures were then isolated using the PixCell II Laser Capture Microdissection system. The laser settings of power at 35mV and size 7.5µm were used. This laser was fired through the film of the Capsure Macro LCM caps at the Collagen IV⁺ cells. This caused the film to melt and capture target cells, as shown in Figure 2.2. After endothelial cells were collected, a new cap was loaded onto the microdissection rig and then the surrounding tumour tissue was collected for comparative RNA values.

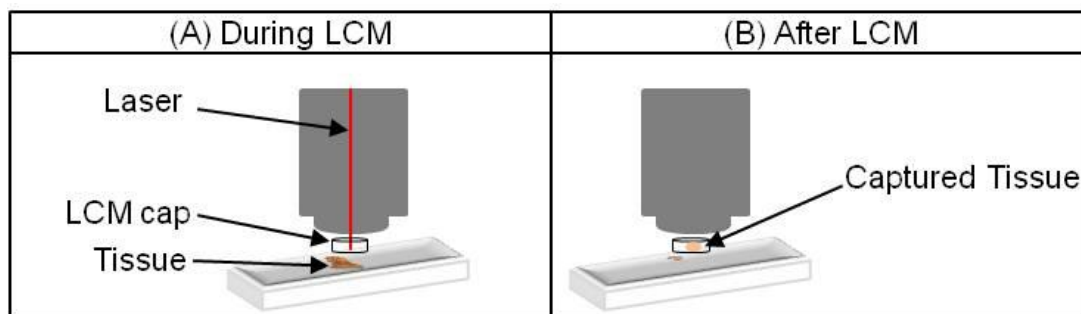


Figure 2.2 Laser capture microdissection.

(A) During laser capture microdissection, slides are placed into a microdissection rig and the laser is fired at the cells of interest. This causes the film of the LCM cap to melt and collects the cells of interest. (B) After the laser is fired, the cells of interest will be captured on the LCM cap for downstream analyses.

2.2.14 Magnetic isolation of CD31⁺ cells from tumour digests

To prepare the magnetic beads, 2×10^7 Sheep anti-rat IgG Dynabeads (50 μ L of bead suspension) were washed twice with 2mL PBS containing 2% FCS. To do this, after suspending the beads in 2mL of wash buffer, they were placed within the DynaMag-15 magnet for 3 minutes, which caused the magnetic beads to move to the sides of the falcon tube by magnetic attraction. This allowed removal of the wash buffer, without disrupting the magnetic beads. The tube was removed from the magnet and the beads were then resuspended in 50 μ L of PBS with 2% FCS and incubated with 3 μ g rat anti-mouse CD31 (clone MEC13.3, BD Pharmingen) for 2 hours rotating at room temperature. Beads were then washed three times in PBS with 2mL of 2% FCS using the DynaMag-15 magnet (as described previously) and finally resuspended in 50 μ L PBS with 2% FCS. Conjugated Dynabeads were stored at 4°C for up to 2 weeks prior to use.

Tumour digests were prepared as described in 2.2.5, and then the cell pellets were resuspended in 1mL Hank's Balanced Salt Solution (HBSS) with 10% FCS. The cell suspension was then incubated with 2.4×10^6 Dynabeads conjugated to anti-mouse CD31 antibody, rocking on ice for 30 minutes. Samples were transferred to a 15mL falcon tube and placed in the DynaMag-15 magnet, and mixed with 2mL of HBSS with 10% FCS. Samples were left within the magnet for 3 minutes, which allowed cells that

were bound to the Dynabeads to migrate to the sides of the falcon tube. A Pasteur pipette was used to carefully remove the HBSS with 10% FCS, to avoid disrupting cells captured by the magnetic field of the DynaMag-15 magnet. The cells were then resuspended by removing the sample from the magnet and mixing cells with 2mL HBSS with 10% FCS. This wash step was repeated six times to remove contaminating non-CD31⁺ cells from the sample. Finally, CD31⁺ cells were collected and centrifuged at 4500rpm for 3 minutes, before resuspending in RLT plus lysis buffer (RNeasy Plus kit) to start the RNA isolation protocol (see 2.2.15).

2.2.15 RNA isolation

RNA was isolated from the different samples using the methods described below. In every case nuclease-free water was used to make solutions required for the isolations, e.g. 70% ethanol, and to elute RNA. Sterile technique was used throughout, and samples and reagents were kept on ice. Following isolation, RNA was stored at -80°C. RNA was quantified using the NanoDrop, and the RNA integrity was quantified using the Agilent Bioanalyzer 2100.

2.2.15.1 RNA isolation from FACS purified cell populations

Cells isolated as described in 2.2.12 were collected into RLT lysis buffer, at a ratio of 3mL RLT lysis buffer per 1mL cells collected. The numbers of cells collected varied from each population – the lowest number of cells was 25000 cells from the CD45⁻ CD31⁺ population. Following this RNA was isolated using the RNeasy Mini kit as per the manufacturer's instructions. Briefly, 70% ethanol was added to the RLT lysis buffer in a 1:1 ratio and 700µL of this mixture was added to the RNeasy spin column. The RNeasy spin column was centrifuged for 15 seconds at 10000 rpm to bind RNA to the column and the flow-through was discarded. This initial step was repeated until all the sample had been passed through the spin column. The column was then washed to

remove impurities initially by adding 700µL buffer RW1 and then centrifuging at 10000 rpm for 15 seconds. The flow through was discarded and the column was then washed with 500µL buffer RPE and centrifuged at 10000 rpm for 15 seconds. This wash step was repeated, but the column was centrifuged for 2 minutes at 10000 rpm to ensure removal of all wash buffer. Following this, the membrane of the spin column was dried by centrifuging the column inside a fresh collection tube at 14000 rpm for 1 minute to increase RNA yields. The column was then transferred to a new collection tube to elute RNA. RNA was eluted from the column using 30µL RNase-free water and centrifuging the column at 10000 rpm for 1 minute. To increase the concentration of RNA, this final elution step was repeated, using the flow-through of the previous elution step to elute any RNA that remained on the column.

2.2.15.2 Isolation of RNA from LCM-captured cells

Laser capture microdissection was carried out on tissue sections as described in 2.2.13. RNA was isolated from these microdissected cells using the PicoPure RNA kit according to the manufacturer's protocol. Sterile forceps were used to remove the film from the Capsure Macro LCM caps and the film was then placed into an eppendorf with 50µL extraction buffer from the PicoPure RNA Isolation kit and incubated for 30 minutes at 42°C to lyse the cells. The RNA purification column was pre-incubated with 250µL of conditioning buffer for 5 minutes at room temperature and centrifuged at 16000 x g for 1 minute. Next 50µL of 70% ethanol was mixed with the cell extract before transferring the solution to the purification column. The column was then centrifuged for 2 minutes at 100 x g and then again for 30 seconds at 16,000 x g to bind the RNA to the column. The purification column was then washed to remove impurities as follows. The column was washed with 100µL of Wash Buffer 1 and centrifuged at 8000 x g for 1 minute. 100µL Wash Buffer 2 was then added to the column before centrifugation at 8000 x g for one minute. This wash step was then repeated, but the column was centrifuged at 16000 x g for 2 minutes to ensure

complete flow through of the final wash step. The purification column was then transferred to a fresh microcentrifuge tube before eluting the RNA. First 11 μ L of elution buffer was incubated on the purification column for 1 minute at room temperature and then the column was centrifuged at 1000 x g for 1 minute. RNA was then eluted by centrifugation of the column at 16000 x g for 1 minute. RNA was then quantified using the Agilent Bioanalyzer 2100 (as detailed in Section 2.2.15.4).

2.2.15.3 RNA isolation from Dynabead collected CD31⁺ cells

Cells were isolated as described in 2.2.14. Cell pellets were first collected and resuspended in 350 μ L RLT plus buffer, as described in the RNeasy Plus kit protocol. These cells were vortexed at room temperature for approximately 30 seconds, or until all cells were visibly lysed, as determined by a lack of cell debris in the solution. As these cells were still attached to the magnetic beads used for their extraction, once the cells had lysed, the cell lysate was placed in a DynaMag-2 magnet for 3 minutes in order to remove the magnetic dynabeads from the cell lysate. The solution was removed and placed in fresh tubes and RNA was isolated from the lysates using the RNeasy Plus kit.

The cell lysate was initially centrifuged in the gDNA eliminator column for 30 seconds at 10000 rpm to remove gDNA from the sample. The flow-through of this column was then mixed with 350 μ L of 70% ethanol and centrifuged in the RNeasy spin column for 15 seconds at 10000 rpm to bind RNA to the column. The flow-through was discarded and the column was washed with 700 μ L of buffer RW1. The column was centrifuged at 10000 rpm for 15 seconds and the flow-through discarded. The column was washed twice more with 500 μ L of buffer RPE. The first buffer RPE wash was removed by centrifuging the column at 10000 rpm for 15 seconds and the second wash was removed with a longer centrifugation step of 2 minutes. The membrane of the spin column was dried to improve RNA yields by centrifuging the column in a fresh collection tube at 14000 rpm for 1 minute. The spin column was transferred to a fresh

collection tube to elute RNA in 30 μ L RNase-free water. RNase free water was added to the spin column and centrifuged at 10000 rpm for 1 minute, to allow the water containing RNA to flow through the column. This step was repeated, using the flow-through of the elution stage to elute any RNA which remained on the spin column, which increased the total RNA concentration of the sample.

2.2.15.4 Quantification of RNA using the Bioanalyzer

RNA isolated using laser capture microdissection (as in section 2.2.15.2) was quantified using the Agilent Bioanalyzer and PicoChip technology (Agilent RNA 6000 Pico kit). This allowed assessment of low RNA yields in the range of 50-5000pg/ μ L, which are typical of samples isolated using laser capture microdissection. The Bioanalyzer not only quantifies RNA concentration, but also allows assessment of RNA quality by the RNA integrity number (RIN). RIN values detail how degraded the RNA is – with intact RNA having a RIN of 10 and highly degraded RNA having a RIN of 1. In order to assess RNA integrity, samples are run alongside an RNA ladder, which allows assessment of RNA fragment size. RNA which is intact should have two peaks at the ribosomal RNA sites 18S and 28S. RNA integrity is important to understand if the RNA can be used in downstream applications.

The PicoChip was prepared by loading 9 μ L of gel mixed with dye into the designated wells of the PicoChip. 9 μ L of RNA conditioning solution was loaded into wells marked with the CS symbol. 5 μ L of RNA marker was then added to wells designated for the ladder and samples. 1 μ L of ladder was added to the designated RNA ladder well and 1 μ L of sample was added to each sample well. The chip was then vortexed at 2400rpm for 1 minute before running on the Agilent Bioanalyzer 2100. In the cases where larger quantities of RNA were purified e.g. when using magnetic isolation (2.2.15.3), the Agilent RNA 6000 Nano kit was used to assess RNA integrity. The protocol for this was similar to the aforementioned PicoChip protocol, only NanoChips were used to allow for the increased concentration of RNA in the sample.

2.2.15.5 Quantification of RNA using the NanoDrop

RNA (of quantities greater than 5ng/μL) was quantified using the NanoDrop. This was used in the first instance for RNA isolated as in 2.2.15.1 and 2.2.15.3, as the NanoDrop was the closest and most readily available machine for quantification. The NanoDrop was first cleaned using RNase-free water (from the RNeasy Plus kit), and then 1μL of RNase-free water was used as a blank reading for the NanoDrop. RNA was then quantified using 1μL of each sample. The NanoDrop uses absorbance to quantify the presence of nucleic acids. 260nm absorbance is used to define nucleic acid presence; 280nm absorbance is usually indicative of proteins and 230nm absorbance is considered to come from sample contamination. A ratio of 260/280 is used to define how pure the sample is and a 260/280 ratio of 2.0 is considered pure for RNA. The 260/230 ratio for RNA should also be around 2.0-2.2. If the 260/230 ratio was lower than 2.0, it suggested that the sample may have contaminants. A likely source of this contamination would be guanidine thiocyanate salts, which could have been left over from the use of RNeasy kits. These contaminations were easily removed using water-saturated butanol as described below.

2.2.15.6 Water-saturated butanol clean-up of RNA

In order to remove contaminating guanidine thiocyanate salts (described in 2.2.15.5), water-saturated butanol was used to clean up the RNA samples. Water saturated butanol was prepared by thoroughly mixing butanol and nuclease-free water in a 1:1 ratio. Following vigorous mixing, two layers formed in the water-butanol mixture: of which, the top layer was water-saturated butanol. Approximately 30μL of RNA in RNase free water (various concentrations) was first mixed with 500μL of water-saturated butanol and then microcentrifuged for 1 minute, until the mixture was clearly separated into two layers, the RNA solution with a water-saturated butanol layer on top, which was then removed. The RNA was washed with water-saturated butanol in this way 5 times. To remove any remaining water-saturated butanol, the RNA was washed

3 times with 300 μ L of di-ethyl ether, by gently layering the ether on top of the RNA layer and then removing it.

2.2.16 cDNA synthesis

RNA was converted to cDNA using the QuantiTect Reverse Transcription kit according to the manufacturer's instructions. Genomic DNA was first eliminated using the gDNA elimination buffer prior to reverse transcription. 12 μ L of sample was mixed with 2 μ L gDNA elimination buffer and incubated for 2 minutes at 42°C. This reaction was then placed on ice and mixed with components for the reverse transcription reaction as follows. Each reverse transcription reaction contained 1 μ L of Quantitect Reverse Transcriptase, 4 μ L Quantitect RT Buffer, 1 μ L RT primer mix and 14 μ L of the gDNA reaction containing the RNA template. 200-500ng of cDNA was synthesised per reaction. The reverse transcriptase reaction was carried out at 42°C for 30 minutes. To inactivate the reverse transcriptase, the reaction was then held at 95°C for 3 minutes. Once synthesised, cDNA was stored at -20°C for a maximum of 2 months until use.

2.2.17 Quantitative PCR

Primers were designed using Primer blast and MFEprimer-2.0 or were previously published. Primers were validated by melt-curve analysis and performing a standard curve analysis to assess efficiency. Quantitative real-time PCR (qPCR) was performed using SYBR green detection and the Applied Biosystems 7900 Real-time PCR machine. In a 384-well plate, each reaction contained 1 μ L cDNA (at a concentration of 1ng-2.5ng depending on the assay, see Chapter 5), 3.4 μ L nuclease-free water and 5 μ L PrecisionPLUS Mastermix premixed with SYBR green and ROX. Each well also contained forward and reverse primers at a concentration of 3pmols. The total reaction volume per well was 10 μ L. Each reaction was run in triplicate (three wells per gene and sample), and Ct values were calculated by determining the number of cycles needed to reach the threshold. The qPCR machine settings were as follows:

1. Hold at 50°C for 2 minutes
2. Hold at 95°C for 10 minutes
3. 40 cycles of 95°C for 15 seconds, and 60°C for 1 minute

Melt-curve analysis (see Figure 2.3) was carried out by adding an additional step in which samples were heated to 95°C for 15 seconds, then the temperature was reduced to 60°C for 15 seconds, before heating to 95°C again. Melt-curves should have one single peak, indicative of one reaction product (Figure 2.3A) rather than multiple or very wide peaks (Figure 2.3B).

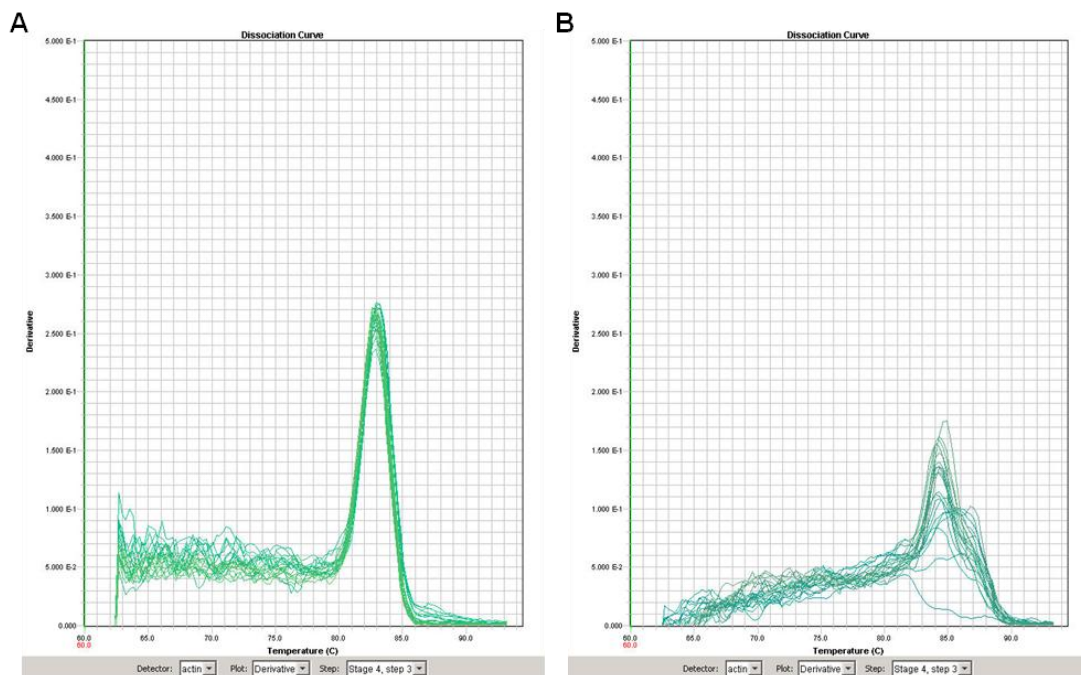


Figure 2.3 Example melt curve analyses.

qPCR was used to amplify genes as described in 2.2.17. Samples were then heated from 60°C to 95°C to create a melt-curve. Melt curves from good primer pairs have a single peak (as in A). (B) shows an example melt curve from a poor primer pair – notice the multiple wide peaks.

$2^{-\Delta\Delta Ct}$ method was used to calculate fold change and gene of interest expression was normalised to *Actb* (β -actin) expression which was used as an endogenous control. β -actin was used as a housekeeper as the Ct values remained consistent between different samples. First, triplicates for each reaction were averaged to find the Ct value. ΔCt values were calculated by subtracting the Ct value of the

housekeeping gene from the Ct value of the gene of interest. $\Delta\Delta\text{Ct}$ values were then calculated by subtracting the ΔCt value of the control group from the ΔCt value of the experimental group. This was then placed into the formula $2^{-\Delta\Delta\text{Ct}}$ to obtain the fold change value.

2.2.18 Data representation and statistical analyses

Data was analysed using GraphPad Prism 7 Software. Graphs represent mean \pm standard error of the mean (SEM) unless otherwise stated. Experiments were carried out a minimum of 3 times. Where possible, normality of these data was checked by performing a Quantile-Quantile plot analysis. If appropriate, samples were matched i.e. when comparing two different areas of the same tumour, samples were matched. Statistical analyses for data with normal distributions were then carried out, including t-tests when comparing two different conditions; One-way ANOVAs when comparing more than one condition and two-way ANOVAs when comparing two-different variables on different treatments. $P < 0.05$ was taken to be significant.

If One-way ANOVAs showed significance, appropriate post-hoc analyses tests (as recommended by Prism software) were used to identify statistical significances between multiple groups and are described in the results. Two way ANOVAs identified whether the effects of doxorubicin treatment or the area analysed (i.e. differences between tumour stroma and tumour cell islands) were significant. This gives two p values of importance: (1) the treatment p value which is DOX having an effect and (2) the area analysed p value which indicates whether the stroma and tumour cell islands are different. Should one of these p values indicate significance, the relevant post-hoc analysis (usually Sidak's multiple comparisons test, as indicated by Graph Pad Prism 7 software) was used to identify which comparisons were of significance.

Chapter 3

Characterisation of key features of mouse mammary (TS1) tumour implants after DOX treatment: *stromal areas versus tumour cell islands.*

3.1 Introduction

As mentioned previously in section 1.2.2, high numbers of TAMs are associated with poor prognosis in many types of cancer [77]. Since then, studies in mouse tumour models have indicated that TAMs also modulate tumour responses to chemotherapeutic agents. For example, TAMs limit the responses of mammary tumours to the cytotoxic agent, paclitaxel [109], [139]. They also promote the regrowth of LLCs after cyclophosphamide treatment [144]. Further studies showed that TAMs which expressed the pro-angiogenic gene, *Vegfa*, were partially responsible for tumour relapse (implanted PyMT tumours) after DOX [144]. TAMs have also been shown to limit the efficacy of chemotherapy in mouse mammary tumours by immunosuppressive mechanisms, such as production of IL-10 [110] and suppression of cytotoxic T cell proliferation [109].

TAMs express both CSF1R [194] and CXCR4 [144] and the ligands for these receptors (CSF1 and CXCL12) help to recruit monocytes into tumours, and are involved in macrophage differentiation [195], [196]. Inhibition of the CSF1-CSF1R and CXCL12-CXCR4 signalling axes in mouse tumour models has been shown to reduce TAM numbers after chemotherapy and significantly improved their response to chemotherapy [109], [144]. Inhibitors of these pathways are currently being tested in clinical trials; however early trials suggest that they may not be as effective in patients as in pre-clinical mouse models [170]. It is, therefore, important to further understand the mechanisms behind monocyte recruitment and 'education' in chemotherapy-treated tumours so new pathways can be identified as therapeutic targets.

A decision was made to study TAMs in a model most relevant to breast cancer, as this is one of the most common types of cancer diagnosed in the UK, with an incidence of 31% of female cancer cases in 2014 [197]. Patients which have smaller, locally restricted tumours have reasonably good prognosis, as at least 88% of stage 2 (and 99% of stage 1) patients go on to survive five years from initial diagnosis [198].

However, patients with larger tumours, which have spread extensively to the lymph nodes (stage 3, locally advanced cancer), have poorer prognosis, with a 5-year survival rate of 55% [198]. There is a need to improve survival rates in this patient population, and so a murine model with mammary tumours was selected for these studies.

Moreover, there is evidence to suggest that TAMs have a role in the progression of breast cancer. For example, breast cancer patients with tumours that had increased TAM infiltration had decreased relapse-free and overall survival [199]. More recently, TAMs were mechanistically shown to influence regrowth of murine mammary tumours following DOX treatment in a VEGF-A dependent manner [144], suggesting that murine models may be one way to understand how TAMs may be contributing to relapse, and potentially allow the investigation of novel targets which could be used to prevent relapse in patients in the future.

An orthotopic mouse tumour model - the orthotopic implant of TS1 cells (a cell line isolated from transgenic MMTV-PyMT tumours [139]) - was used in the studies described in this chapter as this means that tumours form and grow in the correct local tissue environment, and are exposed to signals from the surrounding mammary tissue. The parent, MMTV-PyMT mouse model has also been used to study orthotopic mammary tumours but these mice develop multiple mammary tumours, which are rare in patients [200]. Orthotopic implantation of the TS1 cell line was used here as mice then develop one single mammary tumour, which is more indicative of breast cancer patients.

Anthracyclines are commonly used in the treatment of breast cancer in various different regimens [201]–[203]. DOX, an anthracycline, is offered to patients with advanced triple negative (oestrogen receptor ER⁻, progesterone receptor PR⁻, HER2⁻) breast cancer [204]. The TS1 tumours are ER⁻ and PR⁻, but express HER2 [87]. NICE guidelines indicate that patients with advanced tumours that are HER2⁺, but ER⁻ PR⁻ should receive neoadjuvant DOX in the first instance, and given an anti-HER2 therapy (trastuzumab) if they are not responding to therapy [201]. Therefore DOX was chosen

as an appropriate chemotherapeutic agent for treating TS1 tumours. Moreover previous studies showed DOX treatment of transgenic MMTV-PyMT tumours increased the recruitment of immature myeloid cells and MRC1⁺ TAMs into tumours within 48 hours of treatment [137]. Furthermore, DOX administration resulted in an increase in MRC1⁺ TAMs in well vascularised areas of PyMT tumour implants within seven days of treatment [144].

The hypothesis tested in this chapter was that DOX would trigger changes in the features of TS1 tumours, including the accumulation of TAMs. Tumours were examined 48 hours after a single injection of DOX as this early time point was previously shown to affect the recruitment of both immature myeloid cells and MRC1⁺ TAMs in MMTV-PyMT tumours [137]. The aim of the work described in this chapter was, therefore, to characterise the changes induced in TS1 tumours by DOX - with particular reference to:

- a. Tumour vascularity and hypoxia (as changes in these tumour features could be relevant to changes in TAM accumulation/activation).
- b. Myeloid cell subsets (including F4/80⁺ TAMs and MRC1⁺ TAM subsets, Gr-1⁺ immature myeloid cells and Ly-6G⁺ neutrophils).

3.2 Methods

3.2.1 Immunofluorescent staining of tumours

To understand how DOX impacts on TS1 tumours, immunofluorescent analyses were performed on frozen tumour sections. TS1 tumours were removed from mice after the treatments described in section 2.2.3 and snap frozen in OCT (as described in section 2.2.4). 14µm frozen sections were stained as described in section 2.2.9, using the antibodies at concentrations described below in Table 3.1.

Antibody	Fluorophore	Clone	Conc. (µg/mL)
Rat (m) Anti-Mouse Ly-6G	PE	1A8	4
Rat (m) Anti-Mouse CD31	AlexaFluor647	MEC13.3	5
Rat (m) Anti-Mouse F4/80	AlexaFluor488	Cl:A3-1	2
Rabbit (p) Anti-Mannose Receptor	Unconjugated	ab64693	2.5
Purified Rat (m) Anti-Mouse Gr-1	Unconjugated	RB6-8C5	1
Goat (p) Anti-Rat IgG	AlexaFluor647		10
Goat (p) Anti-Rabbit IgG	AlexaFluor555		10
Mouse (m) Anti-PIMO	Dylight549	4.3.11.3	5

Table 3.1: Antibodies used in immunofluorescent analyses in this chapter.
(m) = monoclonal and (p) = polyclonal antibody.

3.2.2 Analyses of immunofluorescent images

As previously described in section 2.2.11, Fiji was used to analyse images and nuclei (DAPI⁺ events) were counted by the ITCN plugin [191] in the tumour cell islands or by “Analyse particles” in the stroma. Images were taken using at 20x objective lens and at least 5 randomly selected fields of view (FOV) were analysed per tumour section.

The cell counter plugin [192] enabled counting of cells, and allowed counting of cells which were positive, dual-positive or triple positive, by placing markers on cells which could then be applied across multiple colour channels.

CD31 area was calculated by converting the CD31 stain to a binary image (to apply a threshold) and then using Fiji’s analyse particles tool which allowed the percentage of the region of interest covered by CD31 staining to be calculated.

3.3 Results

3.3.1 TS1 tumours contain distinct regions of tumour cell islands and stroma.

Use of haematoxylin and eosin staining showed that these tumours consist largely of two distinct regions - tumour cell islands surrounded by less cellular, stromal areas (Figure 3.1A). This could also be seen on the fluorescent microscope using DAPI nuclear staining (Figure 3.1B). The stroma of these tumours had significantly fewer nuclei (mean= 598.2 ± 40.48 per FOV) than that of the tumour cell islands (mean= 2204 ± 77.12 per FOV, paired t-test $p=0.0006$). Given that the nuclear counts were significantly different between these two tumour areas (Figure 3.1C), it was clear that further analyses of these tumours would need to normalise cell counts to the number of nuclei present in the FOV, when comparing between stroma and tumour cell islands to account for the differences in nuclear density.

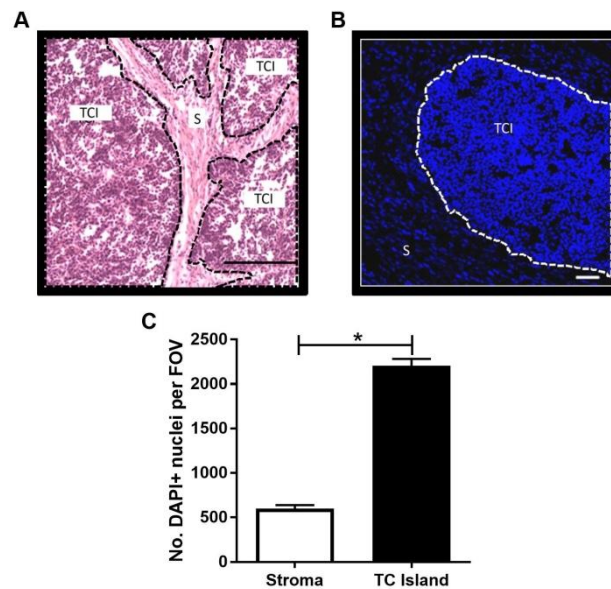


Figure 3.1: TS1 tumours contain two distinct compartments: tumour cell islands and distinct stromal areas.

The tumour cell islands (TCI) contain more nuclei than the stromal compartment (S). These two regions could be identified using haematoxylin and eosin staining (A; scale bar= $200\mu\text{m}$) and DAPI immunofluorescence (B; scale bar= $50\mu\text{m}$) of tumour sections. The total number of nuclei per FOV were counted for the stroma and tumour cell islands (C). * $p\leq 0.001$ $n=4$ tumours.

3.3.2 The stroma of PBS and DOX treated TS1 tumours is normoxic and has increased vascularity compared to tumour cell islands.

It was hypothesised that tumour cell islands and stromal areas might also display differences in other microenvironmental features such as tumour vascularity and hypoxia. These related features were chosen as tumour hypoxia can regulate the phenotype of macrophages, including their expression of *Vegfa* [185], [205]. However, recent studies have shown that ablating hypoxia-inducible factors, 1 and 2 (HIFs 1 and 2) in TAMs has no effect on the regrowth of LLC tumours after chemotherapy [144]. This suggests that hypoxia may not promote the relapse-promoting phenotype of TAMs after chemotherapy [144].

Nevertheless, TS1 tumour bearing mice were injected with PIMO as described in 2.2.3 in order to assess tumour hypoxia. Tumours were then removed, frozen and stained with anti-PIMO (red staining, Figure 3.2) and anti-CD31 (white staining, Figure 3.2) to assess blood vessels as described in 3.2.1. Figure 3.2 shows representative images of the stroma (Figure 3.2A) and tumour cell islands (Figure 3.2B).

Tumour hypoxia was analysed as the percentage of cells which stained PIMO positive out of the total number of cells within the area analysed, to account for different numbers of nuclei in each FOV. Figures 3.2C and 3.2D, alongside the representative staining demonstrate that hypoxia was restricted to the tumour cell islands of the tumours. Tumour cell islands of PBS and DOX treated tumours (PBS mean= 22.86 ± 1.98, DOX mean= 20.59 ± 5.26) were more hypoxic than the stroma (PBS mean=0 ± 0, PBS paired t test p=0.0014, Figure 3.2C, DOX mean= 0 ± 0, DOX paired two tailed t test p=0.0112, Figure 3.2D). Interestingly, within 48 hours, DOX treatment had no effect on the percentage of cells which were hypoxic within TS1 tumours.

Tumour vascularity was assessed by measuring the percentage CD31⁺ area, (i.e. the amount of area covered with CD31 staining). Normoxic regions of PBS treated tumour cell islands (mean= 1.87 ± 0.12) were significantly more vascularised than the hypoxic regions of the tumour cell islands (mean= 0.71 ± 0.15, One way ANOVA

p=0.0153 with Tukey's multiple comparisons test p=0.0202). In PBS-treated tumours, the stroma (mean= 4.89 ± 0.73) had increased vascularity compared to the normoxic tumour cell island, although this was not significantly different (Tukey's multiple comparison test p=0.0718). The stroma of PBS-treated tumours had significantly more CD31⁺ area compared to that of the hypoxic areas found in the tumour cell islands (Tukey's multiple comparisons test p=0.0176; Figure 3.2E).

The normoxic regions of tumour cell islands (mean= 1.67 ± 0.33) were also more vascularised than the hypoxic regions (mean= 0.51 ± 0.10) in DOX-treated tumours (One way ANOVA p=0.0036 with Tukey's multiple comparisons test p=0.0172, Figure 3.2F). In DOX-treated tumours, the stroma (mean= 4.18 ± 0.78) was significantly more vascularised compared to both the normoxic regions of the tumour cell islands (Tukey's multiple comparisons test p=0.0174) and the hypoxic regions of the tumour cell islands (Tukey's multiple comparisons test p=0.0103). DOX did not significantly alter vascularity compared to PBS treated tumours.

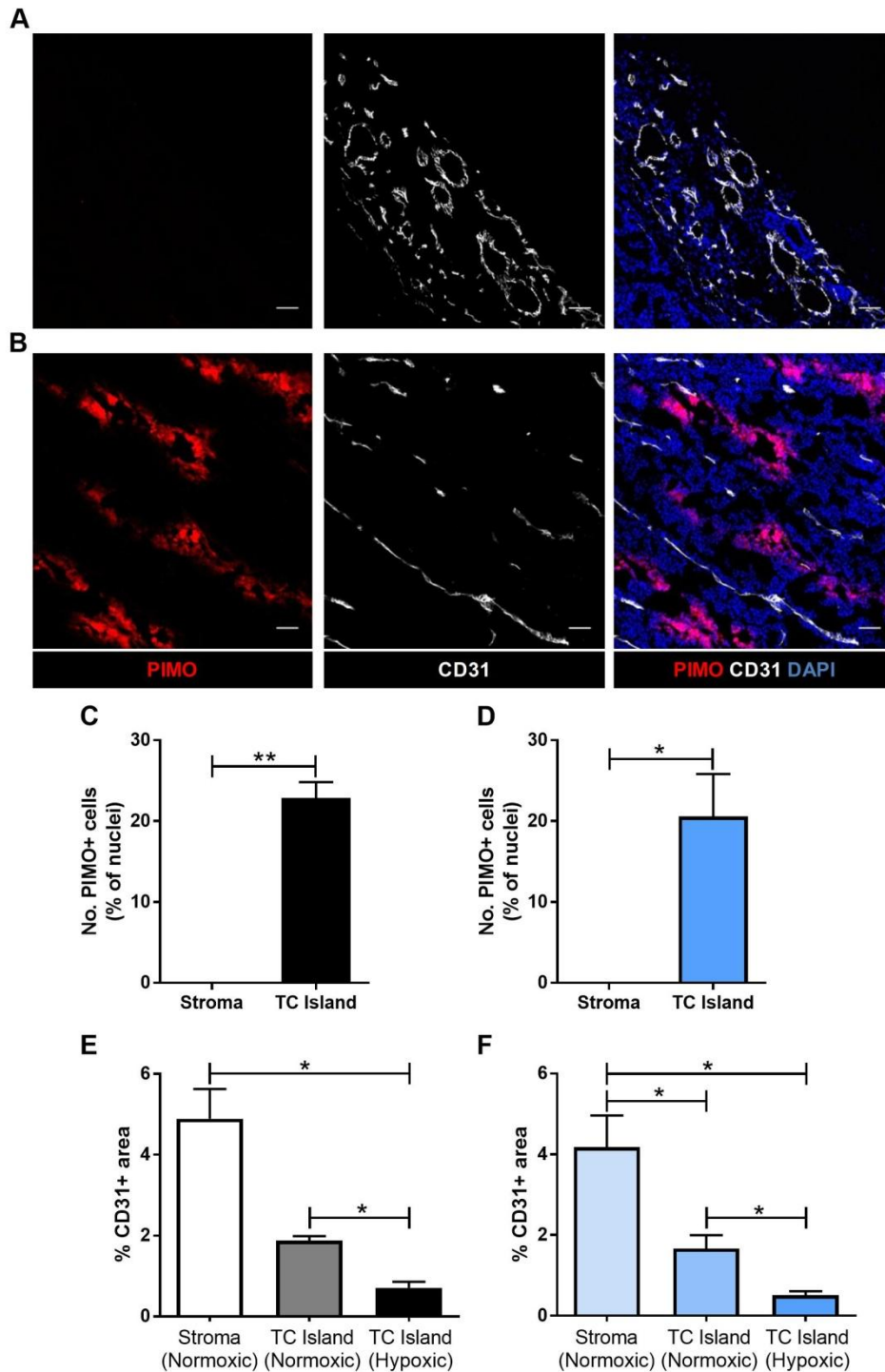


Figure 3.2 The stromal component of TS1 tumours is normoxic and more vascularised compared to the tumour cell islands.

Hypoxic cells (PIMO, red) and blood vessels (CD31, white) were identified using immunofluorescent staining. Representative staining of the stroma (A) and tumour cell islands (B) is shown. Scale bar = 50 μ m. Hypoxia was measured as % PIMO⁺ cells for both PBS (C) and DOX (D) treated tumours. Vascularity of tumours was quantified as % CD31⁺ area (CD31⁺ area as a percentage of total area measured) for PBS (E) and DOX (F) treated tumours. * p<0.05 and ** p<0.01. (n=4 PBS tumours; n=6 DOX treated tumours).

3.3.3 The normoxic stroma of PBS and DOX treated TS1 tumours contain increased numbers of TAMs compared to tumour cell islands.

Previous studies have described TAMs as being located within hypoxic regions of breast carcinomas [78] and murine TS/A tumours [68] and shown that hypoxia can affect the phenotype of TAMs, by causing an upregulation of proangiogenic genes such as *vegfa* [185], [205], [206]. More recently, research has focussed on TAMs located within the normoxic areas of LLCs, demonstrating that such PV TAMs contribute more to tumour relapse after chemotherapy in that tumour model [144]. Given these apparent contradictions, the relationship between hypoxia and TAM density was investigated in TS1 tumour implants. Frozen tumour sections were stained for PIMO (hypoxia; red), CD31 (white) and the macrophage marker F4/80 (green) and representative images of the stroma (Figure 3.3A) and tumour cell islands (Figure 3.3B) are shown.

In PBS-treated tumours there was an increased density of TAMs (total number of TAMs in the area analysed as a percentage of total number of cells in area analysed) in the normoxic stroma (mean= 39.88 ± 4.05), compared to that of the normoxic tumour cell islands (mean= 5.62 ± 0.54 , One way ANOVA $p=0.0032$, Tukey's multiple comparison test $p=0.007$, Figure 3.3C). Hypoxic areas within PBS-treated tumour cell islands also contained F4/80⁺ TAMs (mean= 4.22 ± 1.07) at a lower density than the stroma (Tukey's multiple comparison test $p=0.0074$). There was no significant difference in TAM density between normoxic and hypoxic regions of the tumour cell islands in PBS treated tumours (Tukey's multiple comparison test $p=0.2162$).

The stroma of DOX-treated tumours (mean= 37.87 ± 4.0) had a significantly increased density of TAMs compared to the normoxic regions of the tumour cell islands (mean= 7.51 ± 0.28 , One Way ANOVA $p=0.0004$ with Tukey's multiple comparisons test $p=0.0014$, Figure 3.3D) and hypoxic regions of tumour cell islands (mean= 3.83 ± 0.48 , Tukey's multiple comparisons test $p=0.0006$). In contrast to the PBS treated tumours, in DOX-treated tumours, the hypoxic region of tumour cell islands had a lower

density of TAMs compared to the normoxic regions (Tukey's multiple comparisons test $p=0.0004$). DOX did not impact on the TAM density of these tumours when compared with PBS treated tumours.

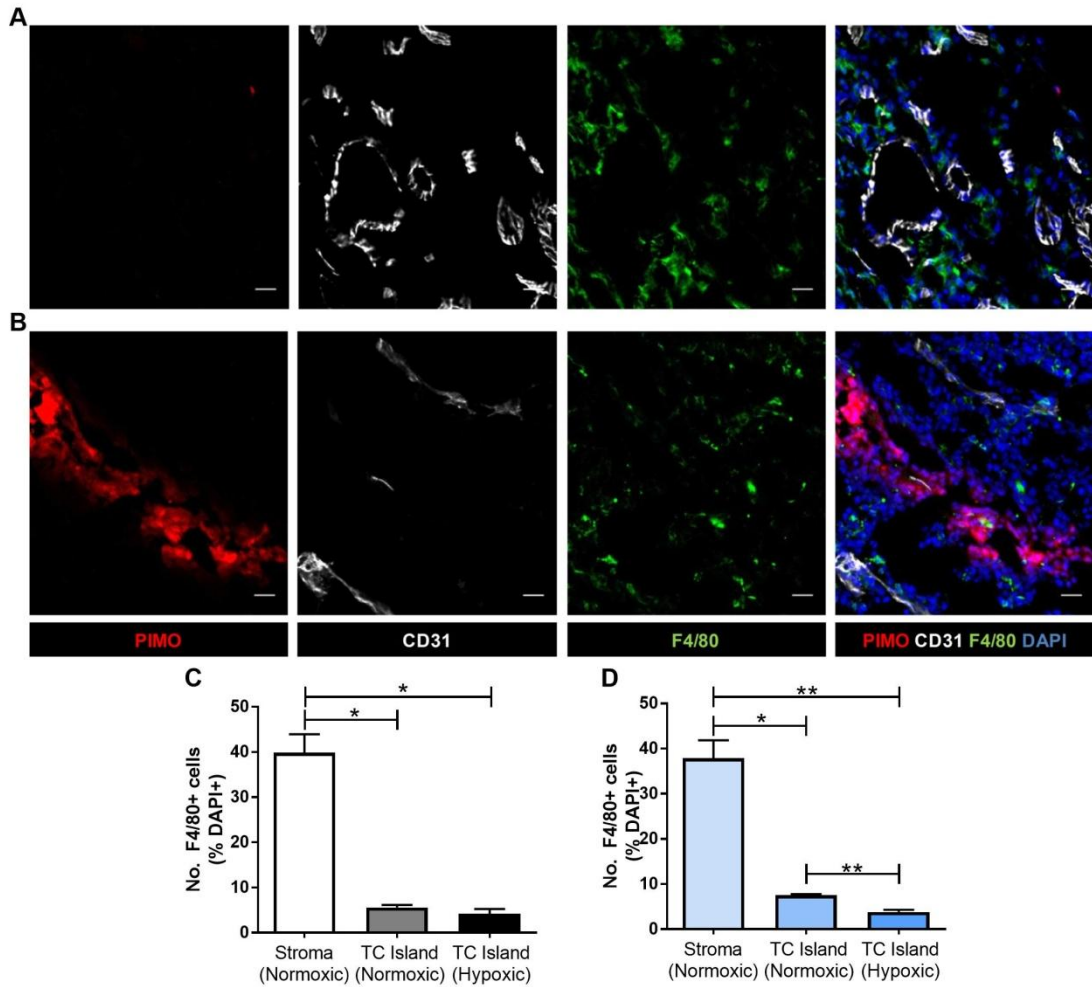


Figure 3.3 The normoxic stroma contained a higher density of TAMs than the more hypoxic, tumour cell islands of TS1 tumours.

Representative hypoxia (PIMO, red); CD31 (white) and F4/80 (green) staining in the stroma (A) and tumour cell islands (B). Scale bar= 20 μ m. The density of F4/80⁺ TAMs was calculated by dividing the total number of F4/80⁺ cells by the number of DAPI⁺ events in each specified region and multiplying by 100. * $p<0.01$ and ** $p<0.001$. (PBS tumours $n=4$; DOX tumours $n=6$).

3.3.4 MRC1⁺ TAMs are present mainly in the stroma of TS1 tumours.

MRC1⁺ TAMs in mouse tumours have previously been shown to stimulate the regrowth of tumour residues after chemotherapy [144]. Therefore, the density and number of F4/80⁺ MRC1⁺ cells was analysed within these tumours by staining for F4/80 (green) and MRC1 (red) as described in section 3.2.1 (Figures 3.4 & 3.5). The number of TAMs per FOV were analysed to understand if TAM recruitment was affected by DOX. TAM density was also analysed to understand the effect of DOX on TAM recruitment, while accounting for the total number of cells per FOV. Representative staining is shown in Figure 3.4A (stroma) and 3.4B (tumour cell islands).

In both DOX and PBS treated tumours, the number of F4/80⁺ TAMs per FOV increased slightly in tumour cell islands (PBS mean= 400.8 ± 108.3, DOX mean= 408.6 ± 61.67) compared to the stroma (PBS mean= 175.1 ± 42.19, DOX mean= 225.1 ± 55.14, Two way ANOVA area analysed p=0.0077). However, post-hoc analyses revealed these trends were just outside of statistical significance (Sidak's multiple comparisons test PBS p=0.0615, DOX p=0.0961). Furthermore, DOX did not change the number of TAMs per FOV in either the stroma or the tumour cell islands (Two way ANOVA treatment p=0.7199, Figure 3.4C).

Next the number of F4/80⁺ MRC1⁺ TAMs were counted per FOV in both tumour regions (Figure 3.4D). The stroma of both PBS (mean= 87.33 ± 28.94) and DOX-treated (mean= 143 ± 39.84) tumours appeared to contain more MRC1⁺ TAMs than the tumour cell islands (PBS mean= 51.88 ± 15.89, DOX mean= 54.93 ± 12.72, Two way ANOVA area analysed p=0.0378). Post-hoc analyses found these differences were not statistically significant (Sidak's multiple comparisons test PBS p=0.6018, DOX p=0.0591) and again DOX did not affect the numbers of F4/80⁺ MRC1⁺ cells per FOV (Two way ANOVA treatment p=0.3454).

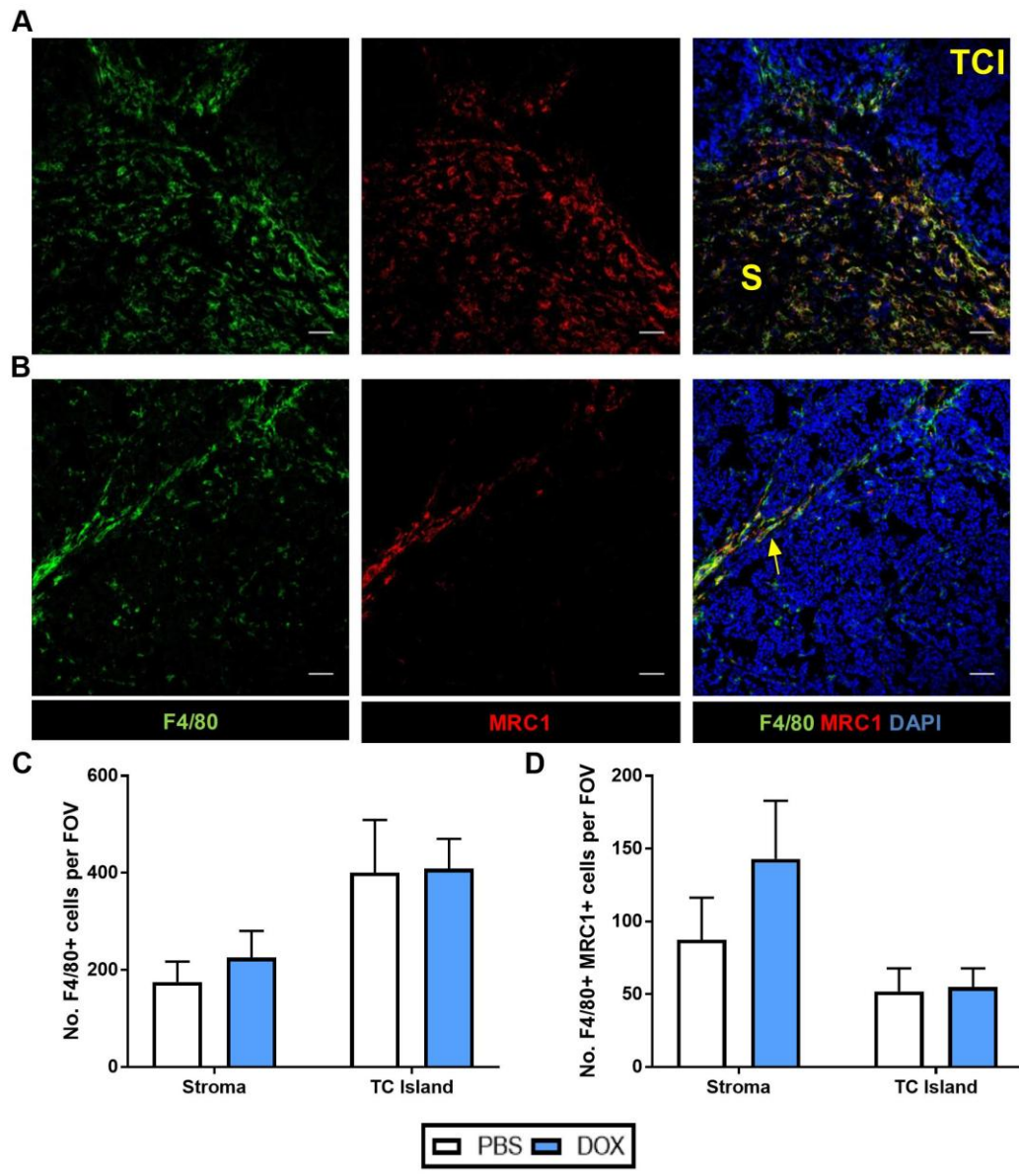


Figure 3.4 Differences in F4/80⁺ and F4/80⁺ MRC1⁺ TAMs between the stromal compartment and tumour cell islands in TS1 implant tumours.

Tumour sections were dual stained for F4/80 (macrophages; green) and MRC1 (red) in the stroma (A) and the tumour cell islands (B). In A, the stroma is denoted with an S, and some tumour cell island (TCI) can be seen at the top of the field of view (FOV). Scale bar = 50µm. F480⁺ MRC1⁺ cells appear yellow in the merged images on the right. MRC1⁺ TAMs were rarely seen in the tumour cell islands, and can be seen in the invading stroma (yellow arrow, B). Both F4/80⁺ (C) and F4/80⁺ MRC1⁺ cells (D) were counted per FOV. Two way ANOVA used (PBS tumours n=5; DOX tumours n=6).

In order to account for the increased density of nuclei in the tumour cell islands, TAM density was calculated as the number of F4/80⁺ cells as a percentage of total cells (Figure 3.5A). The density of F4/80⁺ TAMs was significantly increased in the stroma of PBS treated tumours (mean= 43.57 ± 3.82) compared to tumour cell islands (mean= 12.3 ± 2.91, Two way ANOVA area analysed p<0.0001, Sidak's multiple comparisons test p=0.0001). This was also true in DOX treated tumours (Stroma mean= 44.21 ± 3.73, Tumour cell island mean= 13.8 ± 2.05, Sidak's multiple comparisons test p<0.0001), and again DOX did not change the density of F4/80⁺ cells (Two way ANOVA treatment p=0.7556).

The density of F4/80⁺ MRC1⁺ cells (Figure 3.5B) was then examined. The stroma showed a significant increase (mean= 18.28 ± 4.85) in F4/80⁺ MRC1⁺ cell density compared to tumour cell islands (mean= 1.67 ± 0.37, Two way ANOVA area analysed p<0.0001, Sidak's multiple comparisons test p=0.0095) in PBS-treated tumours. This was also the case in DOX-treated tumours (Stroma mean= 29.05 ± 4.21, Tumour cell island mean = 1.90 ± 0.41, Sidak's multiple comparisons test p=0.0002) and again DOX did not significantly alter the density of F4/80⁺ MRC1⁺ cells (Two way ANOVA treatment p=0.1382).

Finally, the percentage of F4/80⁺ TAMs expressing MRC1 was calculated (as the number of F4/80⁺ MRC1⁺ cells divided by total F4/80⁺ cells multiplied by 100, Figure 3.5C). The stroma of PBS treated tumours (mean= 37.64 ± 10.16) contained a significantly increased percentage of MRC1⁺ TAMs compared tumour cell islands (mean= 16.22 ± 3.48 Two way ANOVA area analysed p<0.0001, Sidak's multiple comparisons test p=0.0112). This was also seen in DOX treated tumours (Stroma mean= 63.94 ± 7.20, Tumour cell island mean= 15.69 ± 4.02, Sidak's multiple comparisons test p<0.0001). Interestingly, there appeared to be a trend for an increase in the percentage of MRC1⁺ TAMs within the stroma of DOX treated tumours compared to PBS treated tumours, but it was not significant (Two way ANOVA treatment p=0.1643).

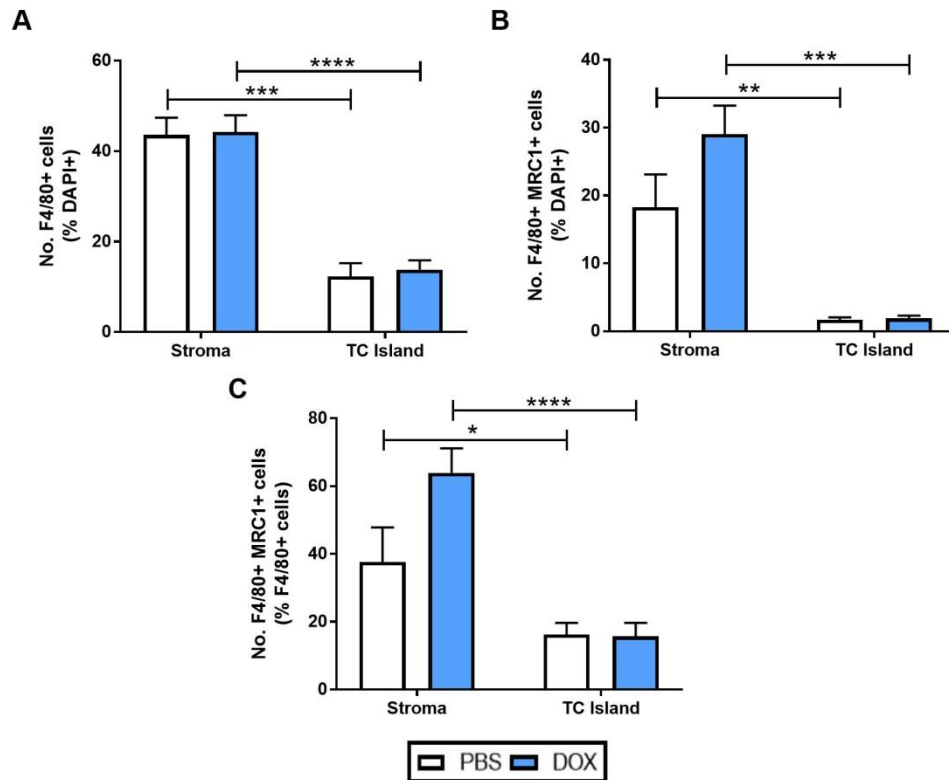


Figure 3.5 Differences in F4/80⁺ and F4/80⁺ MRC1⁺ TAM densities between the stromal compartment and tumour cell islands in TS1 implant tumours.

Both F4/80⁺ (A) and F4/80⁺ MRC1⁺ (B) cells were counted per field of view (FOV) and then calculated as percentage of total cells (DAPI⁺) per FOV to determine their respective densities. The percentage of F4/80⁺ cells in each FOV that were MRC1⁺ was also calculated (C). *p < 0.05 **p < 0.01; ***p < 0.001; ****p < 0.0001. Two way ANOVA used (PBS tumours n=5; DOX tumours n=6)

3.3.5 DOX does not increase infiltration of immature Gr-1⁺ cells.

Although overall TAM infiltration was not affected within 48 hours of DOX treatment, it was deemed possible that the recruitment of TAMs first requires infiltration of immature monocytic cells. Given immature myeloid cells may be a source of TAMs post-chemotherapy, their numbers were examined by counting Gr-1⁺ cells, comprising both monocytes and neutrophils. Therefore Gr-1 staining was carried out as described in section 3.2.1. Gr-1 was used instead of Ly-6C as this was found to co-stain blood vessels (see images in Figure 4.7). Stained Gr-1⁺ cells are shown in white in the

stroma (Figure 3.6A) and tumour cell islands (Figure 3.6B). The number of Gr-1⁺ cells per FOV was quantified (Figure 3.6C) and there were no significant differences between PBS and DOX treated tumours (Two way ANOVA treatment p=0.7533). The stroma of both PBS and DOX treated tumours contained significantly more Gr-1⁺ cells compared to tumour cell islands (Two way ANOVA area analysed p=0.0010, see Table 3.2).

	PBS	DOX
Stroma	103.2 ± 22.32	110.8 ± 22.52
Tumour Cell Island	30.15 ± 4.46	36.05 ± 11.5
Sidak's multiple comparison test	p=0.0120	p=0.0107

Table 3.2 Number of Gr-1⁺ cells per field of view in PBS and DOX treated tumours.

The number of Gr-1⁺ cells per field of view were counted in PBS and DOX treated tumours in the stroma and tumour cell islands. Values are mean ± SEM. Two way ANOVA with Sidak's multiple comparison test showed there were more Gr-1⁺ cells in the stroma of both PBS and DOX treated tumours compared to tumour cell islands.

To allow for the increased nuclear density seen in tumour cell islands, cell counts were normalised by the number of cell nuclei (i.e. by dividing total number of Gr-1⁺ cells by total number of DAPI⁺ nuclei in a FOV and then multiplying by 100 to establish the percentage of cells which were Gr-1⁺, Figure 3.6D). Again, there was no significant difference between PBS- and DOX- treated tumours (Two way ANOVA treatment p=0.7461). The density of Gr-1⁺ cells was significantly increased in the stroma of TS1 tumours, regardless of treatment (Two way ANOVA treatment p=0.0002, see Table 3.3).

	PBS	DOX
Stroma	16.28 ± 2.81	17.45 ± 3.03
Tumour Cell Island	1.42 ± 0.28	1.82 ± 0.56
Sidak's multiple comparison test	p=0.0025	p=0.0019

Table 3.3 Gr-1⁺ cell density in PBS and DOX treated tumours.

The number of Gr-1⁺ cells per field of view were counted and expressed as a percentage of total cells per field of view in the stroma and tumour cell islands of PBS and DOX treated tumours. Values are mean ± SEM. Two way ANOVA with Sidak's multiple comparison test showed there was an increased density of Gr-1⁺ cells in the stroma of both PBS and DOX treated tumours compared to tumour cell islands.

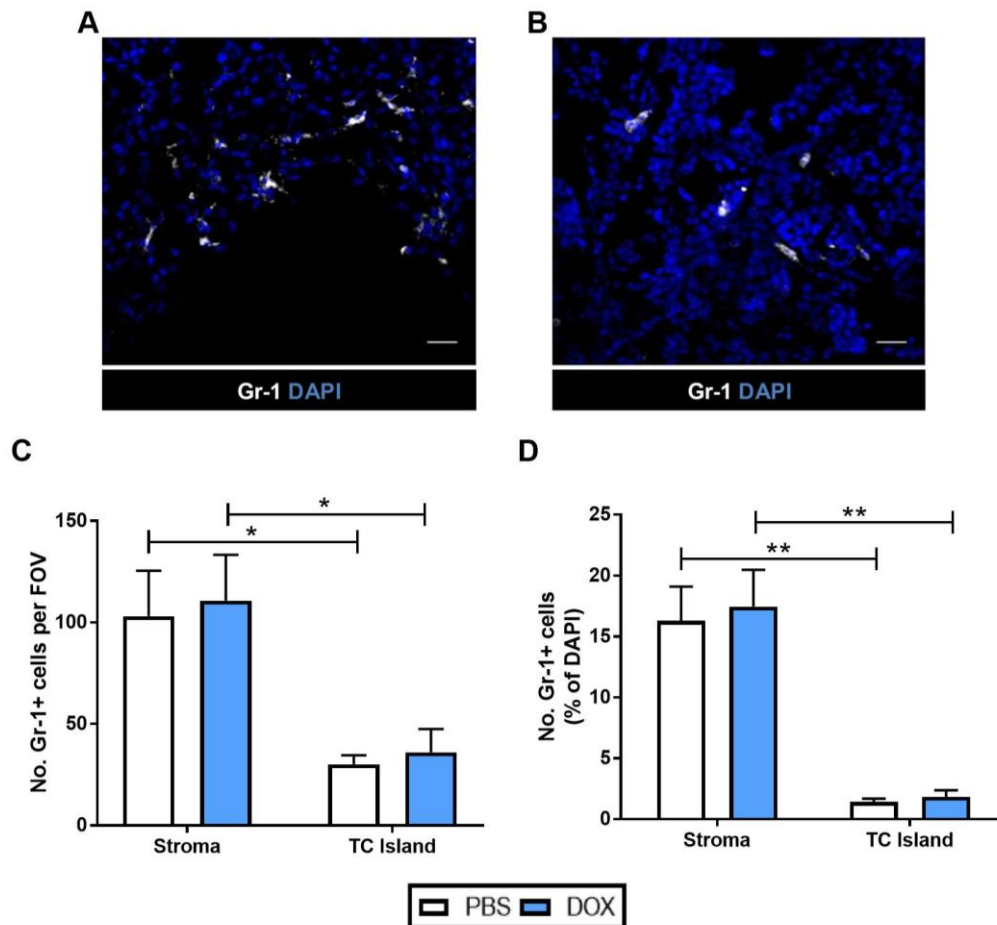


Figure 3.6 The number and density of Gr-1⁺ cells was higher in the stroma compared to the tumour cell islands of TS1 implant tumours.

Gr-1⁺ cells (white) were identified within the stroma (A) and tumour cell islands (B) of TS1 implant tumours. Scale bar= 20µm. Total Gr-1⁺ cells were quantified per FOV (C) and normalised to the number of nuclei (D). *p<0.05; **p<0.01 (n=4 tumours).

3.3.6 DOX does not increase infiltration of Ly-6G⁺ cells.

Neutrophils express Ly-6G [207] so their number can be assessed by staining tumours for this marker, as described in section 3.2.1. The Gr-1 antibody (clone RB6-8C5) used in the previous analysis was reported to inhibit the binding of the Ly-6G antibody (1A8), and so this analysis could not be performed in conjunction with the aforementioned Gr-1 stain. Therefore, we were unable to obtain data about how many of the Gr-1⁺ cells were monocytes and not neutrophils. Nevertheless, Ly-6G⁺ cells (red cells) were present in the stroma (Figure 3.7A) and tumour cell islands (Figure 3.7B) of TS1 tumours.

The number of Ly-6G⁺ cells was counted per FOV (Figure 3.7C) and this was unchanged when comparing DOX and PBS treated tumours (Two way ANOVA treatment $p=0.5536$). The stroma of PBS treated tumours (mean= 15.7 ± 4.34) did not contain more Ly-6G⁺ cells than the tumour cell islands (mean= 11.05 ± 4.08 , Two way ANOVA area analysed $p=0.1754$). This was also true in DOX treated tumours (stroma mean= 21.45 ± 5.08 ; tumour cell island mean= 8.75 ± 4.2). The number of Ly-6G⁺ cells per FOV were then normalised to nuclei per FOV to determine Ly-6G⁺ density (Figure 3.7D), and again Ly-6G⁺ cell density was unaffected by DOX (Two way ANOVA treatment $p=0.3840$). The stroma of PBS treated tumours (mean= 2.84 ± 0.49) had an increased density of Ly-6G⁺ cells compared to tumour cell islands (mean= 0.47 ± 0.13 ; Two way ANOVA area analysed $p=0.0006$; Sidak's multiple comparisons test $p=0.0131$). The stroma of DOX treated tumours (mean= 3.46 ± 0.48) also had an increased density of Ly-6G⁺ cells compared to tumour cell islands (mean= 0.43 ± 0.20 ; Sidak's multiple comparison test $p=0.0041$).

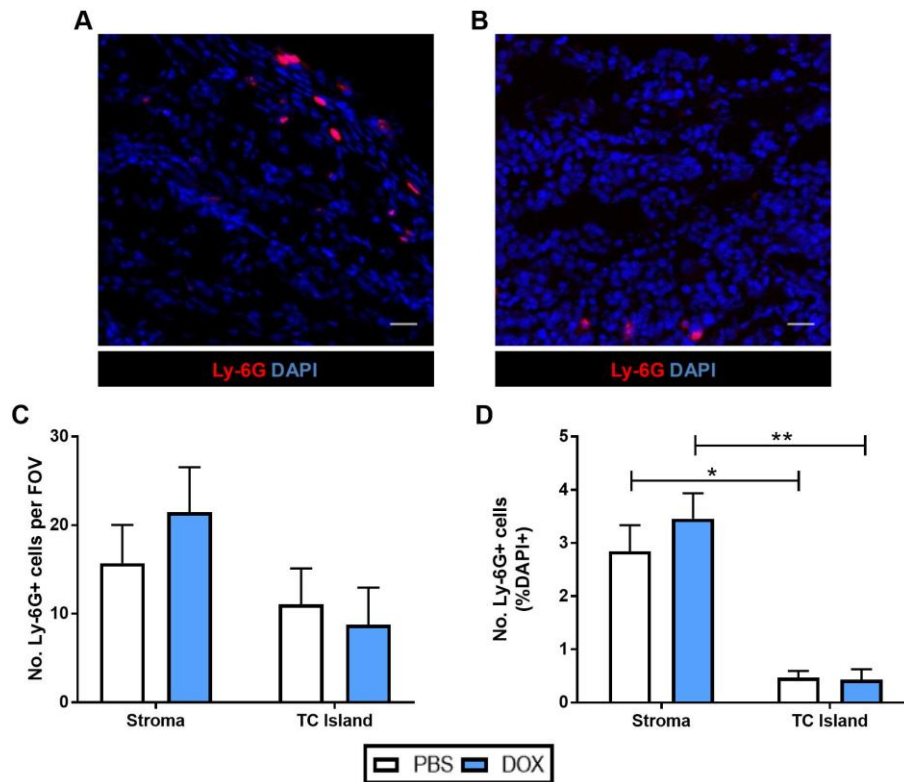


Figure 3.7 The density of Ly-6G⁺ neutrophils is increased in the stroma compared to the tumour cell islands of TS1 implant tumours.

Ly-6G⁺ cells (red) were identified within the stroma (A) and tumour cell islands (B) of TS1 implant tumours. Scale bar= 20µm. Total Ly6G⁺ cells were quantified per field of view (C) and normalised to the number of nuclei (D). *p<0.05; **p<0.01. (n=4 tumours).

3.4 Discussion

In PBS and DOX treated TS1 tumours, two morphologically distinct regions were present: more vascularised, normoxic stromal regions, and less vascularised, more hypoxic tumour cell islands. Interestingly, MRC1⁺ macrophages were more abundant in the former, suggesting their preference for accumulating and/or upregulating MRC1 expression in such vascularised areas in both PBS and DOX treated tumours.

After noting the different nuclear densities of the stroma and the tumour cell islands within these TS1 tumours, it was hypothesised that these two areas may have additional functional differences. Hypoxia was first examined within these two niches as TAMs were previously shown to accumulate in avascular and necrotic areas of breast tumours [78], suggesting that hypoxia may recruit TAMs. Indeed, hypoxia regulates the expression of molecules known to recruit TAMs such as CXCL12 and VEGF-A [208]. In these studies, hypoxia was not affected by DOX in TS1 tumours; however hypoxia was found to be restricted to the tumour cell islands, whereas the stroma remained normoxic.

As maintaining tissue oxygenation relies on functioning blood vessels [209], the vascularity of these two regions was then established. The percentage CD31⁺ area was increased in the stroma of both PBS and DOX treated TS1 tumours, compared to normoxic and hypoxic regions of the tumour cell islands. This increase in vascularity offered a possible explanation as to why the TS1 stroma was normoxic. DOX did not impact on the CD31 area in TS1 tumours, and it was therefore not surprising that tumour hypoxia remained equally unaffected by this treatment. The analysis of tumour blood vessels was carried out by analysing CD31 staining. Other markers of blood vessels include CD34 [139] and endomucin [210]. However, previous studies have often used CD31 as a reliable marker of the tumour vasculature in LLCs, 4T1s and in both transgenic and orthotopically implanted MMTV-PyMT tumours [137], [144]. Therefore, CD31 was used in these current studies. It would be interesting to compare

vascular staining of CD31, CD34 and endomucin in these TS1 tumours, to establish if there is heterogeneity in the expression of these markers by the tumour blood vessels. Only the CD31 area was analysed, rather than analysing the effect of DOX on vessel phenotype. Previous studies demonstrated that cyclophosphamide decreased the length of blood vessels in LLC tumours [144], however this parameter was not measured in these studies. It is possible that the effect of chemotherapy on the tumour vasculature depends on the type of drug, tumour and the time at which the drug was given.

Given the stroma was more normoxic and vascularised it was interesting that TAM density was increased in the stroma compared to areas of hypoxia within the tumour cell islands. This analysis used TAM density rather than raw numbers of TAMs, to account for the different numbers of nuclei in each region. Overall TAM infiltration, as assessed by the number of F4/80⁺ TAMs was unaffected two days after DOX treatment. However, unpublished studies demonstrated that these TS1 tumours do recruit TAMs and MRC1⁺ TAMs within seven days of DOX treatment (Hughes, unpublished); suggesting that this two day time point may be capturing the initial phases of the tumours responding to DOX.

In these TS1 tumours, MRC1⁺ TAMs were mainly located within the stroma of these tumours, suggesting a preferential location of MRC1⁺ pro-tumoural TAMs within the tumour stroma. Previous studies identified MRC1⁺ TAMs within both vascularised and hypoxic areas of untreated LLCs; however cyclophosphamide increased the number of MRC1⁺ TAMs within the normoxic regions of LLCs, but not the hypoxic regions [144]. This suggests that while MRC1⁺ TAMs may be found within hypoxic regions of tumours, they may be specifically recruited to vascularised areas following chemotherapy. In these studies, MRC1 expression was not examined in conjunction with PIMO staining, as the density of TAMs within hypoxic regions was much lower than the rest of the tumour. Moreover, MRC1⁺ TAMs were far more abundant within the normoxic stroma of these tumours, and were a rare occurrence within the tumour cell

islands, suggesting it was unlikely that these TAMs would reside in hypoxic areas of the TS1 tumours. In agreement with these studies, Carmona-Fontaine and colleagues recently demonstrated a spatial segregation of MRC1^{hi} TAMs within MMTV-PyMT tumours [209]. MRC1^{hi} TAMs were mainly found within normoxic regions of these tumours due to differential patterns of metabolites in the hypoxic and normoxic regions of these tumours [209].

Previous studies have shown that MHCII^{lo} TAMs, which also expressed higher amounts of MRC1, were found within hypoxic areas of TS/A tumours [68]. Moreover, hypoxia induced gene expression changes in human MDMs and murine BMDMs *in vitro*, increasing expression of *cxcr4* and *vegfa* amongst other genes [205]. However, more recently, TAMs isolated from less hypoxic tumours (grown in mice which were haplodeficient for the oxygen sensor PHD2) were shown to have similar expression of genes associated with an M2-skewed phenotype such as *mrc1* and *arginase-1* as TAMs isolated from their more hypoxic counterparts [185]. Moreover, ablation of the hypoxia-regulated transcription factors HIF1 and HIF2 in myeloid cells had no effect on the number of MRC1⁺ TAMs within hypoxic or normoxic areas of cyclophosphamide treated LLCs and did not impact upon their regrowth [144]. Therefore, the impact of tumour hypoxia on TAM phenotype is controversial and may be dependent on the model used.

Increased TAM infiltration has been recognised as a feature of poor prognosis in many types of cancer [77]. Studies have now investigated the importance of the spatial organisation of immune cells within breast tumours, which is interesting as the stroma of PBS and DOX treated TS1 tumours had increased densities of TAMs and MRC1⁺ TAMs compared to the tumour cell islands. One study revealed that increased intratumoural TAMs was significantly correlated with decreased disease-free survival in breast cancer patients, and this trend was also true for stromal TAMs, although it was not significant [211]. Conversely, another study demonstrated that breast tumours with an increased density of CD163⁺ TAMs in the tumour stroma were of a higher grade and

more proliferative (as indicated by Ki67 staining), whereas the density of these TAMs in the tumour cell islands did not correlate with any clinicopathological features [212]. Decreased overall survival was also correlated with increased CD163⁺ TAMs in the tumour stroma, yet the presence of these TAMs in the tumour cell islands had no impact on survival [212]. Potentially, the differences between these two studies could be due to differences in TAM detection, as one paper examined CD68⁺ TAMs whereas the other examined TAMs expressing the M2-marker CD163. Further studies in breast cancer demonstrated that increased stromal, but not intratumoural TAMs was correlated with increased tumour grade [213]. Interestingly, tumours with increased numbers of intratumoural TAMs were more likely to have an increased microvascular density, suggesting these TAMs have roles in angiogenesis [213]. This study indicates that TAMs within different tumour microenvironments may have different phenotypes and tumour-promoting functions. Taken together, these studies highlight the importance of characterising niches within tumour microenvironment, as this may have prognostic significance for patients.

As DOX was previously reported to increase the infiltration of immature 7/4⁺ myeloid cells in MMTV-PyMT tumours [137], it was important to examine the effect of DOX on immature myeloid cell infiltration in TS1 tumours. 7/4 staining was attempted on the tumours used in the current study, however it was not successful, so Gr-1 and Ly-6G were instead used as markers of immature myeloid cells (as these staining protocols had previously been optimised in my supervisor's research group). Using Gr-1 as a marker of neutrophils and monocytes, it was clear that DOX did not increase Gr-1⁺ cells within tumours. This contrasted with Nakasone and colleagues who showed an increase in CD11b⁺ 7/4⁺ Gr-1⁺ cells in transgenic MMTV-PyMT tumours 48 hours after DOX treatment [137]. However, this was measured in dissociated tissues by flow cytometry and these TS1 studies used immunofluorescence. Moreover, previous studies used 7/4, a monocyte/neutrophil marker not used in the TS1 model, and Gr-1 was used as a marker instead [137].

Immature myeloid cells have been previously recognised as cells which may impact on the tumour response to chemotherapy [137]. One such study showed that 7/4⁺ cells limit vascular permeability with MMP-9, which results in the decreased efficacy of DOX in MMTV-PyMT tumours [137]. Another study showed that MDSCs (immature CD11b⁺ Gr-1⁺ cells) secrete cathepsin B and IL-1 β to limit the efficacy of 5-fluorouracil in EL4 tumour bearing mice [214]. Other studies suggest different chemotherapy drugs may have beneficial effects on the phenotype of MDSCs [136]. For instance, docetaxel was shown to reduce the number of MDSCs in the spleen of 4T1 tumour bearing mice, and skew these cells towards an M1-like phenotype demonstrated by their increased expression of iNOS and CCR7, and reduced MRC1 expression [136]. While DOX did not affect the number of Gr-1⁺ cells within TS1 tumours, the effect of DOX on the phenotype of these cells themselves, e.g. do they produce cathepsin-B in a manner similar to MDSCs in EL4 tumours [214], was not examined, as this was outside the scope of the project. Future studies could examine these cells in more detail to understand their function within TS1 tumours, and how these cells may influence tumour regrowth.

Interestingly, these data in this chapter show that, in both PBS and DOX treated tumours, Gr-1⁺ cells are located in increased numbers in the stroma of TS1 tumours compared to the tumour cell islands. Previously, studies demonstrated that increased numbers of circulating MDSCs were associated with increased tumour stage in breast cancer patients [215]. Stage IV breast cancer patients with an increased metastatic burden had significantly increased numbers of MDSCs [215]. In another study, pre-operative breast cancer patients had increased circulating MDSCs compared to healthy controls, and stage IV patients with more circulating MDSCs were found to have worse overall survival, than those with fewer MDSCs [216]. While the impact of circulating MDSCs has been established in patients, it would be interesting to see whether the spatial distribution of immature myeloid cells within patient tumours associates with

prognosis, as previously described for stromal and intratumoural TAMs, as this would also give some clinical significance to our findings within the TS1 tumours [211]–[213].

As Gr-1 is also expressed by neutrophils, Ly-6G was then examined within these tumours to understand if they made a significant contribution to the immune cell infiltrate of TS1 tumours. Unsurprisingly, there were fewer Ly-6G⁺ cells within these tumours, compared to the Gr-1⁺ cells, although this is probably because Gr-1 is expressed by immature myeloid cells, such as monocytes, and not just neutrophils. Like the Gr-1⁺ cells, the presence of Ly-6G⁺ cells were not affected by DOX, but they were also found to be at an increased density within the stroma of the TS1 tumours compared to tumour cell islands.

3.5 Concluding remarks

Both PBS and DOX-treated TS1 tumours were divided into distinct stromal areas and tumour cell islands, summarised in Figure 3.8. The stromal areas were more heavily vascularised, less hypoxic and contained an increased density of TAMs. Moreover, MRC1⁺ TAMs were found mainly within the stromal tumour areas, suggesting that the stroma may recruit, retain and/or educate TAMs to become MRC1⁺. As the stroma of TS1 tumours is highly vascularised, future studies should investigate the relationship between MRC1⁺ TAMs and the vasculature, by characterising whether DOX impacts on the number and/or phenotype of PV TAMs.

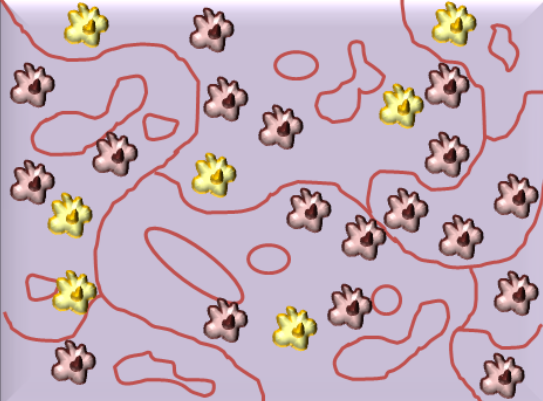
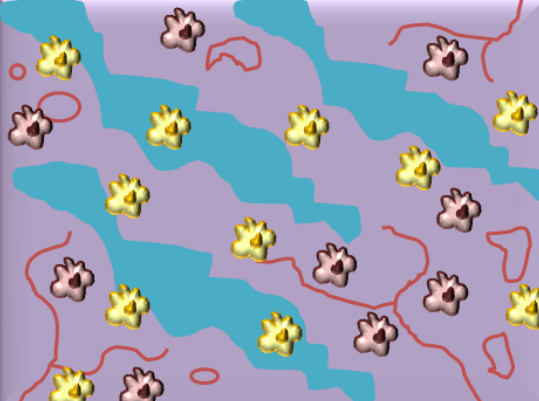




<u>Stroma</u>	<u>Tumour Cell Island</u>
	
<ul style="list-style-type: none"> • Negligible hypoxia • Increased vascularity • Increased MRC1⁺ TAM density 	<ul style="list-style-type: none"> • Increased hypoxia • Decreased vascularity • Decreased MRC1⁺ TAM density
<p><u>Key</u></p> <div style="display: flex; justify-content: space-around;"> <div style="display: flex; align-items: center;">  MRC1⁻ macrophage </div> <div style="display: flex; align-items: center;">  Blood vessels </div> </div> <div style="display: flex; justify-content: space-around; margin-top: 10px;"> <div style="display: flex; align-items: center;">  MRC1⁺ macrophage </div> <div style="display: flex; align-items: center;">  Hypoxia </div> </div>	

Figure 3.8 Summary of differences between stromal and tumour cell island components of TS1 tumours.

The stroma of TS1 tumours was normoxic and had an increase in vascular density. Tumour cell islands were more hypoxic (blue areas) and had fewer blood vessels. TAMs had an increased density in the stroma, and MRC1⁺ TAMs (red cells) were mainly found within the stroma.

Chapter 4

Characterisation of the PV niche in TS1 mammary tumours: *effects of DOX*

4.1 Introduction

In Chapter 3, MRC1⁺ TAMs were shown to be present at a higher density in the well vascularised, oxygenated stroma than in the less vascularised tumour cell islands in TS1 tumours. This was the case in both PBS and DOX-treated tumours. As this TAM subset accumulated in such highly vascularised areas, their direct contact with blood vessels was then investigated. For this, the density of PV TAMs (i.e. TAMs directly abutting the abluminal surface of CD31⁺ blood vessels) was then investigated in both PBS and DOX-treated tumours. This was considered to be of potential functional relevance in TS1 tumours because, as mentioned previously, a recent study showed that such PV TAMs are increased in LLCs treated after cyclophosphamide treatment, and stimulate subsequent tumour regrowth [144]. However, neither their density, origin nor regulation in the PV niche has been investigated in TS1 tumours, to date.

So in this chapter, an attempt was made to quantify their abundance in this type of tumour after exposure to PBS or DOX. Consideration was also given here to the possible origin of these PV cells. Understanding this could lead to the development of new strategies to target the precursors of these PV TAMs in the bloodstream or tumour. While some of the chemokine pathways that attract monocytes into mouse tumours after chemotherapy have been identified (e.g. CSF1 [109] CCL2 [137] and CXCL12 [144]), it is not known whether PV MRC1⁺ TAMs are derived from the recruitment of peripheral blood monocytes (generally or a specific subset), or the local proliferation of TAMs, monocytes or HSCs. One study attempted to address this by injecting BrdU into mice bearing LLCs following their exposure to cyclophosphamide. This showed that TAMs failed to proliferate in this tumour model, nor was there an increase in HSC numbers or any signs of HSC proliferation. This suggests that MRC1⁺ TAMs were likely to be derived from newly recruited peripheral blood monocytes in LLCs [144].

As PV TAMs are in direct contact with blood vessels it is highly likely that the tumour vasculature contributes to their recruitment, retention and phenotype in the PV niche. Indeed, when it comes to the latter of these, there is evidence that endothelial cells can regulate the phenotype of TAMs, even in the absence of chemotherapy. For example, one study showed that *in vitro*, macrophages co-cultured with endothelial cells develop an M2-skewed phenotype, with increased expression of MRC1, TIE2 and arginase-1 [186]. There is also indirect evidence that this phenomenon may occur *in vivo*. For example, agents which alter the vasculature of tumours (e.g. low-dose VEGFR2 inhibitors, overexpression of HRG by tumour cells, and dual inhibition of angiopoietin-2 and VEGF signalling) have been shown to reduce the tumour-promoting phenotype of TAMs [30], [176], [177], [180]. So, the possible effects of DOX on the tumour vasculature (i.e. vessel size, pericyte coverage and vessel patency) were also examined in TS1 tumours to see if these might have impacted upon the recruitment/phenotype of TAMs accumulating in the PV niche after DOX.

Tumour blood vessels are more chaotic, have less pericyte coverage, are more permeable, and carry less regular blood flow than those in normal tissues [217]. Moreover, the tumour vasculature has a completely different structure to the hierarchy of vessels within healthy tissues [217]. In healthy tissues, arteries typically branch into smaller arterioles, which then form capillaries. These capillaries then deliver blood to the surrounding tissue before developing into a network of venules and veins. This is not the case in malignant tumours, as tumour blood vessels lack this structure, and can be identified and categorised as listed in Table 4.1 [217]. These vessel types include 'mother vessels', which can develop into other vessel types including capillaries, glomeruloid microvascular proliferations and vascular malformations which are best recognised on the basis of their morphological features (Table 4.1).

The perfusion of tumour blood vessels is often heterogeneous, with some vessels carrying flow, and others not [217], [218]. One method used to investigate

vessel patency is the perfusion of the vasculature with FITC-lectin, as only flow-carrying vessels are then seen as FITC-lectin⁺ in frozen sections of tumours [137].

Vessel type	Morphological features
Mother vessel	Enlarged hyperpermeable vessels with a degraded basement membrane – first vessel type to develop from pre-existing blood vessels
Capillary	Similar to capillaries found in healthy tissues, usually with a diameter of around 10µm
Glomeruloid microvascular proliferation	Clusters of microvessels which are encased within a poorly organised basement membrane of multiple layers and sporadic pericyte coverage
Vascular malformation	Large vessels coated in a thin layer of smooth muscle cells which are not permeable to macromolecules

Table 4.1 Vessel types found within the abnormal tumour vasculature [217].

The structure of the tumour vasculature differs from that of normal tissues, as tumours do not have the typical arrangement of arteries-arterioles-capillaries-venules and veins. Instead their vessels may be categorised as described above.

Pericyte coverage could also impact on monocyte recruitment into tumours after chemotherapy. These are PV, contractile cells, thought to regulate vessel stability [219]. Pericyte coverage of vessels varies, with more immature, proangiogenic vessels having fewer pericytes than mature, quiescent ones [217], [219], [220]. Current evidence for the effect of pericyte coverage on leucocyte recruitment is conflicting. In murine pancreatic tumours, increased pericyte coverage was associated with increased cytotoxic T cell infiltration, although this study did not examine TAM infiltration [221]. However, other studies have shown leucocyte extravasation occurs at areas of the endothelium not covered in pericytes, suggesting they may impede leucocyte recruitment [222]. In LLCs and B16 tumours, depletion of pericytes resulted in the increased infiltration of immature CD11b⁺ Gr-1⁺ myeloid cells [223].

Recent studies have also focussed on the possible role of high endothelial venules (HEVs) in leucocyte trafficking into tumours. These are specialised vessels characterised by their expression of the protein, peripheral node addressin (PNA_d) [224]. The expression of PNA_d aids the adhesion and rolling of leucocytes in the bloodstream, and HEVs have been shown to be essential for the extravasation of

lymphocytes into lymph nodes [225]. More recently, HEVs have been reported within human breast carcinomas and in Treg-depleted murine fibrosarcomas [226], [227]. T cells are an important feature of tumours, as breast cancer patients with high CD8⁺ cytotoxic T cell densities and low CD4⁺ T cell and CD68⁺ TAM densities have greater recurrence-free survival [109]. Regulatory CD3⁺ CD4⁺ FOXP3⁺ T cells are immunosuppressive and mediate immune escape by mechanisms such as IL-10 production and expression of checkpoint molecules, like CTLA-4, which trigger the inactivation of T cells [105]. Previously, TAMs have been shown to suppress T cell responses in tumours [108], [109], and as HEVs are known to affect T cell infiltration, it was deemed important to establish whether HEVs are present in TS1 tumours, and whether this is altered after DOX treatment. In addition to this, certain chemotherapies have been shown to affect T cell infiltration in murine tumour models [228]. For example, DOX increased the proportion of T cells which were CD8⁺ which infiltrated mammary tumours (OVA expressing AT3 cells) grown subcutaneously [229]. Therefore, the infiltration of T cells within TS1 tumours was also examined.

While it is clear that vascular normalising doses of anti-angiogenic drugs are capable of inducing changes in the tumour vasculature, for example by increasing pericyte coverage and improving vessel functionality [230], few studies have studied whether chemotherapy also has this effect. One study demonstrated that cyclophosphamide did not affect FITC-lectin perfusion of MMTV-PyMT tumours [139]. Another study showed DOX did not affect pericyte coverage of cardiac microvessels in non-tumour bearing mice [231]. Interestingly, some chemotherapy drugs have been shown to inhibit angiogenesis *in vitro* [232], and *in vivo* cyclophosphamide was shown to reduce blood vessel length in LLCs [144]. However, this is controversial as other reports show that both DOX and docetaxel had no effect on microvascular density in stage II and III human breast carcinomas [233]. Conversely, another study showed that treatment with anthracyclines or taxanes actually increased the microvascular density of breast tumours [234]. Therefore, the effect of chemotherapy on tumour blood

vessels could depend on the type of drug used and/or tumour being treated. It will therefore be interesting to examine the effects of DOX on the tumour vasculature of TS1 tumours.

It was therefore hypothesised that DOX would increase the number of MRC1⁺ TAMs in the PV niche (i.e. those making direct contact with blood vessels) of TS1 tumours. Then, changes in the peripheral blood monocytes of such mice were analysed to see if this highlighted one or more monocyte subsets that could have been the precursors for PV MRC1⁺ TAMs. The maturity of MRC1⁺ TAMs in the PV niche was also compared in PBS and DOX-treated TS1 tumours to see if they were immature, newly recruited monocytes/TAMs. Finally, the effect of DOX on vessel size, patency and pericyte coverage was investigated in these tumours.

4.2 Methods

4.2.1 Immunofluorescent staining of tumours

TS1 tumours were grown in mice and treated, as described in section 2.2.3 and prepared for analysis as in section 2.2.4. Tumours were snap frozen in OCT and 14µm sections cut and stained as described in section 2.2.9, using the antibodies listed below in Table 4.2. It is important to note that when both unconjugated rat antibodies and conjugated rat antibodies were used on the same sections, the blocking solution did not contain murine FcR block, as the secondary antibody would have bound to this.

Antibody	Fluorophore	Clone	Conc (µg/mL)
Goat (p) Anti-Rabbit IgG	AlexaFluor555		10
Goat (p) Anti-Rat IgG	AlexaFluor647		10
Goat (p) Anti-Rat IgG	AlexaFluor488		10
Goat (p) Anti-Rat IgG	AlexaFluor555		4
Purified Rat (m) Anti-Mouse Gr-1	unconjugated	RB6-8C5	1
Rabbit (p) Anti- α-smooth muscle actin	unconjugated	ab5694	1
Rabbit (p) Anti-Mannose Receptor	unconjugated	ab64693	2.5
Rat (m) Anti-FOXP3	FITC	FJK-16s	5
Rat (m) Anti-Mouse CD3	AlexaFluor647	17A2	5
Rat (m) Anti-Mouse CD31	AlexaFluor647	MEC13.3	5
Rat (m) Anti-Mouse CD31	AlexaFluor488	MEC13.3	5
Rat (m) Anti-Mouse CD31	PE	MEC13.3	2
Rat (m) Anti-Mouse CD4	AlexaFluor488	GK1.5	5
Rat (m) Anti-Mouse CD4	PE	GK1.5	2
Rat (m) Anti-Mouse CD8α	PE	53-6.7	2
Rat (m) Anti-Mouse F4/80	AlexaFluor488	Cl:A3-1	2
Rat (m) Anti-Mouse Ly-6G	PE	1A8	4
Rat (m) Anti-Mouse MRC1	APC	C068C2	2
Rat (m) Anti-Mouse MRC1	PE	C068C2	2
Rat (m) Anti-PNAd	unconjugated	MECA-79	~10

Table 4.2 Antibodies used in the fluorescent staining of tumours.

(m) indicates monoclonal, **(p)** indicates polyclonal antibody. ~ indicates approximate concentration as the antibody was isolated from ascites.

4.2.2 Flow cytometric analysis of peripheral blood mononuclear cells

Blood was collected from TS1 tumour-bearing mice by flushing the circulation with 0.76% sodium citrate solution (as described in section 2.2.4). While preparing samples for flow cytometry, the peripheral blood samples were kept on ice, in the dark, and with

gentle agitation. Cells were prepared for flow cytometry as described in section 2.2.6, with the antibodies described below in Table 4.3. FACS analysis was performed using the BD LSR II Flow Cytometer. Flow cytometry files (FCS files) were analysed using FlowJo software.

Antibody	Fluorophore	Clone	Conc. (µg/mL)
Rat (m) Anti-CD11b	AlexaFluor488	M1/70	10
Rat (m) Anti-Mouse CXCR4	PE	2B11	4
Rat (m) Anti-Mouse Ly-6C	APC	HK1.4	4
Rat (m) Anti-Mouse Ly-6G	PerCP/Cy5.5	1A8	4
Rat (m) Anti-Mouse MRC1	Brilliant Violet 421	C068C2	2
Rat (m) IgG2a κ	PerCP/Cy5.5		4
Rat (m) IgG2a κ	Brilliant Violet 421		2
Rat (m) IgG2b κ	AlexaFluor488		10
Rat (m) IgG2b κ	PE		4
Rat (m) IgG2c κ	APC		4

Table 4.3 Antibodies and isotype controls used in the flow cytometric analysis of peripheral blood mononuclear cells. (m) = monoclonal antibody.

Isotype controls did not bind non-specifically to peripheral blood mononuclear cells; demonstrating antibody binding was specific, as shown by histograms in Figure 4.1. Histograms show the fluorescence of unlabelled (black) cells and cells incubated with the isotype control (blue). Importantly, the isotype control (blue) histograms do not show increased fluorescence compared to unlabelled samples.

FMO controls (described in section 2.2.7) were used to compensate for spectral overlap in samples and were used to set the gating strategy in these flow cytometry experiments, shown in Figure 4.2. 7 different fluorescent parameters were measured in this experiment, some of which had spectral overlap, therefore FMO controls were the most appropriate control for gating samples.

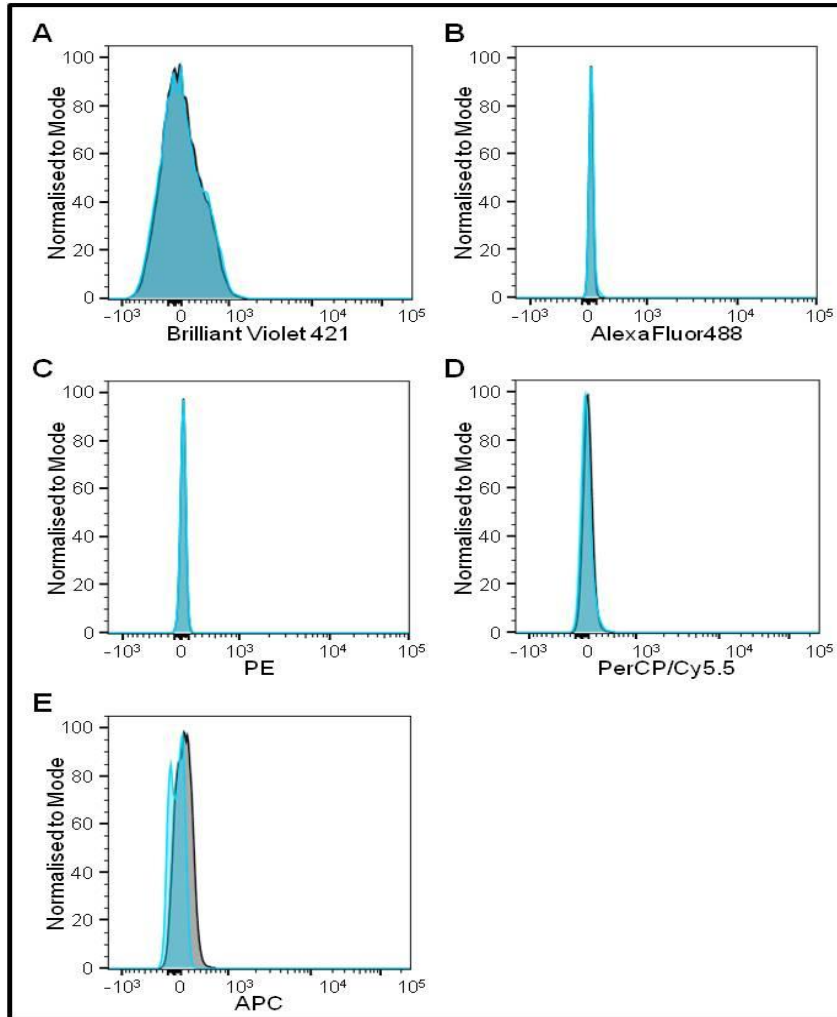


Figure 4.1 Isotype-matched controls do not bind to mouse PBMCs (indicating the specificity of primary antibodies used in the flow cytometric studies described here).

Peripheral blood was collected from FvB/N mice following cervical dislocation by flushing the circulation with 0.76% sodium citrate solution. Cells were then resuspended in FACS buffer and incubated separately with the appropriate isotype-matched IgG. Following staining, erythrocytes were lysed and peripheral blood mononuclear cells were then analysed using the LSR II. Forward scatter and side scatter profiles of the cells were used to eliminate any cell debris. Histograms show unlabelled cells (black) versus cells incubated with control IgGs conjugated to: Brilliant Violet 421 (blue; A); AlexaFluor488 (blue; B); PE (blue; C); PerCP/Cy5.5 (blue; D) and APC (blue; E).

The gating strategy used to identify peripheral blood mononuclear cells (PBMCs) was as follows: cells were selected on the basis of their side scatter-area (SSC-A) and forward scatter-area (FSC-A) profiles – Figure 4.2, gate 1. Single cells (Figure 4.2, gate 2) were then selected based on FSC-A and forward scatter-height (FSC-H). Cells which excluded the viability dye Zombie UV were selected as viable cells (Figure 4.2, gate 3). CD11b⁺ myeloid cells were then selected (Figure 4.2, gate 4). A small population of CD11b^{hi} cells were excluded from this analysis as it was thought these may be cells which had bound excess antibody as these were a low proportion of cells and had increased fluorescence compared to the main CD11b⁺ cell population. CD11b⁺ Ly-6G⁺ cells (Figure 4.2, black circular gate) were excluded from analyses as neutrophils express Ly-6G. Monocytes were therefore selected as CD11b⁺ Ly-6G⁻ (Figure 4.2, gate 5) side-scatter^{lo} cells (Figure 4.2 gate 6). Three monocytic subpopulations could be identified on the basis of their Ly-6C expression: Ly-6C^{lo} non-classical monocytes (Figure 4.2 gate 7a); Ly-6C^{int} intermediate monocytes (Figure 4.2 gate 7b) and Ly-6C^{hi} classical monocytes (Figure 4.2 gate 7c). Using this strategy, the monocytes, neutrophils and monocytic subpopulations were quantified within the peripheral blood of mice bearing TS1 tumours, 48 hours after treatment with either PBS or DOX. MRC1 and CXCR4 expression were also measured on the monocytes and the different monocytic subsets.

4.2.3 Preparation and staining of lymph nodes

Lymph nodes were dissected from healthy female FvB/N mice and frozen in OCT at -80°C. 14µm sections were cut using the cryostat and sections were stained as described in 4.2.1.

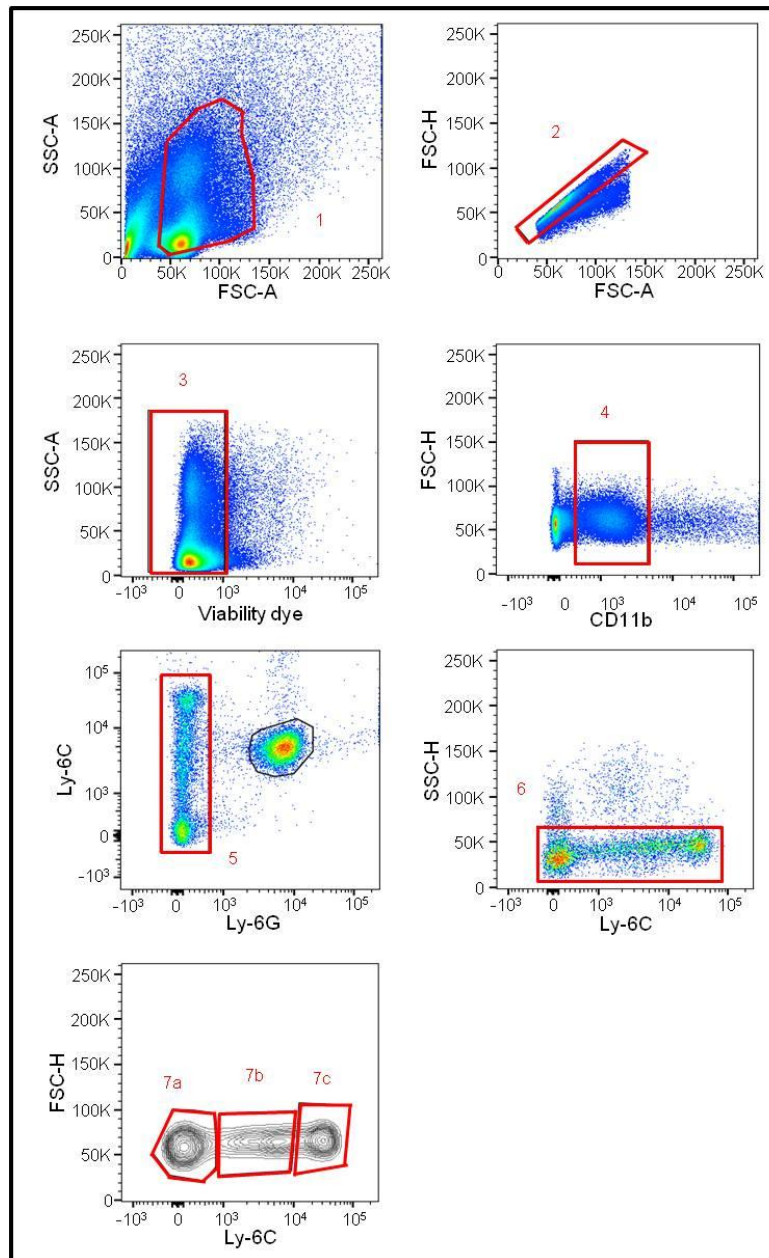


Figure 4.2 Gating strategy for the flow cytometric analysis of murine peripheral blood monocytes.

Cells were first gated using forward scatter and side scatter (1), and then forward scatter-height and forward scatter-area were used to select single cells (2). In order to set additional gates, FMO controls were used. Viable cells (cells unstained by the Zombie UV viability dye) were then selected (3), before gating on the CD11b⁺ myeloid cells (4). CD11b⁺ Ly6G⁺ neutrophils were excluded from this analysis (black circular gate) and CD11b⁺ Ly6G⁻ cells were then selected (red gate 5). As monocytes have a low side scatter profile, cells with a high side scatter were also excluded from the analysis (6). Based on their Ly-6C expression, three monocyte subsets were then identified: Ly-6C^{lo} non-classical monocytes (7a), Ly-6C^{int} intermediate monocytes (7b), and Ly-6C^{hi} classical monocytes (7c).

4.2.4 Image analysis

Fiji was used to analyse images and nuclei (DAPI⁺ events) were counted by the ITCN plugin [191] in the tumour cell islands or by the “Analyse particles” tool in the stroma (section 2.2.11). Images were taken using at 20x objective lens and at least 5 FOV were analysed per tumour. The cell counter plugin was used to mark cells which were positive for various markers [192].

CD31 area was calculated by converting the CD31 stain to binary (to apply a threshold) and then using Fiji's analyse particles tool which allowed the percentage of the region of interest covered by CD31 staining to be calculated.

When analysing the presence of HEVs within tumours, random fields of view did not capture HEVs, suggesting their presence was rare, so the Leica DMI4000B fluorescent microscope was used to scan the whole tumour using the 20x objective lens. 3 tumours per treatment group were scanned in this way.

4.2.4.1 Analysis of vessel patency

Mice bearing TS1 tumours were treated with PBS or DOX as described in section 2.2.3. 48 hours later mice were injected intravenously into the tail vein with FITC-lectin (1mg/mL, administered by Dr. Russell Hughes) and culled 10 minutes later. Post-mortem the circulatory system of the mice was flushed with 0.76% sodium citrate solution. The tumours were then prepared as described in section 2.2.4.

4.2.5 Isolation of BMDMs

BMDMs were isolated from healthy female FvB/N mice as described in section 2.2.2. HSCs were incubated with recombinant murine CSF1 on plastic for 7-14 days to allow macrophages to differentiate [189]. To analyse macrophages, they were removed from plastic by incubating with trypsin and the trypsin was neutralised with FCS once cells had detached.

4.2.6 Flow cytometric analysis of BMDMs

BMDMs were prepared as described in section 2.2.2. These cells were then suspended in FACS buffer and stained with the appropriate antibodies (as described in Table 4.4) and the viability dye Zombie UV (1 μ L in 200 μ L) for 40 minutes, rocking, sheltered from light and on ice. Samples were washed twice in FACS buffer before analysing samples on the LSR II flow cytometer and analysing files with FlowJo software.

Antibody	Fluorophore	Clone	Conc. (μg/mL)
Rat (m) Anti-Mouse CXCR4	PE	2B11	4
Rat (m) Anti-Mouse F4/80	PE/Cy7	BM8	4
Rat (m) Anti-Mouse MRC1	Brilliant Violet 421	C068C2	2
Rat (m) IgG2a κ	Brilliant Violet 421		2
Rat (m) IgG2a κ	PE/Cy7		4
Rat (m) IgG2b κ	PE		4

Table 4.4: Antibodies and isotype controls used in the flow cytometric analysis of BMDMs. (m) = monoclonal antibody.

4.3 Results

4.3.1 DOX significantly increases PV MRC1⁺ TAMs.

In order to assess PV TAMs, immunofluorescent staining of F4/80 (green), MRC1 (red) and CD31 (white) was carried out on sections of TS1 tumours as described in section 4.2.1. Representative staining of the stroma (Figure 4.3A) and tumour cell islands (Figure 4.3B) is shown. PV cells were cells in direct contact with CD31⁺ vessels, and normalised to the percentage area covered by CD31, to control for differing numbers of blood vessels in each FOV. The number of PV F4/80⁺ TAMs in the stroma (Figure 4.3C) was not altered by DOX treatment of tumours (PBS mean= 4.87 ± 1.34, DOX mean= 6.77 ± 0.64, unpaired t test p=0.1036). In contrast, the number of PV F4/80⁺ MRC1⁺ TAMs in the stroma was significantly increased in DOX treated tumours (mean= 5.14 ± 0.47) compared to those treated with PBS (mean= 2.40 ± 0.39, unpaired t test p=0.0010, Figure 4.3D).

In the tumour cell islands there was a non-significant trend for an increase in PV F4/80⁺ TAMs (Figure 4.3E) with DOX treatment (PBS mean= 20.82 ± 3.62, DOX mean= 27.98 ± 2.80, unpaired t test p=0.0731). Again, PV F4/80⁺ MRC1⁺ TAMs were significantly increased in the tumour cell islands of DOX treated tumours (mean= 8.24 ± 1.28) compared to PBS-treated tumour cell islands (mean= 4.10 ± 1.0, unpaired t test p=0.0178, Figure 4.3F). Therefore in both the stroma and tumour cell islands of TS1 tumours, DOX treatment significantly increases the number of PV MRC1⁺ TAMs compared to PBS treated tumours.

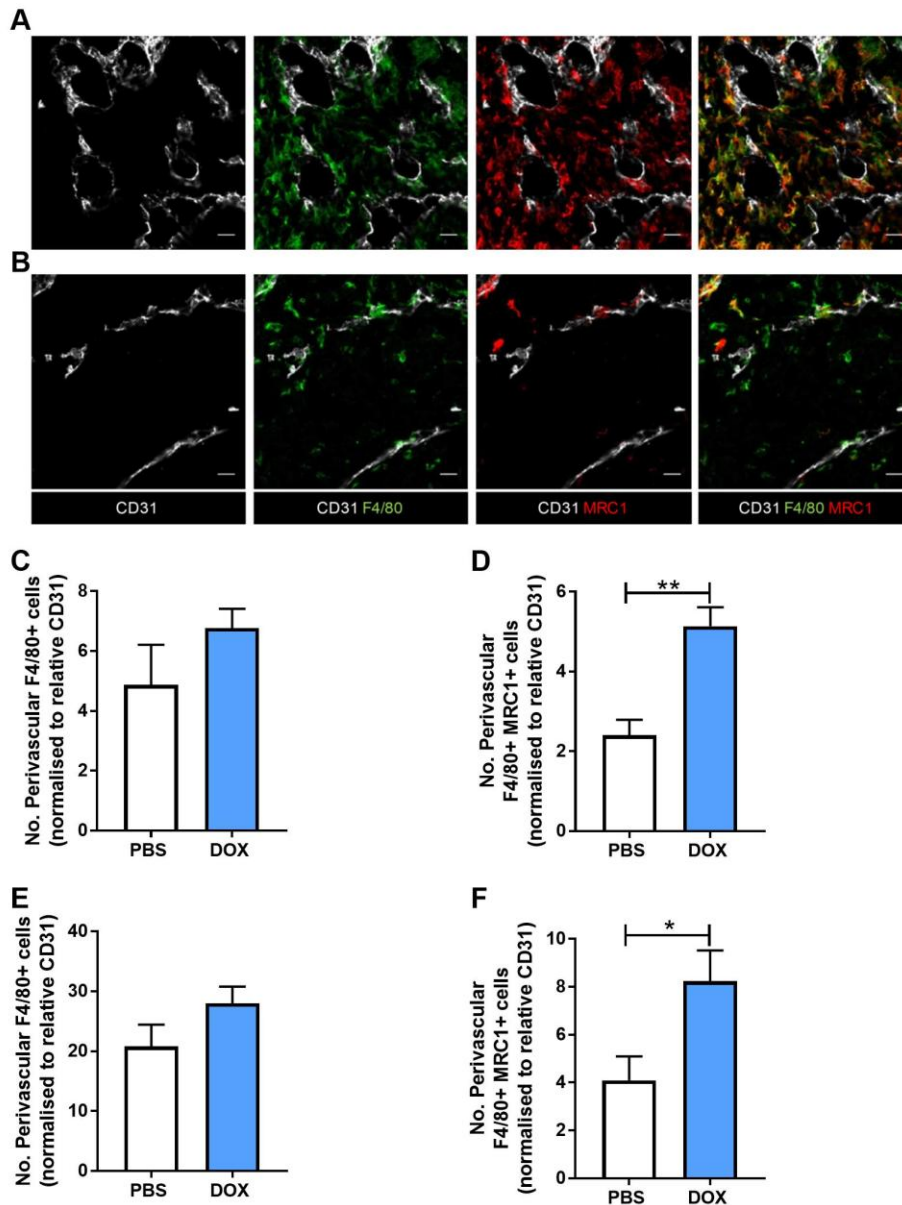


Figure 4.3 DOX increases the density MRC1⁺ TAMs in direct contact with CD31⁺ blood vessels in tumours.

Tumours were stained with anti-F4/80 (TAMs in green), anti-MRC1 (red) and anti-CD31 (white). Examples of stroma (A) and tumour cell island (B) staining are shown. Scale bar = 20 μ m. F480⁺ MRC1⁺ TAMs appear yellow in the far right merged images. PV TAMs i.e. F4/80⁺ cells in direct contact with a CD31⁺ blood vessel were scored and then normalised to the percentage of area covered by CD31 staining in the stroma (C) and the tumour cell islands (E). F4/80⁺ MRC1⁺ PV TAMs were counted and normalised to the percentage CD31⁺ area in the stroma (D) and the tumour cell islands (F). Unpaired t-test test used n=5 PBS tumours and n=6 DOX tumours. * p<0.05; ** p<0.001.

4.3.2 DOX depletes monocytes in TS1 tumour-bearing mice.

Given the PV increase in MRC1⁺ TAMs, the effect of DOX on the abundance and/or phenotype of peripheral blood monocytes was then investigated in TS1 tumour-bearing mice, as these could be a potential source of PV MRC1⁺ TAMs. As described in 4.2.2, peripheral blood cells were prepared for FACS and analysed using the gating strategy in Figure 4.2.

The proportion of monocytes (gated as single viable CD11b⁺ Ly6G⁻ Side-Scatter^{lo}, Ly6C⁺ cells, Figure 4.2 - gate 6) as a percentage of total myeloid cells (single viable CD11b⁺ cells, Figure 4.2 - gate 4) was significantly decreased in the blood of mice treated with DOX (mean= 30.50 ± 1.82, Figure 4.4B) compared to those treated with PBS (mean= 40.84 ± 3.20; unpaired t test p=0.0182). The proportion of neutrophils (gated as single viable CD11b⁺ Ly-6G⁺ cells, Figure 4.2 - black circular gate) out of the total myeloid cells was unaltered by DOX treatment in the blood of tumour bearing mice (PBS mean 50.93 ± 3.90, DOX mean 57.66 ± 2.48, Figure 4.4A; Unpaired t test p=0.1822).

Three monocytic subpopulations were analysed on the basis of their Ly-6C expression; Ly-6C^{lo} monocytes; Ly-6C^{int} monocytes and Ly-6C^{hi} monocytes. DOX did not significantly alter the proportions of these monocytic subpopulations in the blood of tumour bearing mice (Figure 4.4C). Two-way ANOVA revealed that while DOX did not impact on peripheral blood monocyte subpopulations overall (p=0.3553), some subpopulations were more abundant than others in both PBS and DOX treated mice (p<0.0001). Tukey's multiple comparisons test showed that in PBS treated mice, Ly-6C^{lo} monocytes (mean= 48 ± 4.5) were more abundant than Ly-6C^{int} monocytes (mean= 20.51 ± 1.21; p<0.0001) and Ly-6C^{hi} monocytes (mean= 25.43 ± 3.16; p=0.0007), although there was no significant difference in abundance of Ly-6C^{hi} monocytes and Ly-6C^{int} monocytes (p=0.6337). In DOX treated mice Ly-6C^{lo} monocytes (mean= 47.11 ± 4.02) were more abundant than Ly-6C^{int} monocytes (mean= 15.7 ± 2.14 p<0.0001) and Ly-6C^{hi} monocytes (mean= 32.3 ± 2.91 p=0.0398).

DOX treated mice had an increased abundance of Ly-6C^{hi} monocytes compared to Ly-6C^{int} monocytes (p=0.0197). The percentage of myeloid cells which were Ly-6C^{lo} (PBS mean = 20.32 ± 3.17, DOX mean = 14.52 ± 1.70), Ly-6C^{int} (PBS mean = 8.27 ± 0.70, DOX mean = 4.89 ± 0.88) or Ly-6C^{hi} monocytes (PBS mean = 9.84 ± 0.85, DOX mean = 9.64 ± 0.59) was also analysed (Figure 4.4D). DOX appeared to alter the proportions of these monocytic subpopulations (Two-way ANOVA p=0.0290), however post-hoc analysis revealed these trends were not significant (Sidak's multiple comparisons test Ly-6C^{lo} p=0.0528; , Ly-6C^{int} p=0.4023; Ly-6C^{hi} p=0.9997)

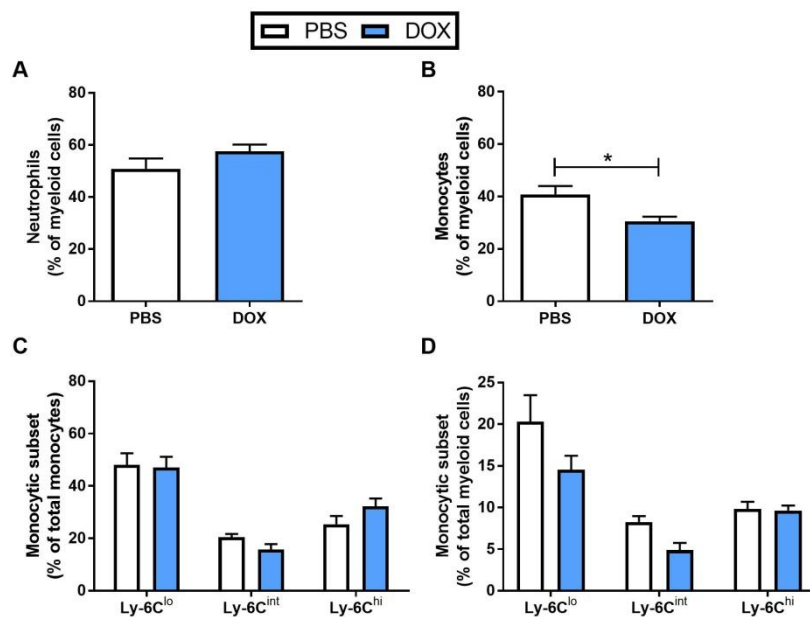


Figure 4.4 DOX significantly lowers the proportion of myeloid cells that are monocytes in the blood of TS1 tumour bearing mice.

FvB/N mice bearing orthotopic TS1 tumours were treated with PBS or DOX (as described in section 2.2.3.) 48 hours later, mice were culled and their peripheral blood collected. The percentage of myeloid cells (CD11b⁺ cells) that were either: (A) neutrophils (CD11b⁺ Ly6G⁺ cells) or (B) monocytes (CD11b⁺ Ly6G⁻ Side-Scatter^{lo}, Ly6C⁺ cells) were assessed. The percentage of total monocytes (CD11b⁺ Ly6G⁻ Side-Scatter^{lo}, Ly6C⁺ cells) that were Ly-6C^{lo}, Ly-6C^{int} or Ly-6C^{hi} was also assessed (C) The percentage of total myeloid cells (CD11b⁺ cells) that were Ly-6C^{lo}, Ly-6C^{int} or Ly-6C^{hi} was also assessed (D). * p<0.05 (PBS n=8 mice; DOX n=7 mice).

4.3.3 DOX slightly increases the abundance of MRC1⁺ monocytes in murine peripheral blood.

As described in section 4.2.2, whole blood was labelled with fluorescent antibodies and analysed using the LSR II. Peripheral blood monocytes were identified using the gating strategy in Figure 4.2 (see gate 6) and were CD11b⁺ Ly6G⁻ Side-Scatter^{lo}, Ly6C⁺ cells. The expression of the M2-skewed marker MRC1 [49] and the receptor CXCR4, known to be important in TAM recruitment [144], were then examined on the surface of monocytes. A small proportion of these monocytes were found to have surface MRC1 expression (Figure 4.5A & B). The proportion of monocytes that were MRC1⁺ was small (approximately 1%) but significantly increased following DOX treatment (mean = 2.34 ± 0.49) compared to monocytes from PBS treated mice (mean = 1.09 ± 0.17 ; unpaired t test $p=0.0240$). Two way ANOVA revealed that DOX had a significant effect on the proportion of MRC1⁺ monocytes within each subset ($p= 0.0395$, Figure 4.5C). When examining MRC1 expression on the monocytic subpopulations, only the Ly-6C^{lo} (PBS mean= 2.00 ± 0.21 ; DOX mean= 4.46 ± 0.91 ; Sidak's multiple comparisons test $p=0.017$) and Ly-6C^{int} subpopulations (PBS mean = 1.88 ± 0.37 ; DOX mean= 4.32 ± 0.89 ; Sidak's multiple comparisons test $p=0.0174$) had an increased proportion of MRC1⁺ cells after DOX treatment, compared to mice treated with PBS. Ly-6C^{hi} monocyte MRC1 expression was unaffected by DOX (PBS mean = 2.69 ± 0.48 ; DOX mean= 2.89 ± 0.52 ; Sidak's multiple comparisons test $p=0.9933$), suggesting differences in response to DOX may depend on the monocytic subset (Two way ANOVA interaction of subpopulation and treatment $p=0.0028$). Monocytic subsets had similar (not significantly different) proportions of MRC1⁺ monocytes within each subset in both PBS and DOX treated mice (Two way ANOVA subpopulation $p=0.4196$).

CXCR4 expression was also examined on monocytes, however the proportion of cells expressing CXCR4 was small (approximately 3%) and the same in PBS (mean= 2.97 ± 0.45) and DOX (mean= 3.36 ± 0.41) treated mice (unpaired t test $p=0.5306$, Figure 4.5D). Two way ANOVA revealed there was no significant difference

between percentage of CXCR4⁺ monocytes within the monocytic subpopulations in PBS and DOX treated mice ($p=0.1788$, Figure 4.5E). However, monocyte subsets had significantly different proportions of CXCR4⁺ monocytes, regardless of treatment (Two way ANOVA $p<0.0001$). PBS treated mice had an increased proportion of CXCR4⁺ monocytes in the Ly-6C^{lo} (mean= 4.93 ± 0.62) subpopulation compared to the Ly-6C^{int} (mean= 1.92 ± 0.36 ; Tukey's multiple comparison test $p<0.0001$) and Ly-6C^{hi} (mean= 0.63 ± 0.09 ; Tukey's multiple comparison test $p<0.0001$) subpopulations. The Ly-6C^{int} subpopulation also contained an increased proportion of CXCR4⁺ monocytes compared to the Ly-6C^{hi} subpopulation in PBS treated mice (Tukey's multiple comparison test $p=0.0311$). DOX treated mice also showed this pattern with an increased proportion of CXCR4⁺ monocytes in the Ly-6C^{lo} subpopulation (mean= 4.96 ± 0.53) compared to the Ly-6C^{int} (mean= 3.55 ± 0.69 ; Tukey's multiple comparison test $p=0.0272$) and Ly-6C^{hi} (mean= 1.33 ± 0.41 , Tukey's multiple comparison test $p<0.0001$) subpopulations. In DOX treated mice the Ly-6C^{int} subpopulation also contained an increased proportion of CXCR4⁺ monocytes compared to the Ly-6C^{hi} subpopulation (Tukey's multiple comparison test $p=0.0005$).

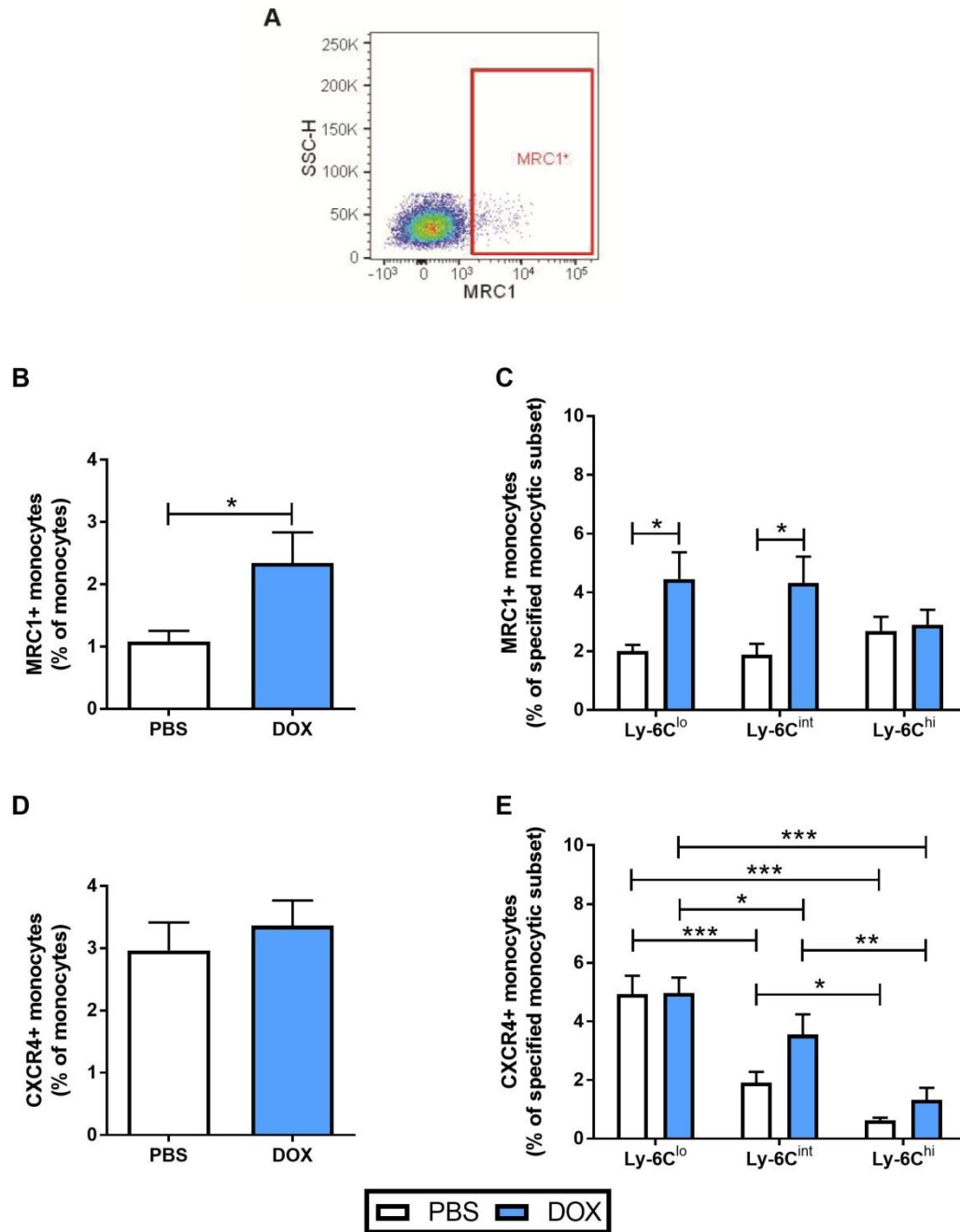


Figure 4.5 DOX increases the small proportion of MRC1⁺ monocytes in the peripheral blood of TS1 bearing mice.

FvB/N mice bearing orthotopic TS1 tumours were treated with PBS or DOX (as described in section 2.2.3.) 48 hours later, mice were culled and their peripheral blood collected by flushing the circulation with 0.76% sodium citrate solution. (A) Demonstrates there were a low number of peripheral monocytes expressing MRC1. The percentage of monocytes (CD11b⁺ Ly6C⁺ Side-Scatter low, Ly6C⁺ cells) expressing MRC1 (B) or CXCR4 (D) were measured. The expression of MRC1 (C) and CXCR4 (E) was then examined on the 3 monocytic subsets (based on the expression of Ly-6C – Ly-6C^{hi}, Ly-6C^{int} and Ly-6C^{lo}). * p<0.05; ** p≤0.001 and *** p≤0.0001 (n=8 PBS mice; n=7 DOX mice).

4.3.4 BMDMs express MRC1 and CXCR4.

As only a small proportion of peripheral blood monocytes were found to express MRC1 and CXCR4 (approximately 1% and 3% respectively), it was important to validate the antibodies used in these FACS analyses. To do this, BMDMs were also examined for their MRC1 and CXCR4 expression. BMDMs were isolated from healthy FvB/N female mice as described in section 2.2.2 and prepared for flow cytometry as described in section 4.2.6. FMO controls were used to set a gating strategy which is shown in Figure 4.6. Cells were first selected on the basis of their FSC and SSC profiles (gates 1 and 2) to exclude debris and identify single cells. Zombie UV viability dye was used to identify viable cells (gate 3), before using F4/80 as a marker of cells which were mature macrophages (gate 4). These F4/80⁺ cells clearly expressed MRC1 (gate 5a) and CXCR4 (gate 5b). Figure 4.6 shows MRC1 and CXCR4 are readily detected on BMDMs, thus validating the antibodies used to analyse their expression on mouse peripheral blood monocytes.

4.3.5 PV MRC1⁺ TAMs were mainly mature, Gr1⁻ cells.

As some peripheral blood monocytes were found to express MRC1, the maturity of PV MRC1⁺ cells was then assessed (i.e. to see if they could be newly recruited from MRC1⁺ monocytes in the blood). Initially it was planned to use Ly-6C, as immature myeloid cells express this marker, however staining revealed some Ly-6C expression on CD31⁺ blood vessels in TS1 tumours (Figure 4.7A, Ly-6C stained in white, CD31 in green), making it difficult to distinguish between PV MRC1⁺ Ly-6C⁺ cells and blood vessels expressing Ly-6C. For this reason Gr-1 was used as an alternative marker of immaturity, even though Gr-1 can be expressed by both monocytes and neutrophils. In order to rule out neutrophil staining, tumours were also stained with Ly-6G, which is exclusively expressed by neutrophils (section 4.3.6). Representative staining of stroma

(Figure 4.7B) and tumour cell islands (Figure 4.7C) are shown, with CD31 in green, MRC1 in red and Gr-1 in white.

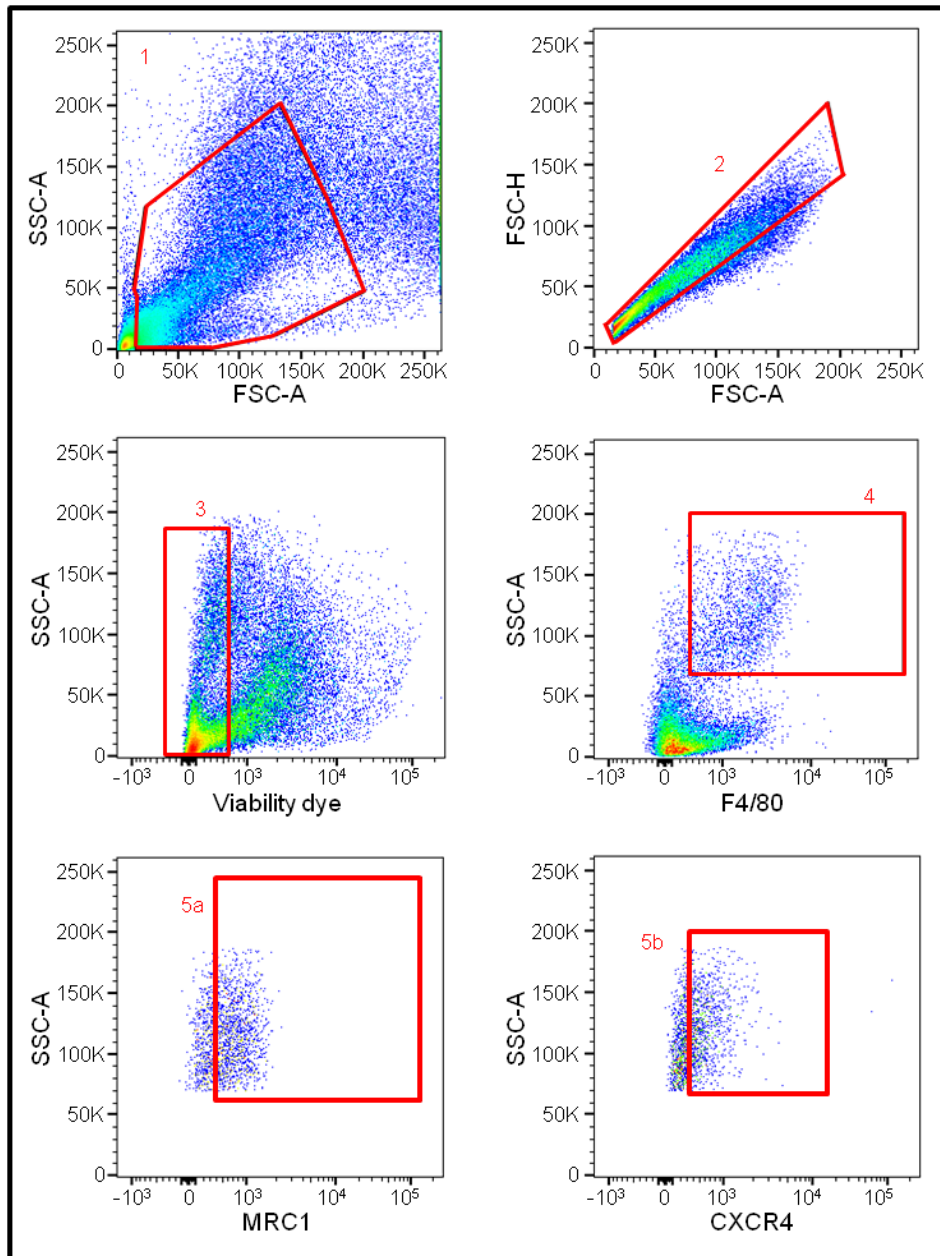


Figure 4.6 Analysis of MRC1 and CXCR4 on the surface of murine BMDMs.

Bone marrow was flushed from the bones of FvB/N mice and HSCs were cultured for 14 days with murine CSF1 to differentiate these cells into BMDMs. BMDMs were labelled with the appropriate antibodies before analysis using the LSR II. Cells were selected on forward scatter (FSC-A) and side scatter profiles (SSC-A)(1) and then singlets were gated using forward scatter height (FSC-H) and area (FSC-A)(2). Viable cells (cells unlabelled by Zombie UV) were then selected (3) and then F4/80⁺ macrophages were selected (4). Surface MRC1 (5a) and CXCR4 (5b) expression were then identified using flow cytometry.

PV MRC1⁺ Gr-1⁺ cells (i.e. cells in contact with CD31⁺ vessels) were counted and divided by the percentage of area covered in CD31 (Figure 4.7D). The stroma of PBS-treated tumours had significantly more PV MRC1⁺ Gr-1⁺ cells (mean= 2.54 ± 0.82) compared to tumour cell islands (mean= 0.28 ± 0.15, Two way ANOVA area analysed p=0.0037 with Sidak's multiple comparisons test p=0.0352). Likewise, DOX treated tumours had significantly more PV MRC1⁺ Gr-1⁺ cells in the stroma (mean= 3.13 ± 0.94) compared to tumour cell islands (mean= 0.84 ± 0.44, Sidak's multiple comparisons test p=0.0339). DOX did not increase the number of PV MRC1⁺ Gr-1⁺ cells (Two way ANOVA treatment p=0.4989), suggesting that while DOX increased numbers of PV MRC1⁺ cells; it did not affect numbers of PV immature MRC1⁺ cells.

The percentage of PV MRC1⁺ cells co-expressing Gr-1 was then calculated (Figure 4.7E). Of note, the majority of PV MRC1⁺ cells were Gr-1⁻ (approximately 75-80% of PV MRC1⁺ cells). In the stroma of PBS (mean= 22.83 ± 8.00) and DOX (mean= 26.1 ± 6.62) treated tumours there was an increased percentage of PV MRC1⁺ cells co-expressing Gr-1 compared to the tumour cell islands (Two way ANOVA area analysed p=0.0019, PBS mean= 4.56 ± 3.26 Sidak's multiple comparisons test p=0.0215, DOX mean= 6.86 ± 2.50 Sidak's multiple comparisons test p=0.0172). Furthermore, DOX did not affect the percentage of PV MRC1⁺ cells co-expressing Gr-1 (Two way ANOVA p=0.7067). In summary, the majority of PV MRC1⁺ cells were mature and did not express Gr-1. Moreover, DOX did not impact on the maturity of these PV MRC1⁺ cells.

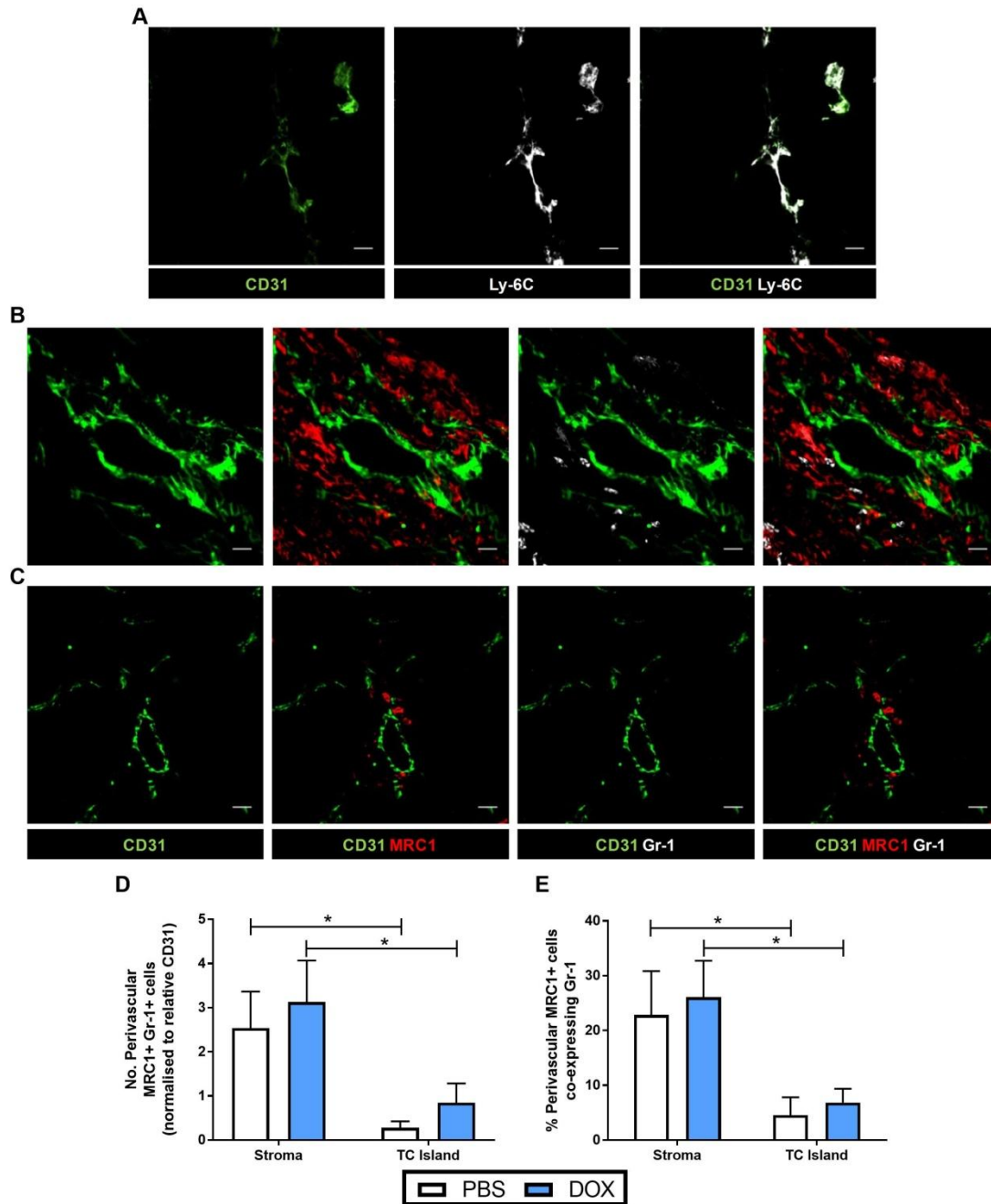


Figure 4.7 DOX did not alter the recruitment of immature PV MRC1⁺ Gr-1⁺ cells in TS1 tumours.

(A) Ly-6C (white) staining within tumours co-localised with CD31 (green), making it difficult to analyse whether or not a PV cell was truly Ly-6C⁺. Gr-1 (white) was used as a surrogate marker to assess maturity of MRC1⁺ (red) PV TAMs next to CD31 staining in green in the stroma (B) and tumour cell islands (C) Scale bar= 20µm. PV MRC1⁺ Gr-1⁺ cells were counted and normalised to percentage area covered with CD31 staining (D) and the percentage of PV MRC1⁺ TAMs co-expressing Gr-1 was calculated (E). Two-way ANOVA n=4 tumours/group * p<0.05.

4.3.6 The majority of PV MRC1⁺ TAMs were Ly-6G⁻.

In order to assess whether the small percentage of PV MRC1⁺ cells co-expressing Gr-1 were neutrophils, MRC1 (white) was co-stained with CD31 (green) and Ly-6G (red, a neutrophil marker) as described in 4.2.1. Representative staining of the stroma and tumour cell islands are shown in Figure 4.8A and 4.8B. PV MRC1⁺ Ly-6G⁺ cells were counted and normalised to percentage of area covered in CD31 staining, to account for different numbers of blood vessels in each FOV. Less than 4% of MRC1⁺ PV cells were Ly-6G⁺. There was a trend for an increase in PV MRC1⁺ Ly-6G⁺ cells in the stroma of PBS treated tumours (mean= 0.35 ± 0.19) compared to tumour cell islands (mean= 0.11 ± 0.08, Two way ANOVA area analysed p=0.0387), however post-hoc analysis revealed this was not significant (Sidak's multiple comparisons test p=0.5232). This was also true in DOX treated tumours (stroma mean= 0.65 ± 0.20, tumour cell island mean= 0.09 ± 0.05, Sidak's multiple comparisons test p=0.0777). DOX did not affect the number of PV MRC1⁺ Ly-6G⁺ cells (Figure 4.8C, Two way ANOVA treatment p=0.3724).

Importantly, the majority (approximately 95%) of MRC1⁺ PV cells were Ly-6G⁻, indicating they were unlikely to be neutrophils (Figure 4.8D). The stroma of both PBS (mean= 1.82 ± 0.91) and DOX (mean= 3.24 ± 0.61) treated tumours did not have significantly different percentages of PV MRC1⁺ cells co-expressing Ly-6G when compared to their tumour cell islands (PBS mean= 3.89 ± 2.89, DOX mean= 0.85 ± 0.50, Two way ANOVA area analysed p=0.9220). Therefore, the majority of PV MRC1⁺ cells were not Ly-6G⁺ and not neutrophils. DOX did not affect the percentage of MRC1⁺ PV cells which co-expressed Ly-6G (Two way ANOVA treatment p=0.6293). Therefore, the small percentage (approximately 25%) of PV MRC1⁺ cells which expressed Gr-1 were likely not Ly-6G⁺ and not neutrophils.

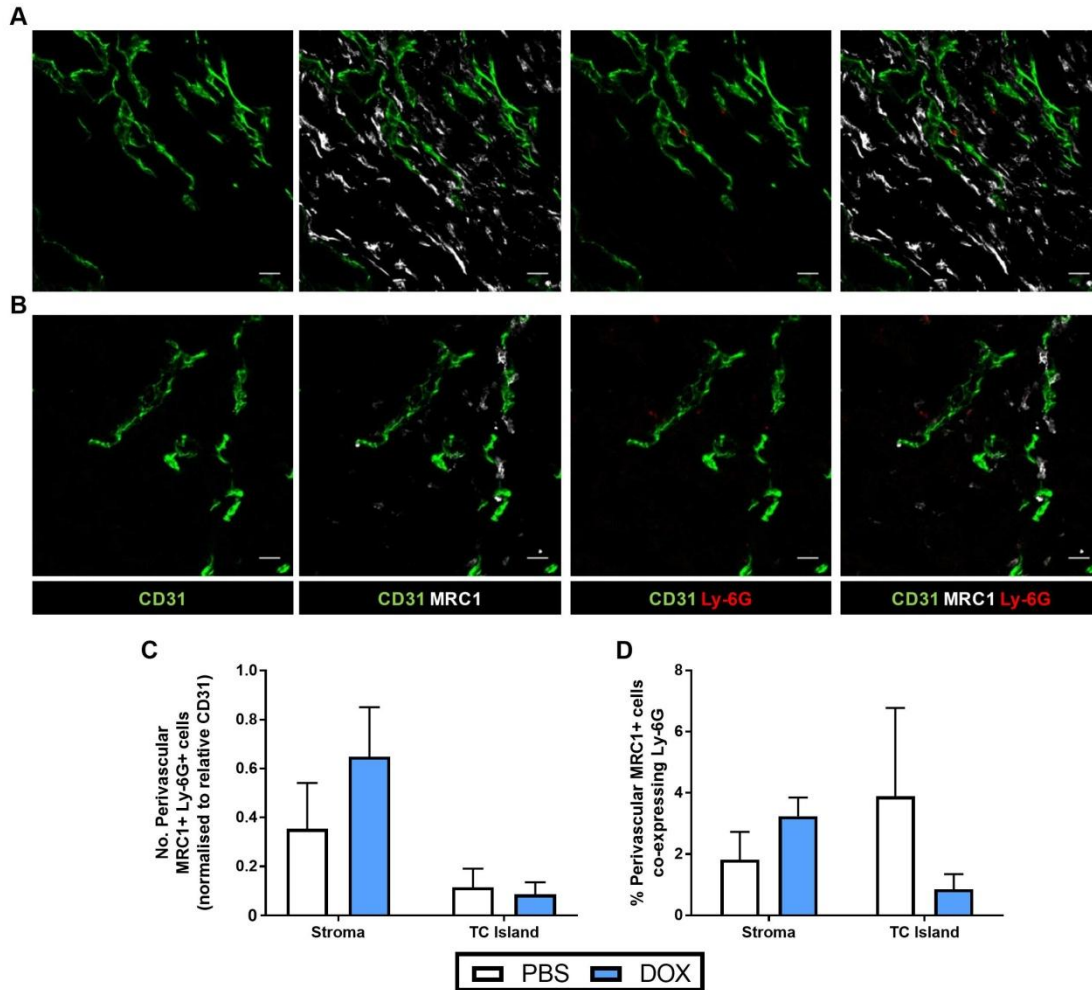


Figure 4.8 PV MRC1⁺ cells expressing Ly-6G were infrequent in PBS and DOX-treated tumours. Ly-6G (red) was stained alongside MRC1 (white) and CD31 (green) in the stroma (A) and tumour cell islands (B). Scale bar = 20 μ m. PV MRC1⁺ Ly-6G⁺ cells were counted and normalised to percentage area covered by CD31 staining (D) and the percentage of PV MRC1⁺ cells co-expressing Ly-6G was calculated (E). 2-way ANOVA. n=4 tumours/group.

4.3.7 CD31⁺ blood vessels had larger luminal areas in the stroma of TS1 tumours than those in the tumour cell islands.

It was thought possible that TAMs may gather around a particular size or type of blood vessel in TS1 tumours. As illustrated in Table 4.1, the tumour vasculature is different from that in healthy tissues, so it was not possible to use typical markers of arterioles and venules in this study. Lumen size was therefore used as a surrogate marker to distinguish between 'capillary-like' CD31⁺ blood vessels (<80 μm^2 - which equates to with a vessel diameter of <10 μm) and larger, non-capillary like CD31⁺ vessels with a lumen area >80 μm^2 [235]. The luminal area of tumour vessels was measured as described in section 2.2.11. First, the distribution of sizes of blood vessels in TS1 tumours was assessed. Figure 4.9 demonstrates the range of lumen sizes. In the stroma of PBS-treated tumours (Figure 4.9A), 37.5% of vessels had luminal areas in the range, 0-80 μm^2 , 56.25% (i.e. the majority of vessels) in the range, 80-1200 μm^2 , and 6.25% were over 1200 μm^2 . Similarly, in DOX treated tumours, 39.42% of vessels had luminal areas in the range, 0-80 μm^2 , 50.96% (i.e. the majority of vessels again) in the range, 80-1200 μm^2 , and 9.62% were over 1200 μm^2 .

In contrast to the stroma, in the tumour cell islands, no vessels had measurable luminal areas over 1200 μm^2 . In these areas of PBS treated tumours (Figure 4.9C), the majority of vessels (64.71%) had luminal areas in the range 0-80 μm^2 , with 35.29% of vessel lumens in the range, 80-1200 μm^2 . This was also true in DOX treated tumours (Figure 4.9D) with 66.7% vessels having a luminal area of 0-80 μm^2 , and 33.3% in the range of 80-1200 μm^2 .

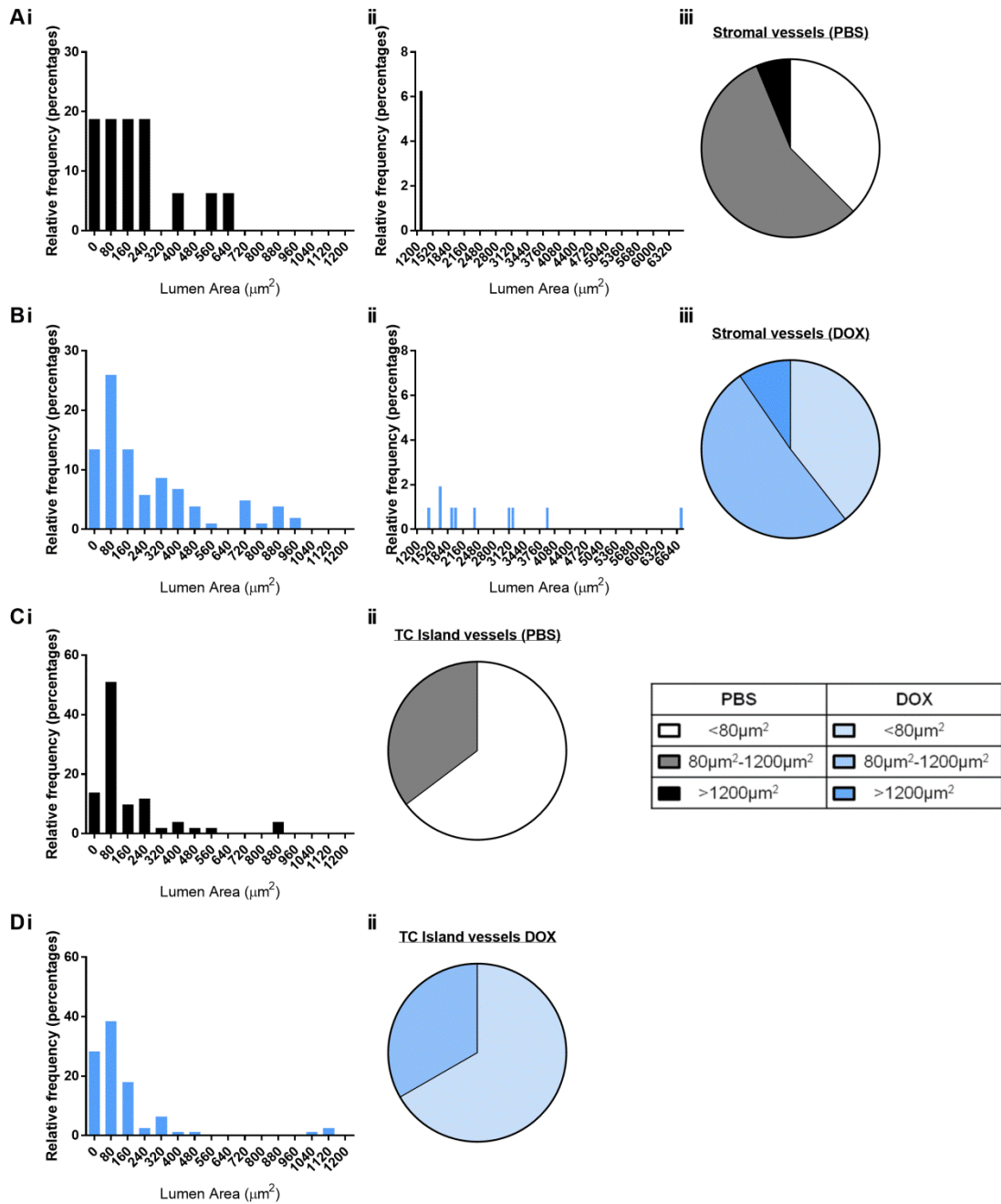


Figure 4.9 Analysis of vessel luminal area (restricted to vessels with a measurable lumen) within tumour cell islands and stroma of TS1 implant tumours, after PBS or DOX treatment.

CD31⁺ vessels within TS1 tumours with a visible lumen were categorised based on their luminal area. The distribution of lumen areas for the stroma of PBS (A) and DOX-treated (B) tumours is shown. A histogram shows the distribution of lumen areas for smaller vessels in (i) (vessels up to the size of 1200μm²; Ai & Bi) and larger vessels (with lumen areas >1200μm² Aii & Bii) and a pie-chart notes the contributions of these vessel sizes to the total vasculature (Aiii & Biii). The distributions of lumen areas within the tumour cell islands of PBS-treated (C) and DOX-treated tumours (D) are shown, with a histogram demonstrating the vessel distributions (Ci & Di) and pie charts noting the contribution of two vessel types to the overall vasculature (Cii & Dii). n=3 tumours per group.

4.3.8 The number of PV TAMs does not correlate with the luminal area of tumour blood vessels.

In order to investigate whether TAMs associate preferentially with vessels of a particular size in TS1 tumours - and whether DOX altered this - tumour vessels with a visible lumen were assessed for both their luminal area and number of PV F4/80⁺ TAMs attached per vessel. [N.B. Vessels which had no PV TAMs were excluded from this analysis].

First, the number of TAMs gathering around vessels of a particular type were counted, and then divided by the total number of TAMs gathering around all vessels analysed (to calculate the percentage of TAMs gathering around a particular subset of vessels). F4/80⁺ TAMs were found to be associated with vessels of a wide variety of sizes. In the stroma of PBS-treated tumours, only 11.48% of PV F4/80⁺ TAMs were found around smaller vessels (0-80 μm^2), and the majority (65.57%) were attached to vessels with a luminal area of 80-1200 μm^2 . Fewer (22.95%) associated with vessels with a larger lumen (>1200 μm^2 in size, Figure 4.10A). In the stroma of DOX treated tumours (Figure 4.10B), the majority of PV TAMs were again mainly (69.29%) located around vessels with lumen areas of 80-1200 μm^2 . There were more TAMs around vessels in the stroma of DOX-treated tumours with luminal areas of 0-80 μm^2 (18.21%) and fewer (12.5%) around vessels with a luminal area of >1200 μm^2 , compared to PBS-treated tumours. There was a significant (Chi-square test $p < 0.0001$) shift in the percentage of TAMs gathering around a particular size of vessel in DOX treated tumours. It appeared that DOX decreased the percentage of TAMs associated with larger vessels (>1200 μm^2) compared to PBS treated tumours, and also increased the percentage of TAMs around smaller vessels, 0-80 μm^2 (Chi-squared test $p < 0.0001$).

In tumour cell islands, PV TAMs were mainly found around vessels with a lumen area of 80-1200 μm^2 in PBS (71.43%, Figure 4.11A) and DOX (70.53%, Figure 4.11B) treated tumours. Fewer numbers of PV TAMs also associated with vessels

which had smaller lumen areas of 0-80 μm^2 in PBS (28.57%) and DOX (29.47%) treated tumours and there was no difference caused by treatment.

As the stroma contained more vessels of the 80-1200 μm^2 subtype, the number of PV TAMs counted was then normalised to the number of vessels within each group for the stroma (Figure 4.10C) and tumour cell islands (Figure 4.11C), to ensure that the increase in PV TAM association was not an artefact of there simply being an increase in vessel number.

In the stroma of PBS treated tumours, lumen size had no impact on the number of PV TAMs counted per vessel (0-80 μm^2 mean= 2.22 \pm 0.48, 80-1200 μm^2 mean= 3.11 \pm 0.60, >1200 μm^2 mean= 4.58 \pm 1.81, Two way ANOVA lumen size $p=0.1546$). This was also true in the stroma of DOX treated tumours (0-80 μm^2 mean= 1.91 \pm 0.21, 80-1200 μm^2 mean= 2.82 \pm 0.47, >1200 μm^2 mean= 3.1 \pm 0.71). Furthermore, DOX did not affect the number of PV TAMs per vessel in the stroma (Two way ANOVA treatment $p=0.3250$).

In the tumour cell islands of PBS treated tumours there were more PV TAMs per vessel in the 80-1200 μm^2 category (mean= 2.65 \pm 0.28), compared to those in the 0-80 μm^2 category (mean= 1.65 \pm 0.22, Two way ANOVA lumen size $p=0.0176$), however this was not significant (Sidak's multiple comparisons test $p=0.0640$). In DOX treated tumours, lumen area did not impact on the number of PV TAMs per vessel (0-80 μm^2 mean= 1.75 \pm 0.15, 80-1200 μm^2 mean= 2.29 \pm 0.33, Sidak's multiple comparisons test $p=0.3287$). DOX did not significantly change the number of PV TAMs gathering around a particular vessel type (Two way ANOVA treatment $p=0.6514$). After quantifying raw numbers of PV TAMs, it appeared there may be a preferential gathering of TAMs around vessels with a lumen area of 80-1200 μm^2 . However following normalisation of numbers of TAMs to the number of vessels counted, it became clear that PV TAMs do not preferentially gather around vessels of a particular size. DOX did not impact on the number of PV TAMs per vessel in this analysis,

matching with the previous analysis examining the total tumour vasculature (Figure 4.1).

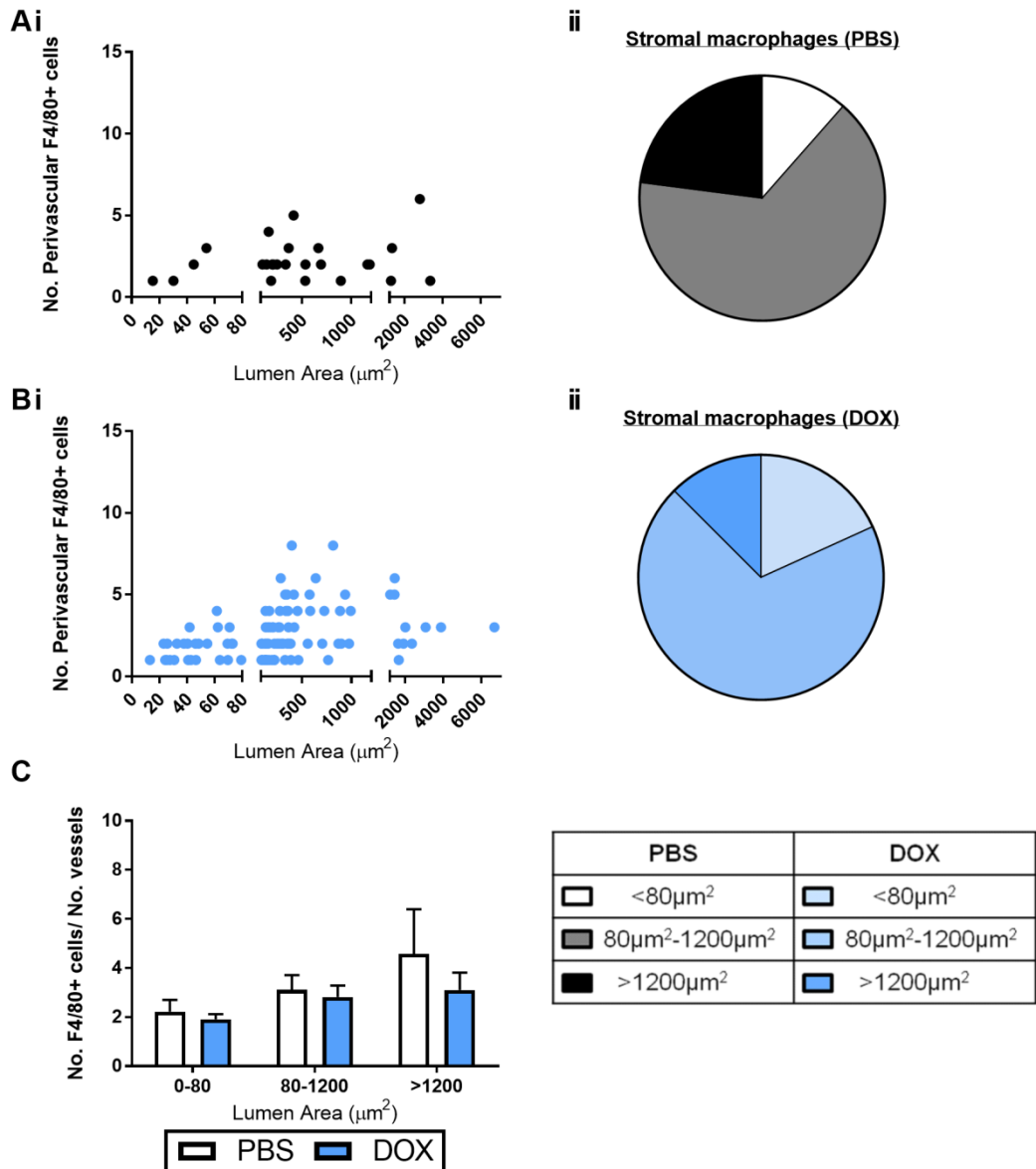


Figure 4.10 Analysis of the distribution of F4/80⁺ TAMs around vessels with a visible lumen in the stroma of TS1 tumours, after PBS and DOX treatment.

Individual vessel lumens were measured and then the number of PV F4/80⁺ TAMs were counted for each vessel. The distribution of PV TAMs around different sized vessels is shown for the stroma of PBS- (A) and DOX-treated (B) tumours, with a histogram demonstrating the number of TAMs attached to a vessel of a particular size (i) and a pie chart which shows the percentage of TAMs which lie in each vessel category (ii). The total number of PV TAMs per vessel category was then normalised to the total number of vessels in each category for the tumour stroma (C). 5 tumours/group; bar charts represent mean + SEM.

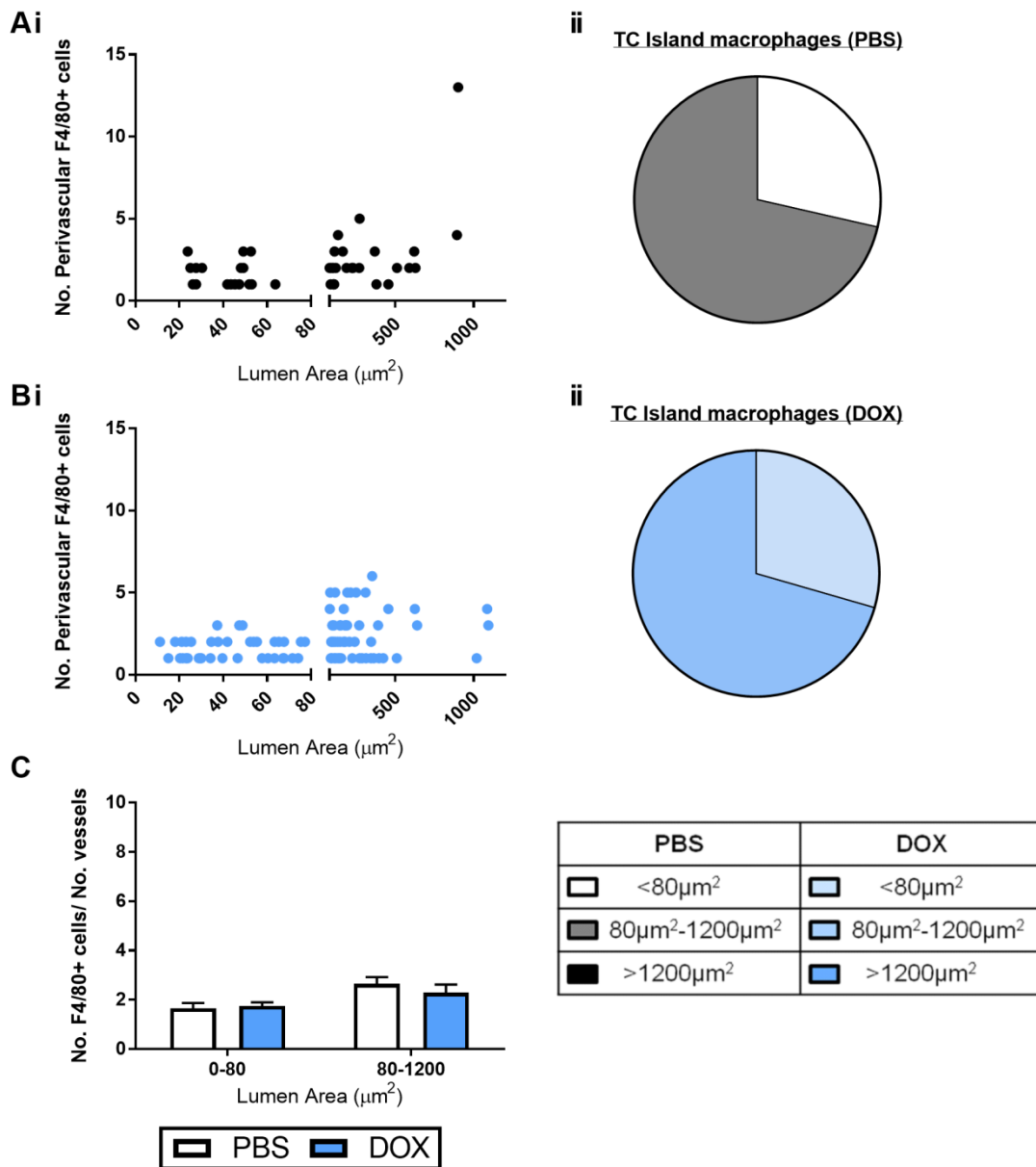


Figure 4.11 Analysis of the distribution of F4/80⁺ TAMs around vessels with a visible lumen in the tumour cell islands, after PBS or DOX treatment.

Individual vessel lumens were measured and then the number of PV F4/80⁺ TAMs were counted for each vessel. The distribution of PV TAMs around different sized vessels is shown for the tumour cell islands of PBS- (A) and DOX-treated (B) tumours, with a histogram demonstrating the number of TAMs attached to a vessel of a particular size (i) and a pie chart which shows the percentage of TAMs which lie in each vessel category (ii). The total number of PV TAMs per vessel category was then normalised to the total number of vessels in each category for the tumour cell islands (C) in PBS and DOX treated tumours. 5 tumours/group; bar charts represent mean + SEM.

4.3.9 Luminal area does not impact on the number of PV MRC1⁺ TAMs per vessel.

The numbers of F4/80⁺ MRC1⁺ TAMs around vessels with a measurable lumen were then counted per vessel to see if this subset of TAMs were gathering around vessels of a particular lumen size (Figures 4.12 and 4.13).

In the stroma of PBS treated tumours, 68.75% of PV F4/80⁺ MRC1⁺ TAMs were located around vessels with a lumen area of 80-1200 μm^2 (Figure 4.12A). F4/80⁺ MRC1⁺ TAMs were also found around vessels with a lumen area of 0-80 μm^2 (9.37%) and >1200 μm^2 (21.88%) in the stroma of these tumours. In the stroma of DOX treated tumours, most PV F4/80⁺ MRC1⁺ TAMs (73.85%) also gathered around vessels with a lumen area of 80-1200 μm^2 (Figure 4.12B), with 16.41% of PV F4/80⁺ MRC1⁺ TAMs found around vessels with a lumen area of 0-80 μm^2 and 9.74% were found around vessels with a lumen area of >1200 μm^2 .

In the tumour cell islands of both PBS- (Figure 4.13A) and DOX- (Figure 4.13B) treated tumours, the majority of PV F4/80⁺ MRC1⁺ TAMs were found around vessels with a lumen area of 80-1200 μm^2 (PBS= 70.83%, DOX= 64.81%). F4/80⁺ MRC1⁺ TAMs were also located around vessels with a lumen area of 0-80 μm^2 (PBS= 29.17%, DOX= 35.19%). While DOX appeared to increase the numbers of PV MRC1⁺ TAMs around vessels which were 0-80 μm^2 , it was then important to normalise the number of TAMs to the number of vessels counted, before concluding if DOX had an effect on vessels of a certain size.

As there were differences in the numbers of vessels for each category, it was then important to normalise the number of PV F4/80⁺ MRC1⁺ TAMs to the number of vessels in each size category, ensuring that increases in TAM numbers were not artefacts of increased numbers of vessels in a particular category. In the stroma of PBS treated tumours, lumen area did not impact on the number of PV F4/80⁺ MRC1⁺ TAMs per vessel (0-80 μm^2 mean= 1.67 \pm 0.88, 80-1200 μm^2 mean= 2.1 \pm 0.61, >1200 μm^2 mean= 2.83 \pm 1.52 Two way ANOVA lumen size p=0.4628). This was also true for the stroma of DOX treated tumours, no particular vessel size had more PV F4/80⁺ MRC1⁺

TAMs per vessel (Two way ANOVA lumen size $p=0.4628$, $0-80\mu\text{m}^2$ mean= 1.27 ± 0.23 , $80-1200\mu\text{m}^2$ mean= 2.13 ± 0.22 $1200\mu\text{m}^2$ mean= 1.93 ± 0.27) In the stroma, the number of PV F4/80⁺ MRC1⁺ TAMs per lumenised vessel was not altered by DOX treatment (Figure 4.12C, Two way ANOVA treatment $p=0.4741$)

Likewise, in PBS-treated tumour cell islands, lumen area did not affect the number of PV F4/80⁺ MRC1⁺ TAMs per vessel ($0-80\mu\text{m}^2$ mean= 0.52 ± 0.24 , $80-1200\mu\text{m}^2$ mean= 0.63 ± 0.21 , Two way ANOVA lumen size $p=0.5198$). This was also true in the tumour cell islands of DOX treated tumours ($0-80\mu\text{m}^2$ mean= 0.50 ± 0.24 , $80-1200\mu\text{m}^2$ mean= 0.72 ± 0.25 , Two way ANOVA lumen size $p=0.5198$). Similarly, in the tumour cell islands, DOX did not alter the number of PV F4/80⁺ MRC1⁺ TAMs per vessel (Figure 4.13C, Two way ANOVA treatment $p=0.8728$). It is possible that had more tumours been analysed, DOX would have had a significant effect on the number of PV F4/80⁺ MRC1⁺ TAMs per vessel, as a power analysis confirmed that the numbers were too small for this analysis to show a significant effect. When analysing the numbers of PV MRC1⁺ TAMs per vessel, there was no significant difference between vessels of different lumen sizes, suggesting that PV MRC1⁺ TAMs do not associate with any one particular size of vessel preferentially. Moreover DOX did not impact on the numbers of PV MRC1⁺ TAMs per vessel, yet showed an effect when the total tumour vasculature was analysed, suggesting that DOX affects the total tumour vasculature, resulting in an increase in PV MRC1⁺ TAMs.

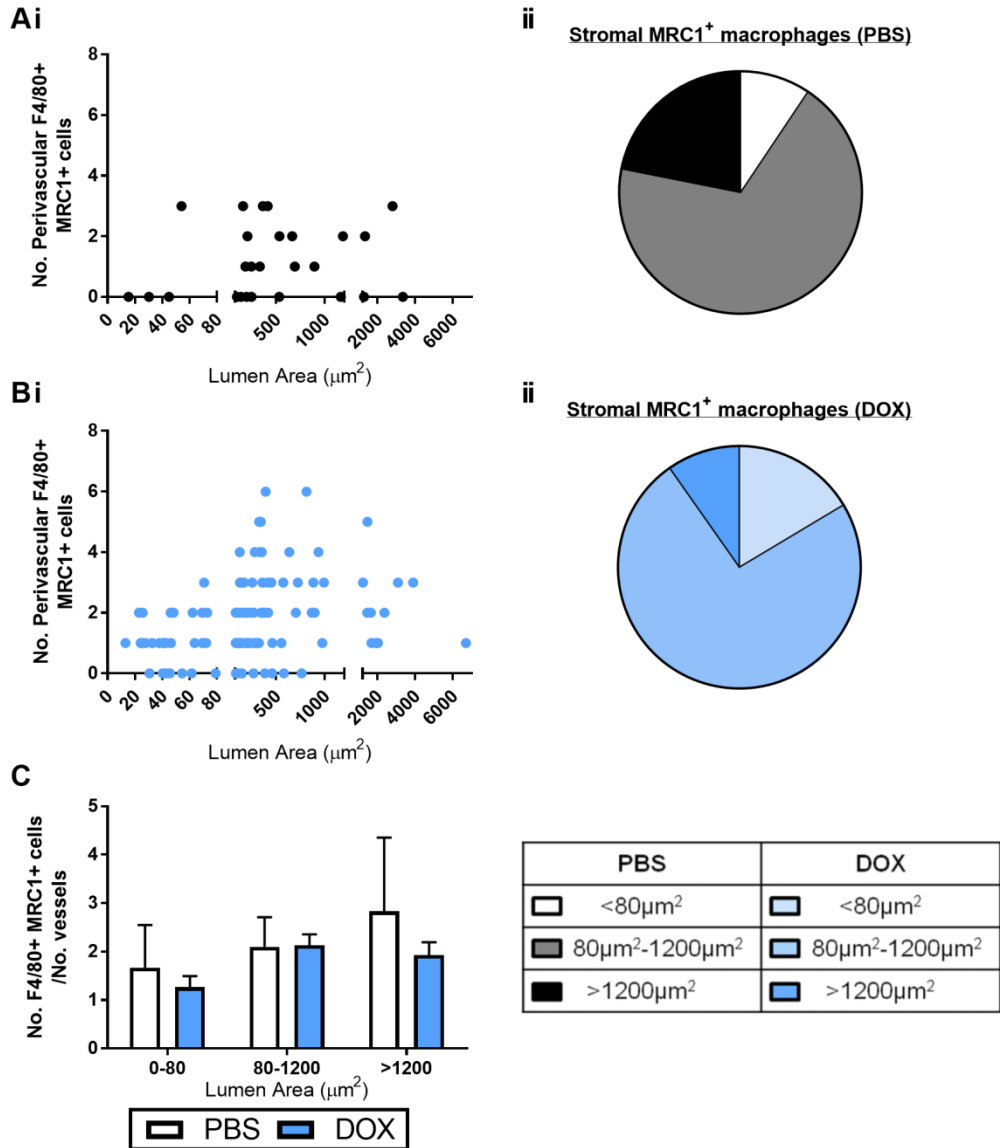


Figure 4.12 Analysis of the distribution of F4/80⁺ MRC1⁺ TAMs around vessels with a measurable lumen in the tumour stroma, after PBS or DOX treatment.

Individual vessel lumens were measured and then the number of PV F4/80⁺ MRC1⁺ TAMs were counted for each vessel. The distribution of PV MRC1⁺ TAMs around different sized vessels is shown for the stroma of PBS- (A) and DOX-treated (B) tumours, with a histogram demonstrating the number of MRC1⁺ TAMs attached to a vessel of a particular size (i) and a pie chart which shows the percentage of MRC1⁺ TAMs which lie in each vessel category (ii). The total number of PV TAMs per vessel category was then divided by the total number of vessels in each category for the stroma (C). 5 tumours/group; bar charts represent mean + SEM.

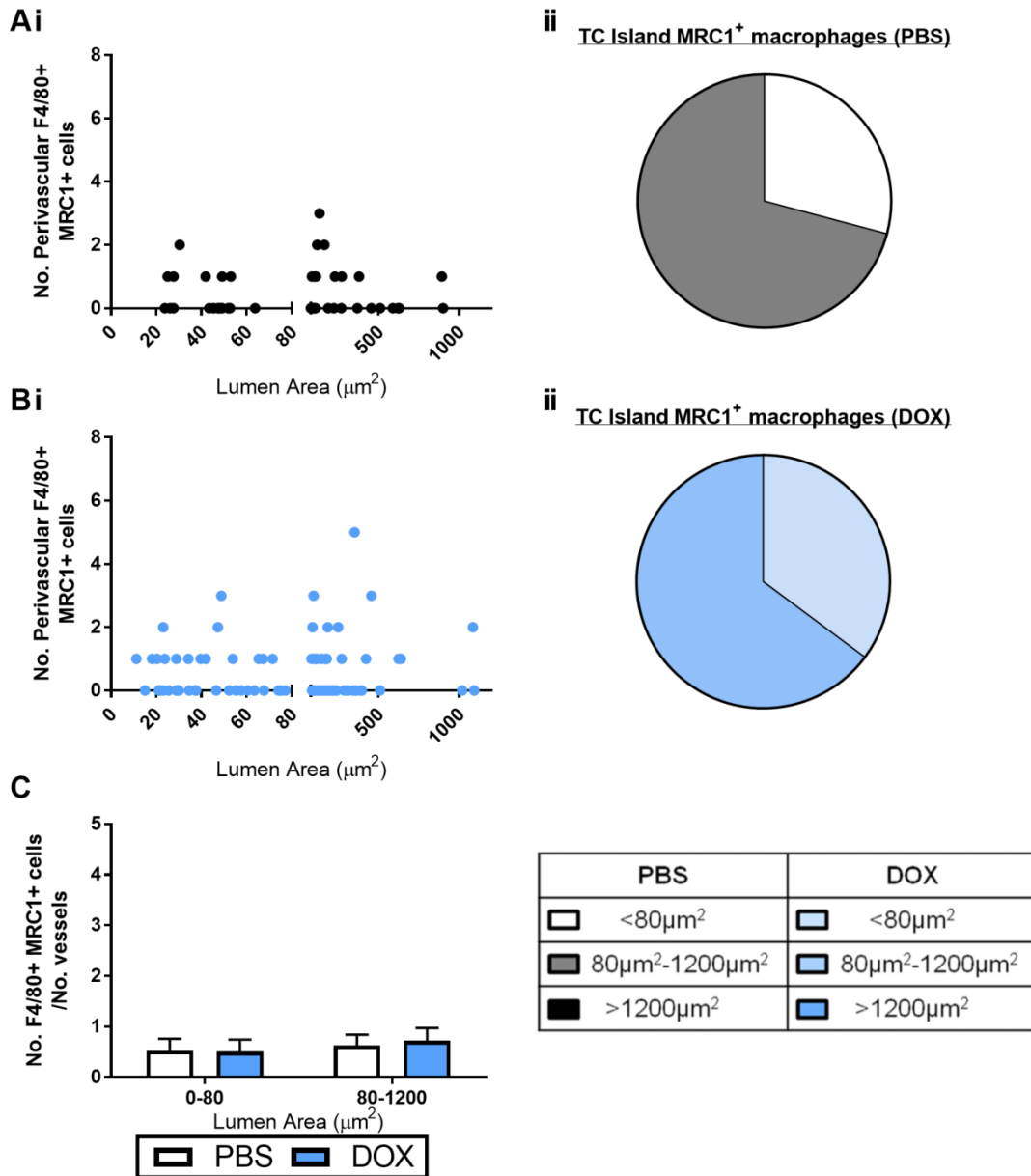


Figure 4.13 Analysis of the distribution of F4/80⁺ MRC1⁺ TAMs around vessels with a measurable lumen in tumour cell islands, after PBS or DOX treatment.

Individual vessel lumens were measured and then the number of PV F4/80⁺ MRC1⁺ TAMs were counted for each vessel. The distribution of PV MRC1⁺ TAMs around different sized vessels is shown for the tumour cell islands of PBS- (A) and DOX-treated (B) tumours, with a histogram demonstrating the number of MRC1⁺ TAMs attached to a vessel of a particular size (i) and a pie chart which shows the percentage of MRC1⁺ TAMs which lie in each vessel category (ii). The total number of PV TAMs per vessel category was then divided by the total number of vessels in each category (C) in PBS and DOX treated tumours. 5 tumours/group; bar charts represent mean + SEM.

4.3.10 HEVs are present in mouse lymph nodes but not TS1 tumours.

Next, the presence of HEVs was examined in TS1 tumours after treatment with PBS or DOX. PNA^d can be identified in tumour sections using the antibody, MECA-79. Lymph nodes were stained for PNA^d as a positive control alongside tumours. Lymph node staining of PNA^d (red) can be seen in Figure 4.14A, with CD31 (green) labelling blood vessels. Blood vessels which were positive for PNA^d (red) are HEVs (Figure 4.14B shows a close-up of a HEV within the lymph nodes). Three tumours from each treatment group were stained for PNA^d (as described, section 4.2.1) and entire sections were scanned for PNA^d⁺ cells using a 20x lens on a fluorescent microscope. As shown in Figure 4.14C, no identifiable PNA^d staining could be observed. From this it was concluded that HEVs were not present in these implanted TS1 tumours, and this was not altered by DOX treatment.

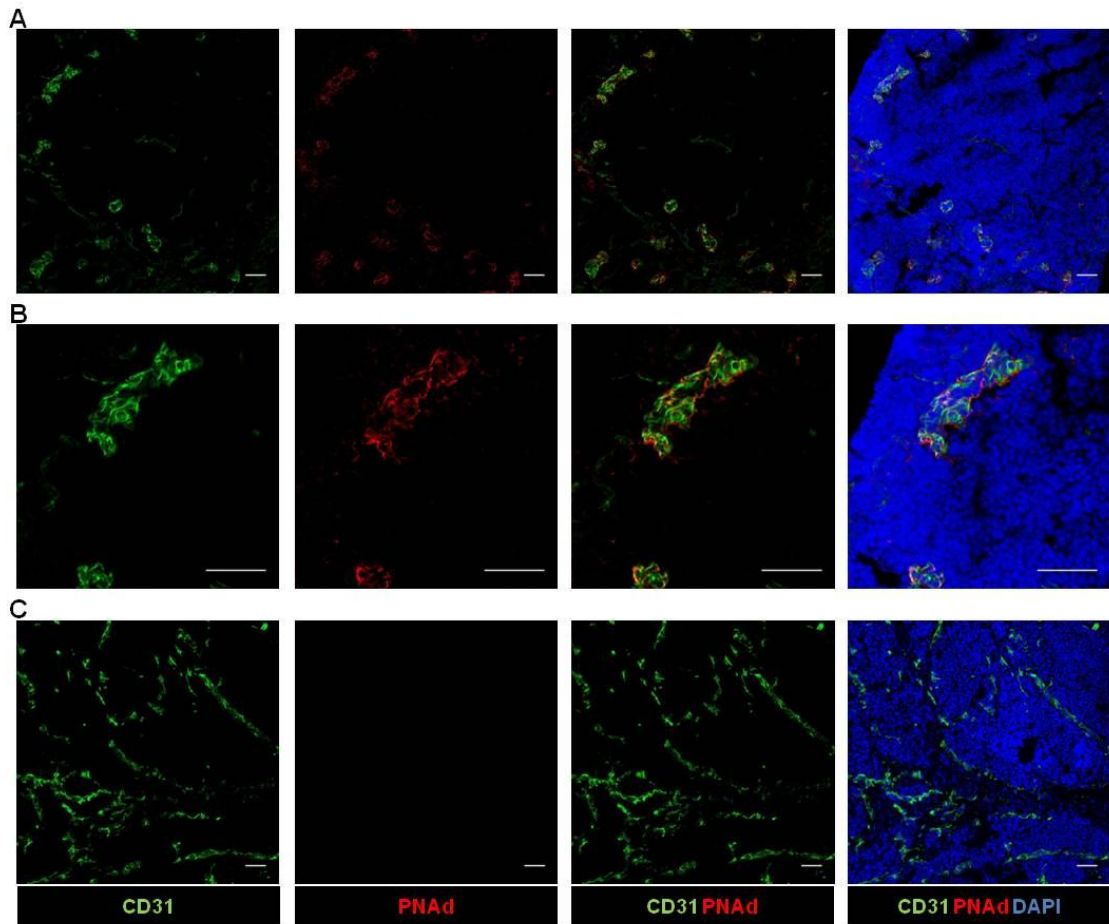


Figure 4.14 TS1 implant tumours do not contain high endothelial venules.

CD31 (green) and peripheral node addressin (PNAAd) (red) expression was analysed using immunofluorescence. Lymph nodes were used as a positive control for PNAAd staining, demonstrating the presence of high endothelial venules (A & B). No PNAAd staining was detectable in tumours (C). Scale bar = 50µm.

4.3.11 Distinct T cell populations are found within the tumour cell islands and stroma of TS1 tumours.

In murine fibrosarcomas (induced by methylcholanthrene), HEVs were only present in tumours with depleted regulatory T cells [227]. Therefore, the T-cell infiltrate of TS1 tumours was examined to establish whether the presence of regulatory T-cells could explain the lack of HEVs in the current model. Tumours were stained for CD3, CD8 and CD4 to identify the different T-cell populations as described in section 4.2.1. CD3 expressing cells are T cells and can be subdivided on the basis of their CD8 (cytotoxic T cells) and CD4 (expressed by both T helper cells and regulatory T cells) expression.

Figure 4.15 shows representative staining of CD3 (white), CD8 (red) and CD4 (green) in the stroma (Figure 4.15A) and tumour cell islands (Figure 4.15B). PBS treated tumours had an increased density of CD3⁺ cells in the stroma (mean= 10.67 ± 2.22) compared to the tumour cell islands (mean= 1.80 ± 0.42, Two way ANOVA area analysed p=0.0004, Sidak's multiple comparisons test p=0.0007). This trend was also seen in DOX treated tumours, although it was not significant (stroma mean= 5.72 ± 0.56, tumour cell island mean= 2.06 ± 0.77, Sidak's multiple comparisons test p=0.0813). DOX did not significantly decrease CD3⁺ T cell density (CD3⁺ T cells as a percentage of total cells, Figure 4.15C), despite a trend for a decrease in CD3⁺ cell density the stroma of these tumours (Two way ANOVA treatment p=0.1238).

The density of CD3⁺ CD4⁺ (T helper and/or regulatory T cells) was then analysed (Figure 4.15D). The stroma of PBS (mean= 6.02 ± 1.26) and DOX (mean= 4.01 ± 0.31) treated tumours had an increased density of CD3⁺ CD4⁺ cells compared to the tumour cell islands (Two way ANOVA area analysed p<0.0001, PBS mean= 0.49 ± 0.14 Sidak's multiple comparisons test p=0.0005, DOX mean= 0.71 ± 0.28 Sidak's multiple comparisons test p=0.0108). DOX did not affect the density of CD3⁺ CD4⁺ cells (Two way ANOVA treatment p=0.2448).

The density of cytotoxic CD3⁺ CD8⁺ T cells was also not affected by DOX (Two way ANOVA treatment p=0.1780, Figure 4.15E). Interestingly, in contrast to CD3⁺

CD4⁺ cells, the CD3⁺ CD8⁺ density was not significantly different in the stroma (mean= 1.38 ± 0.48) and tumour cell islands (0.66 ± 0.17) of PBS treated tumours (Two way ANOVA area analysed p=0.3048) or DOX treated tumours (stroma mean = 0.46 ± 0.08, tumour cell island mean= 0.64 ± 0.24).

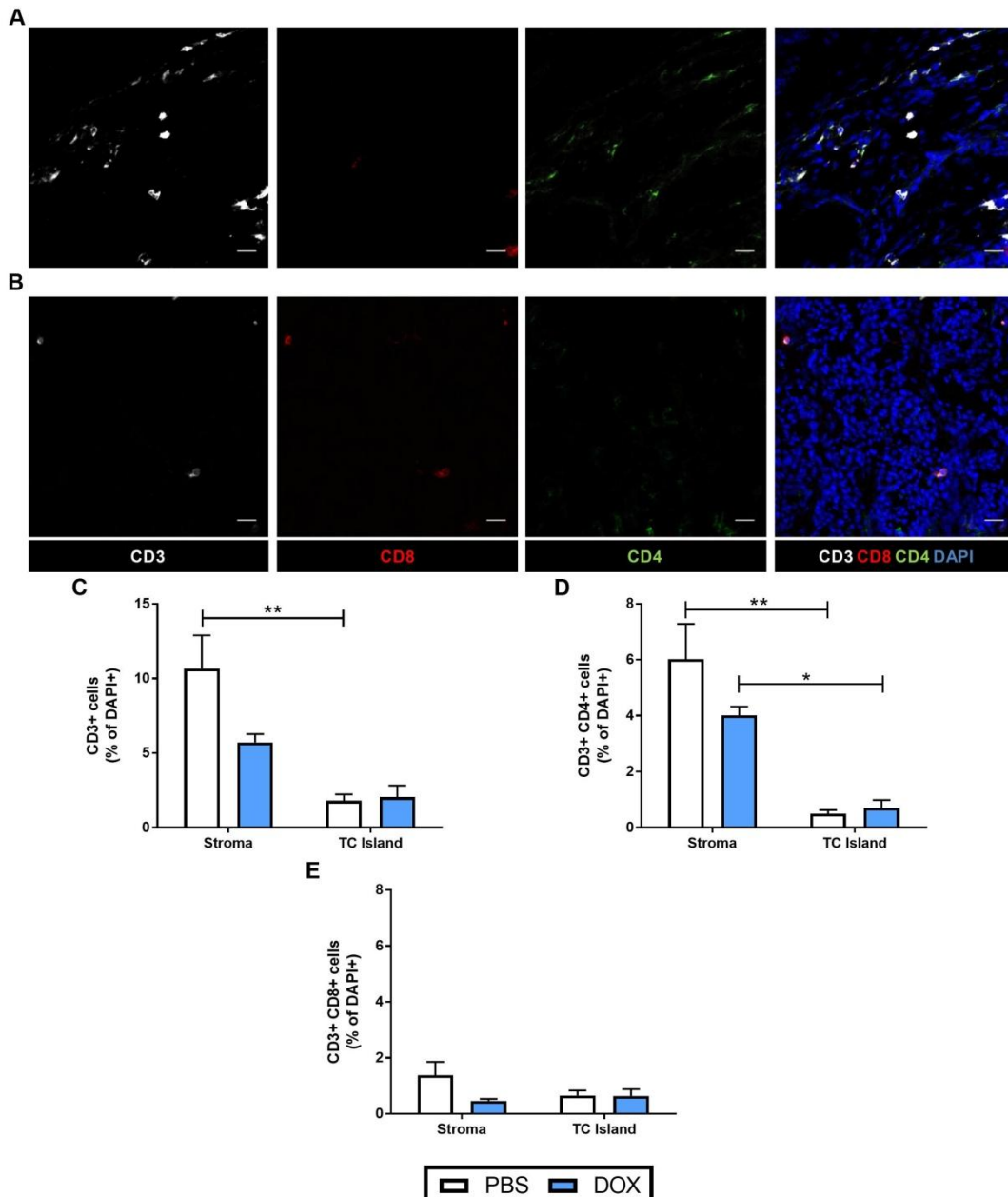


Figure 4.15 Differences in the frequency of T cell subsets between the stroma and tumour cell islands of TS1 tumours after PBS or DOX treatment.

CD3⁺ (white), CD8⁺ (red) and CD4⁺ (green) cells were immunostained and visualised in the stroma (A) and tumour cell islands (B). Scale bar = 20µm. The frequency of these cells was calculated as a percentage of total DAPI⁺ cells (C-E). n=5 tumours/group. 2-way ANOVA used, * p<0.05; ** p<0.001.

The percentages of T cells which expressed CD4 were then calculated by dividing the number of CD3⁺ CD4⁺ cells by total CD3⁺ cells and multiplying by 100 (Figure 4.16A). The percentage of T cells which were CD4⁺ was increased in the stroma of PBS treated tumours (mean= 56.78 ± 4.85) compared to tumour cell islands (mean= 27.69 ± 3.45, Two way ANOVA area analysed p=0.0002, Sidak's multiple comparisons test p=0.0052). The stroma of DOX treated tumours (mean= 68.67 ± 1.62) also had an increased percentage of CD4⁺ T cells compared to the tumour cell islands (mean= 35.22 ± 5.96 Sidak's multiple comparisons test p=0.0022). Interestingly, DOX appeared to increase the percentage of CD4⁺ T cells (Two way ANOVA treatment p=0.0318), however post-hoc analysis revealed these increases were not significant (Sidak's multiple comparisons test stroma p=0.1305, tumour cell island p=0.4104).

The percentage of CD8⁺ T cells was also calculated (Figure 4.16B). The stroma of PBS treated tumours (mean= 11.79 ± 2.11) had a significantly lower percentage of CD8⁺ T cells compared to the tumour cell islands (mean= 36.02 ± 2.20, Two Way ANOVA area analysed p=0.0002, Sidak's multiple comparisons test p=0.0085). This was also true in DOX treated tumours (stroma mean= 9.15 ± 0.56, tumour cell island mean= 39.55 ± 7.41, Sidak's multiple comparisons test p=0.0022). Importantly, DOX did not significantly alter the percentage of T cells which were CD8⁺ (Two way ANOVA treatment p=0.9055).

To understand whether there were more cytotoxic or regulatory T cells, the CD4:CD8 ratio was calculated by dividing the number of CD4⁺ T cells per FOV by the number of CD8⁺ T cells per FOV (Figure 4.16C). In PBS treated tumours, the stroma (mean= 7.35 ± 2.28) had an increased CD4:CD8 ratio compared to tumour cell islands (mean= 1.12 ± 0.20), however this was not significant (Sidak's multiple comparisons test p=0.1521). The stroma of DOX treated tumours (mean= 13.67 ± 3.51) had a significantly increased CD4:CD8 ratio compared to tumour cell islands (mean= 1.08 ± 0.20, Two way ANOVA area analysed p=0.0026, Sidak's multiple comparisons test

p=0.0073). Interestingly, there appeared to be a trend for an increased CD4:CD8 ratio in the stroma of DOX treated tumours, compared to PBS-treated tumours, however this was not significant (Two way ANOVA treatment p=0.1542). Overall, DOX did not impact on the T cell infiltration of these tumours. Importantly CD3⁺ CD4⁺ cells were present in both PBS and DOX treated tumours, possibly explaining the absence of HEVs in these tumours. CD3⁺ CD4⁺ cells can be either T helpers or regulatory T cells, and co-staining CD3 and CD4 with FOXP3 in these tumours should reveal if regulatory T cells are part of the tumour immune infiltrate.

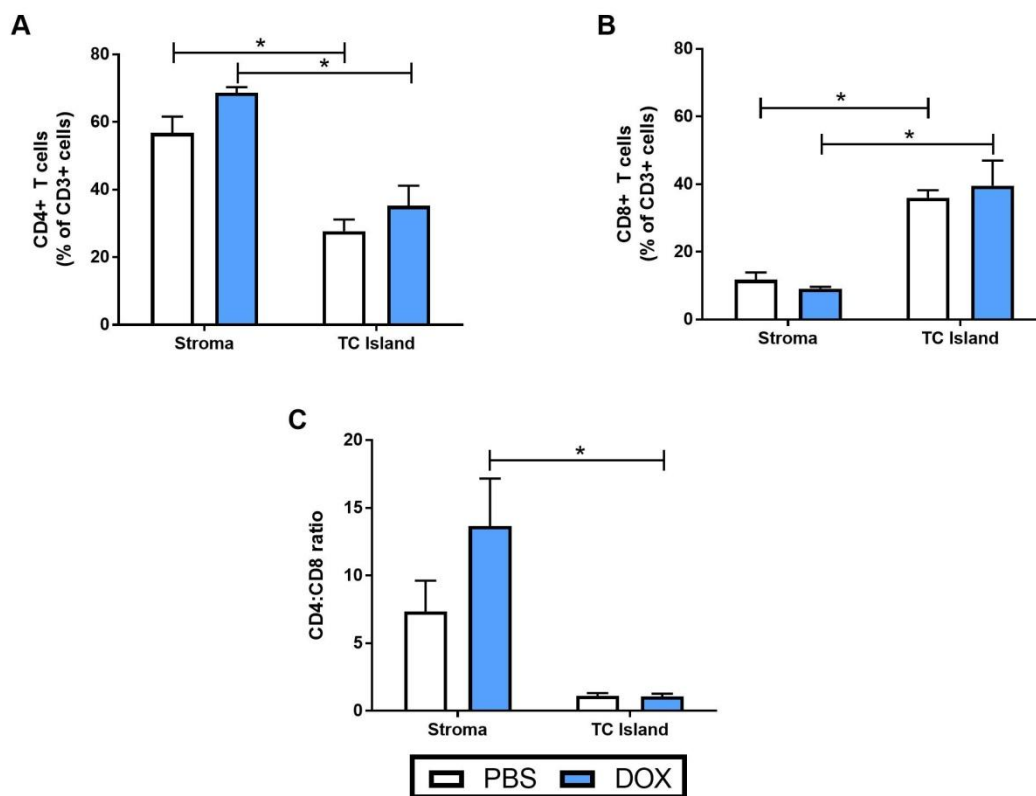


Figure 4.16 Differences in the percentages of CD4⁺ or CD8⁺ T cells between the stroma and tumour cell islands of TS1 tumours after PBS or DOX treatment.

The percentage of CD4⁺ cells/total CD3⁺ cells was calculated (A) as was the percentage of CD8⁺ cells (B). The CD4:CD8 ratio was also calculated (C). n=5 tumours 2-way ANOVA used, * p<0.01.

4.3.12 FOXP3⁺ regulatory T cells are found at an increased density within the stroma than the tumour cell islands of TS1 tumours.

To address whether regulatory T cells were present in these tumours, CD3⁺ CD4⁺ FOXP3⁺ cells were counted. Tumours were stained as in 4.2.1 and typical staining of the stroma (Figure 4.17A) and tumour cell islands (Figure 4.17B) shows CD3 (white), CD4 (red) and FOXP3 (green) staining. The stroma of PBS treated tumours (mean= 2.77 ± 0.86) had an increased density of CD3⁺ CD4⁺ FOXP3⁺ cells (number of CD3⁺ CD4⁺ FOXP3⁺ cells as a percentage of total nuclei, Figure 4.17C) compared to the tumour cell islands (mean= 0.12 ± 0.04, Two way ANOVA area analysed p=0.0070, Sidak's multiple comparisons test p=0.0444). This trend was also seen in DOX treated tumours (stroma mean= 2.26 ± 0.62, tumour cell island mean= 0.17± 0.09) however, this trend was not significant (Sidak's multiple comparisons test p=0.0619). The density of Tregs was not significantly different in DOX treated tumours compared to PBS treated tumours (Two way ANOVA treatment p=0.6599).

The percentage of T (CD3⁺) cells that were Tregs (co-expressing CD4 and FOXP3) was then calculated. There was a trend for an increase in the percentage of T cells which were Tregs in the stroma of both PBS (mean= 33.96 ± 1.68) and DOX (mean= 30.2 ± 5.59) treated tumours compared to tumour cell islands (PBS mean= 12.46 ± 2.23, DOX mean= 12.05 ± 6.05, Two way ANOVA area analysed p=0.0210). However, post-hoc analysis revealed these trends were not significant (Sidak's multiple comparisons test PBS p=0.1218, DOX p=0.1311). Furthermore, DOX did not impact on the percentage of T cells which were Tregs (Figure 4.17D, Two way ANOVA treatment p=0.6099). Importantly, Tregs were present in these TS1 tumours, possibly explaining the lack of HEVs in this model.

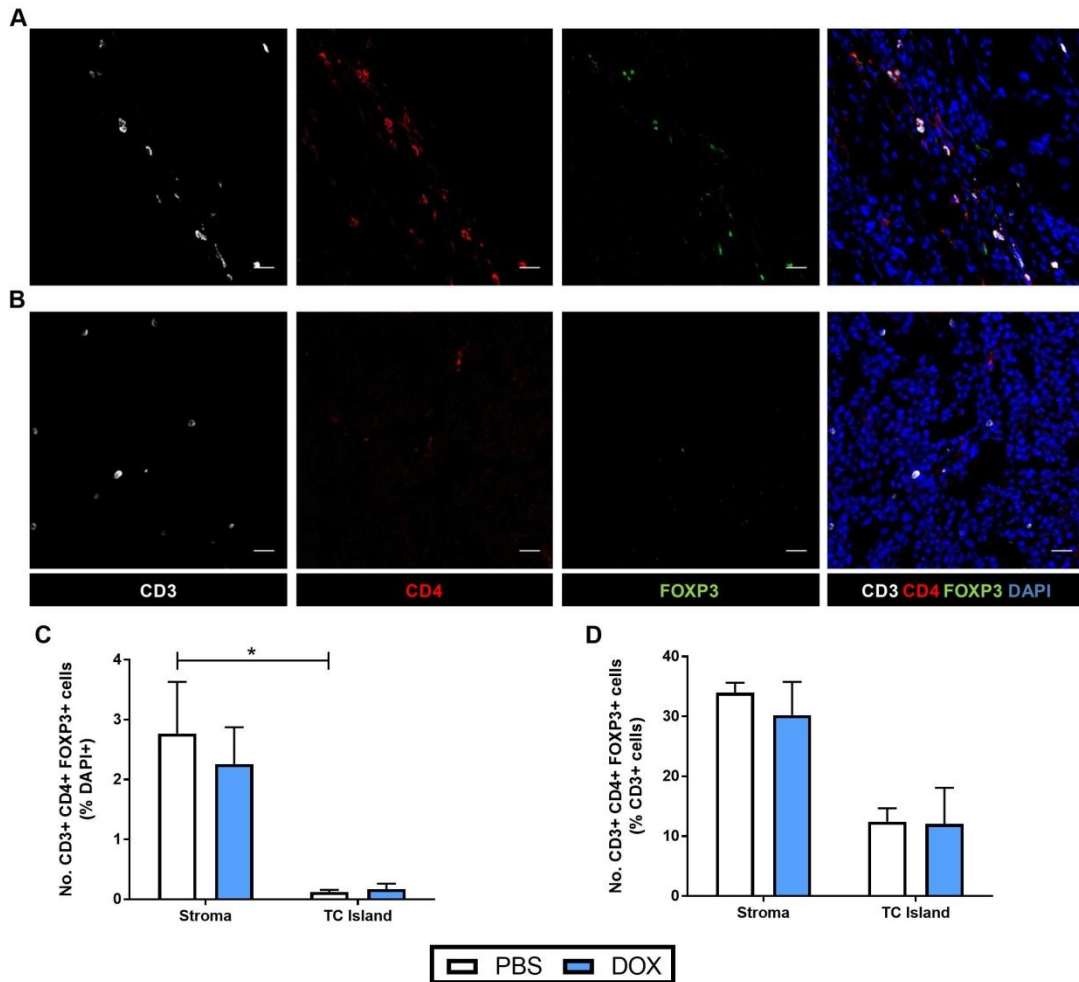


Figure 4.17 Differences in the frequency of regulatory T cells between the stroma and tumour cell islands of TS1 tumours after PBS or DOX treatment.

Immunostaining of CD3⁺ (white); CD4⁺ (red) and FOXP3⁺ (green) cells in the stroma (A) and tumour cell islands (B). Scale bar = 20µm. The frequency of CD3⁺ CD4⁺ FOXP3⁺ Tregs was calculated as a percentage of DAPI⁺ cells (C) or of total CD3⁺ cells (D). n=3-4 tumours/group. 2-way ANOVA used, *p<0.05.

4.3.13 Vessel patency was increased in the stroma of TS1 tumours compared to the tumour cell islands.

The impact of DOX on vessel flow was assessed by analysing whether vessels were patent (i.e. could they be perfused by FITC-lectin - as described in section 4.2.4.1). Mice were injected intravenously with 1mg/mL FITC lectin 10 minutes prior to culling. Tumour sections were stained with CD31 (red in Figure 4.18A-B) as described in 4.2.1 and images show FITC-lectin (green) perfused vessels in the stroma (Figure 4.18A) and the tumour cell islands (Figure 4.18B). CD31 staining was converted into a mask and applied to the FITC-lectin staining, which allowed the percentage of CD31 area co-stained by FITC-lectin to be calculated (Figure 4.18C).

The stroma of both PBS (mean= 51.66 ± 4.31) and DOX (mean = 41.27 ± 5.23) treated tumours had an increased percentage of CD31 area which co-stained for FITC-lectin compared to tumour cell islands (Two way ANOVA area analysed $p=0.0025$, PBS mean= 30.4 ± 9.21 Sidak's multiple comparisons test $p=0.0128$, DOX mean= 23.6 ± 2.56 Sidak's multiple comparisons test $p=0.0244$). However, the percentage of CD31 area co-stained with FITC-lectin was not affected by DOX treatment (Two way ANOVA treatment $p=0.3305$).

To establish whether the proportion of vessels that were patent was affected by DOX treatment, CD31⁺ vessels were identified within tumour sections, and then the number of CD31⁺ FITC-lectin⁺ vessels was expressed as a percentage of total vessels analysed (Figure 4.18D). The stroma of PBS treated tumours (mean= 88.11 ± 4.43) had an increased percentage of FITC-lectin perfused vessels compared to the tumour cell islands (mean= 62.10 ± 9.31 , Two way ANOVA area analysed $p=0.0043$, Sidak's multiple comparisons test $p=0.0444$). This was also true in DOX treated tumours (stroma mean= 87.51 ± 5.27 , tumour cell island mean= 54.16 ± 7.72 , Sidak's multiple comparisons test $p=0.0194$). However, the percentage of FITC-lectin perfused vessels was unaffected by DOX (Two way ANOVA treatment $p=0.6392$).

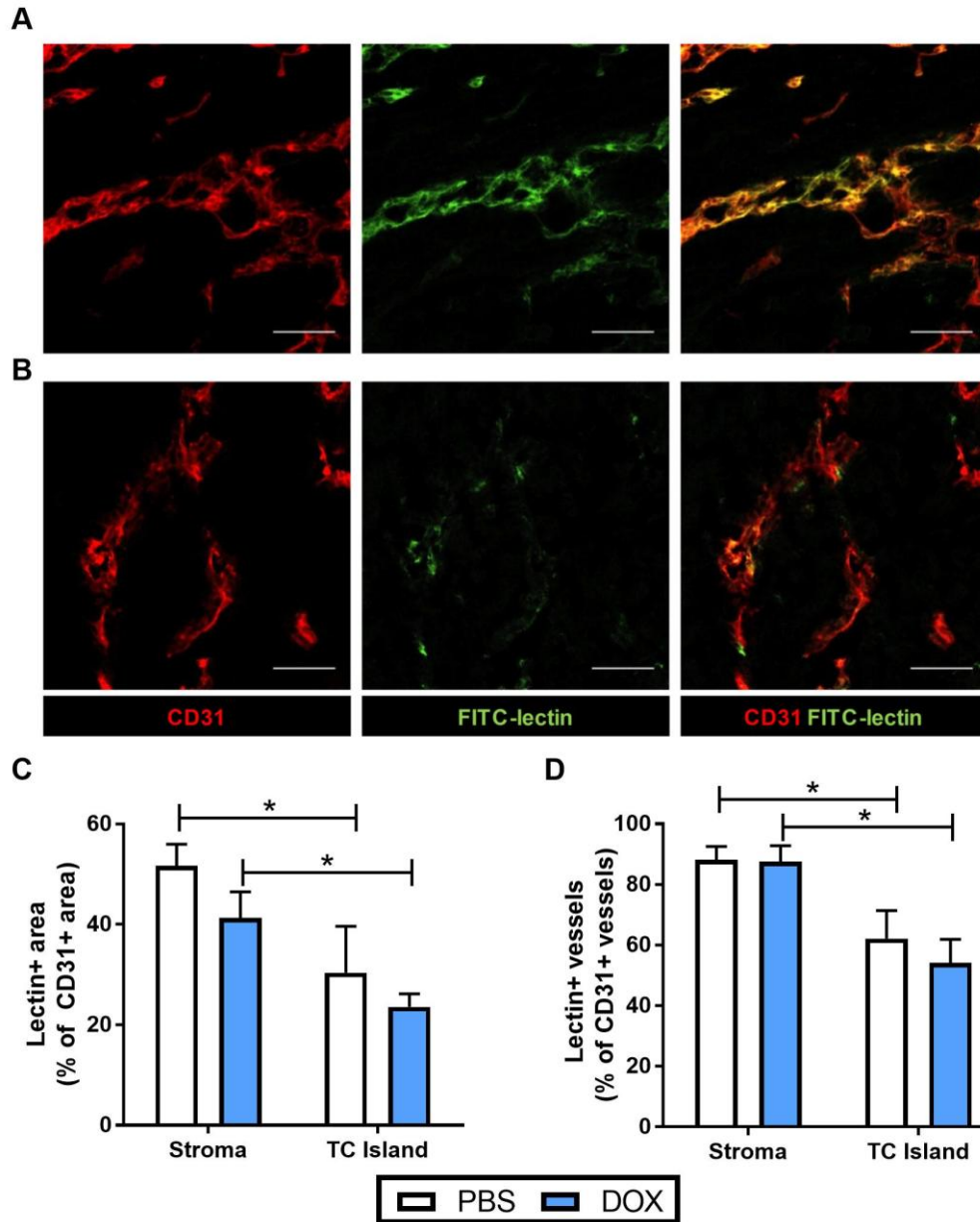


Figure 4.18 DOX did not affect vessel patency in TS1 tumours.

CD31 (red) and FITC-lectin (green) stain vessels within the stroma (A) and tumour cell islands (B). Lectin positive area was calculated as a percentage of the CD31⁺ area mask (C) and the percentage Lectin⁺ vessels out of total CD31⁺ vessels was calculated. 2-way ANOVA used n=3 tumours. Scale bar= 50 μ m * p<0.05.

4.3.14 The majority of vessels in TS1 tumours were associated with pericytes.

The pericyte coverage of vessels was assessed by staining tumours with CD31 (green) and with the pericyte marker α -SMA [220] (red) as described in section 4.2.1. Representative staining of vessels in the stroma (Figure 4.19A) and tumour cell islands (Figure 4.19B) are shown. CD31 staining was converted to a mask and the percentage of CD31⁺ area co-stained by α -SMA was calculated to understand the amount of blood vessel area which was covered by pericytes (Figure 4.19C). The stroma of both PBS (mean 29.56 ± 6.10) and DOX (mean = 27.24 ± 5.33) treated tumours had similar CD31⁺ areas which co-localised with α -SMA staining in their tumour cell islands (PBS mean = 31.04 ± 3.17 , DOX mean = 20.62 ± 3.86 , Two way ANOVA area analysed $p=0.6310$). Thus, DOX did not alter the percentage of CD31⁺ area covered with α -SMA staining (Two way ANOVA treatment $p=0.1978$).

CD31⁺ vessels were counted, and their coverage in PV α -SMA⁺ cells was assessed to give a percentage of vessels which were associated with pericytes out of total vessels analysed (Figure 4.19D). The majority of vessels in the stroma of both PBS (mean = 87.32 ± 3.82) and DOX (mean = 85.52 ± 2.54) treated tumours had pericyte coverage. This was also true for vessels in the tumour cell islands of PBS (mean = 95.59 ± 1.84) and DOX (mean = 85.92 ± 5.20) treated tumours. There was no significant difference in the percentage of pericyte covered vessels between the stroma and tumour cell islands of these tumours (Two way ANOVA are analysed $p=0.2339$). Again DOX did not change the percentage of pericyte covered vessels in either the stroma or tumour cell islands (Two way ANOVA treatment $p=0.1887$).

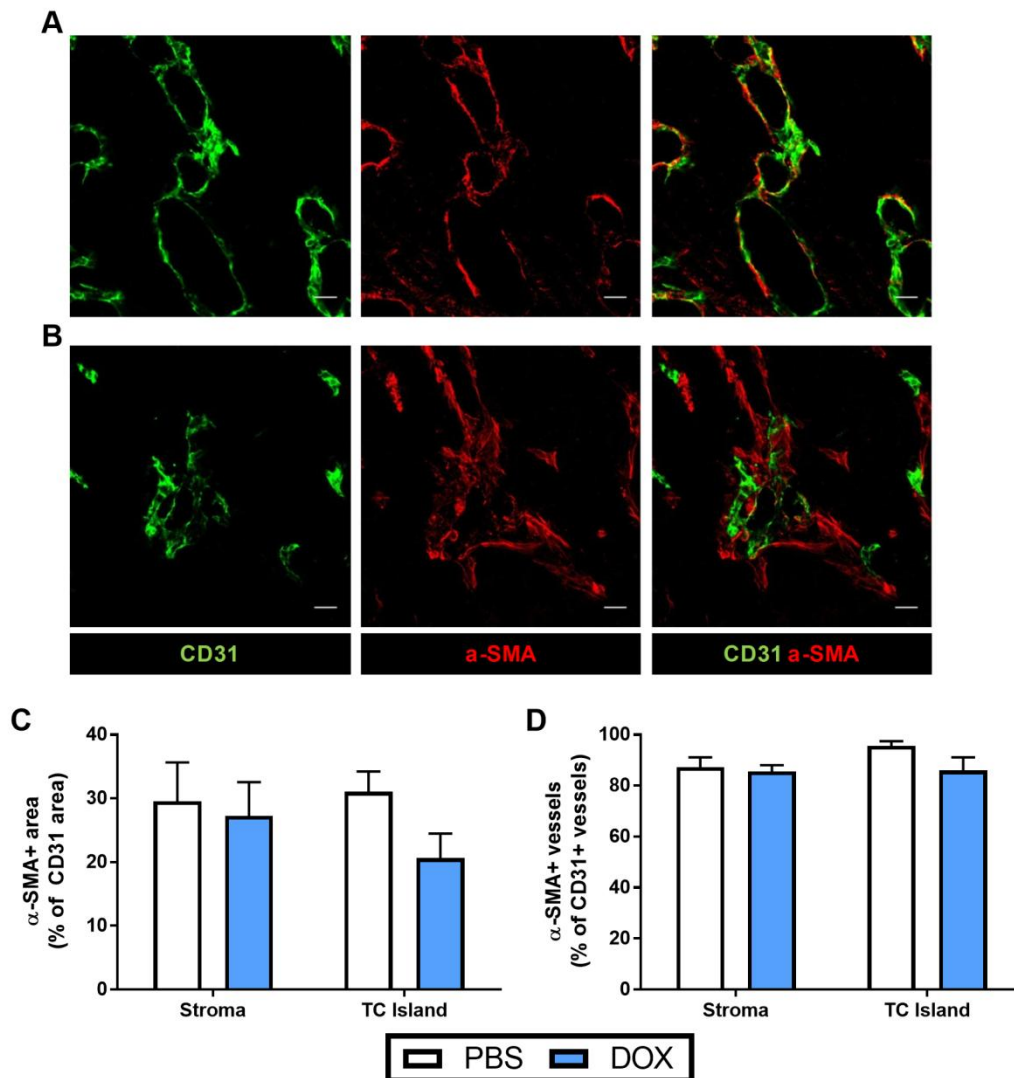


Figure 4.19 The majority of vessels in the stroma and tumour cell islands have pericyte coverage after PBS and DOX treatment.

CD31 (green) and α -SMA (red) demonstrate pericyte coverage of vessels in the stroma (A) and tumour cell islands. Scale bar = 20 μ m. The percentage of CD31 area that co-localised with α -SMA staining was calculated to understand the amount of blood vessel area which was coated by pericytes (C) as was the percentage of vessels which had PV α -SMA⁺ cells, to understand how many vessels were associated with pericytes (D). n=4 tumours.

4.4 Discussion

In this chapter, an increase in PV MRC1⁺ TAMs was demonstrated in TS1 tumours following DOX treatment for this first time. Monocyte subpopulations were also studied in a post-chemotherapy setting in mice bearing such tumours. Interestingly these data demonstrate that while DOX slightly reduces circulating peripheral blood monocytes, there was no significant change in the proportions of the Ly-6C^{hi}, Ly-6C^{int} or Ly-6C^{lo} monocytes present in the blood. However, DOX did induce a small but significant increase in MRC1⁺ monocytes in the Ly-6C^{int} and Ly-6C^{lo} subsets. Further analysis of the PV MRC1⁺ TAMs revealed that these TAMs were mature Gr-1⁻ cells, and were therefore unlikely to be newly recruited from these MRC1⁺ monocytes.

Given the DOX-induced increase in PV MRC1⁺ TAMs it was important to characterise the tumour vasculature of these tumours, as this increase may have been due to changes in the structure of tumour blood vessels after DOX. TAMs were not found to preferentially gather around vessels of a particular luminal size in either the PBS or the DOX-treated tumours. DOX also had no impact on vessel patency or pericyte coverage. However, one interesting finding concerning the vessels was the increase in the patency of vessels in the stroma compared to tumour cell islands. These data in this chapter also demonstrate that HEVs are absent in TS1 tumours, which may have implications for investigating the immune infiltrate of these tumours in future, as HEVs are known to aid in the recruitment of lymphocytes from peripheral blood [224]. In summary, within 48 hours of DOX treatment, there was an increase in both MRC1⁺ monocytes in the blood and TAMs in the PV niche of tumours. However, DOX had no effect on vessel parameters like their size, pericyte coverage, or ability to carry flow.

Although the previous chapter showed DOX had no impact on overall TAM numbers in TS1 tumours, these data in this chapter demonstrate a significant increase in PV MRC1⁺ TAMs in these tumours. This is in keeping with previous studies using

other tumour models (LLCs after cyclophosphamide; 4T1 after paclitaxel and PyMT implanted tumours with DOX), which showed that chemotherapy increased the number of MRC1⁺ TAMs in vascularised areas of tumours [144]. However, it is very interesting that these TAMs were increased specifically in the PV location, but not across the tumour as a whole. This suggests that perhaps the tumour vasculature may influence the retention and/or phenotype of TAMs.

One limitation of these studies is that only MRC1 expression was examined on the PV TAMs. While MRC1 is a commonly used marker of M2-skewed macrophages [49], its presence on PV TAMs in this study does not necessarily mean that these cells are M2-skewed or would have or promoted relapse after DOX. However, unpublished studies carried out by another member of the group, Dr Russell Hughes, during my PhD showed that MRC1⁺ TAMs in TS1 tumours expressed additional M2 markers [42] including CD163 and scavenger receptor A. This suggests that these cells may well have been M2-skewed and, are therefore likely to promote tumour angiogenesis and immunosuppression. This accords with the PV MRC1⁺ TAMs which accumulate and drive relapse in LLCs after cyclophosphamide treatment [144]. In LLCs, these MRC1⁺ TAMs were also shown to express TIE2 [144]. Interestingly, VEGF-A expression was limited to MRC1⁺ TAMs in implanted PyMT tumours and genetic ablation of this delayed relapse following DOX [144]. Although these studies suggest that the PV MRC1⁺ TAMs in TS1 tumours promote relapse after DOX, further studies are needed to provide unequivocal evidence of this.

The peripheral blood monocytes of mice were examined to understand whether DOX was having systemic effects on these mice at this early time point. DOX is known to induce myelosuppression [236], and so DOX depleting monocytes within peripheral blood was not surprising. It is also one of the reasons why peripheral blood was collected from mice 48 hours following the dose of DOX, as earlier time points may have had an increased depletion of monocytes, which would have made studying the monocytic subpopulations difficult. Interestingly, monocyte subpopulation proportions

were unaffected by DOX. Previously, depletion of monocytes with clodronate liposomes demonstrated that Ly-6C^{hi} monocytes appear in circulation approximately 2 days after depletion, whereas the Ly-6C^{lo} subset appeared 7 days after depletion, as the Ly-6C^{hi} monocytes are thought to mature into Ly-6C^{lo} monocytes [11]. This suggests that the different monocytic subsets have different turnovers, with Ly-6C^{hi} monocytes appearing in the blood soon after depletion compared to the Ly-6C^{lo} monocytes. However this was not the case in the current studies using DOX in tumour bearing mice. While total monocytes were depleted, the abundance of the different monocyte subpopulations was unchanged. Further studies with more time points would be needed to accurately study monocyte turnover in this model, and it would be interesting to investigate if the Ly-6C^{lo} monocytes had some survival advantage, which is why they were not depleted 48 hours after DOX, despite an overall decrease in peripheral blood monocytes. Indeed, RAW264.7 macrophages expressing Tie2 were recently shown to have a survival advantage in serum starvation conditions *in vitro*, and TEMs are a subset of non-classical Ly-6C^{lo} monocytes [70], [146]. Perhaps Tie2 expression on a subset of these monocytes could be important for their survival following treatment with DOX.

In this study monocyte subsets were identified on the basis of their Ly-6C expression. It would have been advantageous to include an additional marker of the Ly-6C^{lo} monocytes, such as the fractalkine receptor CX₃CR1, however attempts to detect surface CX₃CR1 expression by flow cytometry in murine peripheral blood mononuclear cells were unsuccessful. This may be why most of the published studies using CX₃CR1 as a marker of the non-classical subset of monocytes often use the CX₃CR1^{GFP/+} mouse, and so non-classical monocytes can be detected on the basis of GFP expression as opposed to directly labelling CX₃CR1 [9]. CX₃CR1^{GFP/+} mice were not used in these studies, mainly due to budget constraints, and had more funds been available, CX₃CR1^{GFP/+} mice may have allowed more accurate assessment of monocytic subsets.

This study indicated that all monocyte subsets were present in murine blood 2-days post DOX treatment, although it was unable to trace monocyte uptake into the chemotherapy treated tumours. Further studies could utilise latex beads [68] to label the different monocytic subsets and provide interesting insights into which subsets are recruited into tumours post-chemotherapy. This method has previously demonstrated that Ly-6C^{hi} monocytes are recruited into tumours, where they differentiate into TAMs, but this was in a non-therapy setting [68]. Intravital imaging could have also provided interesting insights into monocyte recruitment. Previously, intravital imaging described a “patrolling” behaviour of non-classical monocytes in the mouse dermis and mesenteric vessels and demonstrated the early extravasation of these cells in response to inflammation [14]. Whether the same resolution of vessels and monocytes could be achieved within tumours is questionable, although intravital imaging has been used in the MMTV-PyMT model of cancer with some success [116], [137]. Lack of funds and expertise in the area of intravital imaging meant this option was not fully explored in these studies.

Monocyte phenotype was examined using the markers MRC1 and CXCR4. DOX significantly increased the proportion of MRC1⁺ monocytes and this increase was specific to the Ly-6C^{int} and Ly-6C^{lo} subsets. MRC1 was chosen as a marker of ‘pro-tumoural’ phenotype, as it well characterised and is conserved between both mice and humans [53]. DOX did cause a small increase in the number of MRC1⁺ monocytes, which could potentially be due to the effects of DOX on the tumour, for example if DOX caused the tumour to release molecules known to promote MRC1 expression. Further experiments *in vitro* may in future reveal mechanistically how this increase occurred. However, only a small proportion of MRC1⁺ monocytes were detected in murine peripheral blood, possibly reflecting that MRC1 is mainly expressed by more mature cells i.e. TAMs themselves. Moreover, monocytes in healthy female FvB/N mice only constitute 1.07% of white blood cells in peripheral blood [237], and so the biological relevance of this small increase in cells is questionable.

The number of CXCR4 expressing cells was unchanged by DOX, and again circulating CXCR4⁺ monocytes were a very low percentage of total monocytes. Inhibition of CXCR4 with AMD3100 was previously shown to prevent TAM recruitment into tumours after chemotherapy [144], which suggests that TAMs are recruited via CXCL12 into tumours. However in the current model, the peripheral blood monocyte precursors of TAMs rarely expressed CXCR4, which suggests CXCL12-CXCR4 signalling may be impacting TAMs directly, rather than acting on their monocytic precursors. It has previously been shown that CXCR4 is expressed by bone marrow monocytes, but this expression is lost in monocytes as they enter circulation [238], which supports the low proportion of CXCR4⁺ monocytes observed in this study.

One of the limitations of this study was that only two markers of M2-skewed monocyte/macrophage (MRC1 and CXCR4) phenotype were used. This was due to the limited availability of antibodies for M2 markers that would successfully combine with the remainder of essential antibodies needed to label monocyte subsets in the flow cytometry panel. Moreover, as mice only have 2mL of circulating blood, it was not possible to split samples and use this to run different panels of markers, as there would have not been enough cells available for flow cytometric analysis. Had a greater budget for mice been available in my PhD studentship, perhaps more mice could have been used to increase the numbers of markers that could be examined, due to the increased amount of mouse blood available. An alternative to increase the number of markers investigated would have been to extract RNA from the subsets of peripheral blood monocytes. There were several reasons why this was not performed. Firstly, isolating monocyte subsets from the low amounts blood available from each mouse would have been extremely difficult. One published study did isolate RNA from the two major monocytic subsets in mice, however this required pooling the blood of 20 mice to yield enough RNA for an n=1 [71]. For an experiment of n=3 with PBS and DOX treated mice, this would mean 120 mice (60 mice for each treatment group, 20 mice per n) would have had to be used, which was not feasible from a budget or ethical

perspective. Although RNA could have been isolated from whole blood, this would not have yielded information about monocyte subsets. Furthermore, in order to examine monocyte subsets using flow cytometry, all the available murine blood was used, so no material was left over to isolate RNA from.

Previous studies have compared monocytes (selected as CSF1R⁺ cells) from healthy and tumour-bearing mice. These studies showed that monocytes from tumour bearing mice are of a mixed phenotype and had decreased Tie2 and MHCII expression [239]. Gene expression analysis showed monocytes from tumour bearing mice had increases in both pro-inflammatory (e.g. CXCL10, TNF) and immunosuppressive genes (e.g. IL-10) [239]. However, these studies did not examine the impact of chemotherapy on murine monocyte subsets.

Another study examined total monocytes from patients with breast cancer and found these to have decreased IL-6 and TNF production, and to be able to suppress T cells *in vitro* more than those isolated from healthy donors [240]. This suggests that monocytes in breast cancer patients adopt an immunosuppressive phenotype. It was not possible to examine production of cytokines from monocyte subsets in these TS1 studies due to the low yield of cells per mouse, but this could potentially have been very interesting, as this could have revealed whether the MRC1⁺ monocytes were more immunosuppressive than the other monocytes. Further studies utilising patient samples may allow better analysis of monocyte subsets after chemotherapy as a greater volume of blood (and thus monocytes) would be available for analysis.

Potentially, the small increase in MRC1⁺ monocytes in the blood of mice after DOX, observed within 48 hours of treatment, could be a source of PV MRC1⁺ TAMs in DOX treated tumours. Therefore, the maturity of PV TAMs was examined to see if they were immature (and therefore possibly newly recruited from such monocytic precursors) or mature. This was done by co-staining them with Gr-1 and Ly-6G in frozen tumour sections. Gr-1 was used as a surrogate marker for Ly-6C, as this was found to be expressed on CD31⁺ blood vessels. As Gr-1 is also expressed by

neutrophils, Ly-6G was used to identify whether the PV MRC1⁺ cells co-expressing Gr-1 were neutrophils. The majority of PV MRC1⁺ TAMs did not express Gr-1 or Ly-6G, suggesting that they were relatively mature macrophages, and not newly recruited, Ly6C⁺ monocytes. Despite this, these cells may have still been recruited from MRC1⁺ circulating monocytes, and could have matured rapidly into TAMs in the presence of the vasculature. Again, this is relatively unlikely, as previous studies in TS/A bearing mice showed Ly-6C^{hi} monocytes recruited from the peripheral blood did not lose their Ly-6C expression until 12 days after extravasating into these tumours [68]. Indeed, approximately 25% of MRC1⁺ PV TAMs did express Gr-1, although this was not altered by DOX, suggesting that DOX did not cause an increase in recruitment of immature myeloid cells into the PV niche. Another potential mechanism for the increase in PV MRC1⁺ TAMs could be that endothelial cells in DOX treated tumours recruit TAMs from elsewhere in the tumour and/or skew them towards a pro-tumoural phenotype (or at least upregulate their MRC1 expression).

In order to assess whether TAMs were proliferating in this model, tumour bearing mice were injected with BrdU, a marker of cell proliferation. However, due to time constraints it was not possible to follow up on this study and investigate whether the TAMs had actually incorporated the BrdU. Future studies could do this to reveal insights in to whether TAMs accumulate in the PV niche, at least in part, via proliferation. Interestingly, previous studies demonstrated that MRC1⁺ TAMs in cyclophosphamide-treated LLCs did not incorporate BrdU, suggesting their increase in number after chemotherapy was due to recruitment/retention, not proliferation [144].

In order to investigate TAM recruitment and maturation in more detail, more time points, for example 6, 12 and 24 hours after chemotherapy, would be needed. It would also have been interesting to use intravital imaging to understand the origin of MRC1⁺ TAMs within the PV niche. Intravital imaging was not carried out due to budget constraints and the limitations of the multiphoton microscope in the mouse facility. Movahedi and colleagues demonstrated that Ly-6C^{hi} monocytes infiltrate tumours and

develop into TAMs using flow cytometry and fluorescent latex beads, however this approach would not be useful to answer this question, as flow cytometric analysis would not provide spatial information about the location of each TAM subset, so PV TAMs would be indistinguishable from non-PV TAMs [68]. Adoptive transfer of MRC1⁺ monocytes into TS1 tumour bearing mice after DOX administration may have revealed whether these cells are recruited into the PV niche, however as these cells were so low in abundance, many mice would have had to be culled to perform such an experiment.

In a recent study, Hoechst 33342 dye was injected into mice intravenously and allowed to diffuse into tumours, labelling cells (including TAMs) which were close to vasculature, which allowed purification of TAMs in vascularised areas using FACS [180]. This technique made it possible to study the TAMs which were near perfused vessels and those which were not. The limitation of this technique is it only labels TAMs that are 'near' the vasculature, rather than a purely PV population. Therefore, recent advances in labelling techniques developed by Dr. Russell Hughes are very exciting. Intravenous administration of fluorescently-conjugated dextrans have previously been used to label these TAMs within tumours [116], however in this novel technique, mice are culled 30 minutes after dextran administration, and during this time only the PV TAMs take up the fluorescent dextrans (Hughes, unpublished). This means that they can then be isolated from enzymatically dispersed tumours by FACS. Such studies are now being conducted by a postdoctoral scientist in my research group and will, hopefully, allow a detailed investigation into the phenotype of PV MRC1⁺ and non-PV MRC1⁻ TAMs in PBS and chemotherapy-treated tumours. By examining chemokine receptor expression in PV MRC1⁺ TAMs, we may understand other mechanisms by which TAMs are recruited into tumours. Potentially, these studies could reveal novel targets specific to the PV TAMs, so they can be targeted with cytotoxic agents or agents which reprogram these cells towards a more M1-like phenotype.

Given the increase in PV TAMs, the tumour vasculature was characterised to establish whether TAMs were being recruited by, or retained around, a particular type

of vessel. Normal blood vessels are typically described as arterial, venous or capillaries on the basis of features including several markers such as EphB4 (venous fate) and ephrin-B2 (arterial fate) [241]. In these studies, lumen size was used as a surrogate marker to identify different vessel types for several reasons. Firstly, EphB4 is expressed by many different tumour cells, making its detection on the tumour vasculature more complex [242]. Secondly, arterial and venous differentiation depends in part on blood flow, and it is well accepted that in tumours this is heterogeneous and untypical of blood flow which allows the vasculature to remodel into distinct arterial and venous vessels [218], [243]. It is therefore not surprising that the vasculature of tumours has a completely different structure to that seen within healthy tissues (i.e. not arteries-arterioles-capillaries-venules-veins) [217]. In tumours, vessel types include capillaries, glomeruloid microvascular proliferations and vascular malformations and are described in Table 4.1. Given that these vessel types require several morphological features to be defined, including pericyte coverage, it was decided to use lumen area so that CD31 could be utilised as a single marker approach to identify types of tumour blood vessels.

Luminal area was able to classify three different categories of vessels in TS1 tumours. The smallest vessels, $0-80\mu\text{m}^2$ were considered to be capillaries, as this area corresponds to a diameter of $\leq 10\mu\text{m}$ [235]. Any vessels with a lumen area larger than $80\mu\text{m}^2$ were likely to have an arteriole or venule-like structure, and these were subdivided into vessels that had an area smaller or greater than $1200\mu\text{m}^2$ – as histogram analysis showed there was a clear separation of vessels around this size, which allowed the analysis to distinguish between capillaries and larger vessels. Initially lumen size was measured and used to establish whether TAMs gathered around vessels of a particular size. For the first time, it was shown that the stroma of these implantable TS1 tumours had more vessels with a larger lumen area than the tumour cell islands. Both the stroma and tumour cell islands of TS1 tumours appeared to have more PV MRC1⁺ TAMs gathering around vessels which were $80-1200\mu\text{m}^2$ in

size. However, when the number of TAMs was normalised to number of vessels, it was revealed that luminal area did not impact on the number of associated PV TAMs. This suggests that the DOX-induced increase in PV MRC1⁺ TAMs may be a phenomenon which occurred across all vessels, rather than one particular subtype.

It is important to note that there were limitations to this lumen-based approach. Not least of which was that the analysis itself was restricted to vessels with a measurable lumen, in other words, the vessel was cut at a cross-section which made the lumen visible. Some vessels were therefore not analysed in tumour sections, as within the tumour section they were running parallel to the plane in which the tumour section was cut. Furthermore, the number of vessels with a measurable lumen may have been reduced as the lumens of some vessels may have collapsed post-mortem. To avoid this, previous studies have used intra-cardiac administration of PFA to preserve the architecture of the vasculature [69], [70], [137]. However fixing the tumours in this way would have reduced the number of antibodies that could later be used to label cells in tumour sections. Moreover, lumen size was not a primary aim of the *in vivo* study, and PFA perfusion of the vasculature would have preserved the entire tumour, preventing the ability to collect live cells from these tumours for FACS analysis. It is worth noting that when the analysis of PV TAMs was restricted to vessels with a measurable lumen, DOX had no effect on the numbers of PV TAMs when normalised to the number of vessels in each category – this was probably as many vessels were excluded (as they did not have a measurable lumen) and so the total tumour vasculature was not accounted for.

While this lumen area-based analysis did not accurately identify vessel types such as mother vessels and vascular malformations, it did allow the study of the relationship between TAMs and vessels of different sizes. In order to identify additional features of these vessels within the tumours, other parameters such as pericyte coverage, blood flow (FITC-lectin perfusion) and vessel permeability (by administering molecules which could diffuse out of the vasculature, or *Ricinus communis agglutinin I*,

which binds to exposed basement membrane [137]) would have to be analysed in conjunction with CD31 staining. As the aim of this study was to also analyse PV MRC1⁺ TAMs, in conjunction with CD31 staining, it was not possible to simultaneously analyse pericyte coverage, vessel permeability and patency, as confocal microscopy only allows 4 different fluorophores to be imaged at a given time.

HEVs are vessels adapted to promote T lymphocyte extravasation, and are usually found within lymph nodes [224]. More recently, their presence has been described within breast cancer patient samples [226]. Tumours which had increased HEV numbers also had increased infiltration of T cells and B cells and these patients had increased disease-free, metastasis-free and overall survival compared to patients with low numbers of HEVs [226]. Given this impact of HEVs on prognosis, it was interesting to attempt to identify HEVs within these TS1 tumours. However, HEVs (as recognised by PNA_d staining) could not be identified within the PBS and DOX treated TS1 tumours.

Interestingly, in another study, murine fibrosarcomas (induced by the chemical, methylcholanthrene) only contained HEVs after Tregs were depleted (using diphtheria toxin and FOXP3^{DTR} mice to deplete FOXP3⁺ cells) [227], and even then, only half of the tumours which had depleted Tregs showed any positive PNA_d staining. In those cases PNA_d stained less than 1% of the FOV, suggesting that HEVs do not make up a significant part of the vasculature in such tumours. Importantly, in wild-type murine fibrosarcomas containing Tregs, there were no HEVs [227], in agreement with the studies detailed in this chapter using TS1 tumours. These studies call into question the relevancy of HEVs within murine tumour models. The HEV presence within some forms of human tumours, however, cannot be ignored, although there is clearly variability in HEV abundance within patient samples. This may suggest that HEV abundance is a factor which differs between patients and pre-clinical models, and is something which will need to be considered when translating research to patients.

As Tregs suppress HEV formation [227], T cell recruitment was examined in TS1 tumours to identify a potential reason for the lack of HEVs within TS1 tumours. Total T cell recruitment was not significantly altered by DOX, as although there was a trend of an increased CD4:CD8 ratio in the stroma of DOX treated tumours this was not significant. Importantly, Tregs were present in both DOX and PBS treated tumours, which probably explains the lack of HEVs within these tumours.

Intravenous administration of FITC-lectin was used to analyse vessel patency, to further understand the functional status of vessels within these TS1 tumours (i.e. their ability to carry flow). If vessels were patent, it was possible that they could carry circulating monocytes into the tumour where they can extravasate and form TAMs. DOX did not affect vessel patency. In agreement with this, other studies have shown the blood vessel perfusion of MMTV-PyMT tumour bearing mice was not affected by paclitaxel and cyclophosphamide treatment [139]. While vessel patency was not altered by DOX, it was interesting that the majority of vessels within the tumour stroma were patent, whereas the tumour cell island had far fewer patent vessels. These data help to explain the finding in Chapter 3, that the tumour stroma was more normoxic than tumour cell islands.

It would have been interesting to analyse PV TAM recruitment around patent and non-patent vessels, as this might have contributed information on how TAMs arrive at the PV location (e.g. by extravasation vs. chemoattraction from different areas in tumours). Previously, Nakasone and colleagues demonstrated that TAMs and immature myeloid cells limit the permeability of the MMTV-PyMT tumour vasculature in an MMP9-dependant manner, however the location of TAMs in relation to patent and permeable vessels was not explored in this context [137]. Further studies should characterise how vessel patency relates to the location of TAMs. Although, as DOX treatment did not influence vessel patency, it is unlikely that alterations in vessel patency are responsible for the DOX-mediated increase in PV MRC1⁺ TAMs. Studies

utilising *Ricinus communis* lectin may also be useful to understand if PV MRC1⁺ TAMs gather around vessels which are more permeable.

Pericyte coverage of vessels was also analysed, as a measure of blood vessel phenotype. There are conflicting studies regarding the effect of pericytes on macrophage infiltration [220]–[222], [244]–[246]. Total pericyte coverage of vessels as analysed by the CD31 area covered by α -SMA, and the proportion of vessels associated with pericytes, was not altered by DOX. In agreement with this, a study examining pericyte coverage of vessels in murine hearts also showed pericyte coverage was not affected by administration of DOX [231]. Due to time constraints, the number of pericytes per vessel was not analysed in the current study. It would have been interesting to examine this, as pericyte coverage of tumour vessels differs with vessel maturity [220]. As the majority of blood vessels had some form of PV α -SMA⁺ cell, the effect of pericyte coverage on PV TAMs was not examined. However, analysing the number of pericytes per vessel could result in interesting findings by comparing TAM recruitment around vessels with increased pericyte coverage vs. those with few pericytes. As DOX did not impact on the pericyte coverage of vessels, it is unlikely that changes in pericyte coverage could be responsible for the increase in PV MRC1⁺ TAMs.

4.5 Concluding Remarks

DOX-treated TS1 tumours had increased numbers of MRC1⁺ TAMs making direct contact with blood vessels than their PBS-treated counterparts. These TAMs were mature Gr-1⁻ cells, and were therefore unlikely to have been newly recruited from a subset of MRC1⁺ monocytes which were more abundant in DOX treated mice compared to PBS treated mice. The increase in PV MRC1⁺ TAMs suggests that following DOX treatment, the tumour vasculature is altered in a way which promotes the recruitment, retention and/or education of pro-tumoural MRC1⁺ TAMs, and

therefore attempts were made to characterise the tumour vasculature. DOX did not impact on the various vascular parameters analysed including vessel patency and pericyte coverage, suggesting that DOX may affect tumour vasculature in a different manner, which results in an increase in PV MRC1⁺ TAMs. Therefore, the next step to further understand the relationship between the tumour vasculature and TAMs is to purify tumour endothelial cells and identify how their gene expression profile changes following chemotherapy. Potentially TAMs may be attracted to the PV niche by endothelial cells expressing more chemokines after DOX treatment. Additionally, increases in adhesion molecule expression may also result in increased TAM retention in the PV space after DOX. Therefore, the expression of these genes will need to be investigated as these may impact on TAM recruitment, retention or phenotype.

Chapter 5

Effect of DOX on the expression of selected genes by endothelial cells in TS1 tumours

5.1 Introduction

The previous chapter demonstrated an increase in PV MRC1⁺ TAMs 48 hours after DOX treatment. It was unlikely that this was due to the selective recruitment of the small number of MRC1⁺ monocytes induced by DOX in the peripheral blood of such mice, bearing TS1 tumours, as the PV MRC1⁺ TAMs were shown to be mature (lacking Gr-1 expression). In addition to this, there were no obvious morphological changes in the vessels that correlated with this observation. Therefore, the next logical step was to establish whether DOX induced changes in the expression of genes by tumour endothelial cells that encode proteins likely to influence TAMs in the PV niche. Potentially, these could alter the recruitment, retention and/or phenotype of neighbouring TAMs.

Endothelial cells provide a barrier through which monocytes extravasate in order to enter the tumour microenvironment [247]. As will be seen below, a number of studies have shown that endothelial cells can regulate monocytes/macrophages in a number of ways. For example, they express a number of chemokines and/or cell adhesion molecules (CAMs) which influence monocyte recruitment and TAM retention in the PV niche. Examples of the former include CSF1 [186], CXCL12 [248], [249] and angiopoietin-2 [250]. CSF1 is a growth factor, which also acts to promote monocyte viability and differentiation [251]. More recently, CSF1 was shown to increase TAM numbers in both pancreatic tumours treated with gemcitabine, and MMTV-PyMT mammary tumours treated with paclitaxel [108], [109]. CXCL12 was also implicated in TAM recruitment in LLCs treated with cyclophosphamide [144]. Angiopoietin-2 has also shown chemoattractive properties for TEMs [92] and knockdown of its receptor, Tie2 in TAMs reduced the number of TEMs in contact with blood vessels in MMTV-PyMT tumours [102].

Additional studies have shown that these chemokines are also able to stimulate TAMs to express an M2-like phenotype. For example, macrophages co-cultured with

endothelial cells express increased levels of the M2-like markers, MRC1 and arginase-1; whereas M1-like genes like IL-12 and TNF were not upregulated [186]. CSF1 also skews TAMs towards an M2-like phenotype in some mouse tumour models. Treatment of mouse glioblastomas with a CSF1R inhibitor resulted in TAMs expressing a more M1-like phenotype [31]. CXCL12 was shown to increase VEGF and CCL1 expression in human peripheral blood monocytes *in vitro*, suggesting that CXCL12 also acts to increase the proangiogenic activity of these cells [195]. Angiopoietin-2 also exerts a profound effect on TAMs expressing TIE2, enhancing their proangiogenic and immunosuppressive functions [99], [103].

CAMs like vascular cellular adhesion molecule-1 (VCAM-1) are important mediators of monocyte extravasation, acting to aid the rolling and adhesion of monocytes to the surface of endothelial cells [237, 242]. Also, inhibition of Mac-1 (a complex of integrin α M and integrin β 2) prevented regrowth of irradiated Fadu human head and neck squamous cell carcinoma xenografts, via a reduction in the recruitment of relapse-promoting myeloid cells [253]. Furthermore, direct contact with endothelial cells has been shown to promote the development of macrophages from colonies of HSCs *in vitro*, suggesting that endothelial cells express factors (CAMs and/or cytokines) that promote monocyte/macrophage differentiation [186].

Other studies have also inferred the ability of tumour blood vessels to influence TAMs. When the blood vessels of mouse (MCP0008) tumours were 'normalised' by treatment with the VEGFR2 targeted antibody, DC101, TAMs developed an M1-skewed, immunostimulatory phenotype, increasing their expression of *Ii12a*, *Nos2*, *Cxcl9* and *Cxcl11* and reducing their expression of the M2-associated genes, *Ccl17* and *Mmp9* [180]. Vessel normalisation using other methods, such as overexpression of HRG by tumour cells [30] also skewed TAMs towards a tumouricidal phenotype, as depletion of TAMs using clodronate liposomes in these tumours caused them to grow faster [30]. More recently, vessels were normalised in murine models of glioma by simultaneously inhibiting angiopoietin-2 and VEGF signalling [176], [177]. These

tumours had reduced numbers of MRC1⁺ M2-skewed TAMs [177]. Moreover, depletion of TAMs from such mouse gliomas treated with anti-angiopoietin-2 and cediranib (a VEGFR inhibitor), using anti-CSF1 reduced survival of these mice, suggesting that the TAMs in these tumours had become tumouricidal [176].

In order to investigate what, if anything, endothelial cells might express in tumours that stimulate the accumulation of PV MRC1⁺ TAMs after DOX treatment, endothelial cells were purified from TS1 tumours 48 hours after mice were injected with PBS or DOX. Following this, their RNA was isolated and qPCR studies were conducted to analyse the expression of genes encoding 31 selected cytokines and adhesion molecules, all previously shown to be involved in the process of macrophage chemoattraction and/or activation (Table 5.1).

Three different methods were employed to isolate endothelial cells from these mouse tumours: FACS, laser capture microdissection (LCM) and magnetic isolation. Each of these methods provided various advantages, described below.

FACS allows the use of multiple markers (CD45, CD31, etc) to isolate different cell subpopulations from one sample (up to 4 using the BD FACS Aria available in my department), and thus allowed the collection of both endothelial cells and leucocytes from the same tumours. This allows the selection of CD31⁺ cells which are not leucocytes, as TEMs were previously shown to express low levels of CD31 [71]. Previously, my supervisor's group had successfully used FACS to isolate TAMs from mouse tumours but not endothelial cells so a protocol for this had to be established as part of the work outlined in this chapter [144].

LCM is usually used to isolate cell populations located in different areas of the same tissue section (e.g. stroma and tumour cell islands). Previous studies have used LCM to successfully isolate endothelial cells from both murine and human tumour sections [254], [255].

Magnetic isolation of endothelial cells from live cell suspensions derived from tumours has also been used to isolate such cells from tumours [256], [257]. However,

in the latter case, qPCR has to be used to assess the enrichment of endothelial cells in the samples isolated, as an antibody to only one marker (usually CD31) is used to select them [256].

The hypothesis being tested in these studies was that DOX alters the expression of one or more genes in tumour endothelial cells which then contribute(s) to the accumulation of MRC1⁺ TAMs around blood vessels. So, the aims of this chapter were, therefore, to:

1. Develop an effective way to isolate endothelial cells from PBS and DOX treated TS1 tumours.
2. Analyse the expression of 31 selected genes, known to influence macrophage recruitment, retention and/or phenotype, by these endothelial cells, as described in Table 5.1.

Gene name	Abbreviation	Function relevance to PV TAMs	Ref
<i>Angiopoietin-2</i>	<i>Angpt2</i>	Chemoattractant for TEMs, increases immunosuppressive and angiogenic functions in TEMs	[92], [93], [99], [102], [103]
<i>Ccl2</i>	<i>Ccl2</i>	Attracts CCR2 ⁺ monocytes into tumours	[137]
<i>Ccl3</i>	<i>Ccl3</i>	Retains MAMs in lung metastases	[129]
<i>Ccl4</i>	<i>Ccl4</i>	Monocyte/macrophage chemoattractant	[258]
<i>Ccl5</i>	<i>Ccl5</i>	Monocyte/macrophage chemoattractant	[259]
<i>Ccl7</i>	<i>Ccl7</i>	Monocyte/macrophage chemoattractant	[260]
<i>Ccl8</i>	<i>Ccl8</i>	Monocyte/macrophage chemoattractant	[260]
<i>Ccl9</i>	<i>Ccl9</i>	Chemoattractive to immature myeloid cells	[261]
<i>Ccl12</i>	<i>Ccl12</i>	Monocyte/macrophage chemoattractant	[262]
<i>Colony stimulating factor 1</i>	<i>Csf1</i>	Macrophage growth factor and chemoattractant, promotes M2-skew and inhibition reduces TAMs <i>in vivo</i>	[31], [108], [109], [196]
<i>Colony stimulating factor 2</i>	<i>Csf2</i>	Macrophage growth factor, promotes M1-skew	[31], [43]
<i>Cx3cl1</i>	<i>Cx3cl1</i>	Monocyte/macrophage chemoattractant	[263], [264]

<i>Cxcl12</i>	<i>Cxcl12</i>	Regulates macrophage differentiation and interfering with signalling reduces TAMs <i>in vivo</i>	[144], [195]
<i>Endoglin</i>	<i>Eng</i>	Involved in monocyte extravasation	[265]
<i>E-selectin</i>	<i>Sele</i>	Involved in monocyte extravasation	[247], [266]
<i>Fas ligand</i>	<i>FasL</i>	Monocyte/macrophage chemoattractant	[267]
<i>Fibroblast growth factor 1</i>	<i>Fgf1</i>	Decreases monocyte adhesion to endothelial cells	[268]
<i>Fibronectin</i>	<i>FN1</i>	Chemoattractive to monocytes, increases tumouricidal activity of macrophages	[269], [270]
<i>Intercellular adhesion molecule 1</i>	<i>Icam1</i>	Involved in monocyte extravasation	[247], [271]
<i>Intercellular adhesion molecule 2</i>	<i>Icam2</i>	Involved in monocyte extravasation	[247], [271]
<i>Interferon-γ</i>	<i>Ifnγ</i>	Induces 'M1' phenotype in macrophages when combined with other stimuli such as LPS or TNF	[2], [32]
<i>Interleukin-10</i>	<i>Il10</i>	Induces 'M2c' immunosuppressive macrophage phenotype	[2], [42]
<i>Interleukin-1α</i>	<i>Il1a</i>	Affects endothelial CAM expression to increase monocyte adherence	[272], [273]
<i>Interleukin-1β</i>	<i>Il1b</i>	Affects endothelial CAM expression to increase monocyte adherence	[272], [273]
<i>Interleukin-6</i>	<i>Il6</i>	Promotes monocytes to differentiate into macrophages rather than dendritic cells	[274]
<i>Osteopontin</i>	<i>Spp1</i>	Extracellular matrix component and macrophage chemoattractant	[275], [276]
<i>Placental growth factor</i>	<i>Plgf</i>	TAM chemoattractant, promotes M2-skew	[30], [277], [278]
<i>Thrombospondin-1</i>	<i>Thbs1</i>	Chemoattractive to macrophages, increases phagocytic activity	[279]
<i>Tumour necrosis factor</i>	<i>Tnf</i>	Induces 'M1' phenotype in macrophages when combined with IFN-γ	[2]
<i>Vascular cellular adhesion molecule 1</i>	<i>Vcam1</i>	Involved in monocyte extravasation	[252]
<i>Vascular endothelial growth factor A</i>	<i>Vegfa</i>	Monocyte/macrophage chemoattractant	[280]

Table 5.1 Genes assayed using qPCR, for primer sequences see section 2.1.7.

5.2 Methods

The basic steps involved in these three different endothelial cell isolation methods are summarised in Figure 5.1.

For FACS based isolations, there was limited availability of the BD FACS Aria in my Department (which was only available during core facility hours and in fairly constant use). Tumours were, therefore, cut into chunks and preserved in cryopreservation buffer and stored in liquid nitrogen, until the FACS Aria was available for use. The TS1 tumours were enzymatically dispersed (as described in section 2.2.5) and incubated with the antibodies listed in Table 5.2, along with the viability dye Zombie NIR (diluted 1 in 1000), for 40 minutes, whilst covered, rocking and on ice. Samples were then washed twice in FACS buffer before sorting the cells on the FACS Aria. The gating strategy was set using FMO controls and is shown in Figure 5.2. Three subpopulations were then selected on the basis of the expression of a pan-endothelial marker, CD31 [137], [281] and the pan-leucocyte marker CD45: CD31⁻ CD45⁻ cells (gate 3c); CD31⁺ CD45⁻ cells (gate 3a i.e. endothelial cells) and CD31⁻ CD45⁺ cells (gate 3b). Cells were then sorted into RLT lysis buffer (from the RNeasy Mini kit). Finally, RNA was collected from the cells using the RNeasy Mini kit as described in section 2.2.15.1. RNA was quantified using the NanoDrop as described in section 2.2.15.5.

Antibody	Fluorophore	Clone	Conc (µg/mL)
Rat (m) Anti-Mouse CD45	Brilliant Violet 421	30-F11	4
Rat (m) Anti-Mouse CD31	AlexaFluor488	MEC13.3	10

Table 5.2 Antibodies used in FACS sorting of TS1 tumours (m) = monoclonal antibody

LCM was performed as described in section 2.2.13. Briefly, 10µm sections were cut using a cryostat and collected onto uncharged glass slides. The Rapid-Immuno staining protocol was used to stain collagen IV on the basement membrane of

endothelial cells. The Pixcell II LCM system was used to collect collagen IV⁺ cells. RNA was then isolated using the PicoPure kit as described in section 2.2.15.2. RNA quantity and quality was assessed using the Agilent Bioanalyzer 2100, described in section 2.2.15.4.

Magnetic isolation of a CD31-enriched cell fraction was carried out as described in section 2.2.14. Briefly, tumour digests (as described in section 2.2.5) were washed in HBSS with 10% FCS three times. The cell pellet was then resuspended in 1mL HBSS with 10% FCS and 2.4×10^6 Sheep anti-rat IgG Dynabeads conjugated to rat anti-mouse CD31 antibody and left incubating rocking at 4°C for 30 minutes. Following the incubation, the cells were washed using the DynaMag-15 magnet with HBSS with 10% FCS 6 times. RNA was isolated from these cells using the RNeasy Plus Mini kit as described in section 2.2.15.3. RNA was first quantified using the NanoDrop (section 2.2.15.5) and then the RNA integrity was assessed using the Agilent Bioanalyzer 2100 (section 2.2.15.4). RNA isolated from this experiment was converted to cDNA using the QuantiTect Reverse Transcription kit (section 2.2.16).

Enrichment of the CD31-enriched cell fraction isolated via magnetic separation was assessed by qPCR, using the protocol described in section 2.2.17. 2.5ng of cDNA was used per well and the $2^{-\Delta\Delta Ct}$ method was used to compare the expression of *Acta2* (α -SMA, a marker of fibroblasts, pericytes and smooth muscle cells); *Adgre1* (F4/80, a marker of macrophages); *Epcam* (a marker of epithelial and tumour cells); *Ilgam* (CD11b, a marker of myeloid cells) and *Pecam1* (CD31, a marker of endothelial cells) in the CD31-enriched cell fraction with the CD31-depleted cell fraction. *Actb* expression was also measured and used to normalise gene expression as a housekeeper.

Gene expression analysis was performed in the CD31-enriched cell fractions using qPCR as described in section 2.2.17. 1ng of cDNA was used per well and the $2^{-\Delta\Delta Ct}$ method was used to compare the expression of genes, described in Table 5.1, in CD31-enriched cell fractions from both DOX and PBS treated tumours.

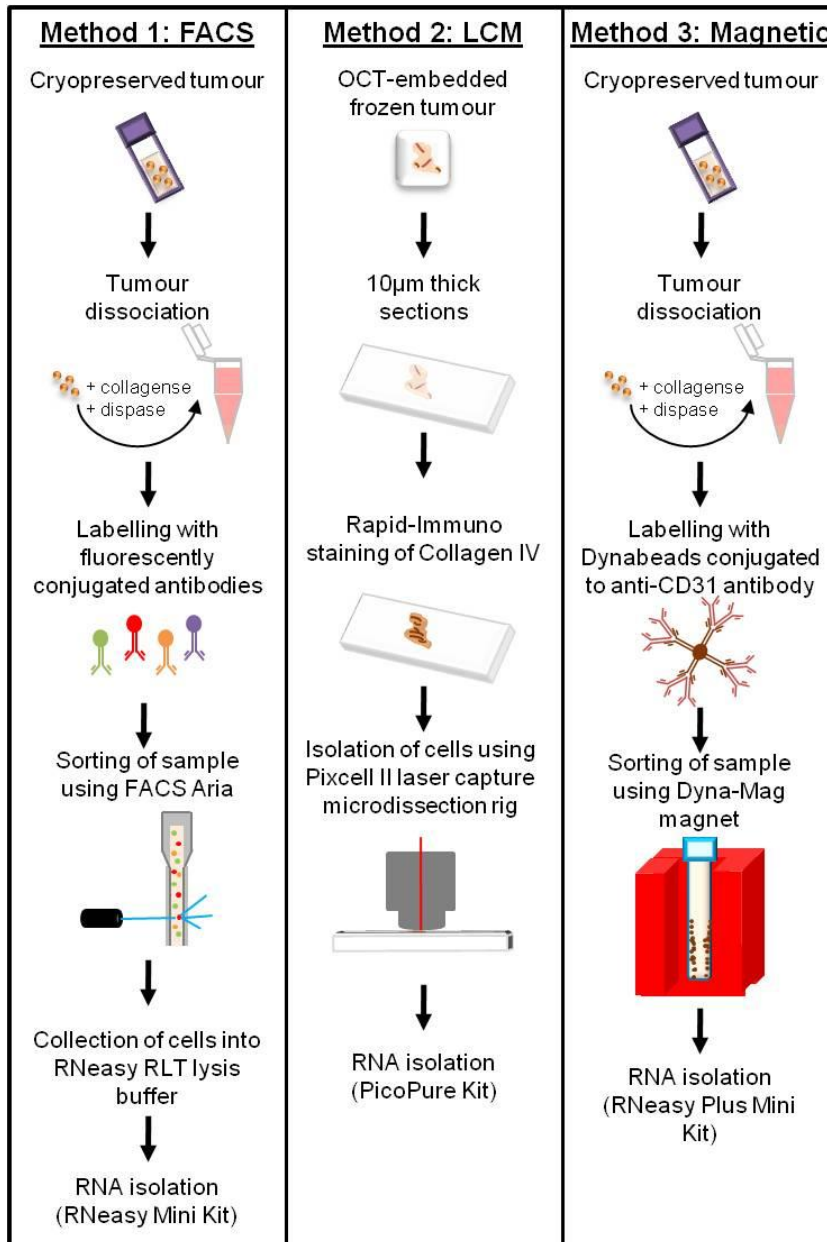


Figure 5.1 Various methods used to isolate tumour endothelial cells.

Method 1 used fluorescently conjugated antibodies and FACS to identify cell populations in tumour digests and sort them accordingly. Laser capture microdissection (LCM, method 2) uses immunohistochemical staining of frozen sections and selection of cells using a laser microdissection rig to isolate cells. Magnetic isolation (method 3) allows sorting of CD31⁺ cells from tumour digests using magnetic Dynabeads conjugated to anti-CD31.

Analysis of selected genes in the CD31-depleted cell fractions was performed as described above to compare gene expression in CD31-depleted cell fractions from PBS and DOX treated tumours. Gene expression analysis was restricted to the genes previously shown to be upregulated by the CD31-enriched cell fraction in response to DOX. Primer sequences for genes analysed can be found in section 2.1.7.

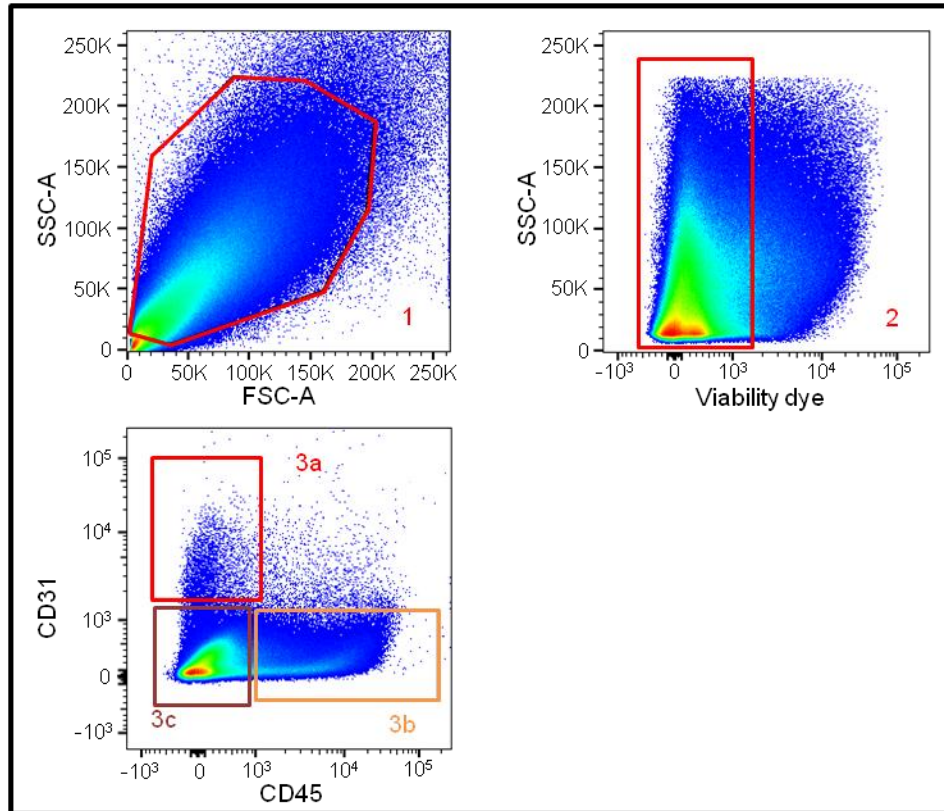


Figure 5.2 Flow cytometric analysis of CD31 and CD45 in digested tumours.

Tumours were digested and labelled with fluorescently conjugated antibodies. The LSR II was used to analyse CD31 and CD45 expression on digested tumours. The gating strategy was set using FMO controls. Cells were selected based on forward scatter and side scatter profiles (1); before gating on viable cells, which excluded the viability dye Zombie NIR (2). Three cell populations can be identified using this method: CD31⁺ CD45⁻ cells (3a); CD45⁺ CD31⁻ cells (3b) and CD45⁻ CD31⁻ cells (3c).

5.3 Results

5.3.1 Isolation of endothelial cells using FACS.

Due to the limited availability of the FACS Aria, the LSR II was first used to determine whether CD31 and CD45 could be detected on cells from the cryopreserved TS1 tumours using flow cytometry. Figure 5.2 shows representative CD31 and CD45 staining on cells in dissociated TS1 tumours, demonstrating that endothelial cells were present and detectable in these samples. RNA yields from the FACS sorting were initially negligible, possibly due to cell death prior to RNA isolation. This could have been due to cells being resuspended in Iscove's Modified Dulbecco's Medium prior to RNA isolation. In order to increase the RNA yield, cells were alternatively collected into RLT lysis buffer from the RNeasy Mini Kit, at a ratio of 1mL sorted cells to 3mL RLT buffer. This allowed cells to lyse on contact with the lysis buffer, thus improving RNA yields.

The FACS Aria was used to identify and isolate the three main different cell populations: CD31⁺ CD45⁻ cells (Figure 5.3A, gate 3a i.e. endothelial cells); CD31⁻ CD45⁺ cells (Figure 5.3A, gate 3b i.e. leucocytes) and CD31⁻ CD45⁻ cells (Figure 5.3A, gate 3c, i.e. a population of any remaining tumour cells and cells like fibroblasts and pericytes). The FACS Aria is only able to record data for 10,000 events in total – and as the endothelial cells were rare events in comparison to the tumour cells and leucocytes, the population inside gate 3a does not appear very abundant. Despite this, 25,000 cells were collected from population 3a.

RNA was isolated from the sorted cells using the RNeasy kit as described in section 2.2.15.1. Figure 5.3B demonstrates the low yield of RNA from the CD31⁺ CD45⁻ cells both before (i) and after (ii) the RNA was cleaned up using water-saturated butanol as described (section 2.2.15.6). Green arrows on the NanoDrop traces indicate where the typical RNA peak is seen at the 260nm wavelength if RNA yields are good.

As the RNA yields were too low to be used in subsequent qPCR analyses, alternative methods to isolate endothelial cell specific RNA were then attempted.

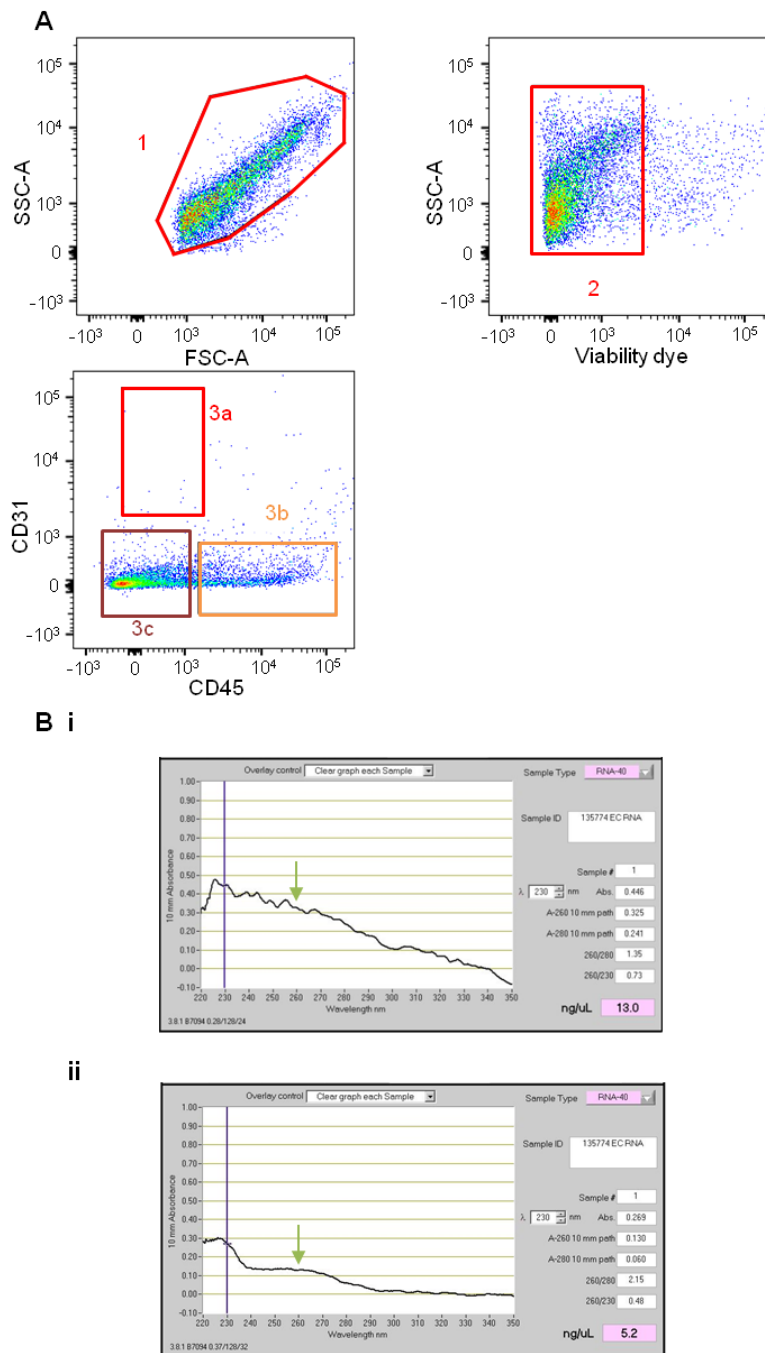


Figure 5.3 FACS isolation of endothelial cells from digested tumours.

Tumours were digested and labelled with fluorescently conjugated antibodies. The FACS Aria machine was then used to separate three different populations from the tumours. The sample gating strategy is shown in A. (1) First cells were selected based on forward scatter and side scatter profiles; (2) before selecting viable cells that excluded Zombie NIR viability dye. Following this three cell populations were sorted: (3a) CD31⁺ CD45⁻ cells; (3b) CD45⁺ CD31⁻ cells and (3c) CD45⁻ CD31⁻ cells. (B i) Example NanoDrop traces from the CD31⁺ CD45⁻ population is shown after RNA isolation and (B ii) following a clean-up of RNA with water-saturated butanol. Green arrows indicate the typical position of a RNA peak at 260nm.

5.3.2 Isolation of endothelial cells using LCM.

As mentioned previously, LCM represents an alternative approach for the isolation of endothelial cells. Previously, a rapid staining protocol was optimised using collagen IV to identify blood vessels (as described in section 2.2.13) by Dr Julie Simpson at the Sheffield Institute of Translational Neuroscience. Collagen IV has been shown to stain the basement membrane of the endothelium in murine tumours (LLCs, RIP-Tag2 pancreatic tumours and MCa-IV mammary tumours), and co-localises with CD31 staining [193]. Representative tumour collagen IV staining is shown in Figure 5.4A. An attempt was therefore made to isolate collagen IV⁺ endothelial cells from frozen TS1 tumour sections.

Figure 5.4B shows images taken during the LCM of blood vessels from these sections. As coverslips were absent during this procedure, the light refraction was less than optimal and so the background staining appears more intense in these images, but this was unavoidable. It was still possible to discern collagen IV⁺ blood vessels from this background staining during the LCM procedure (Figure 5.4Bi, see black arrows). During LCM (Figure 5.4Bii), a 'halo-like' appearance can be noted around the cells which are to be captured. Following capture, gaps can be seen in the tissue (note black arrows in Figure 5.4iii), which indicate the collagen IV⁺ cells have been successfully isolated. As demonstrated by Figure 5.4Biv, LCM collects collagen IV⁺ cells onto the cap of the laser microdissection rig. The RNA was then collected from these cells using the PicoPure RNA Isolation Kit (described in section 2.2.15.2.) It is very important to check the RNA integrity of samples, particularly when dealing with samples isolated using LCM, as the RNA is isolated from tissue which is already dead. Therefore, the Agilent 2100 Bioanalyzer was used to analyse the RNA integrity of the samples isolated.

Figure 5.4C shows a typical trace from an Agilent Bioanalyzer demonstrating that these samples had very poor RNA integrity (as noted by the loss of the peaks at the 18S and 28S ribosomal RNA sites) [282]. The RIN value for the collagen IV⁺ cells

isolated was on average 2.1 out of a possible 10, demonstrating a degradation of the RNA (n=2). As the RNA quality was poor, LCM was deemed an unsuccessful method for isolating endothelial cell RNA and therefore, an alternative method was required.

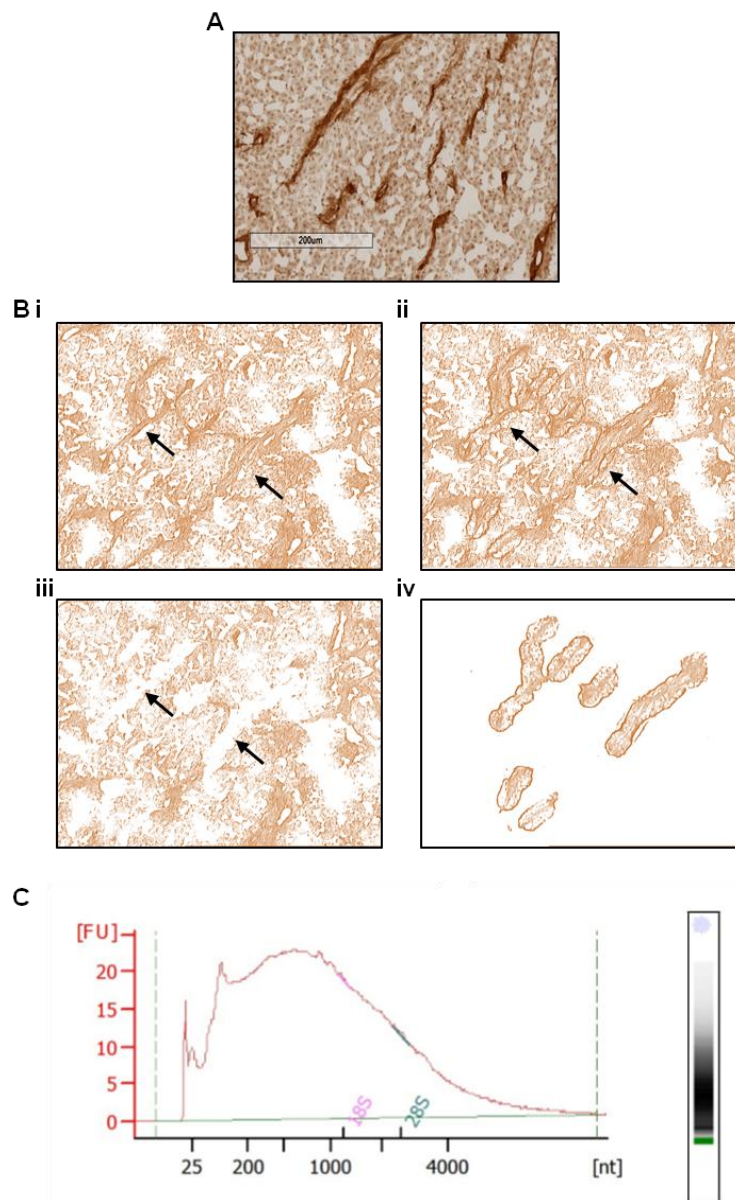


Figure 5.4 Isolation of endothelial cells via Laser Capture Microdissection.

(A) 10µM thick frozen sections were collected onto uncharged glass slides and stained using the described Rapid-Immuno technique for Collagen IV (scale bar= 200µm). Collagen IV⁺ cells were collected using laser capture microdissection. Images in B demonstrate the (i) collagen IV stain before the laser is fired, note the black arrows indicating vessel-like collagen IV⁺ structures; (ii) during the laser being fired - note the halo-like appearance around vessels; (iii) after the laser is fired – the collagen IV⁺ cells have now been collected onto the cap of the dissection rig, note the gaps in tissue, indicated by the black arrows and (iv) an image of the cap, showing the collected cells. (C) RNA was then isolated from the collected cells and the quality was analysed using the Agilent 2100 Bioanalyzer. An example trace from the Bioanalyzer is shown.

5.3.3 Successful isolation of RNA from CD31⁺ cells using magnetic Dynabeads.

As both FACS sorting and LCM failed to produce high yields of intact RNA, a third method for isolating endothelial cells was then attempted. Magnetic Dynabeads conjugated to an anti-CD31 antibody were used to isolate CD31⁺ cells from dissociated tumours, and then the RNA was extracted immediately from these cells. Using this method RNA was isolated successfully from CD31-enriched cells (Figure 5.5Ai) and all other (i.e. CD31-depleted) cells passing through the cell sorting column (Figure 5.5Aii). This yielded improved RNA quality to that seen in the LCM-based isolation methods (Figure 5.5B).

The success of this method can be noted by the clear peak at the 260nm wavelength where RNA is detected, as shown by green arrows on the NanoDrop traces (Figure 5.5A). Having successfully isolated RNA, the integrity was checked using the Agilent Bioanalyzer 2100. As shown in Figure 5.5B the RNA integrity was improved in RNA isolated in this way, with traces taken from the Agilent Bioanalyzer for shown for CD31-enriched (Figure 5.5Bi) and CD31-depleted cell fractions (Figure 5.5Bii). Of note clear peaks are seen at the 18S and 28S ribosomal RNA sites, demonstrating intact RNA. As this magnetic method was able to yield intact RNA from both the CD31-enriched and CD31-depleted cell fractions, this method was employed to isolate RNA from both PBS and DOX treated TS1 tumours (n=3 tumours per group).

5.3.4 Assessing the enrichment of endothelial cells in the CD31-enriched fraction of cells using qPCR.

Having successfully extracted RNA from the CD31-enriched and CD31-depleted cell fractions isolated from tumour samples, qPCR was then used to assess the relative expression of *Pecam1* (CD31, expressed by blood vessels), *Epcam* (a tumour cell marker); *Itgam* (CD11b, a myeloid cell marker); *Adgre1* (F4/80, a macrophage marker); and *Acta2* (α -SMA, a gene expressed by fibroblasts, pericytes and smooth muscle cells) in CD31-enriched and CD31-depleted samples in order to assess whether the

magnetic isolation of endothelial cells had been successful. Figure 5.6A shows the fold change of these genes, as calculated using the $2^{-\Delta\Delta Ct}$ method, normalising gene expression to *Actb* (β -actin).

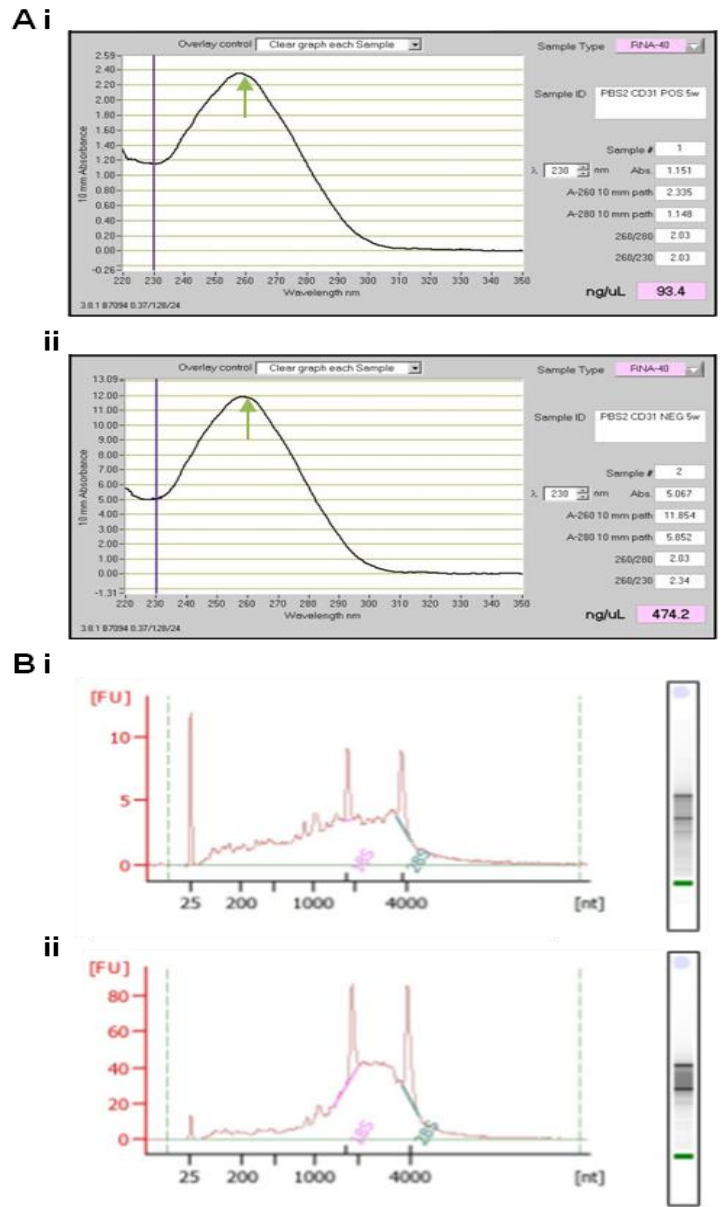


Figure 5.5 Isolation of CD31-enriched cells using magnetic bead isolation.

Tumours were digested and labelled with anti-CD31 conjugated Dynabeads. The DynaMag magnet was then used to isolate the CD31⁺ cells. The RNeasy Plus kit was used to isolate RNA from both the CD31⁺ cells (Ai) and CD31⁻ cells (Aii) as seen in the NanoDrop traces – green arrows indicate peak at 260nm. RNA quality was assessed using the Agilent Bioanalyzer 2100 for both cell populations as shown in B (i – example of a CD31⁺ cell trace; ii- example of a CD31⁻ cell trace).

Expression of the genes of interest were normalised to the housekeeper gene *Actb*, as the Ct values for this gene remained constant amongst samples, regardless of CD31 expression (i.e. CD31-enriched and CD31-depleted samples) and treatment (PBS or DOX). *Pecam1* expression was significantly increased in the CD31-enriched cell fractions, with an average fold change of 54.39 (\pm 12.49) compared to the CD31-depleted cell fractions, demonstrating that the former were enriched for endothelial cells. Expression of *Epcam* was significantly lower in CD31-enriched cell fractions by an average fold change of 0.48 (\pm 0.15) compared to the CD31-depleted cell fractions, demonstrating that they were also not highly contaminated by tumour cells. The *Ilgam* relative expression of the CD31-enriched cell fractions was decreased by an average fold change of 0.60 (\pm 0.13) compared to the CD31-depleted cell fractions, suggesting that the CD31-enriched cell fractions were also not enriched for myeloid cells. Finally, *Adgre1* relative expression was decreased by an average fold change of 0.40 (\pm 0.08) in the CD31-enriched cell fractions compared to the CD31-depleted cell fractions, demonstrating a depletion of macrophages from the CD31-enriched cell fractions.

Acta2 relative expression remained unchanged between the CD31-enriched and CD31-depleted cell fractions (mean fold change 1.26 \pm 0.23), which suggests that transcripts for fibroblast-like cells or pericytes remained unchanged between samples. This is likely explained by pericytes, which coat the vessels of these tumours, remaining attached to the endothelial cells. More vigorous wash steps were introduced to eliminate this possible source of contamination; however this caused all cells to detach from the Dynabeads and resulted in negligible RNA yields. Importantly, the CD31-enriched cell fractions did not have an increase in *Acta2* expression, demonstrating that these samples, while enriched for endothelial cells, were not enriched for pericytes.

Δ Ct values were used to calculate if there were statistically significant changes in gene expression between CD31-enriched and CD31-depleted cell fractions as shown in Figure 5.6 (panels B-F). An increased Δ Ct value indicates a lower expression

of the gene examined. The CD31-enriched cell fractions had significantly lower expression of *Epcam* (mean= 4.24 ± 0.35) compared to the CD31-depleted cell fractions (mean= 2.84 ± 0.20, Paired t-test p=0.0109, Figure 5.6B). *Itgam* expression (Figure 5.6C) was also significantly lower in the CD31-enriched cell fractions (CD31-enriched mean= 9.67 ± 0.30, CD31-depleted mean= 8.63 ± 0.33, Paired t test p=0.0433), as was *Adgre1* expression (CD31-enriched mean= 10.37 ± 0.43, CD31-depleted mean= 8.92 ± 0.27, Paired t test p=0.0020, Figure 5.6D).

Importantly, the CD31-enriched cell fractions had significantly increased *Pecam1* expression (mean= 4.90 ± 0.38) compared to the CD31-depleted cell fractions (mean= 10.49 ± 0.20, Paired t test p<0.0001, Figure 5.6F). *Acta2* expression was consistent between CD31-enriched (mean= 5.94 ± 0.23) and CD31-depleted cell fractions (mean= 6.13 ± 0.31, Paired t test p=0.2819, Figure 5.6E).

Taken together, the above data indicate that the magnetic isolation was relatively successful and the CD31-enriched cell fractions were significantly enriched for endothelial cells.

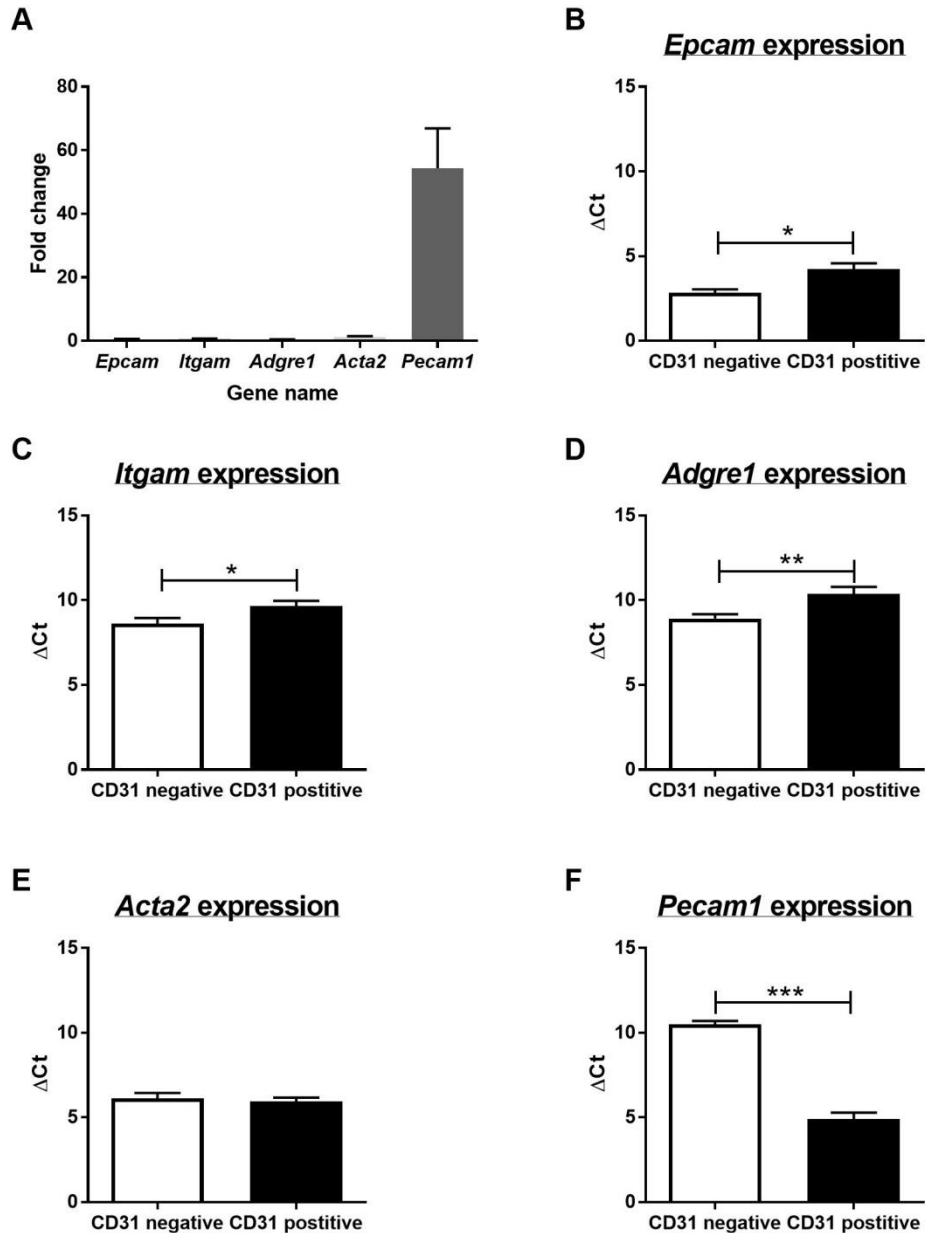


Figure 5.6 Magnetic isolation of CD31⁺ cells enriches *Pecam1* expression and decreases *Epcam*, *Itgam* and *Adgre1* expression in the CD31-enriched fraction of cells compared to CD31-depleted fraction of cells.

RNA was isolated from CD31-enriched cells (as selected using anti-CD31 conjugated Dynabeads) and CD31-depleted cells. Real time qPCR was used to determine the relative expression of 5 different gene transcripts, representative of different cell populations: *Epcam* (protein name: epithelial cell adhesion molecule, a marker of tumour cells), *Itgam* (protein name: integrin α M also known as CD11b, a myeloid cell marker); *Adgre1* (protein name: F4/80, expressed by macrophages); *Acta2* (protein name: α -smooth muscle actin, expressed by fibroblasts, smooth muscle cells and pericytes) and *Pecam1* (protein name CD31; a vascular marker). Fold change (A) was calculated using the $2^{\Delta\Delta Ct}$ method, with gene expression normalised to the housekeeper *Actb* (β -actin). ΔCt values are plotted for the individual genes – B *Epcam* expression; C *Itgam* expression; D *Adgre1* expression; E *Acta2* expression and F *Pecam1* expression. n=6 tumours. Paired t tests *p<0.05; **p<0.01 ***p<0.0001

5.3.5 DOX significantly increases *Angpt2* expression in CD31-enriched cells.

The mRNA levels for the genes listed in Table 5.1 were then assessed in the CD31-enriched and CD31-depleted cell fractions using qPCR.

To understand how PV MRC1⁺ TAMs were increased after DOX, endothelial cell expression of chemokines previously shown to recruit monocytes into tumours were investigated, including *Angpt2*, *Csf1*, *Cxcl12*, and *Plgf* [102], [109], [144], [277]. The level of mRNA expression of these genes was examined in tumour endothelial cells, as increases in these genes may have contributed to the observed increase in PV MRC1⁺ TAMs 48 hours after DOX treatment. Figure 5.7A shows fold change expression of chemokines analysed including *Angpt2*, *Ccl4*, *Ccl5*, *Csf1*, *Cx3cl1*, *Cxcl12*, *Il1b*, *Plgf* and *Vegfa*. *Angpt2* was upregulated by an average of 4.90 (\pm 1.87) fold in the CD31-enriched cell fractions isolated from DOX treated tumours compared to those isolated from PBS treated tumours. *Cx3cl1* was also upregulated in CD31-enriched cell fractions from DOX treated tumours by 5.51 (\pm 1.25) fold, as was *Plgf* (mean= 1.62 fold \pm 0.03) and *Vegfa* (mean= 2.69 fold \pm 0.69), compared to those isolated from PBS treated tumours. The expression of *Ccl4*, *Ccl5*, *Csf1*, *Cxcl12*, and *Il1b* did not change in CD31-enriched cell fractions isolated from tumours treated with DOX compared to those isolated from PBS treated tumours and mean fold change values can be found in Table 5.3. This suggests that in response to DOX treatment, tumour endothelial cells upregulate their expression of *Angpt2*, *Cx3cl1*, *Plgf* and *Vegfa*.

Extravasation of monocytes (TAM precursors) relies on the expression of adhesion molecules on the surface of endothelial cells, like E-selectin and VCAM-1 [247]. Adhesion molecule expression was therefore also analysed and fold change of genes: *Eng*, *Fn1*, *Icam2*, *Sele*, *Spp1*, *Thbs1* and *Vcam1* are shown in Figure 5.7B. *Spp1* expression was increased (mean= 3.84 fold induction \pm 1.26) in the CD31-enriched cell fractions isolated from DOX treated tumours compared to those isolated from PBS treated tumours. Expression of *Eng*, *Fn1*, *Icam2*, *Sele*, *Thbs1* and *Vcam1* were not altered when comparing the CD31-enriched cell fractions from PBS and DOX

treated tumours and mean fold change values can be found in Table 5.3. Therefore, only *Spp1* expression was increased in tumour endothelial cells in response to DOX treatment.

Gene	Fold change (mean \pm SEM)
<i>Ccl4</i>	0.58 \pm 0.15
<i>Ccl5</i>	0.78 \pm 0.16
<i>Csf1</i>	0.78 \pm 0.10
<i>Cxcl12</i>	1.54 \pm 0.52
<i>Il1b</i>	0.57 \pm 0.14
<i>Eng</i>	1.37 \pm 0.51
<i>Fn1</i>	1.18 \pm 0.09
<i>Icam2</i>	0.85 \pm 0.14
<i>Sele</i>	1.11 \pm 0.42
<i>Thbs1</i>	1.08 \pm 0.36
<i>Vcam1</i>	1.13 \pm 0.22

Table 5.3 Comparing gene expression in the CD31-enriched cell fractions isolated from tumours treated with PBS and DOX. n=3 cell fractions per treatment group.

Δ Ct values for genes showing a biologically relevant increase of 1.5 fold change or more (i.e. gene expression had increased by 50% compared to PBS-treated samples [205], [283]) were then plotted and used to calculate if the increases were statistically significant using unpaired t-tests. A lower Δ Ct value indicates increased expression. *Angpt2* expression (Figure 5.7C) was significantly increased in DOX treated CD31-enriched cell fractions (mean= 7.57 \pm 0.55) compared to those isolated from PBS treated tumours (mean= 9.66 \pm 0.19, unpaired t test p=0.0230). *Cx3c1* (Figure 5.7D) showed a trend for an increase in expression in the DOX treated CD31-enriched cell fractions (mean= 7.32 \pm 0.33) compared to those isolated from PBS treated tumours (mean= 9.70 \pm 0.97, unpaired t test p=0.0808). *Plgf* (Figure 5.7E, PBS mean= 5.84 \pm 0.45, DOX mean= 5.14 \pm 0.03, unpaired t test p=0.1961) and *Vegfa* (Figure 5.7F, PBS mean= 8.31 \pm 1.35, DOX mean= 7.01 \pm 0.45, unpaired t test p=0.4116) expression were not significantly different, despite DOX treatment inducing biologically relevant fold increases in gene expression. This was also true for *Spp1* expression (Figure 5.7G, PBS mean= 2.43 \pm 1.07, DOX mean= 0.65 \pm 0.47, unpaired t

test $p=0.2007$). Therefore, while *Angpt2*, *Cx3cl1*, *Plgf*, *Vegfa* and *Spp1* all had a fold induction of at least 1.5 fold in CD31-enriched cell fractions isolated from DOX treated tumours compared to those isolated from tumours treated with PBS; *Angpt2* was the only gene that was statistically significantly upregulated in response to DOX.

5.3.6 DOX significantly increased the mRNA levels for *Angpt2*, *Plgf* and *Spp1* in CD31-depleted cell fractions.

Angpt2, *Cx3cl1*, *Plgf*, *Vegfa* and *Spp1* expression showed biologically relevant increases in the CD31-enriched cell fractions in response to DOX. In order to assess whether the increases in the expression of these genes were specific to the CD31-enriched cell fractions, qPCR was used to analyse expression of these genes in the CD31-depleted cell fractions. Fold change for these genes is shown in Figure 5.8A. *Angpt2* (mean= 4.16 ± 0.94); *Cx3cl1* (mean= 3.21 ± 1.20), *Plgf* (mean= 1.68 ± 0.20) and *Spp1* (mean= 5.29 ± 0.33) were all upregulated in the CD31-depleted cell fractions isolated from DOX treated tumours compared to those isolated from PBS treated tumours. *Vegfa* (mean= 1.03 ± 0.25) was not altered in the CD31-depleted cell fractions isolated from DOX treated tumours compared to those in PBS treated tumours.

Δ Ct values were used to identify genes that had statistically significant increases. *Angpt2* expression (Figure 5.8B) was significantly increased in the CD31-depleted cell fractions isolated from DOX treated tumours (mean= 9.60 ± 0.37) compared to those isolated from PBS treated tumours (mean= 11.57 ± 0.38 , unpaired t test $p=0.0208$). This was also true for *Plgf* expression (Figure 5.8D, PBS mean= 4.34 ± 0.15 , DOX mean= 3.62 ± 0.18 , unpaired t test $p=0.0359$) and *Spp1* expression (Figure 5.8F, PBS mean= 0.31 ± 0.33 , DOX mean= -2.09 ± 0.09 , unpaired t test $p=0.0021$).

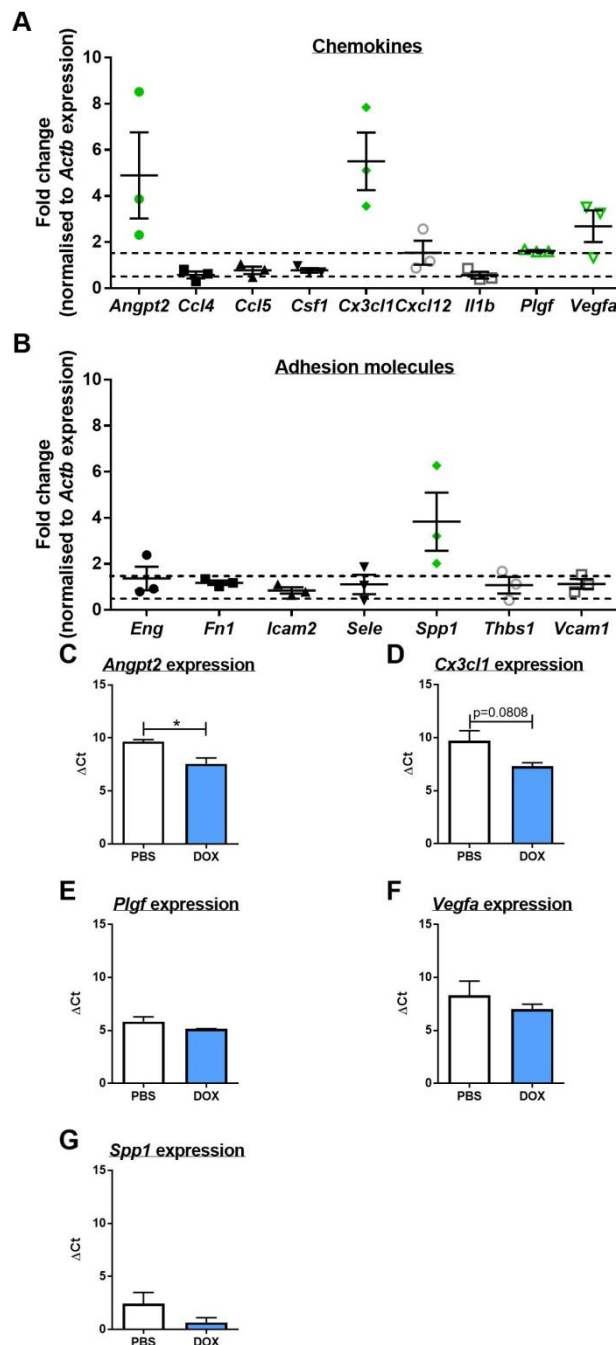


Figure 5.7 DOX significantly increases *Angpt2* expression in the CD31-enriched cell fractions.

qPCR was used to analyse gene expression of several chemokines and adhesion molecules. Fold change of chemokines (A) and adhesion molecules (B) was calculated using the $2^{-\Delta\Delta Ct}$ method normalising gene expression to *Actb*. Each point represents 1 individual tumour and bars show mean with SEM. Dotted lines represent biologically relevant fold changes of 0.5 (i.e. 50% decrease) or 1.5 fold (i.e. 50% increase). Genes which show biologically relevant increases are highlighted with green symbols. ΔCt values for genes showing fold increases of over 1.5 fold are shown with bars representing mean and error bars show SEM: *Angpt2* (C); *Cx3cl1* (D); *Plgf* (E); *Vegfa* (F) and *Spp1* (G). Lower ΔCt values indicate increased gene expression. n=3; Unpaired t-tests *indicates p<0.05.

Cx3cl1 (Figure 5.8C, PBS mean= 8.84 ± 0.72 , DOX mean= 7.33 ± 0.49 , unpaired t test $p=0.1607$) and *Vegfa* (Figure 5.8E, PBS mean= 5.85 ± 0.66 , DOX mean= 5.89 ± 0.37 , unpaired t test $p=0.9588$) were not significantly upregulated in the CD31-depleted cell fractions from DOX treated tumours compared to those isolated from PBS treated tumours. Therefore only *Vegfa* was specifically upregulated in tumour endothelial cells in response to DOX, whereas *Angpt2*, *Cx3cl1*, *Plgf*, and *Spp1* were found to be upregulated in both the CD31-enriched and CD31-depleted cell fractions, suggesting that these changes in mRNA levels are not exclusive to endothelial cells in DOX-treated tumours.

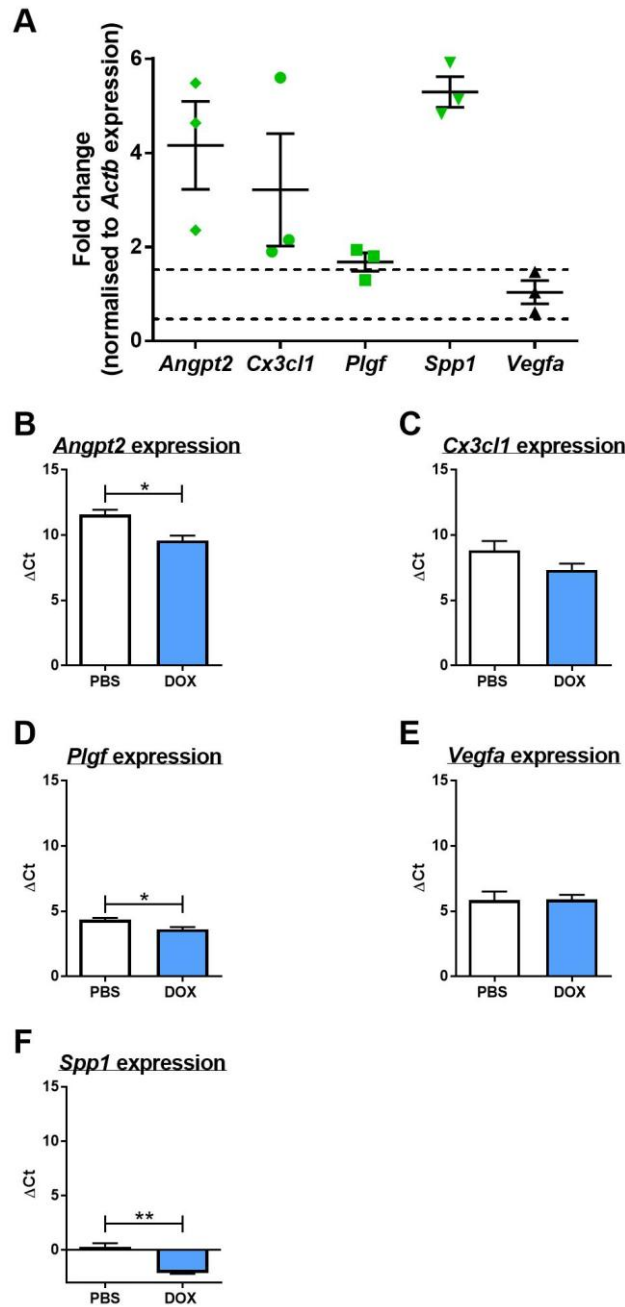


Figure 5.8 DOX increases expression of *Angpt2*, *Cx3cl1*, *Plgf* and *Spp1* but not *Vegfa* in CD31-depleted cell fractions.

qPCR was used to analyse gene expression of molecules previously shown to be upregulated following DOX treatment in the CD31-enriched fraction of cells. Fold change of *Angpt2*, *Cx3cl1*, *Plgf*, *Spp1* and *Vegfa* (A) was calculated using the $2^{-\Delta\Delta Ct}$ method normalising gene expression to *Actb*. Each point represents 1 individual tumour and error bars show mean with SEM. Dotted lines represent biologically relevant fold changes of 0.5 (i.e. 50% decrease) or 1.5 fold (i.e. 50% increase). Genes which are increased by at least 1.5 fold are highlighted with green symbols. ΔCt values are shown with bars representing mean and error bars show SEM. Lower ΔCt value signifies increased expression. *Angpt2* (B); *Cx3cl1* (C); *Plgf* (D); *Vegfa* (E) and *Spp1* (F). n=3; Unpaired two-tailed t-test * indicates $p \leq 0.05$; ** indicates $p \leq 0.01$.

5.4 Discussion

The work described in this chapter aimed to further analyse tumour endothelial cells isolated from TS1 tumours treated with PBS or DOX using qPCR, as changes in the expression of one or more genes for chemokine or adhesion molecules could help to explain the increase in PV MRC1⁺ TAMs present in TS1 tumours after DOX treatment. Three different approaches were taken to isolate tumour endothelial cells, with the most successful being magnetic isolation. Analysing gene expression of the CD31-enriched cell fractions revealed unique insights into their phenotype after DOX treatment; *Vegfa* was specifically upregulated in the CD31-enriched cell fractions isolated from DOX treated tumours compared to those isolated from PBS treated tumours. Both CD31-enriched and CD31-depleted cell fractions also upregulated *Angpt2*, *Cx3cl1*, *Plgf*, and *Spp1* in response to DOX.

Magnetic isolation of endothelial cells was the most successful method for isolating RNA from endothelial cells, as the RNA yields were higher than those obtained from cells isolated via FACS or LCM. Moreover the RNA was of better quality (increased RNA integrity) than samples isolated via LCM. Using magnetic isolation, only two subpopulations of cells were separated from tumours on the basis of their CD31 expression. There were concerns over extending length the isolation protocol by adding in extra magnetic isolation steps as this may have impacted upon cell viability and thus the quality and quantity of the RNA isolated. In future, multiple magnetic isolation steps could be used, which may increase the purity of samples and increase the number of subpopulations isolated.

As samples were isolated using magnetic beads, only CD31 was used to identify cells, rather than using multiple markers to identify endothelial cells. It was therefore imperative to assess the enrichment of these samples. On average, the fold induction of *Pecam1* expression in the CD31-enriched cell fractions was 54.39, however this did vary from sample to sample. A minimum induction of 24.31 fold was

seen in samples, which was deemed sufficient, as previous studies isolating endothelial cells with magnetic beads used samples with a minimum CD31 expression induction of 6 fold [257].

The expression of the myeloid cell transcript marker *Itgam*, macrophage transcript marker *Adgre1* and epithelial and tumour cell marker *Epcam* were significantly decreased in the CD31-enriched cell fractions compared to the CD31-depleted cell fractions. As the magnetic isolation was less rigorous than a multi-panel FACS sort, it was likely that pericytes could still be attached to some of the endothelial cells in the sample. In order to eliminate this, more vigorous wash steps were attempted, but this resulted in negligible RNA yields, so the wash steps were reduced. *Acta2* expression was not changed when comparing CD31-enriched and CD31-depleted cell fractions. This is likely as *Acta2* is marker of smooth muscle cells, fibroblasts and importantly pericytes, which are known to coat the vasculature of these tumours. Importantly, the CD31-enriched cell fraction was not significantly enriched for *Acta2* expression, suggesting that while the pericytes may not have been depleted from the sample, the sample was equally not enriched with pericytes compared to the CD31-depleted cell fractions.

These studies were the first to examine gene expression of tumour endothelial cells which had been exposed to DOX *in vivo*. Four genes were found to be upregulated in both CD31-enriched and CD31-depleted cell fractions isolated from DOX treated tumours compared to those isolated from PBS treated tumours. *Vegfa* was the only gene found to be increased in tumour endothelial cells alone in response to DOX although this increase failed to achieve statistical significance. Previous studies in the MMTV-PyMT and PyMT implanted tumours demonstrate that TAMs constitute the major source of VEGF-A within both untreated and DOX treated tumours [88], [144]. However, those studies examined VEGF-A protein, rather than mRNA. It is possible that use of *in situ* hybridisation for *Vegfa* mRNA might have revealed the presence of additional cell types expressing *Vegfa* mRNA within these tumours (i.e.

cells making *Vegfa* mRNA but not yet the protein). The relevance of cells which express *Vegfa* at the mRNA, but not protein level is questionable however.

The relevance of VEGF signalling in tumours has been explored in depth. VEGF-A is a well-characterised pro-angiogenic molecule and the target of readily available drugs such as bevacizumab (an anti-VEGF targeting antibody) [230], [284]. Others have also demonstrated VEGF-A is a chemoattractive molecule for macrophages [280]. Initially, it was thought that targeting VEGF signalling in tumours would prevent tumour angiogenesis and therefore tumour growth, although drug resistance to these therapies develop rapidly [183]. Standard high doses of anti-angiogenic therapies induce hypoxia which causes an upregulation of other proangiogenic genes, which then lead to revascularisation of the tumour and tumour regrowth [183], [285]. More recently, these anti-angiogenic drugs have been repurposed as drugs for vascular normalisation – the concept of normalising the poorly perfused tumour vasculature, to a ‘normalised’ network of blood vessels that successfully deliver anti-tumour drugs [184].

This current study is the first to show DOX acting to upregulate *Vegfa* in tumoural endothelial cells *in vivo*, although chemotherapy has previously been shown to influence VEGF-A expression by other cell types in mouse tumours. For example, cyclophosphamide was shown to increase the numbers of MRC1⁺ VEGFA⁺ TAMs within LLCs in mice [144]. Moreover, the total TAM population in these cyclophosphamide-treated LLCs were also shown to release more VEGFA than TAMs isolated from tumours treated with PBS [144]. In the current studies, the cell types which express VEGF-A at the protein level were not investigated due to time constraints and would need to be explored further to understand if the increase in VEGF-A expression is limited to endothelial cells in TS1 tumours. According to the qPCR analysis, non-endothelial cells did not alter their *Vegfa* expression 48 hours after DOX treatment in this TS1 model. However, it is possible that there may be discord between the mRNA expression data and protein expression data.

In breast cancer patients, adjuvant chemotherapy (various regimens – all including either DOX or epirubicin) given to patients post-surgery has been shown to increase circulating VEGF [286]. Additional studies also showed serum VEGF concentration to be increased in patients with locally advanced breast cancer following two treatment cycles of chemotherapy (epirubicin/ docetaxel; cyclophosphamide/ epirubicin/ 5-fluorouracil or 5-fluorouracil/ epirubicin/ cyclophosphamide) [287]. These studies support the finding that DOX upregulates *Vegfa* in endothelial cells of TS1 tumours. Another study in breast cancer patients revealed that those with larger tumours (>5cm) had decreased circulating VEGF following chemotherapy (treatment with epirubicin and paclitaxel alone or in combination with cyclophosphamide), suggesting that expression of this cytokine may change depending on the characteristics of the primary tumour [288].

Combining VEGF-targeting therapies with chemotherapy has been explored in the treatment of several types of cancer [230]. In metastatic colorectal cancer, bevacizumab increased both overall and progression free survival of patients treated with fluorouracil alone or those treated with a combination of fluorouracil and irinotecan [289], [290]. Combining anti-angiogenic drugs with chemotherapy (paclitaxel and carboplatin with bevacizumab or docetaxel and ramucirumab - a VEGFR2 blocking antibody) in non-small cell lung cancer (NSCLC) patients significantly increased their overall and progression free survival [291], [292]. The effect of bevacizumab in the treatment of triple negative breast cancer (TNBC) is somewhat controversial. In a phase III trial, bevacizumab was combined with anthracycline or taxane based therapy in TNBC patients in the adjuvant setting (i.e. post-surgery) although this did not seem to affect overall survival of patients [293]. Conversely, studies which combined neoadjuvant epirubicin, cyclophosphamide and docetaxel with bevacizumab significantly increased the pathological complete response rate (recognised as an absence of invasive or noninvasive residual tumour in the breast and lymph nodes), within a cohort of TNBC patients [294]. Perhaps neoadjuvant delivery of bevacizumab is more

effective in TNBC patients, explaining the difference between these studies. It would be interesting to combine bevacizumab with DOX in the treatment of TS1 tumours and see the impact of these therapies on PV MRC1⁺ TAM accumulation and tumour relapse, as VEGF-A may be one of the factors which causes TAMs to increase in the PV niche.

Increases in *Angpt2* mRNA expression were detected within DOX-treated TS1 tumours in both the CD31-enriched and CD31-depleted cell fractions. The CD31-depleted cells which expressed *Angpt2* could potentially be tumour cells or macrophages, as others have previously reported *Angpt2* expression in these cell types [250], [295], [296]. Angiopoietin-2 has multiple effects in tumours including acting as a proangiogenic molecule on the tumour vasculature [99], [101]. Previous studies have shown that TEMs treated with angiopoietin-2 had increased pro-angiogenic and immunosuppressive activities, suggesting that angiopoietin-2 can increase pro-tumoural functions in TEMs [99], [103]. Moreover, inhibiting angiopoietin-2 signalling using an antibody to angiopoietin-2, was shown to significantly inhibit tumour growth and metastasis, suggesting angiopoietin-2 is a molecule which supports tumour progression [102]. DOX treatment was shown to increase PV MRC1⁺ TAMs, and this could be potentially due to the increased *Angpt2* expression, if these cells were also shown to express the Tie2 receptor. Expression of the Tie2 receptor was not examined on PV MRC1⁺ TAMs, however, TEMs are a subset of TAMs, often found within the PV niche of tumours, and express M2-skewed markers such as MRC1 [69], [71]. Therefore, it is possible that these PV MRC1⁺ TAMs co-express Tie2 and accumulate after DOX treatment due to the increased production of *Angpt2*.

In agreement with our TS1 studies, chemotherapy (various regimens, including epirubicin/ docetaxel; cyclophosphamide/ epirubicin/ 5-fluorouracil or 5-fluorouracil/ epirubicin/ cyclophosphamide) was shown to increase circulating angiopoietin-2 in patients with locally advanced primary breast cancer, compared to serum levels measured at time of diagnosis [287]. Had time permitted, it would have been interesting to investigate how serum angiopoietin-2 levels after chemotherapy correlate with

survival and TAM infiltration. It would also be interesting to see if increases in *Angpt2* expression by TS1 tumours following DOX treatment correlated with increased serum angiopoietin-2 levels in the same TS1 tumour bearing mice, as this may increase myeloid cell recruitment from peripheral blood. In future, use of serum angiopoietin-2 could perhaps be used a readout for tumours which may relapse after chemotherapy - although this would need extensive clinical trial data to ratify this idea.

Understanding the possible role of endothelial cell derived angiopoietin-2 in tumour relapse is another question that could be addressed in future studies. As angiopoietin-2 may be causing PV TAMs to gather around blood vessels following DOX treatment, it is possible that these TAMs may then mediate relapse by promoting angiogenesis, as previously described in implanted PyMT tumours and LLCs [144]. One such experiment would be to treat TS1 tumours with DOX and an angiopoietin-2 blocking antibody (although this would block the effects of angiopoietin-2 expressed by other cell types in tumours as well). Previous studies combined various chemotherapies (including 5-fluorouracil, irinotecan, gemcitabine, docetaxel and oxaliplatin) with an anti-angiopoietin-2 antibody known as 3.19.3 to treat xenografted tumours in nude mice, which resulted in decreased tumour growth, compared to using these therapies as single agents, however the effect of these drug combinations on the tumour vasculature or PV TAMs was not established [297]. Additional studies combined administration of a low dose metronomic chemotherapy with an angiopoietin-2 antibody to target metastases [298]. Tumour bearing mice first had their primary tumours resected (4T1 grown in mammary fat pad) and were then treated with metronomic paclitaxel in combination with anti-angiopoietin-2. This caused a reduction in metastases and increased survival of these mice [298]. These studies clearly demonstrate the additive effects of chemotherapy and targeting angiopoietin-2, but did not investigate the impact of these combination therapies on the PV niche.

It is possible that inhibiting angiopoietin-2 helps to 'normalise' the tumour vasculature, allowing for more efficient delivery of chemotherapy and thus results in

improved prevention of tumour growth. Indeed, previous studies showed that combining anti-angiopoietin-2 with cediranib (a VEGFR inhibitor) reduced microvascular density but also increased PV cell coverage, and increased basement membrane coverage of the remaining vessels in murine models of glioma [176]. It is also plausible that inhibiting angiopoietin-2 may impact on the function and phenotype of TAMs and in particular the TEMs. Previous studies have shown angiopoietin-2 can significantly impact on the immunomodulatory functions of TEMs [103], therefore combining an angiopoietin-2 antibody with chemotherapy in the syngenic TS1 tumour model could provide novel insights into the mechanism behind the synergy of these two anti-cancer therapies, as this would allow the studies to investigate whether the cytotoxic T cells of the TS1 tumours are able to target the tumours when angiopoietin-2 is ablated. Mazziari and colleagues previously demonstrated that inhibiting angiopoietin-2 prevented TEMs from interacting with blood vessels and decreased their proangiogenic activity, suggesting that angiopoietin-2 may not only attract TEMs to blood vessels, but also encourage these cells to support blood vessel growth [102]. Potentially, this may be the function of angiopoietin-2 in these TS1 tumours, and purification of PV TAMs from tumours in which the endothelial cells overexpress angiopoietin-2 (as previously described [99]) could reveal the impact of this cytokine on these cells.

Cx3cl1 expression was also increased in CD31-enriched and CD31-depleted cell fractions isolated from DOX treated tumours. This is particularly interesting as CX3CL1 is an established macrophage chemoattractant, known to cause adhesion and endothelial transmigration of monocytes [263], [264]. Moreover, the non-classical subset of monocytes express increased amounts of the CX3CL1 receptor, CX3CR1, suggesting that they are more susceptible to recruitment by CX3CL1 [9]. Indeed, CX3CR1^{hi} non-classical monocytes were shown to patrol blood vessels and extravasate quickly into tissues in response to damage *in vivo* [14]. CX3CL1 may mediate extravasation of non-classical monocytes following DOX-mediated damage to

the TS1 tumours, which could explain the increase in PV MRC1⁺ TAMs. Interestingly, a subset of non-classical monocytes also express Tie2, and these monocytes have been implicated in tumour progression [70], [102].

These studies are not the first to show CX3CL1 expression can be enhanced by chemotherapy - studies investigating Hand-Foot Syndrome, in which chemotherapy induces inflammation in the hands and feet of patients, demonstrated that pegylated liposomal DOX increased CX3CL1 expression in the skin tissue of rat hind-legs [299]. These studies support the finding here that *Cx3cl1* mRNA is upregulated by TS1 tumours after DOX. Interestingly the rats used in the previously mentioned study were not tumour bearing, which may indicate that DOX-mediated *Cx3cl1* upregulation is not a tumour-specific phenomenon and may occur in other healthy tissues. Studies examining paclitaxel induced allodynia in rats, revealed paclitaxel increased CX3CL1 expression in the dorsal root ganglia of the rats, which triggered macrophage activation and recruitment [300]. This study suggests that additional chemotherapy drugs (other than DOX) may induce CX3CL1 expression [300].

CX3CL1 has recently been implicated in TAM infiltration and tumour progression. LLCs grown in *Cx3cl1*-deficient mice contained fewer TAMs and had decreased growth than those grown in wildtype mice [301]. However, the effect of CX3CL1 signalling on cancer prognosis is controversial, with some papers inferring that CX3CL1 has anti-tumoural effects and with others demonstrating it is linked to tumour promotion [302]. For example, in hepatocellular carcinoma patients, those with increased tumour expression of CX3CL1 and its receptor CX3CR1, had increased overall- and disease free-survival, indicating CX3CL1 signalling was associated with a better prognosis in this disease [303]. A study of gastric adenocarcinoma patients showed that tumours with increased CX3CL1 expression had increased infiltration of anti-tumoural CD8⁺ T cells and natural killer cells, and that this correlated with increased disease-free survival compared to those with low tumoural CX3CL1

expression [304]. Finally, low tumour CX3CL1 expression was predictive of increased risk of recurrence in prostate cancer patients [305].

However, increased tumour CX3CL1 expression is associated with a poor outcome in some forms of cancer. Breast cancer patients with high levels of tumour CX3CL1 had worse overall survival than those with lower expression [306]. In addition to this, pancreatic ductal adenocarcinoma patients with increased tumour CX3CL1 expression (or a combination of high CX3CL1 and CX3CR1 expression) had decreased overall survival. [307].

The level of *Plgf* mRNA was also higher in CD31-enriched and CD31-depleted cell fractions isolated from DOX treated tumours compared to those from PBS treated tumours. PLGF is a chemokine which functions as pro-angiogenic molecule and as chemoattractant to macrophages [278]. Targeting PLGF with antibodies results in significantly reduced tumour (Panc02 and B16) growth, demonstrating a role for PLGF in tumour growth and its potential as a new therapeutic target [277]. Combining anti-PLGF treatment with chemotherapy (gemcitabine to treat Panc02; cyclophosphamide to treat B16) resulted in reduced tumour growth compared to tumours treated with chemotherapy or anti-PLGF alone [277]. Moreover, tumours treated with anti-PLGF had decreased TAM infiltration, again demonstrating the chemoattractive properties of PLGF [277].

More recently the role of PLGF in macrophage phenotype was investigated [30]. TAMs isolated from *Plgf*^{-/-} tumours exhibited a more anti-tumoural phenotype (with decreased *Arg1* and *Il10* expression, and increased *Cxcl9* expression) than those isolated from wildtype tumours [30]. These data suggest that PLGF not only attracts TAMs to tumours, but also acts to promote a pro-tumoural phenotype; thus the potential of anti-PLGF to target TAMs is worthy of further investigation. As PLGF acts as a TAM chemoattractant, it is possible that the upregulation of *Plgf* mRNA in DOX-treated TS1 tumours could explain the increase in PV MRC1⁺ TAMs also observed after DOX treatment.

When mice bearing B16F10 melanoma tumours were treated with DOX, serum PLGF decreased, unlike in our TS1 model, in which DOX increased *Plgf* expression. However, paclitaxel increased PLGF in the serum of the B16F10-bearing mice [308]. Although DOX did not induce an increase in serum PLGF in B16F10-bearing mice, this could be due to the differences in the tumour model used; different chemotherapies can have different effects depending on the tumour model. Interestingly, paclitaxel was able to directly upregulate *Plgf* and *Vegfa* in immortalised murine (SVEC-10) endothelial cells and primary lung fibroblasts *in vitro* [308]. These studies support our TS1 model, in that they show chemotherapy is able to induce *Plgf* expression. With some optimisation, tumour endothelial cells could be used in future *in vitro* studies to investigate the direct effects of DOX on their gene expression. Monocyte adhesion assays could also be used to address whether DOX stimulates monocyte adhesion to endothelial cells (and thus potentially tumour infiltration), or causes macrophages to migrate towards endothelial cells, thus explaining how DOX may cause TAM accumulation in the PV niche.

Patients with Her2⁺ breast cancer treated with DOX had increased PLGF in their serum compared to serum levels prior to treatment, and those patients with high concentrations of serum PLGF had an increased risk of cardiotoxicity [309]. These studies suggest that in the context of breast cancer, DOX is capable of inducing increases in PLGF, in agreement with our studies in murine TS1 tumours [309].

PLGF is associated with clinical prognosis in different forms of cancer [310]. Studies in breast cancer patients confirmed *plgf* expression was increased within tumours compared to the normal breast tissue [311]. Moreover, patients with low *plgf* expression had a better prognosis (remaining disease free) compared to those with increased *plgf* expression (poor prognosis – local recurrence, metastasis or death) [311]. Increased tumour PLGF expression was also associated with decreased survival in NSCLC, colorectal, gastric and hepatocellular cancers [312]–[315]. However, not all tumours overexpress *plgf* – for example lung cancer and colon cancer express

relatively low levels of *plgf*, demonstrating the need to target this cytokine in appropriate groups of patients for it to be effective [316].

Serum PLGF has also been measured and used as a biomarker in non-squamous NSCLC patients – those with lower serum PLGF had increased overall survival [317]. This is exciting as monitoring serum biomarkers is a relatively non-invasive procedure which could be carried out over multiple timepoints within a treatment regimen – whether serum PLGF changes during different anti-cancer regimens and if this correlates with treatment outcome should be investigated.

Recently, a phase I clinical trial using an antibody targeting PLGF (TB-403) demonstrated that this treatment was reasonably well-tolerated in patients with solid tumours [318]. Further clinical trials should reveal how effective TB-403 is at reducing tumour growth and whether it can be combined with additional anti-cancer therapies, such as chemotherapy.

SPP1, a chemokine and extracellular matrix component, was found to be upregulated in both CD31-enriched and CD31-depleted cell fractions. SPP1 has roles in bone homeostasis, as well as functions in the regulation of the immune system [275]. Importantly for this work, SPP1 has been shown to be chemoattractive for macrophages [275]. *In vitro*, transmigration assays were used to demonstrate that SPP1 could inhibit the reverse migration of monocytes i.e. once the monocytes had crossed the endothelial cell barrier they did not migrate back, indicating a possible mechanism by which SPP1 can maintain TAM accumulation in the PV niche [276]. Moreover, SPP1 was shown to increase the survival of monocytes grown under serum-starvation conditions, suggesting SPP1 may also increase macrophage viability in stressful conditions [276]. SPP1 protein expression was also correlated with macrophage and neutrophil infiltration in glioblastoma patients, as those with increased SPP1 staining also had increased numbers of macrophages and neutrophils [319]. Interestingly, SPP1 stained more intensely in areas of necrosis and around blood vessels in these patient samples [319]. These studies suggest that SPP1 is another

factor which may be able to cause recruitment or retention of TAMs in the PV niche after DOX treatment.

Previous studies investigating DOX-induced cardiotoxicity demonstrated that DOX induces *Spp1* expression in H9c2 rat heart derived embryonic myocytes *in vitro* [320]. Furthermore, *in vivo*, SPP1 was upregulated in the myocardium of DOX treated rats [321]. These data support our studies which also show DOX upregulates *Spp1* in TS1 tumours. As SPP1 can act as macrophage chemoattractant, it is therefore possible that the increase in *Spp1* expression may mediate the increase in PV MRC1⁺ TAMs after DOX treatment. Further studies revealed that SPP1 deficient mice had less scarring (collagen deposits) in their hearts following DOX treatment [320] suggesting a role for SPP1 in the development of fibrosis. As the present study established *Spp1* was upregulated in TS1 tumours following DOX treatment, it would be interesting to investigate if SPP1 induces fibrotic scarring of tumours after chemotherapy in a similar manner.

In addition to SPP1 affecting macrophages, it is possible that it may affect tumour cell survival during/after DOX treatment. *In vitro*, SPP1 knockdown was shown to increase the sensitivity of MDA-MB-231 breast tumour cells to DOX [322]. This was also shown in PC-3 prostate cancer cells, and believed to be because SPP1 upregulated p-glycoprotein, a mediator of drug resistance [323]. Interestingly, PC-3 tumours were also shown to upregulate SPP1 in response to daunorubicin– much like the response seen in this chapter with TS1 tumours which were treated with DOX [323]. Taken together, these studies implicate SPP1 as a mediator of resistance to chemotherapy and further studies should investigate SPP1 targeting therapies in combination with chemotherapy.

Increased SPP1 expression may also have clinical implications: breast cancer patients treated with cyclophosphamide, methotrexate and fluorouracil had worse prognosis if their tumours expressed high levels of SPP1 [324]. Interestingly the prognosis of patients which were given DOX and cyclophosphamide followed by a

course of cyclophosphamide, methotrexate and fluorouracil showed no such correlation with SPP1 staining [324]. In another cohort of breast cancer patients that received chemotherapy (epirubicin, cyclophosphamide/ methotrexate/ 5-fluorouracil and paclitaxel), patients with high *Spp1* expression had decreased overall and disease-free survival [325]. Future studies could compare SPP1 expression in tumours treated with chemotherapy in the neoadjuvant setting with pre-treatment biopsies in order to analyse the effect of chemotherapy on this. SPP1 is not only important in breast cancer; increased expression of SPP1 was also associated with poor survival in gastric cancer, NSCLC, and prostate cancer patients [326]–[328].

Interestingly, in contrast to the cytokines investigated, the expression of most adhesion molecules, including *Vcam1* and *Sele* (known to be involved in extravasation of leucocytes [247]), were unchanged in CD31-enriched cell fractions isolated from DOX treated TS1 tumours. These data suggest that such molecules involved in the extravasation of monocytes remain unchanged by DOX in tumour endothelial cells. This could indicate that the increased adhesion of monocytes to endothelial cells does not play a part in the increase in PV TAMs in these tumours after DOX.

A major limitation of this study is the lack of protein expression data. It is important to confirm whether the above genes are also upregulated in DOX treated tumours at the protein level. Had time permitted, it would also have been interesting to identify the cell types expressing these proteins in the CD31-depleted cell fractions in TS1 tumours.

Immunofluorescent staining was attempted in order to examine the expression of angiopoietin-2 within these tumours, however this was not successful and the antibody did not detect any discernible patterns of cellular staining. Future attempts could perhaps analyse the expression of this cytokine in at least the CD31-enriched cell fraction from tumours using ELISA or western blotting, as reagents are more readily available for these techniques.

Another limitation of these studies is that it is still unknown if the response to DOX is limited to the tumour vasculature per se, i.e. what effect DOX has on the vasculature of healthy tissues. To investigate this, more studies are needed in which gene expression is analysed in endothelial cells purified from healthy tissues in tumour bearing mice and/or mammary endothelial cells from mammary tissue of healthy mice treated with DOX. Indeed many studies have previously characterised gene expression in healthy endothelial cells and the tumour vasculature, however no such work has examined this in the context of chemotherapy [257], [329].

Moreover, while the gene expression of CD31-enriched and CD31-depleted cell fractions were affected by DOX treatment, it is unknown whether this is a direct effect of DOX on the cells themselves, or due to the indirect effects of DOX on other cells within the tumour microenvironment. It is possible that the increase in PV MRC1⁺ TAMs is because of the increase in chemoattractive genes expressed by CD31-enriched cells within DOX treated tumours, however it is entirely possible that these events occur simultaneously, or that the PV MRC1⁺ TAMs release factors which cause the blood vessels to upregulate their expression of *Angpt2*, *Cx3cl1*, *Plgf*, *Spp1* and *Vegfa*. To further understand these complex interactions, *in vitro* studies may be useful, as this would allow for co-culture experiments with various different cell types including tumour cells, endothelial cells and macrophages.

Due to financial constraints, only 31 genes were analysed in the current studies. RNA sequencing would have identified potential changes in a much broader number of genes, however the cost of this was prohibitive on a PhD studentship. Whole transcriptome amplification is another tool which could have increased the total amount of RNA available for analysis, and thus the amount of genes analysed, but the RNA integrity of the samples did not meet the minimum requirements for this technique. It was therefore decided that RNA would be converted to cDNA using the QuantiTect reverse transcription kit which uses random primers and converts to cDNA from both 5'

and 3' ends, to enable reliable cDNA synthesis even if RNA has been partially degraded.

The CD31-depleted cell fraction could potentially include tumour cells, TAMs and other tumour-infiltrating cells such as T lymphocytes and neutrophils as well as fibroblasts. Further studies profiling the expression of the above mRNA transcripts and/or proteins in these different cell populations could lead to a better understanding of how they are regulated by DOX in different cell types in tumours. In order to purify these different cell populations, FACS sorting could be used for cell populations that are more abundant than endothelial cells, such as TAMs [144].

More recently, unpublished work by Professor Lewis' group has focused on the purification of PV TAMs, using fluorescently conjugated dextrans. The dextrans are injected into the tail veins of mice 30 minutes prior to culling – this allows the fluorescent dextrans to diffuse into the tissues where they are engulfed by macrophages. The time window of 30 minutes means that the dextrans are only engulfed by PV TAMs, as the dextrans do not permeate the whole tumour in this period of time (Hughes, unpublished). Studies like this could be very illuminating – it would of course be appealing to investigate if these PV TAMs express receptors for the molecules these studies have identified e.g. TIE2, CX3CR1, VEGFR1 and VEGFR2, which would indicate that the chemokines upregulated by endothelial cells and the rest of the tumour in DOX treated tumours can signal to the PV TAMs.

5.5 Concluding remarks

In this chapter, we show for the first time that tumoural CD31-enriched cells exclusively upregulate *Vegfa* mRNA expression within 48 hours of DOX treatment. In addition to this, *Angpt2*, *Cx3cl1*, *Plgf*, and *Spp1* were upregulated within both CD31-enriched and CD31-depleted cell fractions after DOX treatment. As these genes have all been previously implicated in macrophage chemoattraction, this increase in expression may

well explain the increase in PV MRC1⁺ TAMs also seen two days after DOX is administered to TS1 bearing mice. In future, studies should focus on confirming the protein expression of these genes, before deciding whether any of these genes are worthy targets for novel TAM-disrupting drugs.

Chapter 6

General Discussion

6.1 Summary of major findings.

In the implantable TS1 tumour model used in this thesis, the majority of MRC1⁺ TAMs were found to reside mainly in the normoxic, more vascularised stroma rather than in tumour cell islands. When TS1 tumours were treated with DOX there was no change in total TAM recruitment within 48 hours, however there was a significant increase in MRC1⁺ TAMs directly abutting tumour blood vessels. As TAMs in untreated tumours are derived from blood monocytes, it was assumed that this PV accumulation was due to increased recruitment of these precursors from the blood. However, these PV TAMs were shown to be relatively mature and, therefore, more likely to have been attracted into the PV niche from elsewhere in these tumours during/after DOX treatment (e.g. deeper in the stroma, the tumour cell islands or from surrounding normal tissue outside the tumour).

Given this pronounced change in TAMs near blood vessels, the tumour vasculature was characterised, to determine if this increase was due to changes in the morphology or phenotype of endothelial cells. While DOX treatment did not alter vascular parameters like lumen size, vessel patency (as measured by FITC-lectin perfusion) or pericyte coverage, it induced increases in the expression of *Vegfa*, *Angpt2*, *Cx3cl1*, *Plgf* and *Spp1* by tumour endothelial cells. Interestingly, the expression of the last four of these genes was also seen in other, undefined CD31-depleted cells from these tumours (Figure 6.1).

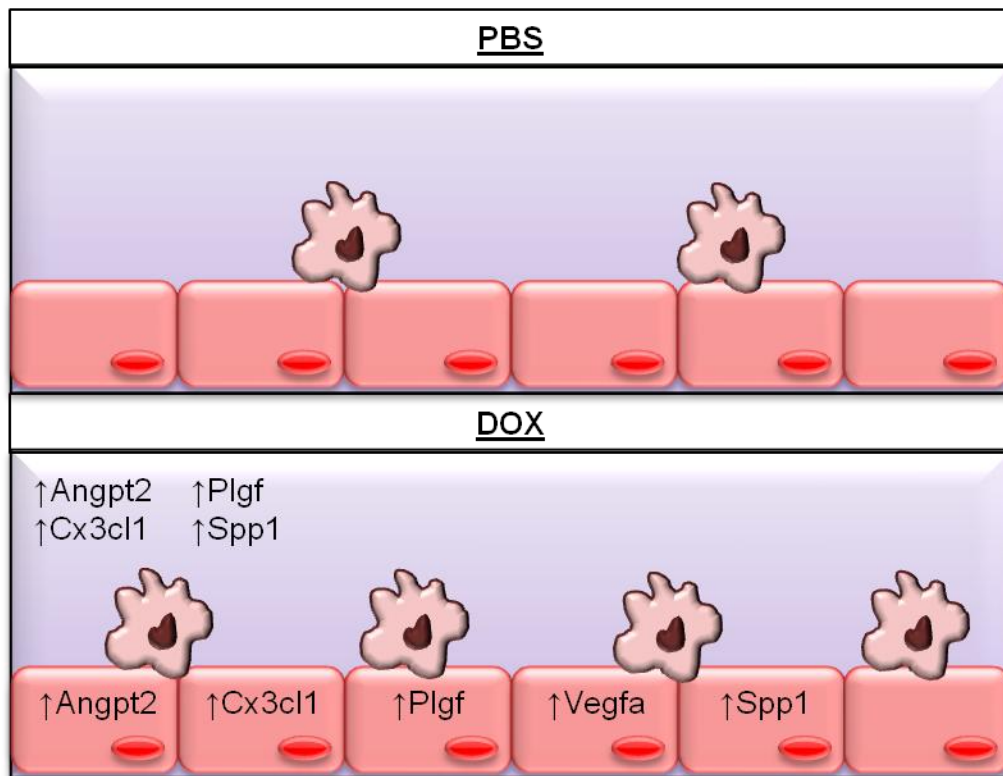


Figure 6.1 Summary of the effects of DOX on the PV niche.

DOX significantly increases PV MRC1⁺ TAMs and induces gene expression changes. *Angpt2*, *Cx3cl1*, *Plgf* and *Spp1* were all upregulated by both CD31-enriched and CD31-depleted cell fractions in DOX treated tumours. CD31-enriched cells isolated from DOX treated tumours also had increased *Vegfa* expression.

6.2 DOX induces changes within the PV niche of TS1 tumours.

These studies further demonstrate that chemotherapy is capable of inducing changes within the tumour microenvironment that can impact on the behaviour of both TAMs and endothelial cells. To further understand the dynamics of PV TAMs following DOX, intravital imaging could be employed to study if these cells accumulate rapidly after the administration of DOX, or if these cells only start to accumulate two days after treatment. Indeed, intravital imaging was previously used to demonstrate non-classical monocytes rapidly extravasate from blood vessels in the dermis and into damaged tissues [14]. Moreover, intravital imaging demonstrated that CSF1R⁺ cells (likely monocytes or macrophages) infiltrate MMTV-PyMT tumours following DOX treatment

[137]. These studies however did not specifically examine the PV niche, possibly as achieving the resolution needed to examine individual blood vessels within such tumours is not yet possible. By studying additional early and later time points, it would of course be possible to learn more about the recruitment of these PV MRC1⁺ TAMs, and immunofluorescent analyses could show if they appear as PV MRC1⁻ TAMs or even PV immature Gr-1⁺ cells at an earlier time point. Additionally, FACS sorting of PV TAMs using fluorescent dextrans at different time points would allow an in-depth study of how these cells change e.g. maturation status, expression of pro-angiogenic and immunosuppressive genes, in response to DOX.

In these studies, PV TAMs were examined but other leucocyte subpopulations were not studied in relation to vasculature. Future studies could examine whether these additional populations, including immature myeloid cells, associate with either the PV TAMs or the blood vessels themselves. Potentially, while DOX did not increase the overall infiltration of Gr-1⁺ cells, DOX could increase PV Gr-1⁺ cells. Immunofluorescent analyses of whether immature myeloid cells are found specifically around patent FITC-lectin perfused blood vessels could give insight as to how these cells are recruited from the vasculature.

As the T cell infiltrate of tumours can affect the outcome of chemotherapy [109], it would be interesting to establish if these cells exist within the PV niche of TS1 tumours. Previously, endothelial cell FasL expression has been shown to effect T cell infiltration of murine ID8-VEGF tumours, as when mice were treated with anti-FasL, they had an increased CD8⁺ T cell infiltrate [330]. This suggests that endothelial cells themselves may prevent recruitment of anti-tumoural T cells by expression of factors such as FasL. MRC1⁺ TAMs are increased in the PV niche of these tumours and so the PV niche may act as an immunosuppressive barrier. Understanding whether these PV MRC1⁺ TAMs express immunosuppressive molecules such as IL-10 [110] or checkpoint molecules such as PD-L1 [112], may help establish if they are able to suppress anti-tumoural T cells. In the TS1 tumours, cytotoxic T cells were observed

within the tumour cell islands, but rarely within the tumour stroma. It would also be interesting to establish the activation status of these cytotoxic T cells, particularly if they are in close proximity to PV MRC1⁺ TAMs.

Inhibiting TAM infiltration of tumours has shown promising results when combined with chemotherapy. For example inhibition of TAMs using anti-CSF1 in both mammary (MMTV-PyMT) and pancreatic models significantly decreases tumour growth in combination with chemotherapy [108], [109]. Similarly, inhibiting TAM recruitment by blocking CXCR4 signalling with the drug AMD3100 vastly reduced tumour regrowth following chemotherapy [144].

While there are clear benefits to inhibiting TAMs in murine models of cancer, some of these experimental therapies are yet to show such promising results in patients. The CSF1R inhibitor PLX3397 has now been trialled as single agent, and effectively caused tenosynovial giant cell tumours to regress, although this was likely as these tumours overexpress CSF1 [171]. In a phase II trial of recurrent glioma patients, however, PLX3397 failed to show any benefit, demonstrating that these CSF1R inhibitors may not be as successful at treating human cancer [172]. While well-tolerated, combining carboplatin and etoposide chemotherapy with the CXCR4 antagonist, LY2510924, had no effect progression-free or overall survival in NSCLC patients [163].

Given that MRC1⁺ TAMs were previously shown to promote relapse in LLC and PyMT implanted tumours, it is possible that targeting TAMs using nanobodies may be another potential therapy that could be used in future. Previously, an MRC1 targeting nanobody was developed and labelled with the isotope Technetium-99m and was used to image TAMs in TS/A and MMTV-PyMT tumours *in vivo* [331]. It is therefore possible, that this nanobody could be coupled to toxins in future, and used to ablate TAMs as a novel anti-cancer therapy, although care should be taken to analyse the effects of this nanobody on additional macrophage populations within the body, such as alveolar macrophages or Kupffer cells. In mice bearing S180 tumours, treatment with a

mannose-receptor targeted glucomannan conjugated to alendronate (ALN-BSP) decreased the number of TAMs, tumour growth and the number of vessels within such tumours [332]. In addition to this, ALN-BSP was capable of decreasing tumour expression of IL-10 and increasing tumour IFN- γ , suggesting that this therapy decreased the immunosuppressive activity of the tumour microenvironment by eliminating TAMs. Using MRC1 to target TAMs may therefore have some advantages in the treatment of cancer, although the effect of targeting MRC1 on healthy tissues needs to be established. Purifying PV macrophages from tumours and healthy tissues would allow the study of targets which may be exclusively expressed in PV TAMs, and therefore allow the design of therapeutics which specifically ablate TAMs and not resident tissue macrophages.

For the first time, DOX was shown to also upregulate five mRNA transcripts in tumour endothelial cells (with *Vegfa* being the only gene exclusively upregulated in endothelial cells), all of which have been shown to affect macrophage recruitment, retention and/or regulation [30], [92], [99], [103], [263], [264], [275]–[277], [280]. Further studies are now warranted to see if and how these gene products influence TAMs in the PV niche of chemotherapy-treated tumours and if this then impacts on tumour relapse.

6.3 Limitations of studies

One of the major limitations of these studies is that only one mouse model of cancer was used. It would be important to verify some of the key findings of the studies in this thesis in other mouse mammary tumour models, and in response to different, clinically relevant chemotherapeutics. However, the finding that PV MRC1⁺ TAMs accumulate in TS1 tumours after DOX treatment is in agreement with previous studies which demonstrated that relapse promoting PV MRC1⁺ TAMs are increased after cyclophosphamide treatment of LLCs [144]. This suggests that the phenomenon of PV

TAMs accumulating in chemotherapy treated tumours may be applicable to different cancer types and models, other than the one studied in this thesis. Isolating tumour endothelial cells from LLCs treated with cyclophosphamide may reveal whether the genes in our TS1 studies are also potentially responsible for the accumulation of PV TAMs in LLCs. It is of course important not to extrapolate too much from murine tumours before confirming findings in human tumours. Previous studies showed there was an increased percentage of MRC1⁺ cells in vascularised areas of human breast carcinomas treated with paclitaxel, compared to the avascular areas [144], however further studies should confirm if PV TAMs contribute to the relapse-free survival of these patients. Indeed, previous studies have analysed gene expression in endothelial cells isolated from human tumours and healthy organs [257], but it would be very interesting to compare the expression profile of endothelial cells in breast cancer pre-treatment biopsies and tumours taken after chemotherapy, again to confirm if the findings in the TS1 model are relevant to patients.

Xenograft models using human tumour cell lines could have been used instead of TS1 cells, but this would have meant the mice themselves would not have had a fully competent immune system. An immunocompetent, syngeneic mouse model (TS1 orthotopic implants) was used instead, as previous studies have shown TAMs can reduce the efficacy of chemotherapy by inhibiting T cell responses in mice [108]–[110]. Intraperitoneal administration of 8mg/kg DOX was previously shown to induce necrosis and cause immature myeloid cell infiltration in transgenic MMTV-PyMT tumours [137], so this DOX regimen was selected for our implantable orthotopic (MMTV-PyMT derived) TS1 model. It was thought the TS1 tumours would respond in a similar way to these MMTV-PyMT transgenic tumours, as they are established from the same tumour cell line, and so the intrinsic properties of the cancer cells should be similar. The TS1 model was previously well-established and used alongside the parent MMTV-PyMT transgenic tumours by others [139]. Indeed, studies characterising the molecular characteristics of these two tumour cell types (transgenic and TS1), and reporting if

there are any differences between them, would be very useful to further understand these models. The implantable tumour models, however are more likely to be used in future research projects, as these allow the study of one tumour mass at an orthotopic site, rather than multiple tumours arising in different mammary glands.

DOX was considered to be the most clinically relevant drug, as NICE recommends that patients with locally advanced, hormone receptor negative breast cancer are treated with DOX, or another anthracycline drug, in the first instance [201], [204]. TS1 tumours are also hormone receptor negative, and so their treatment with DOX bears clinical relevance [87]. In patients who cannot be treated with anthracycline drugs, patients may be treated with docetaxel, vinorelbine or capecitabine [204]. It would have been interesting to establish the effects of these alternative chemotherapeutic regimens on TAMs and the tumour microenvironment, but due to time and budget constraints, only DOX could be investigated in these studies. Previously, the effect of paclitaxel (which belongs to the taxane family of drugs), has been established in two murine models, increasing MRC1⁺ TAMs in vascularised areas of 4T1 tumours and generally increasing TAM recruitment in the MMTV-PyMT model [109], [144]. More recently, trials have started to investigate immunotherapy in patients and it would therefore be important to investigate whether the tumour microenvironment responds to checkpoint inhibitors, such as antibodies targeting PD1 or PD-L1 [111], in a similar way to that seen in TS1 tumours treated with DOX in order to understand potential mechanisms by which tumours may relapse following checkpoint inhibitor therapy.

Another limitation of these studies is that it is not understood exactly how DOX causes the upregulation of 5 different genes within tumour endothelial cells, and other unspecified cells. It is possible that DOX may cause changes in mRNA expression by directly affecting the cells involved. This could be addressed by *in vitro* experiments, however tumour endothelial cells are notoriously difficult to grow *in vitro* [333], and so murine endothelial cell lines may need to be used for these assays instead. Potentially

DOX impacts on tumour cells e.g. could induce cell death, which causes a release of factors which then impact on the endothelial cells, in which case co-culture experiments with endothelial cells and tumour cells should be optimised. Conditioned media from DOX treated endothelial cells could be taken and placed onto BMDMs or freshly isolated TAMs to understand the direct effects of endothelial cell produced cytokines on these cells which gather in the PV niche of TS1 tumours.

6.4 Clinical implications

Breast cancer is one of the most common types of cancer diagnosed in the UK, accounting for 31% of female cancer cases in 2014 [197]. There are multiple subtypes of breast cancer, defined by their molecular and pathological characteristics, making it a complex disease. Patients that present with smaller, locally restricted tumours e.g. stage 1 or stage 2 patients are usually treated with surgery to remove the tumour, and may also receive radiotherapy post-surgery to kill any remaining cancer cells. These patients have the best response to therapy, as at least 88% of stage 2 (and 99% of stage 1) patients go on to survive five years from initial diagnosis [198]. Unfortunately for patients presenting with larger tumours, which have spread extensively to the lymph nodes (stage 3, locally advanced cancer), the 5 year survival rate is 55% [198]. These patients are usually given chemotherapy or endocrine therapy in the neoadjuvant setting to shrink their tumours before removing the tumour with surgery [204]. The survival rate for patients with metastatic breast cancer (stage 4), which has spread to distant sites within the body (including brain, bone and lungs) is only 15% [198]. Therefore, there is clearly a need to improve survival rates of patients with stages 3-4 of breast cancer.

Currently breast cancer can be treated with a number of drugs including chemotherapy (usually taxane based or anthracycline based) and endocrine therapies. When considering treating patients with breast cancer, the patient biopsy is tested for

the expression of three receptors: ER, PR and the HER2 receptor [202]. Patients with oestrogen and progesterone receptors will respond to endocrine therapies, such as tamoxifen [202]. Tumours which are HER2 positive can also be treated with trastuzumab (also known by the drug name Herceptin) [202]. However, TNBC does not respond to endocrine therapies or trastuzumab, as the tumours do not express ER, PR or HER2 receptors. In the UK approximately 15% of breast cancer cases are TNBC [334]. These patients have more limited treatment options, usually only surgery and chemotherapy. It is therefore very important to investigate new pathways which can be manipulated in order to improve the response to chemotherapy and to develop new, more targeted therapies for these patients.

More recently, molecular characterisation of tumours has been considered to further personalise treatments. Luminal-A, Luminal-B, HER2-enriched, Basal-like and Claudin-low describe the five main molecular subtypes of human breast cancer [335]. Luminal-A and Luminal-B tumours express hormone receptors (ER⁺ PR⁺) and are associated with a better outcome compared to the other molecular subtypes (with Luminal-A tumours having the best prognosis as it is less proliferative than Luminal-B tumours) [335]. HER-2 enriched tumours, express HER2, and therefore will respond to trastuzumab [335]. Basal-like tumours are often triple negative, as are Claudin-low tumours, which represent tumours which are more difficult to treat [335].

Previously, microarray analysis of transgenic MMTV-PyMT tumours showed that they model the 'luminal' molecular subtype of human breast cancer [336]. However, unlike this form of human cancer, they lack ER and PR expression [87], [336]. This lack of hormone receptors demonstrates they would not respond to endocrine therapy, much like patients with TNBC [335]. However, MMTV-PyMT tumours express the HER2 receptor (ErbB2/Neu), and in the clinic, patients with tumours expressing HER2 can be treated with trastuzumab [87], [201]. NICE guidelines indicate that trastuzumab is only administered to patients with locally advanced HER2⁺ breast cancer if they are unable to be treated with anthracycline based chemotherapy,

such as DOX [201]. Therefore, in the first instance, most ER⁻ PR⁻ HER2⁺ cases are given DOX or another anthracycline, much like patients with TNBC. Therefore, while the MMTV-PyMT tumours express ErbB2/Neu, it is still a clinically relevant model for analysing the response of tumours to DOX. I considered alternative murine models of cancer that could have been used to accurately model triple negative cancer, such as the 4T1 model, however 4T1 tumours are exceptionally inflammatory, and as these studies were focussed on the immune system, the decision was made not to use this model [337].

One of the most novel findings of this thesis is that TS1 tumours upregulate *Angpt2*, *Cx3cl1*, *Spp1*, *Plgf* in response to DOX. Endothelial cells also upregulated *Vegfa* in DOX treated tumours. Previous studies have demonstrated roles for each of these genes in macrophage recruitment and often correlated their high expression with poor prognosis [250], [306], [311], [324], [338]. Inhibiting one of these molecules alongside chemotherapy, could result in a better outcome for patients, although rigorous trials would be needed to understand the side effects of combining these therapies. It is possible that drugs which may also exert effects on the tumour vasculature, rather just the TAMs themselves e.g. anti-VEGFA or anti-PLGF, may result in cardiovascular events such as thromboembolism due to vascular collapse. For some of these molecules (e.g. VEGF-A), drugs which inhibit them already exist and are being used in the clinic [230], [284]. However some molecules, such as SPP1, have only been inhibited using shRNA [323], rather than small-molecule inhibitors that could be more easily translated into patients, and so therapies targeting SPP1 may take longer to receive clinical approval.

Angiopoietin-2 is a molecule characterised by its effects on both the tumour vasculature and a subset of TAMs which express Tie2 (TEMs) [99], [101], [103]. *In vitro* studies demonstrated that angiopoietin-2 is a chemoattractant for TEMs, and enhances their proangiogenic and immunosuppressive functions which are known to aid tumour progression [92], [99], [103]. Moreover, inhibition of the Angiopoietin2-Tie2 signalling

axis in pre-clinical murine mouse models has revealed promising results, as an antibody raised to angiopoietin-2 was shown to reduce tumour growth and metastasis of murine tumours, demonstrating a role for angiopoietin-2 in tumour progression [102]. Furthermore, the antibody 3.19.3 which targets angiopoietin-2 was successfully combined with chemotherapy in a variety of xenograft mouse models of cancer, and significantly increased tumour shrinkage [297]. Low dose metronomic chemotherapy was also combined with angiopoietin-2 targeted antibodies to halt growth of murine metastases [298]. These studies all demonstrate the promise of combining anti-angiopoietin-2 therapies with chemotherapy, although the effects of these on preventing TAM induced relapse have yet to be fully established. It is entirely possible that the PV MRC1⁺ TAMs in the TS1 tumours also express TIE2, as TEMs are heavily M2 skewed and have been known to express MRC1 [71]. Moreover, previous studies showed that MRC1⁺ TAMs in LLCs also expressed TIE2 [144].

Breast cancer patients with increased angiopoietin-2 expression have decreased overall and disease-free survival [250]. Interestingly, studies have demonstrated that patients with locally advanced breast cancer have increased circulating angiopoietin-2 following treatment with chemotherapy, suggesting that they may also respond to chemotherapy in a similar way to our model [287]. These studies demonstrate angiopoietin-2 may be a potential novel target for breast cancer patients receiving chemotherapy. Recently, early clinic trials revealed the anti-angiopoietin-2 antibody, MEDI3617, was well-tolerated in patients in combination with carboplatin and paclitaxel [173] and the longer term outcomes of these trials are awaited with interest.

CX3CL1 is a chemokine which attracts and aids the extravasation of monocytes into tissues [263], [264]. In breast cancer patients, high tumour CX3CL1 levels are associated with poor prognosis [306], suggesting that inhibition of this signalling pathway may improve the response of patients to current therapies. Studies should now focus on whether interfering with CX3CL1 signalling improves the outcome of chemotherapy regimens.

PLGF was demonstrated to be a proangiogenic molecule, which also acts as a macrophage chemoattractant and is known to be involved in skewing TAMs towards a pro-tumoural phenotype in murine models of cancer [30], [277]. *Plgf* is also associated with poor prognosis in breast cancer [311], and HER2⁺ breast cancer patients were shown to increase their circulating PLGF levels following treatment with DOX, demonstrating that our murine studies may mimic what is occurring in this subset of patients [309]. Taken together, these studies suggest that PLGF may be a potential novel target for improving the response to chemotherapy. Indeed, in pancreatic and B16 murine tumours, anti-PLGF antibodies were combined with chemotherapy which resulted in increased shrinkage of tumours [277]. In attempts to translate these studies towards clinical use, an antibody targeting PLGF was successfully delivered to patients with solid tumours and was well-tolerated, suggesting that there are therapies available to target PLGF signalling in patients [318]. Further trials should examine whether anti-PLGF therapy can improve current chemotherapy regimens.

VEGF signalling is the target of many anti-angiogenic drugs [230], [284]. While most studies confirm VEGF is important in the stimulation of angiogenesis, others have shown VEGF is a chemoattractant for macrophages [280]. Therefore, the DOX-mediated upregulation of *Vegfa* in endothelial cells may offer an explanation as to why there was an increase in PV MRC1⁺ TAMs. Previously, murine studies revealed that TAM derived VEGF-A supports tumour regrowth following DOX treatment in implanted PyMT tumours, demonstrating this molecule is involved in tumour relapse [144]. Moreover, two separate studies have shown increased circulating VEGF in breast cancer patients following chemotherapy [286], [287]. However, another study showed circulating VEGF was decreased after chemotherapy in breast cancer patients with tumours larger than 5cm, suggesting that this may be a more complex regulation [288]. Perhaps in patients with larger tumours, the baseline circulating VEGF level is higher than in patients with smaller tumours, as there is a likely an increase in necrosis and hypoxia within these tumours, which results in an increase in VEGF-producing cells. If

chemotherapy causes tumour shrinkage, it may ablate some of the VEGF-producing cells, resulting in an overall decrease in circulating VEGF. Patients with smaller tumours on the other hand, may have fewer VEGF producing cells to start with, and the response to the chemotherapy in these patients causes the tumours to upregulate VEGF. While combining bevacizumab (an anti-VEGFA antibody) with chemotherapy was not successful when administered to patients in the adjuvant post-surgery setting [293], delivering this combination in the neoadjuvant setting effectively increased the pathological complete response rate of a cohort of breast cancer patients [294]. These studies suggest that targeting VEGFA may be useful in improving the response to chemotherapy; however the timing of when these drugs are given is very important to their clinical benefit.

SPP1 also acts as a macrophage chemoattractant, as well as having many other functions including being a component of the extracellular matrix [275]. Breast cancer patients with increased expression of SPP1 had decreased survival compared to those with low SPP1 expression [325]. Moreover, increased SPP1 expression was associated with poor response to chemotherapy in another cohort of breast cancer patients [324]. Again, these studies indicate SPP1 may also have potential as a new therapeutic target in patients, and further studies should reveal if inhibiting SPP1 improves the response of tumours to chemotherapy.

In summary, each of these genes are associated with poor prognosis in breast cancer patients and are capable of regulating macrophages. It is, therefore, highly likely that combining chemotherapy with therapies that target one or more of these genes could benefit patients. Further work is needed to characterise the safety and efficacy of these approaches.

6.5 Further work and directions

The most important step in continuing this research would be to examine the expression of the proteins encoded by the five genes up-regulated by DOX treatment in TS1 tumours (i.e. to confirm whether these novel transcriptional changes are translated to the protein, and specifically which cellular compartments of the tumour they are found in).

Ideally, flow cytometry would be used to analyse protein expression, as this would allow protein expression to be analysed in a range of different cell types e.g. compare protein expression in endothelial cells, TAMs and tumour cells. Moreover, as flow cytometry allows the measurement of fluorescent intensity, this would allow the detection of whether these proteins were upregulated after DOX, giving this method a clear advantage over immunofluorescent staining, in which quantification of protein expression is far more subjective. Unfortunately there were no antibodies designed for the flow cytometric analysis of these proteins.

In future, use of ELISAs or western blotting may be more useful, as reagents designed to measure angiopoietin-2, VEGF-A, PLGF, SPP1 and CX3CL1 protein expression by these methods are readily available. Ideally, this would be performed on the lysates of individual cell types isolated from dispersed tumours (e.g. CD31-enriched endothelial cells, etc).

Should any of the above genes show the same regulation at the protein level, it would be crucial to understand the role, if any, of each of these in the regulation of PV MRC1⁺ TAMs (and whether endothelial cell expression of these is particularly important given the proximity of endothelial cells to PV TAMs). Transgenic mice could be used to induce deletion of these genes specifically in endothelial cells following DOX treatment of tumours. One such model could use a Tie1 promoter [100] to drive expression of a tamoxifen-inducible Cre protein [127], which could then specifically ablate the expression of floxed genes. This study would allow the role of endothelial cell-specific

genes in the recruitment of PV TAMs, and potentially tumour regrowth to be studied. Importantly, an inducible model would allow the role of these genes in TAM recruitment and/or education to be studied at multiple timepoints such as before and after chemotherapy administration. Monoclonal antibodies targeting the upregulated genes could also be used to investigate whether any of these genes could be targeted to improve response to chemotherapy, however this would not establish the role of endothelial-cell specific proteins.

A new technique developed by our research group allows purification of PV TAMs from murine tumours (Hughes, unpublished). This technique utilises fluorescent dextrans which diffuse into the tumour and are engulfed by PV TAMs. Studies isolating these cells are now underway in my research group and will hopefully show whether PV MRC1⁺ TAMs express the receptors for the above genes. If so, the *ex vivo* effect of each of these proteins could be examined on the phenotype and function of PV MRC1⁺ TAMs isolated from chemotherapy-treated tumours.

In summary, these studies have revealed novel insights into the PV niche following DOX treatment. Further work should reveal if any of the five genes identified by qPCR studies are also upregulated at the protein level and if they are suitable candidates for preventing tumour regrowth after chemotherapy.

References

- [1] S. Gordon, "Elie Metchnikoff: father of natural immunity.," *Eur. J. Immunol.*, vol. 38, pp. 3257–3264, 2008.
- [2] D. M. Mosser and J. P. Edwards, "Exploring the full spectrum of macrophage activation," *Nat. Rev. Immunol.*, vol. 8, no. 12, pp. 958–969, 2008.
- [3] S. J. Galli, N. Borregaard, and T. a Wynn, "Phenotypic and functional plasticity of cells of innate immunity: macrophages, mast cells and neutrophils.," *Nat. Immunol.*, vol. 12, no. 11, pp. 1035–44, Nov. 2011.
- [4] A. Volkman and J. L. Gowans, "The Origin of Macrophages From Bone Marrow in the Rat.," *Br. J. Exp. Pathol.*, vol. 46, no. 1, pp. 62–70, Feb. 1965.
- [5] T. R. Bradley and D. Metcalf, "The growth of mouse bone marrow cells in vitro.," *Aust. J. Exp. Biol. Med. Sci.*, vol. 44, no. 3, pp. 287–300, Jun. 1966.
- [6] R. van Furth and Z. A. Cohn, "The origin and kinetics of mononuclear phagocytes.," *J. Exp. Med.*, vol. 128, no. 3, pp. 415–35, Sep. 1968.
- [7] T. J. L. M. Goud, C. Schotte, and R. van Furth, "Identification and Characterization of the Monoblast in Mononuclear Phagocyte Colonies Grown In Vitro," *J. Exp. Med.*, vol. 142, no. 5, pp. 1180–1199, 1975.
- [8] R. van Furth and M. M. C. Diesselhoff-Den Dulk, "The Kinetics of Promonocytes and Monocytes in the Bone Marrow," *J. Exp. Med.*, vol. 132, no. 4, pp. 813–828, 1970.
- [9] F. Geissmann, S. Jung, and D. R. Littman, "Blood monocytes consist of two principal subsets with distinct migratory properties.," *Immunity*, vol. 19, no. 1, pp. 71–82, Jul. 2003.
- [10] B. Passlick, D. Flieger, and H. W. L. Ziegler-Heitbrock, "Identification and Characterization of a Novel Monocyte Subpopulation in Human Peripheral Blood," *Blood*, vol. 74, pp. 2527–2534, 1989.
- [11] C. Sunderkötter *et al.*, "Subpopulations of mouse blood monocytes differ in maturation stage and inflammatory response," *J. Immunol.*, vol. 172, pp. 4410–4417, Apr. 2004.
- [12] C. Weber *et al.*, "Differential chemokine receptor expression and function in human monocyte subpopulations," *J. Leukoc. Biol.*, vol. 67, pp. 699–704, 2000.
- [13] S. Gordon and P. R. Taylor, "Monocyte and macrophage heterogeneity," *Nat. Rev. Immunol.*, vol. 5, pp. 953–64, Dec. 2005.
- [14] C. Auffray *et al.*, "Monitoring of blood vessels and tissues by a population of monocytes with patrolling behavior.," *Science*, vol. 317, no. 5838, pp. 666–70, Aug. 2007.
- [15] M. Nahrendorf *et al.*, "The healing myocardium sequentially mobilizes two monocyte subsets with divergent and complementary functions," *J. Exp. Med.*, vol. 204, no. 12, pp. 3037–3047, 2007.
- [16] C. Shi and E. G. Pamer, "Monocyte recruitment during infection and inflammation," *Nat. Rev. Immunol.*, vol. 11, no. 11, pp. 762–774, Nov. 2011.
- [17] E. Gomez Perdiguero and F. Geissmann, "The development and maintenance of

- resident macrophages," *Nat. Immunol.*, vol. 17, no. 1, pp. 2–8, 2016.
- [18] J. Y. Bertrand, A. Jalil, S. Jung, A. Cumano, and I. Godin, "Three pathways to mature macrophages in the early mouse yolk sac," *Blood*, vol. 106, no. 9, pp. 3004–3011, 2005.
- [19] K. E. Mcgrath *et al.*, "Distinct Sources of Hematopoietic Progenitors Emerge before HSCs and Provide Functional Blood Cells in the Mammalian Embryo," *Cell Rep.*, vol. 11, no. 12, pp. 1892–1904, 2015.
- [20] Y. Lavin, A. Mortha, A. Rahman, and M. Merad, "Regulation of macrophage development and function in peripheral tissues," *Nat. Rev. Immunol.*, vol. 15, pp. 731–744, 2015.
- [21] S. Gordon and L. Martinez-Pomares, "Physiological roles of macrophages," *Pflugers Arch.*, vol. 469, pp. 365–374, 2017.
- [22] N. Garbi and B. N. Lambrecht, "Location, function, and ontogeny of pulmonary macrophages during the steady state," *Pflugers Arch.*, vol. 469, pp. 561–572, 2017.
- [23] D. H. Kaplan, "In vivo function of Langerhans cells and dermal dendritic cells," *Trends Immunol.*, vol. 31, pp. 446–451, 2010.
- [24] H. Kettenmann, U.-K. Hanisch, M. Noda, and A. Verkhratsky, "Physiology of Microglia," *Physiol. Rev.*, vol. 91, pp. 461–553, 2011.
- [25] W. J. Boyle, W. S. Simonet, and D. L. Lacey, "Osteoclast differentiation and activation," *Nature*, vol. 423, pp. 337–342, 2003.
- [26] Z. Abdullah and P. A. Knolle, "Liver macrophages in healthy and diseased liver," *Pflugers Arch.*, vol. 469, pp. 553–560, 2017.
- [27] M. Bilzer, F. Roggel, and A. Gerbes, "Role of Kupffer cells in host defense and liver disease," *Liver Int.*, vol. 26, pp. 1175–1186, 2006.
- [28] F. O. Martinez and S. Gordon, "The M1 and M2 paradigm of macrophage activation : time for reassessment," *F1000Prime Rep.*, vol. 6, p. 13, 2014.
- [29] T. Hagemann *et al.*, "'Re-educating' tumor-associated macrophages by targeting NF- κ B.," *J. Exp. Med.*, vol. 205, pp. 1261–1268, 2008.
- [30] C. Rolny *et al.*, "HRG inhibits tumor growth and metastasis by inducing macrophage polarization and vessel normalization through downregulation of PlGF.," *Cancer Cell*, vol. 19, pp. 31–44, 2011.
- [31] S. M. Pyonteck *et al.*, "CSF-1R inhibition alters macrophage polarization and blocks glioma progression," *Nat. Med.*, vol. 19, pp. 1264–1272, 2013.
- [32] C. F. Nathan, H. W. Murray, M. E. Wiebe, and B. Y. Rubin, "Identification of Interferon- γ as the Lymphokine that Activates Human Macrophage Oxidative Metabolism and Antimicrobial Activity," *J. Exp. Med.*, vol. 158, pp. 670–689, 1983.
- [33] F. O. Martinez, S. Gordon, M. Locati, and A. Mantovani, "Transcriptional Profiling of the Human Monocyte-to-Macrophage Differentiation and Polarization: New Molecules and Patterns of Gene Expression," *J. Immunol.*, vol. 117, pp. 7303–7311, 2006.

- [34] D. D. Taub *et al.*, "Recombinant Human Interferon-inducible Protein 10 Is a Chemoattractant for Human Monocytes and T Lymphocytes and Promotes T Cell Adhesion to Endothelial Cells," *J. Exp. Med.*, vol. 177, pp. 1809–1814, 1993.
- [35] M. A. Collart, D. Belin, J.-D. Vassalli, S. De Kossodo, and P. Vassalli, "γ-Interferon Enhances Macrophage Transcription of the Tumor Necrosis Factor/Cachectin, Interleukin 1, and Urokinase Genes, which are Controlled by Short-Lived Repressors," *J. Exp. Med.*, vol. 164, pp. 2113–2118, 1986.
- [36] C. Bogdan, M. Röllinghoff, and A. Diefenbach, "The Role of Nitric Oxide in Innate Immunity," *Immunol. Rev.*, vol. 173, pp. 17–26, Feb. 2000.
- [37] S. Kurosawa *et al.*, "Early-Appearing Tumour-Infiltrating Natural Killer Cells Play a Crucial Role in the Generation of Anti-Tumour T Lymphocytes," *Immunology*, vol. 85, pp. 338–346, Jun. 1995.
- [38] K. Hariharan, G. Braslawsky, A. Black, S. Raychaudhuri, and N. Hanna, "The Induction of Cytotoxic T Cells and Tumor Regression by Soluble Antigen Formulation," *Cancer Res.*, vol. 55, pp. 3486–3489, 1995.
- [39] S. Goerdts and C. E. Orfanos, "Other Functions, Other Genes: Alternative Activation of Antigen-Presenting Cells," *Immunity*, vol. 10, pp. 137–142, 1999.
- [40] B. Mues, D. Langer, G. Zwadlo, and C. Sorg, "Phenotypic characterization of macrophages in human term placenta," *Immunology*, vol. 67, pp. 303–307, 1989.
- [41] D. R. Herbert *et al.*, "Alternative Macrophage Activation Is Essential for Survival during Schistosomiasis and Downmodulates T helper 1 Responses and Immunopathology," *Immunity*, vol. 20, pp. 623–635, 2004.
- [42] A. Mantovani, A. Sica, S. Sozzani, P. Allavena, A. Vecchi, and M. Locati, "The chemokine system in diverse forms of macrophage activation and polarization.," *Trends Immunol.*, vol. 25, pp. 677–686, 2004.
- [43] D. C. Lacey *et al.*, "Defining GM-CSF- and Macrophage-CSF-Dependent Macrophage Responses by In Vitro Models," *J. Immunol.*, vol. 188, pp. 5752–5765, 2012.
- [44] R. P. Donnelly, M. J. Fenton, D. S. Finbloom, and T. L. Gerrard, "Differential Regulation of IL-1 Production in Human Monocytes by IFN-γ and IL-4," *J. Immunol.*, vol. 145, pp. 569–575, 1990.
- [45] C. Bogdan, Y. Vodovotz, J. Paik, Q. Xie, and C. Nathan, "Mechanism of suppression of nitric oxide synthase expression by interleukin-4 in primary mouse macrophages," *J. Leukoc. Biol.*, vol. 55, pp. 227–233, 1994.
- [46] I. M. Corraliza, G. Soler, K. Eichmann, and M. Modolell, "Arginase Induction by Suppressors of Nitric Oxide Synthesis (IL-4, IL-10 and PGE2) in Murine Bone-Marrow-Derived Macrophages," *Biochem. Biophys. Res. Commun.*, vol. 206, pp. 667–673, 1995.
- [47] M. J. Fenton, J. A. Buras, and R. P. Donnelly, "IL-4 Reciprocally Regulates IL-1 and IL-1 Receptor Antagonist Expression in Human Monocytes," *J. Immunol.*, vol. 149, pp. 1283–1288, 1992.
- [48] D. Ruckerl, M. Heßmann, T. Yoshimoto, S. Ehlers, and C. Hölscher,

- “Alternatively activated macrophages express the IL-27 receptor alpha chain WSX-1,” *Immunobiology*, vol. 211, pp. 427–436, 2006.
- [49] M. Stein, S. Keshav, N. Harris, and S. Gordon, “Interleukin 4 Potently Enhances Murine Macrophage Mannose Receptor Activity: A Marker of Alternative Immunologic Macrophage Activation,” *J. Exp. Med.*, vol. 176, no. July, pp. 287–292, 1992.
- [50] M. Munder, K. Eichmann, and M. Modolell, “Alternative Metabolic States in Murine Macrophages Reflected by the Nitric Oxide Synthase/Arginase Balance: Competitive Regulation by CD4 + T Cells Correlates with Th1/Th2 Phenotype,” *J. Immunol.*, vol. 160, pp. 5347–5354, 1998.
- [51] G. Raes, P. De Baetselier, W. Noël, A. Beschin, F. Brombacher, and G. Hassanzadeh Gh, “Differential expression of FIZZ1 and Ym1 in alternatively versus classically activated macrophages,” *J. Leukoc. Biol.*, vol. 71, pp. 597–602, 2002.
- [52] C. J. Scotton *et al.*, “Transcriptional Profiling Reveals Complex Regulation of the Monocyte IL-1 β System by IL-13,” *J. Immunol.*, vol. 174, pp. 834–845, 2005.
- [53] F. O. Martinez *et al.*, “Genetic programs expressed in resting and IL-4 alternatively activated mouse and human macrophages: similarities and differences,” *Blood*, vol. 121, pp. e57–e69, 2013.
- [54] X. Liao *et al.*, “Krüppel-like factor 4 regulates macrophage polarization,” *J. Clin. Invest.*, vol. 121, pp. 2736–2749, 2011.
- [55] M. Rehli *et al.*, “Transcription Factor Tfec Contributes to the IL-4-Inducible Expression of a Small Group of Genes in Mouse Macrophages Including the Granulocyte Colony-Stimulating Factor Receptor,” *J. Immunol.*, vol. 174, pp. 7111–7122, 2005.
- [56] C. El Chartouni, L. Schwarzfischer, and M. Rehli, “Interleukin-4 induced interferon regulatory factor (Irf) 4 participates in the regulation of alternative macrophage priming,” *Immunobiology*, vol. 215, pp. 821–825, 2010.
- [57] J. P. Edwards, X. Zhang, K. A. Frauwirth, and D. M. Mosser, “Biochemical and functional characterization of three activated macrophage populations,” *J. Leukoc. Biol.*, vol. 80, pp. 1298–1307, 2006.
- [58] K.-H. Park-Min, T. T. Antoniv, and L. B. Ivashkiv, “Regulation of macrophage phenotype by long-term exposure to IL-10,” *Immunobiology*, vol. 210, pp. 77–86, 2005.
- [59] J. Ehrchen *et al.*, “Glucocorticoids induce differentiation of a specifically activated, anti-inflammatory subtype of human monocytes,” *Blood*, vol. 109, pp. 1265–1274, 2007.
- [60] M. D. B. van de Garde, F. O. Martinez, B. N. Melgert, M. N. Hylkema, R. E. Jonkers, and J. Hamann, “Chronic Exposure to Glucocorticoids Shapes Gene Expression and Modulates Innate and Adaptive Activation Pathways in Macrophages with Distinct Changes in Leukocyte Attraction,” *J. Immunol.*, vol. 192, pp. 1196–1208, 2014.
- [61] A. Mantovani, S. Sozzani, M. Locati, P. Allavena, and A. Sica, “Macrophage polarization: tumor-associated macrophages as a paradigm for polarized M2

- mononuclear phagocytes.," *Trends Immunol.*, vol. 23, no. 11, pp. 549–55, Nov. 2002.
- [62] H. Fang and Y. A. DeClerck, "Targeting the Tumor Microenvironment: From Understanding Pathways to Effective Clinical Trials," *Cancer Res.*, vol. 73, pp. 4965–4977, 2013.
- [63] D. F. Quail and J. A. Joyce, "Microenvironmental regulation of tumor progression and metastasis," *Nat. Med.*, vol. 19, pp. 1423–1437, 2013.
- [64] C. E. Lewis and J. W. Pollard, "Distinct Role of Macrophages in Different Tumor Microenvironments," *Cancer Res.*, vol. 66, pp. 605–612, 2006.
- [65] M. De Palma and C. E. Lewis, "Macrophage Regulation of Tumor Responses to Anticancer Therapies," *Cancer Cell*, vol. 23, pp. 277–286, 2013.
- [66] R. Noy and J. W. Pollard, "Tumor-Associated Macrophages: From Mechanisms to Therapy," *Immunity*, vol. 41, pp. 49–61, 2014.
- [67] F. Tacke, F. Ginhoux, C. Jakubzick, N. van Rooijen, M. Merad, and G. J. Randolph, "Immature monocytes acquire antigens from other cells in the bone marrow and present them to T cells after maturing in the periphery," *J. Exp. Med.*, vol. 203, pp. 583–597, 2006.
- [68] K. Movahedi *et al.*, "Different tumor microenvironments contain functionally distinct subsets of macrophages derived from Ly6C(high) monocytes," *Cancer Res.*, vol. 70, pp. 5728–39, Jul. 2010.
- [69] M. De Palma, M. A. Venneri, C. Roca, and L. Naldini, "Targeting exogenous genes to tumor angiogenesis by transplantation of genetically modified hematopoietic stem cells," *Nat. Med.*, vol. 9, pp. 789–795, 2003.
- [70] M. De Palma *et al.*, "Tie2 identifies a hematopoietic lineage of proangiogenic monocytes required for tumor vessel formation and a mesenchymal population of pericyte progenitors," *Cancer Cell*, vol. 8, pp. 211–226, 2005.
- [71] F. Pucci *et al.*, "A distinguishing gene signature shared by tumor-infiltrating Tie2-expressing monocytes, blood 'resident' monocytes, and embryonic macrophages suggests common functions and developmental relationships.," *Blood*, vol. 114, pp. 901–914, 2009.
- [72] F. K. Swirski *et al.*, "Identification of Splenic Reservoir Monocytes and Their Deployment to Inflammatory Sites," *Science (80-.)*, vol. 325, pp. 612–616, 2009.
- [73] V. Cortez-Retamozo *et al.*, "Origins of tumor-associated macrophages and neutrophils," *Proc. Natl. Acad. Sci. U. S. A.*, vol. 109, pp. 2491–2496, 2012.
- [74] F. H. W. Shand *et al.*, "Tracking of intertissue migration reveals the origins of tumor-infiltrating monocytes," *Proc. Natl. Acad. Sci. U. S. A.*, vol. 111, pp. 7771–7776, 2014.
- [75] R. A. Franklin *et al.*, "The Cellular and Molecular Origin of Tumor-Associated Macrophages," *Science (80-.)*, vol. 344, pp. 921–925, 2014.
- [76] C. Schulz *et al.*, "A Lineage of Myeloid Cells Independent of Myb and Hematopoietic Stem Cells," *Science (80-.)*, vol. 336, pp. 86–90, 2012.

- [77] L. Bingle, N. J. Brown, and C. E. Lewis, "The role of tumour-associated macrophages in tumour progression: implications for new anticancer therapies.," *J. Pathol.*, vol. 196, pp. 254–265, 2002.
- [78] R. D. Leek, R. J. Landers, A. L. Harris, and C. E. Lewis, "Necrosis correlates with high vascular density and focal macrophage infiltration in invasive carcinoma of the breast," *Br. J. Cancer*, vol. 79, pp. 991–995, 1999.
- [79] T. Hanada, M. Nakagawa, A. Emoto, T. Nomura, N. Nasu, and Y. Nomura, "Prognostic value of tumor-associated macrophage count in human bladder cancer.," *Int. J. Urol.*, vol. 7, pp. 263–269, Jul. 2000.
- [80] N. Koide, A. Nishio, T. Sato, A. Sugiyama, and S. Miyagawa, "Significance of macrophage chemoattractant protein-1 expression and macrophage infiltration in squamous cell carcinoma of the esophagus," *Am. J. Gastroenterol.*, vol. 99, pp. 1667–1674, 2004.
- [81] Y. Yao, T. Kubota, K. Sato, and R. Kitai, "Macrophage Infiltration-associated Thymidine Phosphorylase Expression Correlates with Increased Microvessel Density and Poor Prognosis in Astrocytic Tumors," *Clin. Cancer Res.*, vol. 7, pp. 4021–4026, 2001.
- [82] M. Ryder, R. A. Ghossein, J. C. M. Ricarte-Filho, J. A. Knauf, and J. A. Fagin, "Increased density of tumor-associated macrophages is associated with decreased survival in advanced thyroid cancer.," *Endocr. Relat. Cancer*, vol. 15, pp. 1069–1074, 2008.
- [83] D. Hanahan and R. A. Weinberg, "Hallmarks of Cancer: The Next Generation," *Cell*, vol. 144, pp. 646–674, 2011.
- [84] J. Folkman, P. Cole, and S. Zimmerman, "Tumor Behavior in Isolated Perfused Organs: In Vitro Growth and Metastases of Biopsy Material in Rabbit Thyroid and Canine Intestinal Segment," *Ann. Surg.*, vol. 164, pp. 491–502, Sep. 1966.
- [85] M. Skobe, P. Rockwell, N. Goldstein, S. Vosseler, and N. E. Fusenig, "Halting angiogenesis suppresses carcinoma cell invasion," *Nat. Med.*, vol. 3, pp. 1222–1227, 1997.
- [86] L. Bingle, C. E. Lewis, K. P. Corke, M. W. R. Reed, and N. J. Brown, "Macrophages promote angiogenesis in human breast tumour spheroids in vivo," *Br. J. Cancer*, vol. 94, pp. 101–107, 2006.
- [87] E. Y. Lin *et al.*, "Progression to Malignancy in the Polyoma Middle T Oncoprotein Mouse Breast Cancer Model Provides a Reliable Model for Human Diseases," *Am. J. Pathol.*, vol. 163, pp. 2113–2126, Nov. 2003.
- [88] E. Y. Lin *et al.*, "Macrophages Regulate the Angiogenic Switch in a Mouse Model of Breast Cancer," *Cancer Res.*, vol. 66, pp. 11238–11246, 2006.
- [89] W. Wiktor-Jedrzejczak *et al.*, "Total absence of colony-stimulating factor 1 in the macrophage-deficient osteopetrotic (op/op) mouse," *Proc. Natl. Acad. Sci. U. S. A.*, vol. 87, pp. 4828–4832, 1990.
- [90] S. M. Zeisberger, B. Odermatt, C. Marty, A. H. M. Zehnder-Fjällman, K. Ballmer-Hofer, and R. A. Schwendener, "Clodronate-liposome-mediated depletion of tumour-associated macrophages: a new and highly effective antiangiogenic therapy approach.," *Br. J. Cancer*, vol. 95, pp. 272–281, 2006.

- [91] T. M. Schlaeger *et al.*, "Uniform vascular-endothelial-cell-specific gene expression in both embryonic and adult transgenic mice.," *Proc. Natl. Acad. Sci. U. S. A.*, vol. 94, pp. 3058–3063, 1997.
- [92] C. Murdoch, S. Tazzyman, S. Webster, and C. E. Lewis, "Expression of Tie-2 by human monocytes and their responses to angiopoietin-2," *J. Immunol.*, vol. 178, pp. 7405–7411, 2007.
- [93] M. A. Venneri *et al.*, "Identification of proangiogenic TIE2-expressing monocytes (TEMs) in human peripheral blood and cancer.," *Blood*, vol. 109, pp. 5276–5285, 2007.
- [94] T. Matsubara *et al.*, "TIE2-expressing monocytes as a diagnostic marker for hepatocellular carcinoma correlates with angiogenesis.," *Hepatology*, vol. 57, pp. 1416–1425, 2013.
- [95] B. D. Brown, M. A. Venneri, A. Zingale, L. Sergi Sergi, and L. Naldini, "Endogenous microRNA regulation suppresses transgene expression in hematopoietic lineages and enables stable gene transfer.," *Nat. Med.*, vol. 12, pp. 585–591, 2006.
- [96] C.-Z. Chen, L. Li, H. F. Lodish, and D. P. Bartel, "MicroRNAs Modulate Hematopoietic Lineage Differentiation.," *Science (80-.)*, vol. 303, pp. 83–86, 2004.
- [97] S. García *et al.*, "Tie2 Signaling Cooperates with TNF to Promote the Pro-Inflammatory Activation of Human Macrophages Independently of Macrophage Functional Phenotype," *PLoS One*, vol. 9, p. e82088, 2014.
- [98] P. C. Maisonpierre *et al.*, "Angiopoietin-2, a Natural Antagonist for Tie2 That Disrupts *in vivo* Angiogenesis," *Science (80-.)*, vol. 277, pp. 55–60, 1997.
- [99] S. B. Coffelt *et al.*, "Angiopoietin-2 regulates gene expression in TIE2-expressing monocytes and augments their inherent proangiogenic functions.," *Cancer Res.*, vol. 70, no. 13, pp. 5270–80, Jul. 2010.
- [100] Y. Reiss *et al.*, "Angiopoietin-2 Impairs Revascularization after Limb Ischemia," *Circ. Res.*, vol. 101, pp. 88–96, 2007.
- [101] H. G. Augustin, G. Y. Koh, G. Thurston, and K. Alitalo, "Control of vascular morphogenesis and homeostasis through the angiopoietin–Tie system," *Nat. Rev. Mol. Cell Biol.*, vol. 10, pp. 165–177, 2009.
- [102] R. Mazziere *et al.*, "Targeting the ANG2/TIE2 Axis Inhibits Tumor Growth and Metastasis by Impairing Angiogenesis and Disabling Rebounds of Proangiogenic Myeloid Cells," *Cancer Cell*, vol. 19, no. 4, pp. 512–26, 2011.
- [103] S. B. Coffelt *et al.*, "Angiopoietin 2 Stimulates TIE2-Expressing Monocytes To Suppress T Cell Activation and To Promote Regulatory T Cell Expansion," *J. Immunol.*, vol. 186, pp. 4183–4190, 2011.
- [104] M. R. Young, E. Wheeler, and M. Newby, "Macrophage-Mediated Suppression of Natural Killer Cell Activity in Mice Bearing Lewis Lung Carcinoma," *J. Natl. Cancer Inst.*, vol. 76, no. 4, pp. 745–750, 1986.
- [105] S. A. Quezada, K. S. Peggs, T. R. Simpson, and J. P. Allison, "Shifting the equilibrium in cancer immunoediting: from tumor tolerance to eradication," *Immunol. Rev.*, vol. 241, pp. 104–118, 2011.

- [106] B. Sheid and J. Boyce, "Inhibition of lymphocyte mitogenesis by factor(s) released from macrophages isolated from ascitic fluid of advanced ovarian cancer patients," *Cancer Immunol. Immunother. Immunother.*, vol. 17, pp. 190–194, Jan. 1984.
- [107] J. R. Oehler, D. a Campbell, and R. B. Herberman, "In vitro inhibition of lymphoproliferative responses to tumor associated antigens and of lymphoma cell proliferation by rat splenic macrophages.," *Cell. Immunol.*, vol. 28, no. 2, pp. 355–70, Feb. 1977.
- [108] J. B. Mitchem *et al.*, "Targeting Tumor-Infiltrating Macrophages Decreases Tumor-Initiating Cells, Relieves Immunosuppression, and Improves Chemotherapeutic Responses," *Cancer Res.*, vol. 73, pp. 1128–1141, 2013.
- [109] D. G. DeNardo *et al.*, "Leukocyte Complexity Predicts Breast Cancer Survival and Functionally Regulates Response to Chemotherapy," *Cancer Discov.*, vol. 1, pp. 54–67, 2011.
- [110] B. Ruffell *et al.*, "Macrophage IL-10 Blocks CD8+ T Cell-Dependent Responses to Chemotherapy by Suppressing IL-12 Expression in Intratumoral Dendritic Cells," *Cancer Cell*, vol. 26, pp. 623–637, 2014.
- [111] A. V. Balar and J. S. Weber, "PD-1 and PD-L1 antibodies in cancer: current status and future directions," *Cancer Immunol. Immunother.*, vol. 66, pp. 551–564, 2017.
- [112] Y. Zhu *et al.*, "CSF1 / CSF1R Blockade Reprograms Tumor-Infiltrating Macrophages and Improves Response to T-cell Checkpoint Immunotherapy in Pancreatic Cancer Models," *Cancer Res.*, vol. 74, pp. 5057–5069, 2014.
- [113] O. Bloch, C. A. Crane, R. Kaur, M. Safaee, M. J. Rutkowski, and A. T. Parsa, "Gliomas Promote Immunosuppression through Induction of B7-H1 Expression in Tumor-Associated Macrophages," *Clin. Cancer Res.*, vol. 19, pp. 3165–3175, 2013.
- [114] S. Goswami *et al.*, "Macrophages Promote the Invasion of Breast Carcinoma Cells via a Colony-Stimulating Factor-1/Epidermal Growth Factor Paracrine Loop," *Cancer Res.*, vol. 65, pp. 5278–5283, Jun. 2005.
- [115] J. Wyckoff *et al.*, "A Paracrine Loop between Tumor Cells and Macrophages Is Required for Tumor Cell Migration in Mammary Tumors," *Cancer Res.*, vol. 64, pp. 7022–7029, 2004.
- [116] J. B. Wyckoff *et al.*, "Direct Visualization of Macrophage-Assisted Tumor Cell Intravasation in Mammary Tumors," *Cancer Res.*, vol. 67, pp. 2649–2656, 2007.
- [117] E. Y. Lin, A. V. Nguyen, R. G. Russell, and J. W. Pollard, "Colony-stimulating factor 1 promotes progression of mammary tumors to malignancy.," *J. Exp. Med.*, vol. 193, pp. 727–739, 2001.
- [118] T. Hagemann, S. C. Robinson, M. Schulz, L. Trümper, F. R. Balkwill, and C. Binder, "Enhanced invasiveness of breast cancer cell lines upon co-cultivation with macrophages is due to TNF- α dependent up-regulation of matrix metalloproteases," *Carcinogenesis*, vol. 25, pp. 1543–1549, 2004.
- [119] S. Hiratsuka *et al.*, "MMP9 induction by vascular endothelial growth factor receptor-1 is involved in lung-specific metastasis," *Cancer Cell*, vol. 2, pp. 289–

300, 2002.

- [120] J. S. Lewis, R. J. Landers, J. C. Underwood, A. L. Harris, and C. E. Lewis, "Expression of Vascular Endothelial Growth Factor by Macrophages is Up-Regulated in Poorly Vascularized Areas of Breast Carcinomas," *J. Pathol.*, vol. 192, pp. 150–158, 2000.
- [121] M. Mazzone *et al.*, "Heterozygous Deficiency of PHD2 Restores Tumor Oxygenation and Inhibits Metastasis via Endothelial Normalization," *Cell*, vol. 136, pp. 839–51, 2009.
- [122] W. Wang *et al.*, "Identification and Testing of a Gene Expression Signature of Invasive Carcinoma Cells within Primary Mammary Tumors," *Cancer Res.*, vol. 64, pp. 8585–8594, 2004.
- [123] S. Goswami *et al.*, "Identification of invasion specific splice variants of the cytoskeletal protein Mena present in mammary tumor cells during invasion in vivo," *Clin Exp Metastasis*, vol. 26, pp. 153–159, 2009.
- [124] A. S. Harney *et al.*, "Real-Time Imaging Reveals Local, Transient Vascular Permeability, and Tumor Cell Intravasation Stimulated by TIE2 hi Macrophage-Derived VEGFA," *Cancer Discov.*, vol. 5, pp. 932–943, 2015.
- [125] T. E. Rohan *et al.*, "Tumor Microenvironment of Metastasis and Risk of Distant Metastasis of Breast Cancer," *J. Natl. Cancer Inst.*, vol. 106, p. dju136, 2014.
- [126] B. Qian *et al.*, "A Distinct Macrophage Population Mediates Metastatic Breast Cancer Cell Extravasation, Establishment and Growth," *PLoS One*, vol. 4, p. e6562, 2009.
- [127] B.-Z. Qian *et al.*, "CCL2 recruits inflammatory monocytes to facilitate breast-tumour metastasis," *Nature*, vol. 475, pp. 222–225, 2011.
- [128] L. Bonapace *et al.*, "Cessation of CCL2 inhibition accelerates breast cancer metastasis by promoting angiogenesis," *Nature*, vol. 515, pp. 130–133, 2014.
- [129] T. Kitamura *et al.*, "CCL2-induced chemokine cascade promotes breast cancer metastasis by enhancing retention of metastasis-associated macrophages," *J. Exp. Med.*, vol. 212, pp. 1043–1059, 2015.
- [130] B.-Z. Qian *et al.*, "FLT1 signaling in metastasis-associated macrophages activates an inflammatory signature that promotes breast cancer metastasis," *J. Exp. Med.*, vol. 212, pp. 1433–1448, 2015.
- [131] V. Malhotra and M. C. Perry, "Classical Chemotherapy: Mechanisms, Toxicities and the Therapeutic Window," *Cancer Biol. Ther.*, vol. 2, pp. S2–S4, 2003.
- [132] Macmillan Cancer Support, "Individual chemotherapy drugs," 2013. [Online]. Available: <http://www.macmillan.org.uk/Cancerinformation/Cancertreatment/Treatmenttypes/Chemotherapy/Individualdrugs/Individualdrugs.aspx>. [Accessed: 19-Jan-2014].
- [133] J. L. Guerriero, D. Ditsworth, Y. Fan, F. Zhao, H. C. Crawford, and W.-X. Zong, "Chemotherapy Induces Tumor Clearance Independent of Apoptosis," *Cancer Res.*, vol. 68, pp. 9595–9600, 2008.
- [134] P. Scaffidi, T. Misteli, and M. E. Bianchi, "Release of chromatin protein HMGB1 by necrotic cells triggers inflammation," *Nature*, vol. 418, pp. 191–195, 2002.

- [135] J. L. Guerriero *et al.*, “DNA Alkylating Therapy Induces Tumor Regression through an HMGB1-Mediated Activation of Innate Immunity.,” *J. Immunol.*, vol. 186, pp. 3517–3526, 2011.
- [136] K. N. Kodumudi, K. Woan, D. L. Gilvary, E. Sahakian, S. Wei, and J. Y. Djeu, “A Novel Chemoimmunomodulating Property of Docetaxel: Suppression of Myeloid-Derived Suppressor Cells in Tumor Bearers,” *Clin. Cancer Res.*, vol. 16, pp. 4583–4594, 2010.
- [137] E. S. Nakasone *et al.*, “Imaging Tumor-Stroma Interactions during Chemotherapy Reveals Contributions of the Microenvironment to Resistance,” *Cancer Cell*, vol. 21, pp. 488–503, 2012.
- [138] V. Gocheva *et al.*, “IL-4 induces cathepsin protease activity in tumor-associated macrophages to promote cancer growth and invasion,” *Genes Dev.*, vol. 24, pp. 241–255, 2010.
- [139] T. Shree *et al.*, “Macrophages and cathepsin proteases blunt chemotherapeutic response in breast cancer,” *Genes Dev.*, vol. 25, pp. 2465–2479, 2011.
- [140] L. Ireland *et al.*, “Chemoresistance in Pancreatic Cancer Is Driven by Stroma-Derived Insulin-Like Growth Factors,” *Cancer Res.*, vol. 76, pp. 6851–6863, 2016.
- [141] C. E. Lewis, A. S. Harney, and J. W. Pollard, “The Multifaceted Role of Perivascular Macrophages in Tumors,” *Cancer Cell*, vol. 30, pp. 18–25, 2016.
- [142] B. E. Clausen, C. Burkhardt, W. Reith, R. Renkawitz, and I. Förster, “Conditional gene targeting in macrophages and granulocytes using LysMcre mice,” *Transgenic Res.*, vol. 8, pp. 265–277, 1999.
- [143] C. Stockmann *et al.*, “Deletion of vascular endothelial growth factor in myeloid cells accelerates tumorigenesis,” *Nature*, vol. 456, pp. 814–818, 2008.
- [144] R. Hughes *et al.*, “Perivascular M2 Macrophages Stimulate Tumor Relapse after Chemotherapy,” *Cancer Res.*, vol. 75, pp. 3479–3491, 2015.
- [145] G. A. Donzella *et al.*, “AMD3100, a small molecule inhibitor of HIV-1 entry via the CXCR4 co-receptor,” *Nat. Med.*, vol. 4, pp. 72–77, 1998.
- [146] L. Chen *et al.*, “Tie2 Expression on Macrophages Is Required for Blood Vessel Reconstruction and Tumor Relapse after Chemotherapy,” *Cancer Res.*, vol. 76, pp. 6828–6838, 2016.
- [147] P. Paulus, E. R. Stanley, R. Schäfer, D. Abraham, and S. Aharinejad, “Colony-Stimulating Factor-1 Antibody Reverses Chemoresistance in Human MCF-7 Breast Cancer Xenografts,” *Cancer Res.*, vol. 66, pp. 4349–4356, 2006.
- [148] S. Y. Lim, A. E. Yuzhalin, A. N. Gordon-Weeks, and R. J. Muschel, “Targeting the CCL2-CCR2 signaling axis in cancer metastasis,” *Oncotarget*, vol. 7, pp. 28697–28710, 2016.
- [149] S. K. Sandhu *et al.*, “A first-in-human, first-in-class, phase I study of carlumab (CNTO 888), a human monoclonal antibody against CC-chemokine ligand 2 in patients with solid tumors,” *Cancer Chemother. Pharmacol.*, vol. 71, pp. 1041–1050, 2013.
- [150] I. Brana *et al.*, “Carlumab, an anti-C-C chemokine ligand 2 monoclonal antibody,

in combination with four chemotherapy regimens for the treatment of patients with solid tumors : an open-label, multicenter phase 1b study,” *Target. Oncol.*, vol. 10, pp. 111–123, 2015.

- [151] K. J. Pienta *et al.*, “Phase 2 study of carlumab (CNTO 888), a human monoclonal antibody against CC-chemokine ligand 2 (CCL2), in metastatic castration-resistant prostate cancer,” *Invest. New Drugs*, vol. 31, pp. 760–768, 2013.
- [152] A. F. Welford *et al.*, “TIE2-expressing macrophages limit the therapeutic efficacy of the vascular-disrupting agent combretastatin A4 phosphate in mice,” *J. Clin. Invest.*, vol. 121, pp. 1969–1973, 2011.
- [153] M. Kioi, H. Vogel, G. Schultz, R. M. Hoffman, G. R. Harsh, and J. M. Brown, “Inhibition of vasculogenesis but not angiogenesis, prevents the recurrence of glioblastoma after irradiation in mice,” *J. Clin. Invest.*, vol. 120, pp. 694–705, 2010.
- [154] S. V. Kozin, W. S. Kamoun, Y. Huang, M. R. Dawson, R. K. Jain, and D. G. Duda, “Recruitment of Myeloid but not Endothelial Precursor Cells Facilitates Tumor Regrowth after Local Irradiation,” *Cancer Res.*, vol. 70, pp. 5679–5685, 2010.
- [155] I. Kalatskaya, Y. A. Berchiche, S. Gravel, B. J. Limberg, J. S. Rosenbaum, and N. Heveker, “AMD3100 Is a CXCR7 Ligand with Allosteric Agonist Properties,” *Mol. Pharmacol.*, vol. 75, pp. 1240–1247, 2009.
- [156] M. Deichmann, R. Kronenwett, and R. Haas, “Expression of the Human Immunodeficiency Virus Type-1 Coreceptors CXCR-4 (fusin, LESTR) and CKR-5 in CD34+ hematopoietic progenitor cells.,” *Blood*, vol. 89, pp. 3522–3528, May 1997.
- [157] W. C. Liles *et al.*, “Mobilization of hematopoietic progenitor cells in healthy volunteers by AMD3100, a CXCR4 antagonist,” *Blood*, vol. 102, pp. 2728–2730, Oct. 2003.
- [158] H. E. Broxmeyer *et al.*, “Rapid mobilization of murine and human hematopoietic stem and progenitor cells with AMD3100, a CXCR4 antagonist,” *J. Exp. Med.*, vol. 201, pp. 1307–1318, Apr. 2005.
- [159] E. De Clercq, “The AMD3100 story: The path to the discovery of a stem cell mobilizer (Mozobil),” *Biochem. Pharmacol.*, vol. 77, pp. 1655–1664, Jun. 2009.
- [160] S. Scala, “Molecular Pathways : Targeting the CXCR4 – CXCL12 Axis — Untapped Potential in the Tumor Microenvironment,” *Clin. cancer Res.*, vol. 21, pp. 4278–4285, 2015.
- [161] S.-B. Peng *et al.*, “Identification of LY2510924, a Novel Cyclic Peptide CXCR4 Antagonist That Exhibits Antitumor Activities in Solid Tumor and Breast Cancer Metastatic Models,” *Mol. Cancer Ther.*, vol. 14, pp. 480–490, 2015.
- [162] M. D. Galsky *et al.*, “A Phase I Trial of LY2510924, a CXCR4 Peptide Antagonist, in Patients with Advanced Cancer,” *Clin. cancer Res.*, vol. 20, pp. 3581–3588, 2014.
- [163] R. Salgia *et al.*, “A randomized phase II study of LY2510924 and carboplatin/etoposide versus carboplatin/etoposide in extensive-disease small

- cell lung cancer,” *Lung Cancer*, vol. 105, pp. 7–13, 2017.
- [164] D. J. Ceradini *et al.*, “Progenitor cell trafficking is regulated by hypoxic gradients through HIF-1 induction of SDF-1,” *Nat. Med.*, vol. 10, pp. 858–864, 2004.
- [165] J. Xu *et al.*, “CSF1R Signaling Blockade Stanches Tumor-Infiltrating Myeloid Cells and Improves the Efficacy of Radiotherapy in Prostate Cancer,” *Cancer Res.*, vol. 73, pp. 2782–2794, 2013.
- [166] S. J. Priceman *et al.*, “Targeting distinct tumor-infiltrating myeloid cells by inhibiting CSF-1 receptor: combating tumor evasion of antiangiogenic therapy.,” *Blood*, vol. 115, pp. 1461–1471, 2010.
- [167] T. D. Eubank, M. Galloway, C. M. Montague, W. J. Waldman, and C. B. Marsh, “M-CSF Induces Vascular Endothelial Growth Factor Production and Angiogenic Activity from Human Monocytes,” *J. Immunol.*, vol. 171, pp. 2637–2643, 2003.
- [168] R. J. Tushinski, I. T. Oliver, L. J. Guilbert, P. W. Tynan, J. R. Warner, and E. R. Stanley, “Survival of Mononuclear Phagocytes Depends on a Lineage-Specific Growth Factor That the Differentiated Cells Selectively Destroy,” *Cell*, vol. 28, pp. 71–81, 1982.
- [169] T. D. Eubank *et al.*, “Granulocyte Macrophage Colony-Stimulating Factor Inhibits Breast Cancer Growth and Metastasis by Invoking an Anti-Angiogenic Program in Tumor-Educated Macrophages,” *Cancer Res.*, vol. 69, pp. 2133–2140, 2009.
- [170] A. Buqué *et al.*, “Trial Watch — Small molecules targeting the immunological tumor microenvironment for cancer therapy,” *Oncoimmunology*, vol. 5, pp. e1149674-2-e1149674-25, 2016.
- [171] W. D. Tap *et al.*, “Structure-Guided Blockade of CSF1R Kinase in Tenosynovial Giant-Cell Tumor,” *N. Engl. J. Med.*, vol. 373, pp. 428–437, 2015.
- [172] N. Butowski *et al.*, “Orally administered colony stimulating factor 1 receptor inhibitor PLX3397 in recurrent glioblastoma: an Ivy Foundation Early Phase Clinical Trials Consortium phase II study,” *Neuro. Oncol.*, vol. 18, pp. 557–564, 2016.
- [173] D. M. Hyman *et al.*, “A phase 1 study of MEDI3617, a selective angiopoietin-2 inhibitor, alone and in combination with carboplatin/paclitaxel, paclitaxel, or bevacizumab in patients with advanced solid tumors,” *J. Clin. Oncol.*, vol. 32, p. (suppl; abstr 3012), 2014.
- [174] A. Gollerkeri *et al.*, “Phase Ib safety trial of CVX-060, an intravenous humanized monoclonal CovX body inhibiting angiopoietin 2 (Ang-2), with axitinib in patients with previously treated metastatic renal cell cancer (RCC).,” *J. Clin. Oncol.*, vol. 31, p. suppl; abstr 2533, 2013.
- [175] Y. Kienast *et al.*, “Ang-2-VEGF-A CrossMab, a Novel Bispecific Human IgG1 Antibody Blocking VEGF-A and Ang-2 Functions Simultaneously, Mediates Potent Antitumor, Antiangiogenic, and Antimetastatic Efficacy,” *Clin. Cancer Res.*, vol. 19, pp. 6730–6740, 2013.
- [176] T. E. Peterson *et al.*, “Dual inhibition of Ang-2 and VEGF receptors normalizes tumor vasculature and prolongs survival in glioblastoma by altering macrophages,” *Proc. Natl. Acad. Sci. U. S. A.*, vol. 113, pp. 4470–4475, 2016.
- [177] J. Kloepper *et al.*, “Ang-2/VEGF bispecific antibody reprograms macrophages

- and resident microglia to anti-tumor phenotype and prolongs glioblastoma survival,” *Proc. Natl. Acad. Sci. U. S. A.*, vol. 113, pp. 4476–4481, 2016.
- [178] D. S. Mendelson *et al.*, “First-in-human dose-escalation safety and PK trial of a novel humanized monoclonal CovX body dual inhibitor of angiopoietin 2 and vascular endothelial growth factor,” *J. Clin. Oncol.*, vol. 29, p. (suppl; abstr 3055), 2011.
- [179] National Institutes of Health, “ClinicalTrials.gov Study Record for trial NCT01004822,” 2015. [Online]. Available: <https://clinicaltrials.gov/show/NCT01004822>. [Accessed: 26-Apr-2017].
- [180] Y. Huang *et al.*, “Vascular normalizing doses of antiangiogenic treatment reprogram the immunosuppressive tumor microenvironment and enhance immunotherapy,” *Proc. Natl. Acad. Sci. U. S. A.*, vol. 109, pp. 17561–17566, 2012.
- [181] M. M. Kaneda *et al.*, “PI3K γ is a molecular switch that controls immune suppression,” *Nature*, vol. 539, pp. 437–442, 2016.
- [182] National Institutes of Health, “ClinicalTrials.gov Study Record for trial NCT02637531,” 2017. [Online]. Available: <https://clinicaltrials.gov/show/NCT02637531>. [Accessed: 28-Apr-2017].
- [183] G. Bergers and D. Hanahan, “Modes of Resistance to Anti-Angiogenic Therapy,” *Nat. Rev. Cancer*, vol. 8, pp. 592–603, 2008.
- [184] R. K. Jain, “Normalization of Tumor Vasculature: an Emerging Concept in Antiangiogenic Therapy,” *Science (80-)*, vol. 307, pp. 58–62, 2005.
- [185] D. Laoui *et al.*, “Tumor Hypoxia Does Not Drive Differentiation of Tumor-Associated Macrophages but Rather Fine-Tunes the M2-like Macrophage Population,” *Cancer Res.*, vol. 74, pp. 24–30, 2014.
- [186] H. He *et al.*, “Endothelial cells provide an instructive niche for the differentiation and functional polarization of M2-like macrophages,” *Blood*, vol. 120, pp. 3152–3162, 2012.
- [187] W. Qu *et al.*, “MFEprimer-2.0: a fast thermodynamics-based program for checking PCR primer specificity,” *Nucleic Acids Res.*, vol. 40, pp. W205–W208, 2012.
- [188] J. Schindelin *et al.*, “Fiji : an open-source platform for biological-image analysis,” *Nat. Methods*, vol. 9, pp. 676–682, 2012.
- [189] X. Zhang, R. Goncalves, and D. M. Mosser, “The Isolation and Characterization of Murine Macrophages,” *Curr. Protoc. Immunol.*, vol. 83, p. 14.1.1–14.1.14., 2008.
- [190] L. A. Herzenberg, J. Tung, W. A. Moore, L. A. Herzenberg, and D. R. Parks, “Interpreting flow cytometry data: a guide for the perplexed,” *Nat. Immunol.*, vol. 7, no. 7, pp. 681–685, 2006.
- [191] T. Kuo and J. Byun, “Image-based Tool for Counting Nuclei (ITCN) Plugin.” 2006.
- [192] K. De Vos, “Cell Counter ImageJ Plugin.” 2001.

- [193] P. Baluk, S. Morikawa, A. Haskell, M. Mancuso, and D. M. McDonald, "Abnormalities of Basement Membrane on Blood Vessels and Endothelial Sprouts in Tumors," *Am. J. Pathol.*, vol. 163, pp. 1801–1815, 2003.
- [194] R. Tang, F. Beuvon, M. Ojeda, V. Mosseri, P. Pouillart, and S. Scholl, "M-CSF (Monocyte Colony Stimulating Factor) and M-CSF Receptor Expression by Breast Tumour Cells: M-CSF Mediated Recruitment of Tumour Infiltrating Monocytes?," *J. Cell. Biochem.*, vol. 50, pp. 350–356, 1992.
- [195] L. Sánchez-Martín, A. Estecha, R. Samaniego, S. Sánchez-Ramón, M. Á. Vega, and P. Sánchez-Mateos, "The chemokine CXCL12 regulates monocyte-macrophage differentiation and RUNX3 expression," *Blood*, vol. 117, pp. 88–97, 2011.
- [196] F. J. Pixley and E. R. Stanley, "CSF-1 regulation of the wandering macrophage: complexity in action," *Trends Cell Biol.*, vol. 14, pp. 628–638, 2004.
- [197] Cancer Research UK, "The Three Most Common Cancers: 2014," *The Three Most Common Cancers in females: 2014*, 2014. [Online]. Available: <http://www.cancerresearchuk.org/health-professional/cancer-statistics/incidence/common-cancers-compared#heading=Two>. [Accessed: 05-Jun-2017].
- [198] Cancer Research UK, "Five Year Relative Survival (%) by Stage in Breast Cancer," 2006. [Online]. Available: <http://www.cancerresearchuk.org/health-professional/cancer-statistics/statistics-by-cancer-type/breast-cancer/survival#heading=Three>. [Accessed: 06-Jun-2017].
- [199] R. D. Leek, C. E. Lewis, R. Whitehouse, M. Greenall, J. Clarke, and A. L. Harris, "Association of Macrophage Infiltration with Angiogenesis and Prognosis in Invasive Breast Carcinoma," *Cancer Res.*, vol. 56, pp. 4625–4629, 1996.
- [200] M. A. Chaudary *et al.*, "Bilateral primary breast cancer: a prospective study of disease incidence," *Br. J. Surg.*, vol. 71, pp. 711–714, 1984.
- [201] National Institute for Health and Care Excellence, "NICE pathway: Managing advanced breast cancer," 2016. [Online]. Available: <https://pathways.nice.org.uk/pathways/advanced-breast-cancer#path=view%3A/pathways/advanced-breast-cancer/managing-advanced-breast-cancer.xml&content=view-index>. [Accessed: 06-Jun-2017].
- [202] National Institute for Health and Care Excellence, "Adjuvant therapy for early and locally advanced breast cancer," 2017. [Online]. Available: <http://pathways.nice.org.uk/pathways/early-and-locally-advanced-breast-cancer>. [Accessed: 08-Jun-2017].
- [203] National Institute for Health and Care Excellence, "Early and locally advanced breast cancer overview," 2017. [Online]. Available: <http://pathways.nice.org.uk/pathways/early-and-locally-advanced-breast-cancer>. [Accessed: 01-Aug-2017].
- [204] National Institute for Health and Care Excellence, "Advanced breast cancer (update)," 2014. [Online]. Available: <http://www.nice.org.uk/guidance/cg81/chapter/1-Recommendations>. [Accessed: 20-Aug-2014].
- [205] H.-Y. Fang *et al.*, "Hypoxia-inducible factors 1 and 2 are important transcriptional

- effectors in primary macrophages experiencing hypoxia," *Blood*, vol. 114, pp. 844–859, 2009.
- [206] C. Murdoch, M. Muthana, and C. E. Lewis, "Hypoxia Regulates Macrophage Functions in Inflammation," *J. Immunol.*, vol. 175, pp. 6257–6263, 2005.
- [207] S. Rose, A. Misharin, and H. Perlman, "A novel Ly6C/Ly6G-based strategy to analyze the mouse splenic myeloid compartment," *Cytom. Part A*, vol. 81, pp. 343–350, 2012.
- [208] C. Hitchon, K. Wong, G. Ma, J. Reed, D. Lyttle, and H. El-Gabalawy, "Hypoxia-Induced Production of Stromal Cell-Derived Factor 1 (CXCL12) and Vascular Endothelial Growth Factor by Synovial Fibroblasts," *Arthritis Rheum.*, vol. 46, pp. 2587–2597, 2002.
- [209] C. Carmona-Fontaine, M. Deforet, L. Akkari, C. B. Thompson, J. A. Joyce, and J. B. Xavier, "Metabolic origins of spatial organization in the tumor microenvironment," *Proc. Natl. Acad. Sci. U. S. A.*, vol. 114, pp. 2934–2939, 2017.
- [210] J. Decock, W. Hendrickx, S. Thirkettle, A. Gutiérrez-Fernández, S. D. Robinson, and D. R. Edwards, "Pleiotropic functions of the tumor- and metastasis-suppressing matrix metalloproteinase-8 in mammary cancer in MMTV-PyMT transgenic mice," *Breast Cancer Res.*, vol. 17, p. 38, 2015.
- [211] J. M. Gwak, M. H. Jang, D. Il Kim, A. N. Seo, and S. Y. Park, "Prognostic Value of Tumor-Associated Macrophages According to Histologic Locations and Hormone Receptor Status in Breast Cancer," *PLoS One*, vol. 10, p. e0125728, 2015.
- [212] C. Medrek, F. Pontén, K. Jirström, and K. Leandersson, "The presence of tumor associated macrophages in tumor stroma as a prognostic marker for breast cancer patients," *BMC Cancer*, vol. 12, p. 306, 2012.
- [213] E. S. Ch'ng, S. Emilia, T. Sharif, and H. Jaafar, "In human invasive breast ductal carcinoma, tumor stromal macrophages and tumor nest macrophages have distinct relationships with clinicopathological parameters and tumor angiogenesis," *Virchows Arch.*, vol. 462, pp. 257–267, 2013.
- [214] M. Bruchard *et al.*, "Chemotherapy-triggered cathepsin B release in myeloid-derived suppressor cells activates the Nlrp3 inflammasome and promotes tumor growth.," *Nat. Med.*, vol. 19, pp. 57–64, 2013.
- [215] C. M. Diaz-Montero, M. L. Salem, M. I. Nishimura, E. Garrett-Mayer, D. J. Cole, and A. J. Montero, "Increased circulating myeloid-derived suppressor cells correlate with clinical cancer stage, metastatic tumor burden, and doxorubicin–cyclophosphamide chemotherapy," *Cancer Immunol. Immunother.*, vol. 58, pp. 49–59, 2009.
- [216] K. Gonda *et al.*, "Myeloid-derived suppressor cells are increased and correlated with type 2 immune responses, malnutrition, inflammation, and poor prognosis in patients with breast cancer," *Oncol. Lett.*, vol. 14, pp. 1766–1774, 2017.
- [217] J. A. Nagy, S.-H. Chang, S.-C. Shih, A. M. Dvorak, and H. F. Dvorak, "Heterogeneity of the Tumour Vasculature," *Semin. Thromb. Hemost.*, vol. 36, pp. 321–331, 2010.

- [218] R. J. Gillies, P. A. Schornack, T. W. Secomb, and N. Raghunand, "Causes and Effects of Heterogeneous Perfusion in Tumors," *Neoplasia*, vol. 1, pp. 197–207, 1999.
- [219] A. Raza, M. J. Franklin, and A. Z. Dudek, "Pericytes and vessel maturation during tumor angiogenesis and metastasis," *Am. J. Hematol.*, vol. 85, pp. 593–598, 2010.
- [220] A. Armulik, G. Genové, and C. Betsholtz, "Pericytes: Developmental, Physiological, and Pathological Perspectives, Problems, and Promises," *Dev. Cell*, vol. 21, pp. 193–215, 2011.
- [221] J. Hamzah *et al.*, "Vascular normalization in Rgs5-deficient tumours promotes immune destruction," *Nature*, vol. 453, pp. 410–414, 2008.
- [222] M.-B. Voisin, D. Pröbstl, and S. Nourshargh, "Venular Basement Membranes Ubiquitously Express Matrix Protein Low-Expression Regions: Characterization in Multiple Tissues and Remodeling during Inflammation," *Am. J. Pathol.*, vol. 176, pp. 482–495, 2010.
- [223] J. Hong *et al.*, "Role of Tumor Pericytes in the Recruitment of Myeloid-Derived Suppressor Cells," *J. Natl. Cancer Inst.*, vol. 107, p. djv209, 2015.
- [224] A. Ager and M. J. May, "Understanding high endothelial venules: Lessons for cancer immunology," *Oncoimmunology*, vol. 4, pp. e1008791-1-e1008791-14, 2015.
- [225] J.-P. Girard and T. A. Springer, "High endothelial venules (HEVs): specialized endothelium for lymphocyte migration," *Immunol. Today*, vol. 16, pp. 449–457, 1995.
- [226] L. Martinet *et al.*, "Human Solid Tumors Contain High Endothelial Venules: Association with T- and B-Lymphocyte Infiltration and Favorable Prognosis in Breast Cancer," *Cancer Res.*, vol. 71, pp. 5678–5687, 2011.
- [227] J. P. Hindley *et al.*, "T-Cell Trafficking Facilitated by High Endothelial Venules Is Required for Tumor Control after Regulatory T-Cell Depletion," *Cancer Res.*, vol. 72, pp. 5473–5482, 2012.
- [228] L. Bracci, G. Schiavoni, A. Sistigu, and F. Belardelli, "Immune-based mechanisms of cytotoxic chemotherapy: implications for the design of novel and rationale-based combined treatments against cancer," *Cell Death Differ.*, vol. 21, pp. 15–25, 2014.
- [229] S. R. Mattarollo, S. Loi, H. Duret, Y. Ma, L. Zitvogel, and M. J. Smyth, "Pivotal Role of Innate and Adaptive Immunity in Anthracycline Chemotherapy of Established Tumors," *Cancer Res.*, vol. 71, pp. 4809–4820, 2011.
- [230] R. R. Ramjiawan, A. W. Griffioen, and D. G. Duda, "Anti-angiogenesis for cancer revisited: Is there a role for combinations with immunotherapy?," *Angiogenesis*, vol. 20, pp. 185–204, 2017.
- [231] V. Chintalgattu *et al.*, "Coronary microvascular pericytes are the cellular target of sunitinib malate induced cardiotoxicity," *Sci. Transl. Med.*, vol. 5, p. 187ra69, 2013.
- [232] D. S. Grant, T. L. Williams, M. Zahaczewsky, and A. P. Dicker, "Comparison of Antiangiogenic Activities using Paclitaxel (Taxol) and Docetaxel (Taxotere)," *Int.*

- J. cancer*, vol. 104, pp. 121–129, 2003.
- [233] K. D. Miller *et al.*, “Randomized phase II trial of the anti-angiogenic potential of doxorubicin and docetaxel; primary chemotherapy as Biomarker Discovery Laboratory,” *Breast Cancer Res. Treat.*, vol. 89, pp. 187–197, 2005.
- [234] G. Luengo-Gil *et al.*, “Effects of conventional neoadjuvant chemotherapy for breast cancer on tumor angiogenesis,” *Breast Cancer Res. Treat.*, vol. 151, pp. 577–587, 2015.
- [235] W. F. Boron and E. L. Boulpaep, *Medical Physiology*, Second Edi. Philadelphia: Saunders Elsevier, 2009.
- [236] S. Gibaud, J. P. Andreux, C. Weingarten, M. Renard, and P. Couvreur, “Increased Bone Marrow Toxicity of Doxorubicin Bound to Nanoparticles,” *Eur. J. Cancer*, vol. 30A, pp. 820–826, 1994.
- [237] The Jackson Laboratory, “Mouse Phenome Database -MPD:22934 Hematological survey of 11 strains of mice.,” 2006. [Online]. Available: <http://phenome.jax.org>. [Accessed: 05-May-2017].
- [238] Y. Wang *et al.*, “CCR2 and CXCR4 regulate peripheral blood monocyte pharmacodynamics and link to efficacy in experimental autoimmune encephalomyelitis,” *J. Inflamm.*, vol. 6, p. 32, 2009.
- [239] R. Caso, R. Silvera, R. Carrio, V. Iragavarapu-Charyulu, R. R. Gonzalez-Perez, and M. Torroella-Kouri, “Blood monocytes from mammary tumor-bearing mice: Early targets of tumor-induced immune suppression ?,” *Int. J. Oncol.*, vol. 37, pp. 891–900, 2010.
- [240] C. Bergenfelz *et al.*, “Systemic Monocytic-MDSCs Are Generated from Monocytes and Correlate with Disease Progression in Breast Cancer Patients,” *PLoS One*, vol. 10, p. e0127028, 2015.
- [241] H. U. Wang, Z.-F. Chen, and D. J. Anderson, “Molecular Distinction and Angiogenic Interaction between Embryonic Arteries and Veins Revealed by ephrin-B2 and Its Receptor Eph-B4,” *Cell*, vol. 93, pp. 741–753, 1998.
- [242] N. K. Noren and E. B. Pasquale, “Paradoxes of the EphB4 Receptor in Cancer,” *Cancer Res.*, vol. 67, pp. 3994–3997, 2007.
- [243] V. L. Bautch and K. M. Caron, “Blood and Lymphatic Vessel Formation,” *Cold Spring Harb. Perspect. Biol.*, vol. 7, p. a008268, 2015.
- [244] R. Daneman, L. Zhou, A. A. Kebede, and B. A. Barres, “Pericytes are required for blood-brain barrier integrity during embryogenesis,” *Nature*, vol. 468, pp. 562–566, 2010.
- [245] L. E. Olson and P. Soriano, “PDGFR β Signaling Regulates Mural Cell Plasticity and Inhibits Fat Development,” *Dev. Cell*, vol. 20, pp. 815–826, 2011.
- [246] W. Chen *et al.*, “Reduced mural cell coverage and impaired vessel integrity after angiogenic stimulation in the Alk1-deficient brain,” *Arterioscler. Thromb. Vasc. Biol.*, vol. 33, pp. 305–310, 2013.
- [247] D. Vestweber, “How leukocytes cross the vascular endothelium,” *Nat. Rev. Immunol.*, vol. 15, pp. 692–704, 2015.

- [248] K. Yamada *et al.*, "CXCL12–CXCR7 axis is important for tumor endothelial cell angiogenic property," *Int. J. cancer*, vol. 137, pp. 2825–2836, 2015.
- [249] A. Salmaggi *et al.*, "CXCL12 in malignant glial tumors: a possible role in angiogenesis and cross-talk between endothelial and tumoral cells," *J. Neurooncol.*, vol. 67, pp. 305–317, 2004.
- [250] C. Sfiligoi *et al.*, "Angiopoietin-2 Expression in Breast Cancer Correlates with Lymph Node Invasion and Short Survival," *Int. J. cancer*, vol. 103, pp. 466–474, 2003.
- [251] J. M. Wang, J. D. Griffin, A. Rambaldi, Z. G. Chen, and A. Mantovani, "Induction of monocyte migration by recombinant macrophage colony-stimulating factor," *J. Immunol.*, vol. 141, pp. 575–579, 1988.
- [252] J. Meerschaert and M. B. Furie, "Monocytes use either CD11/CD18 or VLA-4 to migrate across human endothelium in vitro," *J. Immunol.*, vol. 152, pp. 1915–1926, 1994.
- [253] G.-O. Ahn, D. Tseng, C.-H. Liao, M. J. Dorie, A. Czechowicz, and J. M. Brown, "Inhibition of Mac-1 (CD11b/CD18) enhances tumor response to radiation by reducing myeloid cell recruitment," *Proc. Natl. Acad. Sci. U. S. A.*, vol. 107, pp. 8363–8368, 2010.
- [254] T. Kaneko, T. Okiji, R. Kaneko, H. Suda, and J. E. Nör, "Gene Expression Analysis of Immunostained Endothelial Cells Isolated from Formaldehyde-fixed Paraffin Embedded Tumors Using Laser Capture Microdissection – a Technical Report," *Microsc. Res. Tech.*, vol. 72, pp. 908–912, 2009.
- [255] F. Visioli *et al.*, "Glucose-Regulated Protein 78 (Grp78) Confers Chemoresistance to Tumor Endothelial Cells under Acidic Stress," *PLoS One*, vol. 9, p. e101053, 2014.
- [256] K. Hida *et al.*, "Tumor-Associated Endothelial Cells with Cytogenetic Abnormalities," *Cancer Res.*, vol. 64, pp. 8249–8255, 2004.
- [257] J. W. Wragg *et al.*, "MCAM and LAMA4 Are Highly Enriched in Tumor Blood Vessels of Renal Cell Carcinoma and Predict Patient Outcome," *Cancer Res.*, vol. 76, pp. 2314–2326, 2016.
- [258] M. Uguccioni, M. D. Apuzzo, M. Loetscher, B. Dewald, and M. Baggiolini, "Actions of the chemotactic cytokines MCP-1, MCP-2, MCP-3, RANTES, MIP-1 α and MIP-1 β on human monocytes," *Eur. J. Immunol.*, vol. 25, pp. 64–68, 1995.
- [259] T. J. Schall, K. Bacon, K. J. Toy, and D. V. Goeddel, "Selective attraction of monocytes and T lymphocytes of the memory phenotype by cytokine RANTES," *Nature*, vol. 347, pp. 669–671, 1990.
- [260] J. Van Damme, P. Proost, J.-P. Lenaerts, and G. Opdenakke, "Structural and Functional Identification of Two Human, Tumor-derived Monocyte Chemotactic Proteins (MCP-2 and MCP-3) Belonging to the Chemokine Family," *J. Exp. Med.*, vol. 176, pp. 59–65, 1992.
- [261] T. Kitamura *et al.*, "SMAD4-deficient intestinal tumors recruit CCR1+ myeloid cells that promote invasion," *Nat. Genet.*, vol. 39, pp. 467–475, 2007.
- [262] M. N. Sarafi, E. A. Garcia-Zepeda, J. A. MacLean, I. F. Charo, and A. D. Luster, "Murine Monocyte Chemoattractant Protein (MCP)-5: A Novel CC Chemokine

- That Is a Structural and Functional Homologue of Human MCP-1," *J. Exp. Med.*, vol. 185, pp. 99–109, 1997.
- [263] T. Imai *et al.*, "Identification and molecular characterization of fractalkine receptor CX3CR1, which mediates both leukocyte migration and adhesion," *Cell*, vol. 91, pp. 521–30, 1997.
- [264] A. M. Fong *et al.*, "Fractalkine and CX3CR1 Mediate a Novel Mechanism of Leukocyte Capture, Firm Adhesion, and Activation under Physiologic Flow," *J. Exp. Med.*, vol. 188, pp. 1413–1419, 1998.
- [265] E. Rossi *et al.*, "Endothelial endoglin is involved in inflammation: role in leukocyte adhesion and transmigration," *Blood*, vol. 121, pp. 403–415, 2013.
- [266] G. Walz, A. Aruffo, W. Kolanus, M. Bevilacqua, and B. Seed, "Recognition by ELAM-1 of the Sialyl-Lex Determinant on Myeloid and Tumor Cells," *Science (80-.)*, vol. 250, pp. 1132–1135, 1990.
- [267] K. Seino *et al.*, "Cutting Edge: Chemotactic Activity of Soluble Fas Ligand Against Phagocytes," *J. Immunol.*, vol. 161, pp. 4484–4488, 1998.
- [268] H. Zhang and A. C. Issekutz, "Down-Modulation of Monocyte Transendothelial Migration and Endothelial Adhesion Molecule Expression by Fibroblast Growth Factor Reversal by the Anti-Angiogenic Agent SU6668," *Am. J. Pathol.*, vol. 160, pp. 2219–2230, 2002.
- [269] D. A. Norris, R. A. F. Clark, L. M. Swigart, J. C. Huff, W. L. Weston, and S. E. Howell, "Fibronectin fragment(s) are chemotactic for human peripheral blood monocytes," *J. Immunol.*, vol. 129, pp. 1612–1618, 1982.
- [270] R. T. Perri, N. E. Kay, J. McCarthy, R. L. Vessella, H. S. Jacob, and L. T. Furcht, "Fibronectin Enhances In Vitro Monocyte-Macrophage-Mediated Tumoricidal Activity," *Blood*, vol. 60, pp. 430–435, 1982.
- [271] A. R. Schenkel, Z. Mamdouh, and W. A. Muller, "Locomotion of monocytes on endothelium is a critical step during extravasation," *Nat. Immunol.*, vol. 5, pp. 393–400, 2004.
- [272] M. P. Bevilacqua, J. S. Pober, M. . E. Wheeler, R. S. Cotran, and M. A. Gimbrone Jr, "Interleukin I Acts on Cultured Human Vascular Endothelium to Increase the Adhesion of Polymorphonuclear Leukocytes , Monocytes , and Related Leukocyte Cell Lines," *J. Clin. Invest.*, vol. 76, pp. 2003–2011, 1985.
- [273] B. S. Bochner *et al.*, "Adhesion of Human Basophils , Eosinophils , and Neutrophils to Interleukin 1-activated Human Vascular Endothelial Cells: Contributions of Endothelial Cell Adhesion Molecules," *J. Exp. Med.*, vol. 173, pp. 1553–1556, 1991.
- [274] P. Chomarat, J. Banchereau, J. Davoust, and A. K. Palucka, "IL-6 switches the differentiation of monocytes from dendritic cells to macrophages," *Nat. Immunol.*, vol. 1, pp. 510–514, 2000.
- [275] F. Kahles, H. M. Findeisen, and D. Bruemmer, "Osteopontin: A novel regulator at the cross roads of inflammation, obesity and diabetes," *Mol. Metab.*, vol. 3, pp. 384–393, 2014.
- [276] T. H. Burdo, M. R. Wood, and H. S. Fox, "Osteopontin Prevents Monocyte Recirculation and Apoptosis," *J. Leukoc. Biol.*, vol. 81, pp. 1504–1511, 2007.

- [277] C. Fischer *et al.*, “Anti-PlGF Inhibits Growth of VEGF(R)-Inhibitor-Resistant Tumors without Affecting Healthy Vessels,” *Cell*, vol. 131, pp. 463–75, 2007.
- [278] M. Dewerchin and P. Carmeliet, “PlGF: A Multitasking Cytokine with Disease-Restricted Activity,” *Cold Spring Harb. Perspect. Med.*, vol. 2, p. a011056, 2012.
- [279] T. Kirsch *et al.*, “Endothelial-derived thrombospondin-1 promotes macrophage recruitment and apoptotic cell clearance,” *J. Cell. Mol. Med.*, vol. 14, pp. 1922–1934, 2010.
- [280] B. Barleon, S. Sozzani, D. Zhou, H. A. Weich, A. Mantovani, and D. Marmé, “Migration of Human Monocytes in Response to Vascular Endothelial Growth Factor (VEGF) Is Mediated via the VEGF Receptor flt-1,” *Blood*, vol. 87, pp. 3336–3343, 1996.
- [281] M. J. Smith, R. W. Berger, K. Minhas, R. A. Moorehead, and B. L. Coomber, “Heterogeneity of vascular and progenitor cell compartments in tumours from MMTV-PyVmT transgenic mice during mammary cancer progression,” *Int. J. Exp. Pathol.*, vol. 92, pp. 106–116, 2011.
- [282] A. Schroeder *et al.*, “The RIN: an RNA integrity number for assigning integrity values to RNA measurements,” *BMC Mol. Biol.*, vol. 7, p. 3, 2006.
- [283] M. C. Bosco *et al.*, “Hypoxia Modifies the Transcriptome of Primary Human Monocytes: Modulation of Novel Immune-Related Genes and Identification Of CC-Chemokine Ligand 20 as a New Hypoxia-Inducible Gene,” *J. Immunol.*, vol. 177, pp. 1941–1955, 2006.
- [284] N. Ferrara, K. J. Hillan, and W. Novotny, “Bevacizumab (Avastin), a humanized anti-VEGF monoclonal antibody for cancer therapy,” *Biochem. Biophys. Res. Commun.*, vol. 333, pp. 328–335, 2005.
- [285] O. Casanovas, D. J. Hicklin, G. Bergers, and D. Hanahan, “Drug resistance by evasion of antiangiogenic targeting of VEGF signaling in late-stage pancreatic islet tumors,” *Cancer Cell*, vol. 8, pp. 299–309, 2005.
- [286] P. J. Mills *et al.*, “Predictors of inflammation in response to anthracycline-based chemotherapy for breast cancer,” *Brain. Behav. Immun.*, vol. 22, pp. 98–104, 2008.
- [287] G. Fürstenberger *et al.*, “Circulating endothelial cells and angiogenic serum factors during neoadjuvant chemotherapy of primary breast cancer,” *Br. J. Cancer*, vol. 94, pp. 524–531, 2006.
- [288] S. Kümmel *et al.*, “Changes in the Circulating Plasma Levels of VEGF and VEGF-D after Adjuvant Chemotherapy in Patients with Breast Cancer and 1 to 3 Positive Lymph Nodes,” *Anticancer Res.*, vol. 26, pp. 1719–1726, 2006.
- [289] B. F. Kabbinavar *et al.*, “Phase II, Randomized Trial Comparing Bevacizumab Plus Fluorouracil (FU)/Leucovorin (LV) With FU/LV Alone in Patients With Metastatic Colorectal Cancer,” *J. Clin. Oncol.*, vol. 21, pp. 60–65, 2003.
- [290] H. Hurwitz *et al.*, “Bevacizumab plus Irinotecan, Fluorouracil, and Leucovorin for Metastatic Colorectal Cancer,” *N. Engl. J. Med.*, vol. 350, pp. 2335–2342, 2004.
- [291] A. Sandler *et al.*, “Paclitaxel–Carboplatin Alone or with Bevacizumab for Non–Small-Cell Lung Cancer,” *N. Engl. J. Med.*, vol. 355, pp. 2542–2550, 2006.

- [292] E. B. Garon *et al.*, "Ramucirumab plus docetaxel versus placebo plus docetaxel for second-line treatment of stage IV non-small-cell lung cancer after disease progression on platinum-based therapy (REVEL): a multicentre, double-blind, randomised phase 3 trial," *Lancet*, vol. 384, pp. 665–673, 2014.
- [293] D. Cameron *et al.*, "Adjuvant bevacizumab-containing therapy in triple-negative breast cancer (BEATRICE): primary results of a randomised , phase 3 trial," *Lancet Oncol.*, vol. 14, pp. 933–942, 2013.
- [294] B. Gerber *et al.*, "Neoadjuvant bevacizumab and anthracycline–taxane-based chemotherapy in 678 triple-negative primary breast cancers; results from the geparquinto study (GBG 44)," *Ann. Oncol.*, vol. 24, pp. 2978–2984, 2013.
- [295] N. E. Hubbard, D. Lim, M. Mukutmoni, A. Cai, and K. L. Erickson, "Expression and regulation of murine macrophage angiopoietin-2," *Cell. Immunol.*, vol. 234, pp. 102–109, 2005.
- [296] K. Koga *et al.*, "Expression of Angiopoietin-2 in Human Glioma Cells and Its Role for Angiogenesis," *Cancer Res.*, vol. 61, pp. 6248–6254, 2001.
- [297] J. L. Brown *et al.*, "A Human Monoclonal Anti-ANG2 Antibody Leads to Broad Antitumor Activity in Combination with VEGF Inhibitors and Chemotherapy Agents in Preclinical Models," *Mol. Cancer Ther.*, vol. 9, pp. 145–156, 2010.
- [298] K. Srivastava *et al.*, "Postsurgical Adjuvant Tumor Therapy by Combining Anti-Angiopoietin-2 and Metronomic Chemotherapy Limits Metastatic Growth," *Cancer Cell*, vol. 26, pp. 880–895, 2014.
- [299] N. Yokomichi *et al.*, "Pathogenesis of Hand-Foot Syndrome induced by PEG-modified liposomal Doxorubicin," *Hum. Cell*, vol. 26, pp. 8–18, 2013.
- [300] Z.-Z. Huang *et al.*, "CX3CL1-mediated macrophage activation contributed to paclitaxel-induced DRG neuronal apoptosis and painful peripheral neuropathy," *Brain. Behav. Immun.*, vol. 40, pp. 155–165, 2014.
- [301] A. Schmall *et al.*, "Macrophage and Cancer Cell Cross-talk via CCR2 and CX3CR1 Is a Fundamental Mechanism Driving Lung Cancer," *Am. J. Respir. Crit. Care Med.*, vol. 191, pp. 437–447, 2015.
- [302] W. Liu *et al.*, "Role of CX3CL1 in Diseases," *Arch. Immunol. Ther. Exp. (Warsz.)*, vol. 64, pp. 371–383, 2016.
- [303] T. Matsubara, T. Ono, A. Yamanoi, M. Tachibana, and N. Nagasue, "Fractalkine-CX3CR1 Axis Regulates Tumor Cell Cycle and Deteriorates Prognosis After Radical Resection for Hepatocellular Carcinoma," *J. Surg. Oncol.*, no. 95, pp. 241–249, 2007.
- [304] M. Hyakudomi *et al.*, "Increased Expression of Fractalkine is Correlated with a Better Prognosis and an Increased Number of Both CD8+ T Cells and Natural Killer Cells in Gastric Adenocarcinoma," *Ann. Surg. Oncol.*, vol. 15, pp. 1775–1782, 2008.
- [305] D. L. Blum *et al.*, "Chemokine Markers Predict Biochemical Recurrence of Prostate Cancer following Prostatectomy," *Clin. Cancer Res.*, vol. 14, pp. 7790–7797, 2008.
- [306] J. Y. S. Tsang *et al.*, "CX3CL1 expression is associated with poor outcome in breast cancer patients," *Breast Cancer Res. Treat.*, vol. 140, pp. 495–504, 2013.

- [307] X. Xu *et al.*, "High Expression of CX3CL1/CX3CR1 Axis Predicts a Poor Prognosis of Pancreatic Ductal Adenocarcinoma," *J. Gastrointest. Surg.*, vol. 16, pp. 1493–1498, 2012.
- [308] G. Liu *et al.*, "Specific chemotherapeutic agents induce metastatic behaviour through stromal- and tumour-derived cytokine and angiogenic factor signalling," *J. Pathol.*, no. 237, pp. 190–202, 2015.
- [309] M. Putt *et al.*, "Longitudinal Changes in Multiple Biomarkers Are Associated with Cardiotoxicity in Breast Cancer Patients Treated with Doxorubicin, Taxanes, and Trastuzumab," *Clin. Chem.*, vol. 61, pp. 1164–1172, 2015.
- [310] C. Fischer, M. Mazzone, B. Jonckx, and P. Carmeliet, "FLT1 and its ligands VEGFB and PlGF: drug targets for anti-angiogenic therapy?," *Nat. Rev. Cancer*, vol. 8, pp. 942–956, 2008.
- [311] C. Parr, G. Watkins, M. Boulton, J. Cai, and W. G. Jiang, "Placenta growth factor is over-expressed and has prognostic value in human breast cancer," *Eur. J. Cancer*, vol. 41, pp. 2819–2827, 2005.
- [312] S.-C. Wei *et al.*, "Placenta growth factor expression is correlated with survival of patients with colorectal cancer," *Gut*, vol. 54, pp. 666–672, 2005.
- [313] C.-N. Chen *et al.*, "The significance of placenta growth factor in angiogenesis and clinical outcome of human gastric cancer," *Cancer Lett.*, vol. 213, pp. 73–82, 2004.
- [314] M.-C. Ho *et al.*, "Placenta growth factor not vascular endothelial growth factor A or C can predict the early recurrence after radical resection of hepatocellular carcinoma," *Cancer Lett.*, vol. 250, pp. 237–249, 2007.
- [315] L. Zhang, J. Chen, Y. Ke, R. E. Mansel, and W. G. Jiang, "Expression of Placenta growth factor (PlGF) in non-Small cell Lung cancer (NSCLC) and the clinical and prognostic significance," *World J. Surg. Oncol.*, vol. 3, p. 68, 2005.
- [316] L. Xu and R. K. Jain, "Down-Regulation of Placenta Growth Factor by Promoter Hypermethylation in Human Lung and Colon Carcinoma," *Mol. Cancer Res.*, vol. 5, pp. 873–880, 2007.
- [317] B. S. Jones *et al.*, "Pilot phase II study of metronomic chemotherapy in combination with bevacizumab in patients with advanced non-squamous non-small cell lung cancer," *Lung Cancer*, vol. 106, pp. 125–130, 2017.
- [318] U. Lassen *et al.*, "A phase I, dose-escalation study of TB-403, a monoclonal antibody directed against PlGF, in patients with advanced solid tumours," *Br. J. Cancer*, vol. 106, pp. 678–684, 2012.
- [319] N. A. Atai *et al.*, "Osteopontin is up-regulated and associated with neutrophil and macrophage infiltration in glioblastoma," *Immunology*, vol. 132, pp. 39–48, 2010.
- [320] K. J. Schunke, L. Coyle, G. F. Merrill, and D. T. Denhardt, "Acetaminophen Attenuates Doxorubicin-Induced Cardiac Fibrosis Via Osteopontin and GATA4 Regulation: Reduction of Oxidant Levels," *J. Cell. Physiol.*, vol. 228, pp. 2006–2014, 2013.
- [321] Y. Mori, C. Kondo, Y. Tonomura, M. Torii, and T. Uehara, "Identification of potential genomic biomarkers for early detection of chemically induced cardiotoxicity in rats," *Toxicology*, vol. 271, pp. 36–44, 2010.

- [322] L. Yang *et al.*, “Down-regulation of osteopontin expression by RNA interference affects cell proliferation and chemotherapy sensitivity of breast cancer MDA-MB-231 cells,” *Mol. Med. Rep.*, vol. 5, pp. 373–376, 2012.
- [323] I.-S. Hsieh, W.-H. Huang, H.-C. Liou, W.-J. Chuang, R.-S. Yang, and W.-M. Fu, “Upregulation of Drug Transporter Expression by Osteopontin in Prostate Cancer Cells,” *Mol. Pharmacol.*, vol. 83, pp. 968–977, 2013.
- [324] K. Zduniak, A. Agrawal, S. Agrawal, M. M. Hossain, P. Ziolkowski, and G. F. Weber, “Osteopontin splice variants are differential predictors of breast cancer treatment responses,” *BMC Cancer*, vol. 16, p. 441, 2016.
- [325] A. Psyrris *et al.*, “Association of osteopontin with specific prognostic factors and survival in adjuvant breast cancer trials of the Hellenic Cooperative Oncology Group,” *J. Transl. Med.*, vol. 15, p. 30, 2017.
- [326] M. Di Bartolomeo *et al.*, “Osteopontin, E-cadherin, and β -catenin expression as prognostic biomarkers in patients with radically resected gastric cancer,” *Gastric Cancer*, vol. 19, pp. 412–420, 2016.
- [327] P. C. Mack *et al.*, “Lower Osteopontin Plasma Levels Are Associated With Superior Outcomes in Advanced Non-Small-Cell Lung Cancer Patients Receiving Platinum-Based Chemotherapy: SWOG Study S0003,” *J. Clin. Oncol.*, vol. 26, pp. 4771–4776, 2008.
- [328] J. W. Thoms *et al.*, “Plasma osteopontin as a biomarker of prostate cancer aggression: relationship to risk category and treatment response,” *Br. J. Cancer*, vol. 107, pp. 840–846, 2012.
- [329] J. M. J. Herbert, D. Stekel, S. Sanderson, V. L. Heath, and R. Bicknell, “A novel method of differential gene expression analysis using multiple cDNA libraries applied to the identification of tumour endothelial genes,” *BMC Genomics*, vol. 9, p. 153, 2008.
- [330] G. T. Motz *et al.*, “Tumor Endothelium FasL Establishes a Selective Immune Barrier Promoting Tolerance in Tumors,” *Nat. Med.*, vol. 20, pp. 607–615, 2014.
- [331] K. Movahedi *et al.*, “Nanobody-Based Targeting of the Macrophage Mannose Receptor for Effective In Vivo Imaging of Tumor-Associated Macrophages,” *Cancer Res.*, vol. 72, pp. 4165–4177, 2012.
- [332] X. Zhan *et al.*, “Targeted depletion of tumour-associated macrophages by an alendronate-glucomannan conjugate for cancer immunotherapy,” *Biomaterials*, vol. 35, pp. 10046–10057, 2014.
- [333] A. C. Dudley, “Tumor Endothelial Cells,” *Cold Spring Harb. Perspect. Med.*, no. 2, p. a006536, 2012.
- [334] Cancer Research UK, “Triple Negative Breast Cancer,” 2016. [Online]. Available: <http://www.cancerresearchuk.org/about-cancer/breast-cancer/stages-types-grades/types/triple-negative-breast-cancer>. [Accessed: 06-Jun-2017].
- [335] A. Prat *et al.*, “Clinical implications of the intrinsic molecular subtypes of breast cancer,” *The Breast*, vol. 24, pp. S26–S35, 2015.
- [336] J. I. Herschkowitz *et al.*, “Identification of conserved gene expression features between murine mammary carcinoma models and human breast tumors,” *Genome Biol.*, vol. 8, p. R76, 2007.

- [337] S. A. DuPré, D. Redelman, and K. W. Hunter Jr, "The mouse mammary carcinoma 4T1: characterization of the cellular landscape of primary tumours and metastatic tumour foci," *Int. J. Exp. Pathol.*, vol. 88, pp. 351–360, 2007.
- [338] G. Gasparini, "Prognostic Value of Vascular Endothelial Growth Factor in Breast Cancer," *Oncologist*, vol. 5, pp. 37–44, 2000.